GoNEXUS

Tools and solutions for governing the nexus

Final Synthesis on River Basin WEFE Models

Deliverable D4.1 – WP4

September 2023

GoNEXUS has received funding from the European Union's Horizon 2020 research and innovation programme under grant agreement number 101003722.

www.gonexus.eu

Version 0.5
September 2023

Deliverable D4.1: Final Synthesis on River Basin WEFE Models

Lead by POLIMI
Wyatt Arnold, Andrea Ficchì, Matteo Giuliani, Paolo Gazzotti, Giorgio Guariso, Matteo Sangiorgio, Andrea Castelletti (POLIMI); Hector Macian-Sorribes, Manuel Pulido Velazquez, Amparo Martinez-Domingo UPV); Adrian Gonzalez-Rosell (UPM); Scott Sinclair, Dennis Eberli, Matthias Häfliger, Luca Franzetti, Anna Costa, Paolo Burlando (ETHZ); Janos Feher (FAMIFE), Rens van Beek (UU)

Dissemination level of document
Public

Abstract
This deliverable discusses the different WEFE models developed in the 6 case studies, including the description of the steps required for developing the models and reporting on the model performance.

GoNEXUS has received funding from the European Union's Horizon 2020 research and innovation programme under grant agreement number 101003722.

Version History

Version	Date	Authors	Description
V0.1	07/03/2023	Wyatt Arnold, Matteo Giuliani, Andrea Castelletti (POLIMI)	Proposed structure of the report
V0.2	08/03/2023	Wyatt Arnold, Matteo Sangiorgio (POLIMI); Scott Sinclair (ETH); Desamparados Martinez Domingo (UPV); Vahid Espanmanesh , Amaury Tilmant (ULAVAL)	First Draft
V0.3	09/13/2023	Wyatt Arnold, Matteo Giuliani, Andrea Castelletti (POLIMI)	WP-Internal Review
V0. 4	09/26/2023	Desamparados Martinez Domingo, Ivan Gerardo Lagos Castro, Sebastian Arias, Valentina Monico, Eulalia Gomez Martin (UPV); Adrian Humberto Gonzales Rosell (UPM); Rens van Beek (UU); Wyatt Arnold, Matteo Sangiorgio (POLIMI);	WP-External Review; Edits to application chapters; Addition of Danube application; Addition of List of Abbreviations
V0. 5	09/29/2023	POLIMI	Final review and submittal

Table of contents

List of Abbreviations

AWE-GEN-2d - Advanced WEather GENerator for a two-dimensional grid
CAP - Common Agricultural Policy
CAPEX - Capital Expenditure
CMIP - Coupled Model Intercomparison Project
CSG-SDDP - Combined Surface-Groundwater Stochastic Dual Dynamic Programming
DAFNE - Decision-Analytic Framework to explore the water-energy-food Nexus
UC/ED - Unit Commitment/Economic Dispatch
EMM - Embedded Multi-reservoir Model
EMODPS - Evolutionary Multi-Objective Direct Policy Search
ESPAT - Explicit Stochastic Programming Advanced Tool
FAO - Food and Agriculture Organization of the United Nations
FCM - Fuzzy Cognitive Map
FPV - Floating solar photovoltaic
FRB - Fuzzy Rule-Based model
GLM - General Lake Model
GMB - Group Model Building
HEM - Hydro-Economic Model
HPU - Potential Useful Habitat
IHA - Indicators of Hydrologic Alteration
JRB - Júcar River Basin
LCB - Lake Como Basin
LHS - Latin Hypercube Sampling
MEF - Minimum Environmental Flow
MOEA - Multi-Objective Evolutionary Algorithm
MORDM - Many-Objective Robust Decision Making
MPAR - Multisite Periodic Autoregressive Model
NTU - Nephelometric Turbidity Unit
OPEX - Operating Expenditure
PRIM - Patient Rule Induction Method
RBF - Radial Basis Function
RDM - Robust Decision Making
SD - System Dynamics
SDDP - Stochastic Dual Dynamic Programming
SRB - Segura River Basin
SRI - Standardized Runoff Index
SSP - Shared Socioeconomic Pathway
TOPKAPI-ETH - Physically-based hydrological model
TRB - Tagus River Basin
TSA - Tagus-Segura Aqueduct
WEFE - Water-Energy-Food-Ecosystem
ZWC - Zambezi Watercourse

1 Introduction

This report synthesizes the development and application of diverse water-energy-food-environment (WEFE) modelling approaches across six river basin case studies in the GoNEXUS project. The overarching goal of the modelling work is to provide quantitative evidence on WEFE nexus tradeoffs and synergies to support stakeholder dialogue and decision-making in the river basins.

The report is structured in three parts:

Part 1 describes the methodological frameworks applied to conduct WEFE modelling in GoNEXUS. Four modelling approaches are utilized: (1) High-resolution WEFE modelling integrates detailed physically based hydrological modelling with other sectoral models to evaluate WEFE indicators at local scales. (2) Many-objective robust decision making (MORDM) combines simulation-optimization with deep uncertainty analysis to design resilient infrastructure planning and management strategies. (3) Hydroeconomic modelling optimizes water allocation decisions based on economic objectives and constraints. (4) System dynamics modelling represents feedback mechanisms and nonlinearities between modelled variables. For each approach, the key components, modules, and connections to other work packages are outlined.

Part 2 provides an overview of the six river basin case studies: Zambezi Watercourse, Lake Como, Júcar, Tagus-Segura, Senegal, and Danube. The unique settings, nexus challenges, and involved stakeholders are described for each basin. This context sets the stage for the basin-specific modelling efforts documented in Part 3. Major nexus concerns include climate change impacts, water scarcity, energy transition, food production sustainability, and ecosystem preservation.

Part 3 documents the development and application of the WEFE models introduced in Part 1 to the case studies in Part 2. For each modelling framework, the configuration, key features, and initial results are reported for one or more case studies. This includes describing how the models are tailored to the individual basins and demonstrating their capability to address the nexus challenges identified by stakeholders. The models provide quantitative evidence on tradeoffs and synergies across the WEFE sectors under diverse scenarios. A crosswalk of the methodological frameworks applied to the six river basin case studies is shown in Figure 1.

In summary, this report synthesizes the cross-case learning in applying diverse modelling techniques to represent the complexity of managing water-energy-food-environment interlinkages in river basins. The models enhance understanding of nexus dynamics and generate insights to support dialogue and decision-making for equitable and sustainable management of natural resources.

As shown by the GoNEXUS interactions depicted in Figure 2, the WEFE models and applications developed under WP4 will be used in connection with Scenarios (WP2) and Large-scale WEFE Modelling (WP3) as the basis for WEFE Evidence (WP5), and, through interaction with stakeholders in the Nexus Dialogues (WP6), the development of WEFE Solutions (WP7).

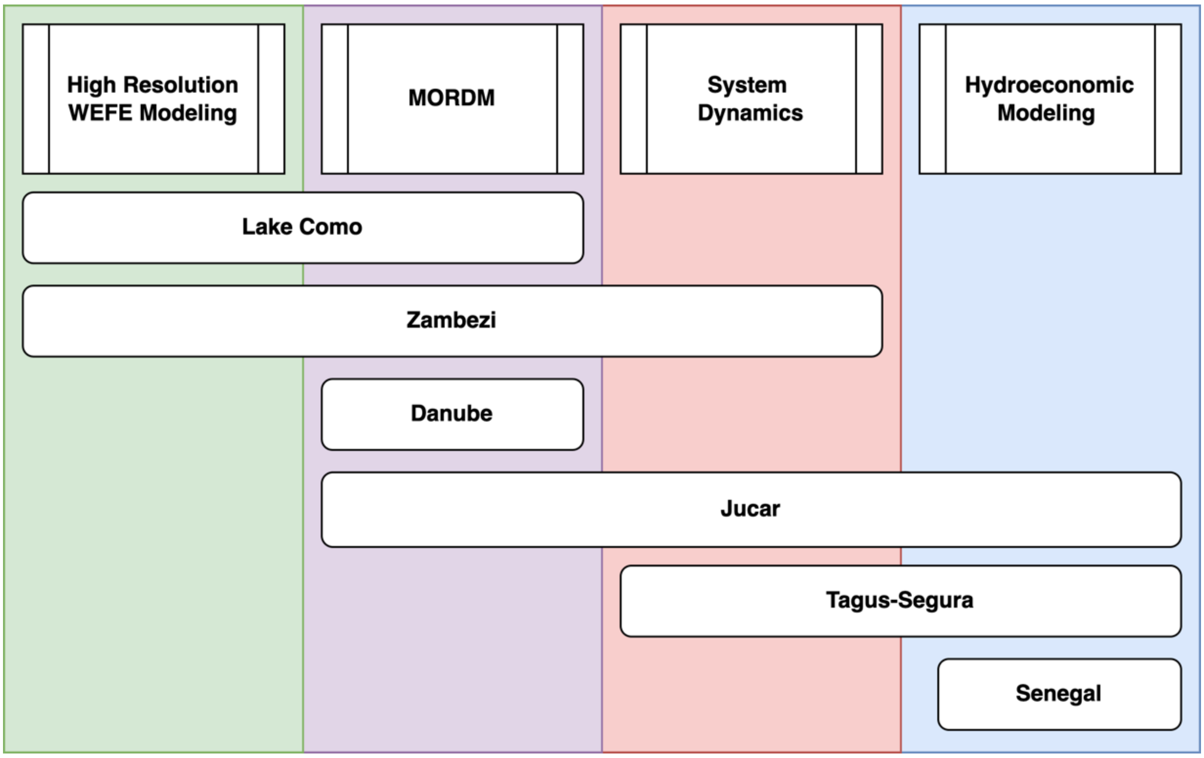

Figure 1. Crosswalk of Methods and Frameworks to River Basin Case Studies.

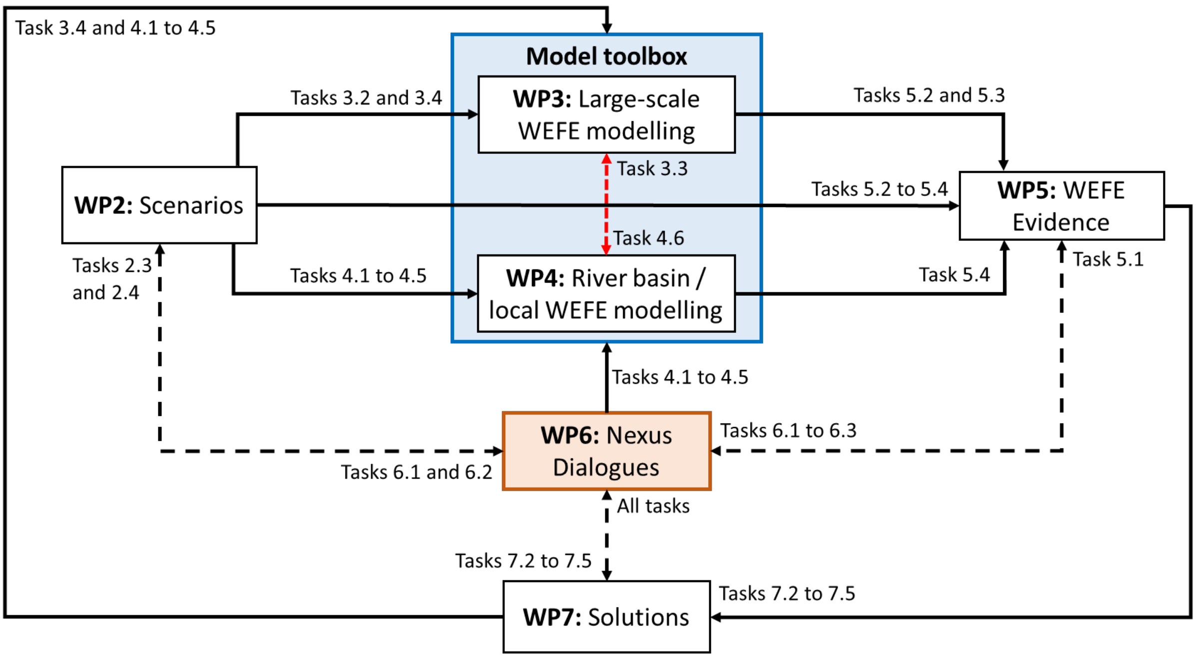

Figure 2. GoNEXUS Interconnections.

2 Methods and Frameworks

2.1 High-resolution WEFE Modelling

2.1.1 Introduction

The impacts of different system management operations, planning and development options on the components of the WEFE nexus are location specific. Figure 3 illustrates the wide variety of components that should be modelled together to obtain a comprehensive picture of the inter-connections and tradeoffs. The main goal of the high-resolution WEFE modelling framework described here, is to provide a quantitative tool for evaluating nexus indicators at a range of locations and at various space and timescales within a river basin. The framework can be subjected to different scenarios of projected climate, land-use and socio-economic scenarios, and system operations to aid in robust planning and development for an uncertain future.

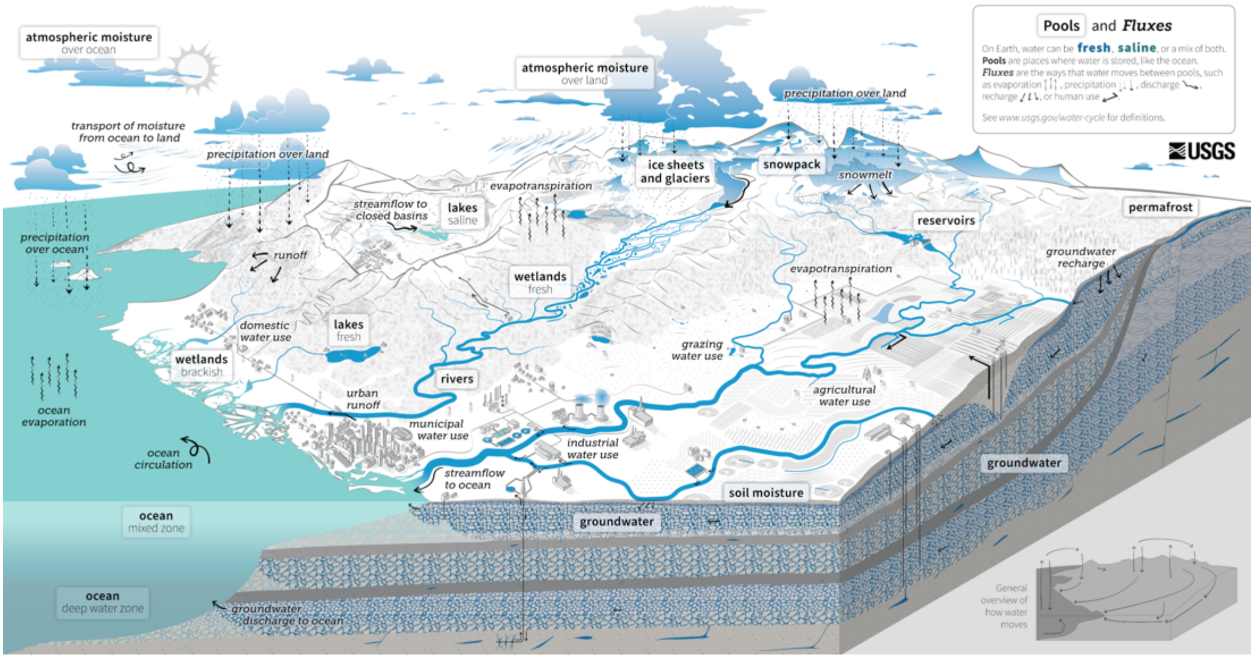

Figure 3. Schematic illustrating the typical components of the water cycle, including anthropogenic uses, which must be included in nexus modelling efforts to assess the WEFE components at basin scales (figure source: United States Geological Survey)

The concept developed and applied in the Decision-Analytic Framework to explore the water-energy-food NExus in complex transboundary water resource systems of fast developing countries (DAFNE, 2018) and being further refined in GoNEXUS makes use of a two level modelling approach to quantify the impacts:

- First, the Many-objective Robust Decision Making (MORDM) provides basin development pathways and infrastructure operations policies. This analysis is implemented using a strategic optimization model, which is used to assess tradeoffs among the policies and objectives set for the different sectors using key design indicators.
- Next, the high-resolution WEFE simulation model, can be used to quantify in greater detail the impact on a broader set of evaluation indicators to given alternative options

and corresponding policies. This is done by implementing the developments and policies in the high-resolution model and simulating under various future climate and socio-economic scenarios.

- Based on a concise description of basin and infrastructures, the strategic model produces the operating policies through optimization with respect to objectives set for each indicator.

The high-resolution WEFE model is based on a detailed description of a river basin and infrastructures and simulates the WEFE nexus at high spatial and temporal resolution using the optimized policies coming from the strategic model. The goal is to compute an extended set of evaluation indicators.

2.1.2 Components and Modules

The High-resolution WEFE model is composed of three main components as shown in Figure 4: first, the statistical down-scaling weather generator model AWE-GEN-2d (Peleg et al., 2017); second the high-resolution physically explicit hydrological model TOPKAPI-ETH (e.g., (Fatichi et al., 2015); and a third possibility of complementary models to extend the scope of possible indicators to be evaluated. The high-resolution WEFE modelling concept is linked with, and dependent on, the MORDM through the functionality of TOPKAPI-ETH to directly ingest system operation policies (e.g., reservoirs, irrigation allocations) designed by the decision analytic framework.

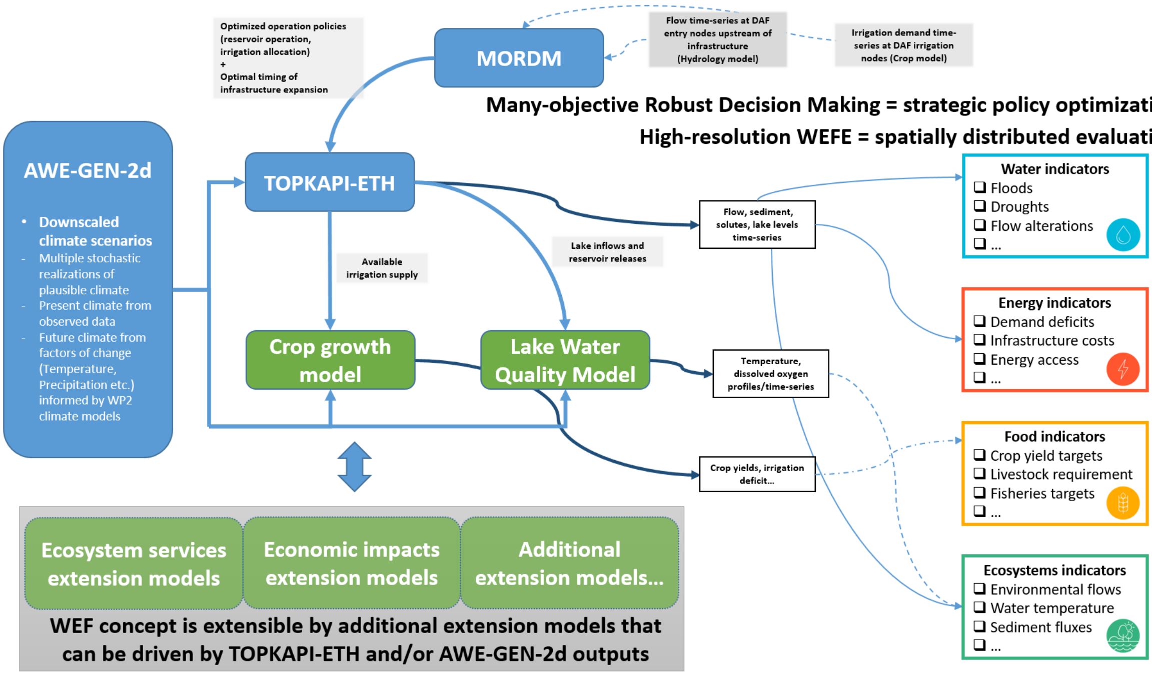

Figure 4. Components of the high-resolution WEFE model.

2.1.2.1 Down-scaling weather generator AWE-GEN-2d

The Advanced WEather GENerator for a two-dimensional grid (AWE-GEN-2d) (Peleg et al., 2017) can be used to generate stochastic ensembles of future climate variables using locally projected trends of these variables derived from climate models. This provides an alternative downscaling methodology compared with commonly used statistical down-scaling techniques, with the advantage of accounting for internal climate variability (Peleg et al., 2019).

As shown in Figure 5, the down-scaled climate ensembles can be used to derive WEFE indicators either directly from the climate variables or indicators obtained by running the ensembles through the hydrological model.

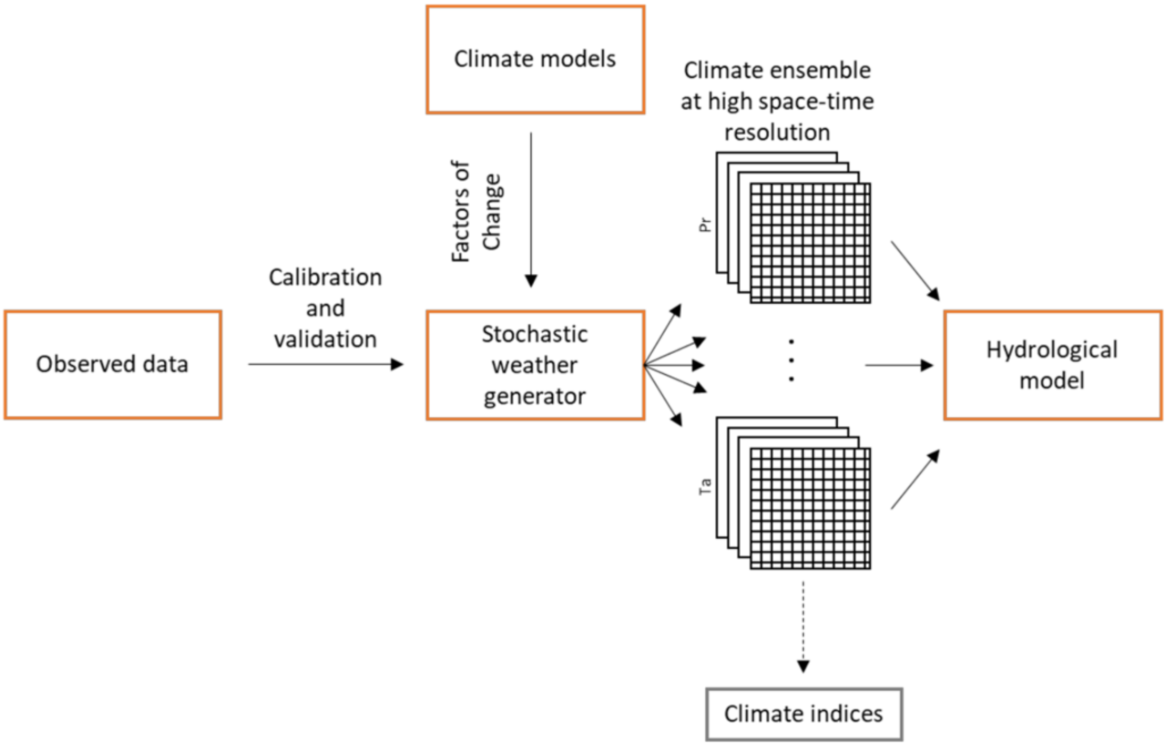

Figure 5. Methodological workflow for applying AWE-GEN-2d to the assessment of climate indices (future climate impacts) and forcing of the hydrological model TOPKAPI-ETH. Figure sourced from Peleg et al. (2020) .

2.1.2.2 Hydrological modelling TOPKAPI-ETH

The main water fluxes in a basin are modelled by TOPKAPI-ETH, forced by the down-scaled climate ensemble of AWE-GEN-2d, and with major infrastructures operated according to the MORDM policies.
The WEF hydrology model can simulate the following (and more), which can be assessed at multiple locations within the basin, according to specific WEFE challenges:

- Overland and river flows
- Evapotranspiration
- Dynamics of soil water content
- Groundwater storage
- Snow and glaciers mass balance
- Reservoir and lake levels and volumes
- Sediment production and transport
- Irrigation return flow
- Hydropower production
- Solute transport

and can account for:

- Water abstractions (irrigation and domestic/industrial water supply)
- River diversions and inter-basin transfers

- Coordinated reservoir and lakes release policies

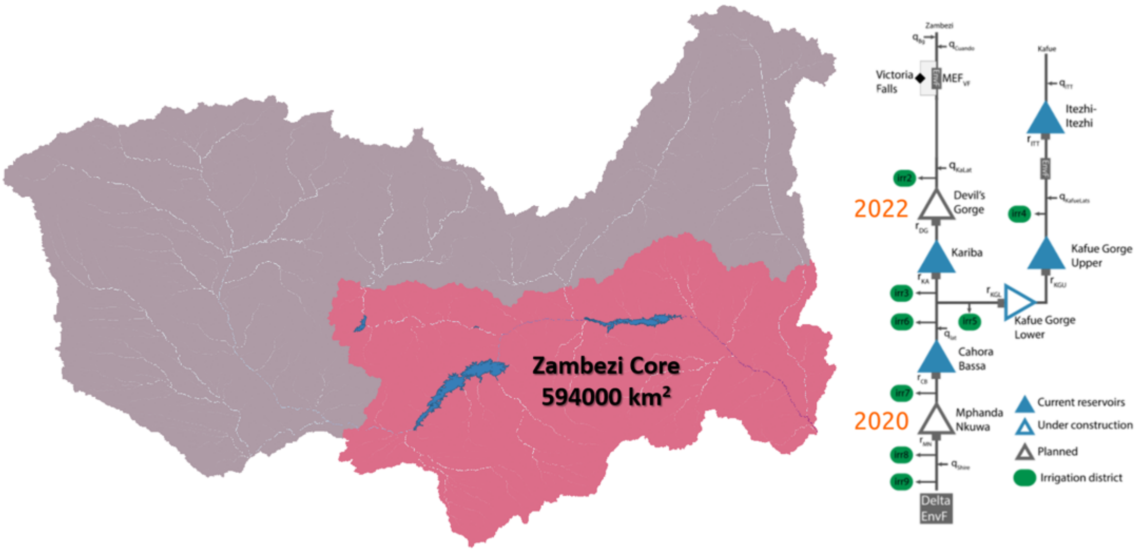

Figure 6. An illustration of the implementation of MORDM designed infrastructure timing into the TOPKAPI-ETH model of the Zambezi watercourse (ZWC).

2.1.2.3 Complementary models and post-processing to compute WEFE indicators

The derivation of WEFE indicators as illustrated in Figure 4 will either be the result of post-processing model outputs or chaining additional models to allow the evaluation of other processes. An unimplemented workflow designed in DAFNE is shown in Figure 7 where it is technically feasible to evaluate water quality variables like water temperature and dissolved oxygen for Lake Kariba in the Zambezi watercourse. In this example the Generalized Lake Model (GLM) implementation of Calamita et al. (2021) could be forced by the climate ensembles and, inflow/outflow series according to the TOPKAPI-ETH simulation using the MORDM operational policy.

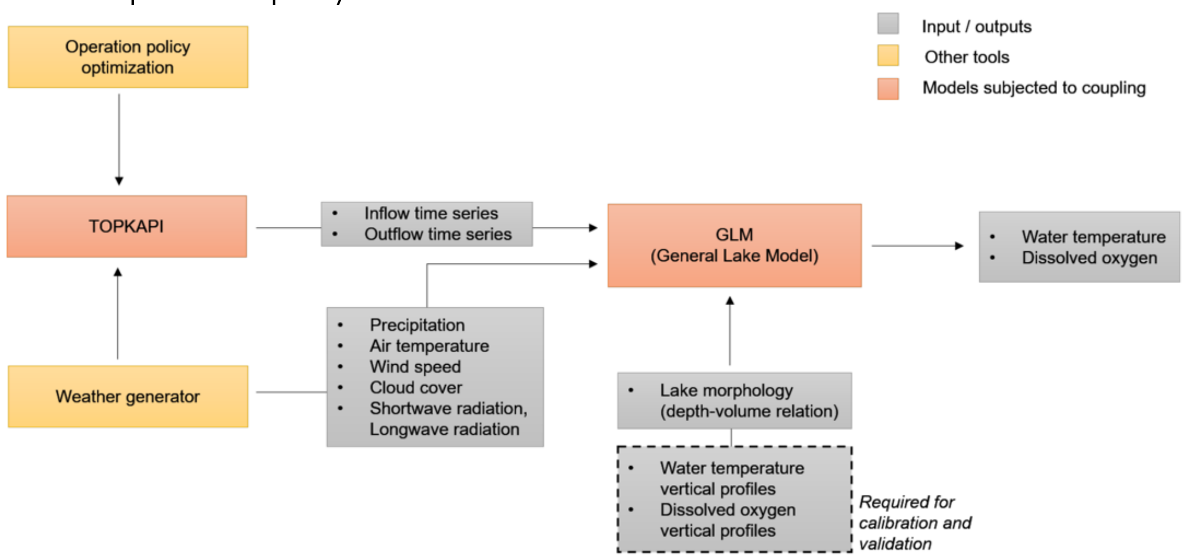

Figure 7. Methodological workflow designed for using forcing from AWE-GEN-2d, and the hydrological model TOPKAPI-ETH to drive the Generalized Lake Model of Lake Kariba, which was implemented by Calamita et al. (2021). Figure sourced from DAFNE .

2.1.3 GoNEXUS Interconnections

This modelling component has linkages to almost all the GoNEXUS work packages. Specifically:

- A connection to WP2 through the input of climate, land-use, socio-economic scenarios required to force and configure the model.
- A direct connection with the MORDM within WP4, by ingesting the system infrastructure operations policies designed by the optimization framework.
- Links to WP5 through the calculation of WEFE indicators using the SAF to provide WEFE evidence at basin scales.
- Two connections to WP6; the first through stakeholder information (challenges) and co-design of basin scenarios from the dialogues; the second by evaluation of the evidence developed through WP5 in subsequent dialogues.
- WP7 through the implementation of identified WEFE solutions in the modelling.
-

2.2 Many-objective Robust Decision Making

2.2.1 Introduction

Many-objective Robust Decision Making (MORDM) combines many-objective evolutionary optimization (MOEA) and robust decision making (RDM) into a framework for planning and management of complex human-environmental systems under deep uncertainty (Kasprzyk et al., 2013). MOEA uses simulation-optimization with evolutionary algorithms to increase the level of model complexity and the number of objectives included in the decision problem. RDM is used to guide decision-making through a systematic and rigorous evaluation of a wide range and sources of uncertainty. These uncertainties are referred to as "deep" when agreement on the likelihood of any one scenario or condition cannot be reached and arise from sampling, parametric, and structural sources that combine to create many plausible "states of the world" (Srikrishnan et al., 2022).

2.2.2 Components and Modules

The design of the robust solutions is performed according to the four steps of the taxonomy framework shown in Figure 8 (Herman et al., 2015).These steps are introduced under the four respective subsections below.

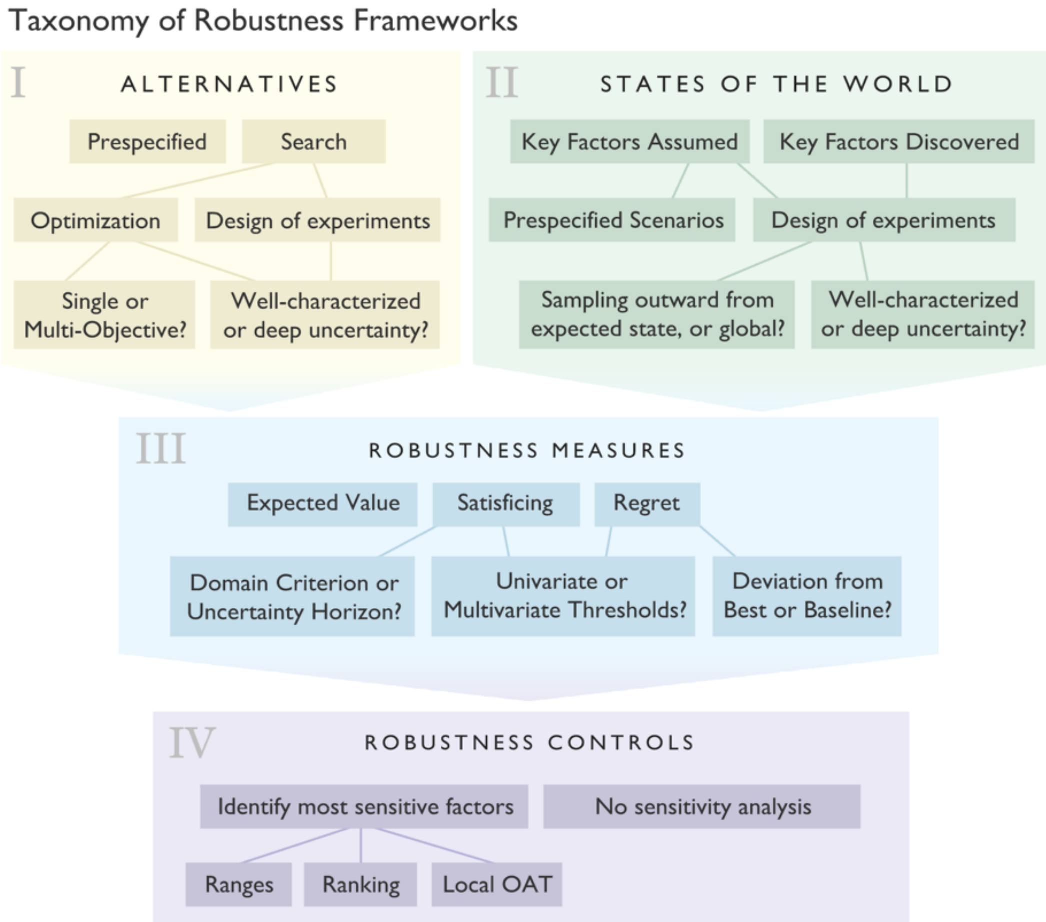

Figure 8. Taxonomy of robustness frameworks (Herman et al., 2015).

Step 1 – Alternatives

The first step of many-objective robust decision-making is identification of the decision alternatives. Alternatives can be "soft" policy, management, and operational changes, or "hard" physical infrastructure modifications and additions. A set of discrete alternatives may be prespecified in the simplest case, but alternatives can also be developed through computational search, relying on an enumeration of the decision space (Matrosov et al., 2013) or on an optimization routine (Kasprzyk et al., 2013). When optimized with respect to a multidimensional objective space, alternatives consist of a Pareto-optimal set of solutions where the choice among alternatives necessarily involves trading performance between objectives (i.e., tradeoffs). Thus, multi-objective optimization finds the best possible decision alternatives given the constraints, conflicts, and synergies within the system of interest.

Step 2 – States of the World

The second step is the enumeration of uncertain states of the world (i.e., scenarios), which expands evaluation of decision alternatives' performance beyond the ranges of uncertain factors considered when initially identifying the alternatives. A subset of uncertain factors deemed important to decision-makers may be pre-specified a priori; alternatively, additional uncertain factors may be sampled with the understanding that some might be found inconsequential. Once the uncertain factors are identified, they are combined to create an ensemble of scenarios (Mahmoud et al., 2009) or generated via sampling techniques (Groves & Lempert, 2007). This sampling is typically performed over noninformative priors, reflecting the exploratory nature of deep uncertainty analyses; however, a well-characterized probability distribution can also be used if known.

Step 3 – Robustness Measures

The third step is the evaluation of the robustness of the decision alternatives. Robustness can be defined in several ways, and the way in which it is formulated can influence the preferred alternative of decision-makers (Giuliani & Castelletti, 2016; McPhail et al., 2018). In water resources management, decision-makers have been shown to sacrifice expected performance to improve the robustness of selected solutions (DiFrancesco & Tullos, 2014; Lempert, 2002; Walker et al., 2013). In general, robust solutions are whose performance is least sensitive to sampling uncertainty and ensure performance across the plausible states of the world considered. The most commonly adopted robustness metrics, which can be employed in either a univariate or multivariate context, can be classified as follows (McPhail et al., 2018):

- Expected value metrics (Wald, 1950) which indicate an expected level of performance across a range of scenarios.
- Metrics of higher-order moments, such as variance and skew (Kwakkel et al., 2016) which provide information on how the expected level of performance varies across multiple scenarios.
- Regret-based metrics (Savage, 1951) where the regret of a decision alternative is defined as the difference between the performance of the selected option for a particular plausible condition and the performance of the best possible option for that condition.
- Satisficing metrics (Simon, 1956) which calculate the percentage of scenarios that have acceptable performance relative to a specified threshold.

Step 4 – Robustness Controls

The final step is the identification of uncertain factors that tend to be associated with system failure. Also known as "scenario discovery", this step can be considered a consequence-oriented sensitivity analysis (Herman et al., 2015) or factor mapping (Saltelli et al., 2008). One of the most widely adopted methods is the Patient Rule Induction Method (PRIM (Friedman & Fisher, 1999)), a data mining technique that isolates areas of the multi-dimensional space of uncertain factors where system failures are likely to occur (Kasprzyk et al., 2013; Kwakkel & Jaxa-Rozen, 2016; Trindade et al., 2017). Alternatively, global sensitivity analysis methods (Sobol, 2001) can also support the ranking of the uncertain factors in order of their sensitivity (Herman et al., 2015).

2.2.3 GoNEXUS Interconnections

WP2 outputs from climate scenarios (Task 2.1) and land use and socioeconomic scenarios (Task 2.3) are post-processed to modify hydrology and demand components in the river basin simulation models. WP3 outputs of the large-scale WEFE models may be used directly or indirectly depending on the spatial coverage and configuration of each case study (e.g., several EU-based models do not represent regions in Africa). Outputs of the river basin case studies will provide the basis for evidence building in WP5 (Task 5.4). Finally, the WP6 dialogues provide a venue for stakeholders to evaluate the tradeoffs across many Pareto-optimal alternatives developed in WP4 and choose WEFE solutions for subsequent robustness analysis.

2.3 Hydroeconomic Modelling

2.3.1 Introduction

Hydroeconomic modelling can be defined as a modelling strategy in which water resource systems are jointly characterized from a hydrologic, engineering, environmental and economic aspects (Harou et al., 2009). This explicit inclusion of economic features is the main distinctive characteristic of hydroeconomic models compared to traditional water resource system models. Although their applicability range is wide, covering the scope of traditional water resource system models, their main purpose is to evaluate water resource management from an economic point of view at the system scale (benefits and costs for water users; value of water in reservoirs, aquifers and streams; economic analysis of investments, etc.) and use economics as the main driver of any system modification (e.g., modify water allocation to maximize revenues). The use of hydroeconomic models can be traced back to the 1960s in water-scarce regions. They have gained momentum in parallel to the exhaustion of traditional supply-side water measures in part of the world (e.g. dam building), the increased acknowledgement of the link between water use and economic welfare and the adoption of economic principles and tools in the water sector such as cost recovery, polluter pays, ecosystem services and payment for them, use of economic instruments (pricing policies, water markets, insurances) and cost-benefit and cost-efficiency analyses. In Europe, one of the main landmarks for the rise of hydroeconomic models was the adoption of the Water Framework Directive, which introduced some of these principles and methodologies in water planning and management of European watercourses.
Currently, hydroeconomic models show a wide range of application from the continental (Burek et al., 2018; Olesen & Bindi, 2002) international (Hossen et al., 2021; Tilmant et al., 2011) national (Gil et al., 2011; Satti et al., 2015; Tesfaye et al., 2016) river basin (Goor et al., 2010; Marques & Tilmant, 2013) to local scales (Lopez-Nicolas et al., 2017). Areas of application include the definition of economic-efficient water resource management rules (Harou & Lund, 2008); optimal adaptation portfolios against climate change impacts (Girard et al., 2015; Kahil et al., 2015); economic evaluation of ecosystem services (Momblanch et al., 2016); definition of economic instruments (Denaro et al., 2020; Macian-Sorribes et al., 2014); and exploration of economic synergies among the WEFE nexus (Do et al., 2020).

2.3.2 Components and Modules

Hydroeconomic modelling relies on the quantification of each water use in a common monetary unit, providing a homogeneous framework for the evaluation of alternatives across water uses and easing the identification of tradeoffs and synergies to achieve optimality. Such a homogenization allows an efficient identification of optimal solutions through single-objective optimization algorithms. On the other hand, quantification of all water uses into a single monetary unit may be challenging and usually requires distinct amounts of information not directly available. There are several alternatives to quantify each water use depending on the type of use, data availability and the purpose of the model. Consumptive water uses such as urban, agricultural and industrial, can be quantified through demand curves or benefit functions, whose particular building strategy depends on the type of use (Harou et al., 2009). Non-consumptive water uses such as hydropower production or ecosystem services can be quantified using diverse economic valuation techniques tailored to each particular use (Harou et al., 2009; Tietenberg & Lewis, 2012). If economic quantification is not possible for one or several water uses, a common strategy consists in prescribing different fixed amounts of satisfaction of them and evaluating the economic impact that an increase of satisfaction levels has in the rest of the water uses (Guisández et al., 2013).

The components of a hydroeconomic model are similar than standard water resource system models, which the addition of the economic features or quantifications of each water use previously mentioned. A generic view of these components with examples of input information is provided in Figure 4 below, although hydroeconomic models can accommodate different configurations of components and inputs in a flexible environment (e.g., rainfall-runoff modelling embedded, inclusion of agronomic models, several mathematical representations of system operation). This flexibility is crucial to adapt the modelling strategy to the requirements and data availability of each water resource system. Hydroeconomic model outputs are similar than those from water resource management models, with the addition of economic results, which mostly refer to the economic revenues of water uses and water values. While the output set depends on the features of the model, in a similar way than inputs, an example is provided in Figure 9 below.

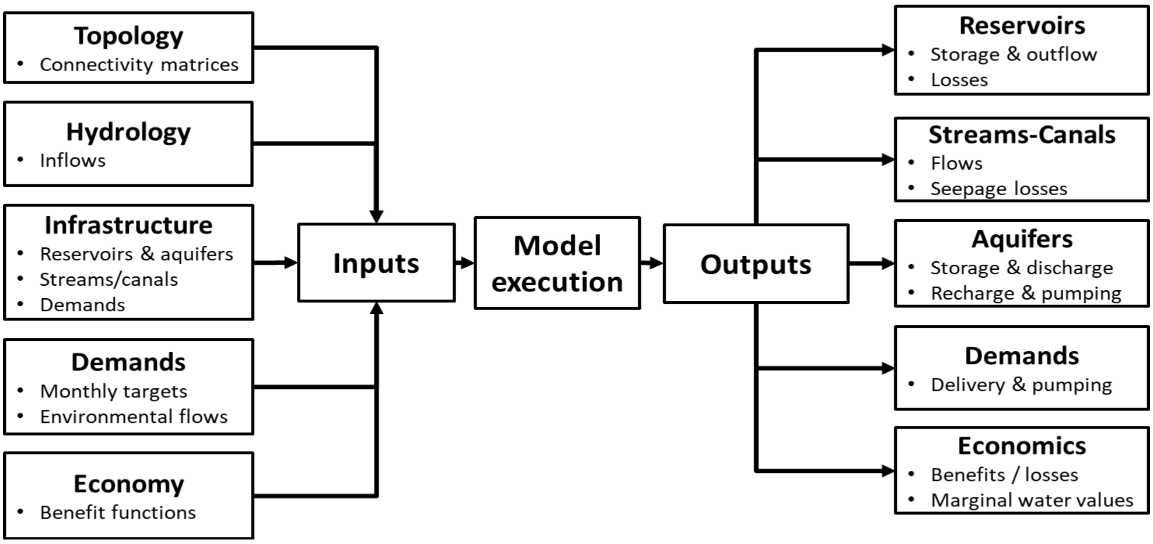

Figure 9. Standard components of a hydroeconomic model.

2.3.3 GoNEXUS Interconnections

Hydroeconomic models share interconnections with GoNEXUS WP2, WP3, WP5 and WP6. WP2 and WP3 will mostly provide inputs, WP5 will mostly receive outputs from hydroeconomic models while WP6 will provide insights to modify the model configuration. In particular:

- WP2 scenarios: hydroeconomic models will use climate scenarios (Task 2.1) and local land use and socioeconomic scenarios (Task 2.3) as direct inputs to modify their hydrology and the demand components. Policy scenarios (Task 2.4) will be indirectly implemented by modifying the infrastructure, demands and economy component accordingly. The latter will also be performed through WP3.
- WP3 large-scale modelling: outputs from WP3 models will be used directly or indirectly depending on the configuration of hydroeconomic models. As an example, energy prices resulting from continental water and energy production availability together with continental policies is an output whose inclusion in hydroeconomic

models would be straightforward. The inclusion of other WP3 model outputs variables such as crop prices and biodiversity status would vary depending on the model configuration.

- WP5 evidence: outputs from hydroeconomic models of WP4 will provide the basis for evidence building in WP5 (Task 5.4). Hydroeconomic models could be modified to align their formulation and output provision to the indicators defined in WP5.
- WP6 dialogues: the dialogues will provide requirements to modify or adapt hydroeconomic models to address particular features. These requirements may include the modelling of solutions, which is linked to WP7 as well.

2.4 System Dynamics Modelling

2.4.1 Introduction

System dynamics is a methodology and mathematical modelling technique to conceptualize, comprehend and discuss complex issues and problems. The primary purpose of a system dynamics analysis is to understand how and why the dynamics of concern are generated and to look for managerial policies that can improve the system's performance (Mirchi et al., 2012; Simonovic, 2020). In system dynamics, the system structure is defined by the positive and negative relationships between variables, feedback loops, logical statements, and delays (Sterman, 2000). The application of system dynamics in water resource management has grown since the 90s. Nowadays, we find applications of system dynamics modelling to study a large variety of water resource issues (Winz et al., 2009). They range from region-scale models with multiple demands and frequent water scarcity events to models coupling surface and groundwater dynamics for a basin, flood management or predicting models, reservoir operation and water supply for multiple water users, and the design of water pricing policies (Ahmad & Prashar, 2010; Correia de Araujo et al., 2019; L. Li & Simonovic, 2002; Qaiser et al., 2011; Sehlke & Jacobson, 2005; Susnik et al., 2022). The application of the methodology to the NEXUS projects has been explored in the past in contributions from Albrecht et al. (2018), Yung et al. (2019), and González-Rosell et al. (2020).

2.4.2 Components and Modules

This methodology focuses on understanding how the physical processes, information flows, and managerial policies interact to create the dynamics of the different variables of interest. The system's structure defines its behaviour, and sometimes systems behave in ways that are not easy to predict using a compartmented view. Qualitative/conceptual and quantitative/numerical modelling methods are applied to create and analyse the systems.
Qualitative modelling (e.g., causal loops diagrams and definition of the positive and negative connections between variables) improves our conceptual system understanding (Winz & Brierley, 2007). This type of modelling is often seen as a previous step to quantitative modelling, where the behaviour of the system and the effects of different intervention policies can be visualized through simulation. Qualitative models can be further developed into quantitative models. The jump from qualitative to quantitative models requires a deep knowledge of the physical, analytical, and statistical relationships between the system's variables (Rubio-Martin et al., 2020). In system dynamics, the relationships between variables can be expressed by linear, non-linear mathematical equations and logical expressions, such

as IF-THEN statements, to introduce management policies and rules. Models are validated by comparing their results to the available historical records to assess their skill.
NEXUS components in the model can be separated in different subsystems to facilitate the conceptual understanding of each subsystem and to facilitate the definition of the linkages existing between the components of the different subsystems. Quantitative and qualitative inputs can be integrated in the same framework to integrate all available information in a single modelling environment.

2.4.1 Participatory modelling and System Dynamics

The governance practices embedded in the NEXUS involve various actors with diverse perspectives, values, assumptions, and knowledge, which can lead to conflicts and hinder the long-term effectiveness of measures and strategies. Proactive stakeholder engagement is crucial to overcome these challenges and promoting transparency, equity, trust, and ambition in policy change. However, stakeholder participation in co-creating water governance measures within NEXUS is currently low. Therefore, further studies are needed to integrate multi-stakeholder participatory processes (NEXO dialogues) with modelling tools that allow for a comprehensive and systemic analysis of different components (Johnson and Walker, 2000; Pagano et al., 2019; Ridder and Pahl-Wostl, 2005).
Participatory modelling plays a vital role in decision-making by involving key stakeholders in co-creating conceptual models and designing actions and strategies. It fosters active collaboration and rigorous integration of diverse expertise and interdisciplinary skills, building trust in the models (Zomorodian et al., 2018). Group Model Building (GMB) activities enhance stakeholder communication, facilitate consensus building, and create a shared vision on specific issues. Participatory modelling, including GMB, has been widely used to gather bottom-up information and organize stakeholders' collective knowledge in a graphical structure that captures the system's main dynamics. It offers advantages at both individual and collective levels, improving problem formulation and perception at the individual level while facilitating group involvement and achieving consensus at the collective level.
System dynamics modelling and participatory modelling are complementary approaches that can be used together to address complex problems. System dynamics modelling provides a quantitative and analytical framework to understand the dynamics of a system. In contrast, participatory modelling incorporates the perspectives and knowledge of stakeholders, fostering collaboration and ownership of the modelling process. By combining these approaches, stakeholders can actively co-create conceptual models, design actions, and develop strategies. This collaborative effort enhances the accuracy and relevance of the models, improves problem understanding, and facilitates stakeholder consensus-building.

2.4.2 GoNEXUS Interconnections

The system dynamics modelling framework enables the analysis of the complex interaction between quantitative and qualitative inputs, offering insights into the interlinkages among various variables, such as water and energy usage, energy production, and the impact of policy, infrastructure, or operational changes within the system.
The modelling framework incorporates a participatory phase, involving key system stakeholders in co-creating qualitative system dynamics models. This participatory process and the resulting qualitative model serve two primary purposes: a) they provide the

foundational structure for the development of the stock and flow SD model, and b) they aid in the creation of a semi-quantitative fuzzy cognitive map, a tool for supporting the co-design of local scenarios during the second dialogue (WP6). The developed framework and the step-by-step process for constructing a quantitative SD model from the participatory phase are illustrated in Figure 10, which also highlights the framework's connection to other WP (Work Packages).

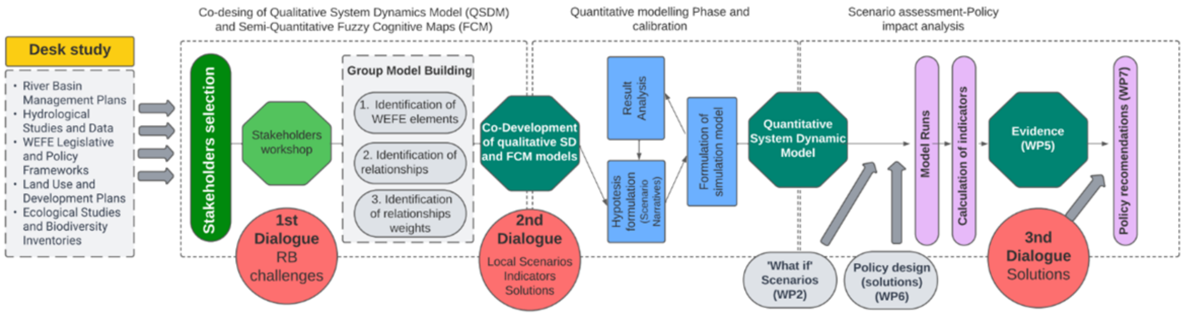

Figure 10. Showing the participatory system dynamics framework

In section 4, we will delve into the quantitative phase of the framework. Subsequently, the following section will focus on the essential steps for co-designing qualitative system dynamic models. This means that the upcoming section will be dedicated to the first phase of the framework, which includes.

Step 1: Stakeholder selection

To enhance the effectiveness of the decision-making process, it is crucial to grasp the implications of each decision and action on various stakeholders, such as the impact of ecological flow increase, restoration of riparian areas, and water tax adjustments. Equally important is identifying the responsible actors who hold the authority to implement these actions, as they significantly influence the outcomes achieved. These actors may include farmers' associations and river basin authorities (Reed et al., 2009; Santoro et al., 2019).

To facilitate the participatory modelling exercise, it becomes essential to carefully select stakeholders representing different levels of governance and representatives from various Water-Energy-Food-Environment (WEFE) sectors. The number of stakeholders chosen should align with the objectives and expected outcomes of the participatory activity. This inclusive approach ensures that diverse perspectives are considered, leading to more informed and impactful decisions.

Step 2: Development of a Causal Loop Diagram

Causal Loop Diagrams (CLDs) depict causal relationships among various concepts, factors, variables, or nodes within a system. These relationships are illustrated using links that connect the different concepts. A positive or negative symbol indicates the direction of each causal relationship.

In the CLD, a positive sign (+) denotes positive causal relationships between two concepts or variables. This implies that an increase/decrease in a variable Vi results in a corresponding increase/decrease in variable Vj. On the other hand, a negative symbol (–) signifies negative causal relationships, indicating an inverse correlation. In such cases, an increase in variable Vi leads to a decrease in variable Vj and vice versa.

The CLD (Causal Loop Diagram) development employs group model building (GMB) techniques to foster consensus among stakeholders, enhance communication, and promote a shared vision. GMB plays a vital role in instilling confidence among stakeholders regarding the utilization of system ideas. Typically, this process unfolds in a two-hour workshop attended by selected stakeholders (step 1).

In this workshop, stakeholders actively contribute to identifying key factors within the system, focusing on the Water-Energy-Food-Environment (WEFE) aspects of the basin system. The participants then represent and establish relationships between variables and their polarities (positive or negative). During the GMB session, it is natural for differences of opinion or discrepancies among participants to surface. When possible, reaching a consensus among the participants is essential. This is where the facilitator's role becomes pivotal, as they aid in elucidating knowledge within the group, uncovering hidden assumptions and differences, and guiding the process towards a consensus view of the problem.

In cases where an agreement cannot be reached, the final decision lies with the expert group. Subsequently, to facilitate the post-processing of the Causal Loop Diagram, the resulting model is digitized using Vensim software. This digital representation streamlines further analysis and interpretation.

Step 3: Development of a fuzzy cognitive map from the CLD

Fuzzy Cognitive Maps (FCMs) originated from graph theory and were first introduced by Bart Kosko in 1986. As a mathematical modelling tool, FCMs represent and analyse complex systems, finding broad applications in addressing various intricate problems, from climate change adaptation to landscape and forest management (Martinez et al., 2018). While FCMs do not provide precise quantitative predictions, they excel in indicating changes in system behaviour patterns resulting from alterations in the relationships between factors. Consequently, FCMs enable the assessment of the effects of different policies under hypothetical "what-if" scenarios.

An FCM is an extension of the causal loop diagram, distinguished by its representation of relationships between concepts using fuzzy values (between 0 and 1) rather than binary values (0 or 1). This characteristic allows for a more refined and nuanced depiction of the system's dynamics. To transform the CLD into an FCM, the strength of impacts among the elements constituting the map is also indicated. This strength is represented by assigning weights, describing the intensity of relationships (weak, medium, strong) between variables or nodes. During the participatory activity, participants express the strength of a relationship by adjusting the thickness of the links between concepts within the FCM. This interactive process aids in developing a comprehensive and detailed FCM that captures the complexities of the system's interconnections. After the participatory modelling phase, each fuzzy weight (weak, medium, strong) was translated into a numerical value. The weights ranged in an interval of $\{-1,0,1\}$. The value 1 represents a positive causality and the strongest relationship. The closer the values approach 0, the weaker the relationships are. For weak relationships, a value of 0.3 was assigned. For relationships of medium strength, a value of 0.6 was given. Finally, value 1 was used for the strongest links.

It is important to note that the participatory phase described above has only been implemented in the Tagus-Segura case. The participatory phase for the Jucar and Zambezi systems was carried out in other projects before GoNEXUS.

The System Dynamics approach is being applied to the Júcar and the Tagus-Segura case studies in Spain, including assessing different policies and management practices within the water resource system and the interaction with the energy and food production systems. The system dynamics (SD) approach, including the participatory modelling, is connected to different work packages:

- **WP2 scenarios:** SD models will use inputs from climate scenarios (Task 2.1) and local land use and socioeconomic scenarios (Task 2.3). Policy scenarios (Task 2.4) will be implemented by modifying the infrastructure, demands, and economy components quantitative or qualitatively.
- **WP5 evidence:** outputs from SD models will provide the basis for evidence building in WP5 (Task 5.4)
- **WP6 dialogues:** The dialogues will help shape the SD models to address particular features. These requirements may include modelling solutions, which are also linked to WP7. Furthermore, the insights and outcomes obtained from the participatory modelling activities, including using Fuzzy Cognitive Maps conducted in the Tagus-Segura basins, will serve as valuable inputs for the upcoming dialogue sessions centred around local scenarios.

3 Case Study Descriptions

3.1 Zambezi Watercourse

3.1.1 Basin Setting

The Zambezi Watercourse is the fourth largest basin of Africa and is shared by eight countries (Angola, Botswana, Malawi, Mozambique, Namibia, Tanzania, Zambia, and Zimbabwe) and populated by around 40 million inhabitants (Figure 11) The climate of the Zambezi Watercourse follows a seasonal pattern associated with the Intertropical Convergence Zone: a rainy season from November to April and a dry season from May to October. While the average annual rainfall in the basin is high (950 mm/year), it is unevenly distributed across the basin and the interannual variability is substantial. Up to 1,400 mm/year are observed in the northern and eastern parts of the basin, whereas 400 mm/year characterizes the southern and western regions. A large amount of water is lost by evaporation due to the high evaporation rates.

The Zambezi River originates in eastern Angola and northwest Zambia and flows for 2,700 km through plains, gorges, and marshlands, with an average annual discharge of 2,600 m^3/s into the delta in Mozambique. Whereas the source of the Zambezi is in the humid tropical climate zones and hence discharges water on a continuous basis, the pronounced seasonality of rainfall at more southern latitudes introduces greater variability of the seasonal discharge regime. Information on groundwater resources in the Zambezi Watercourse is relatively scarce so that water availability from groundwater bodies cannot be properly quantified even at coarse temporal and spatial scales. Finally, the basin is home to many wetlands, which provide a broad range of ecosystem services.

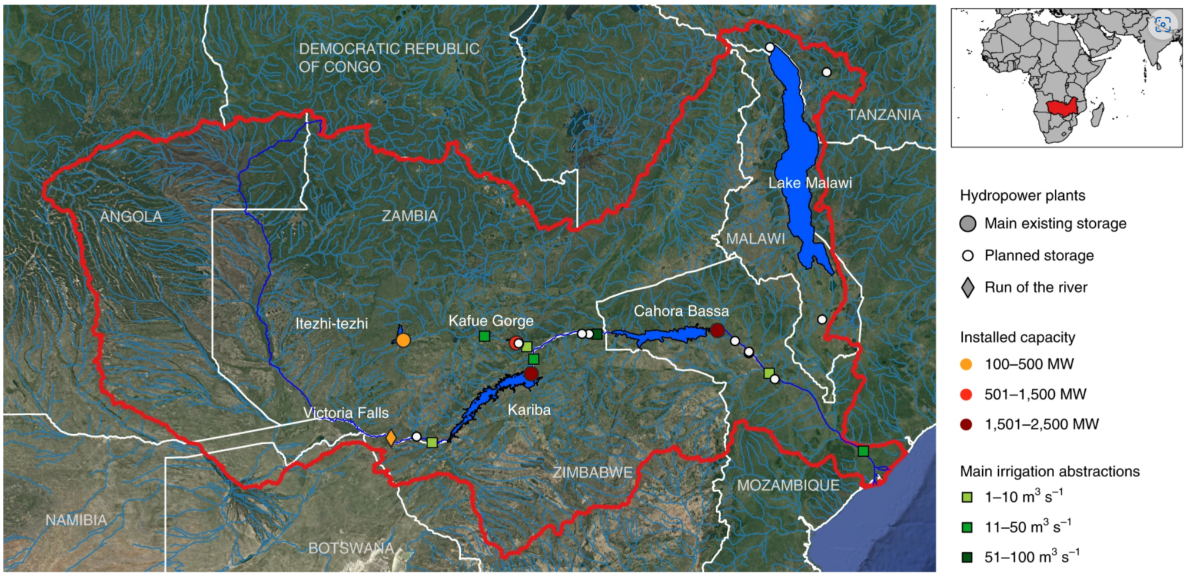

Figure 11. Four dams and six power plants currently in operation and 8 irrigation abstraction locations representing 182,000 ha of irrigated areas in the Zambezi Watercourse (Giuliani et al., 2022).

3.1.2 Nexus Challenges

3.1.2.1 Water

By the late 1970s, dam operations had significantly changed the natural flow pattern, affecting some of the wetland ecosystems in the middle and lower courses and favoring expansion of irrigated agriculture. Currently, water requirements are smaller than the estimated water available in the Zambezi Watercourse. Nevertheless, possible conflicts between riparian countries can arise due to the asymmetry between resource availability and the fact that riparian countries have different investment potential and shares of the river basin, thus determining a different capability to access and use water.

The largest consumptive use of water is through evaporation losses from reservoirs (estimated at 12,300 hm^3/year - 16,400 hm^3/year, 15-20% of the annual runoff). Irrigated agriculture consumes an average of 1,700 $hm^{3/}$year and consumption by animal livestock estimated at 170 hm^3/year (DAFNE, 2018). The total annual consumption of water by private households is estimated at 200 hm3/year (DAFNE, 2018). Industrial water consumption, estimated at around 300 $hm^{3/}$year (Lautze et al., 2017) is confined to a few major industry sectors, namely brewing, cement producing and sugar refining plants in central Zambia, copper mines concentrated in Zambia's north central region (the "Copperbelt"), and coal mining in the Tete province of Mozambique.

In the future, expansion of irrigated agriculture, additional hydropower schemes and expanding tourism in important areas of biodiversity (Lake Malawi, floodplains of Barotseland, Busanga and Kafue in Zambia, Zambezi delta and the protected areas in northern Zimbabwe and the Luangwa Valley in eastern Zambia) could spark regional and international conflicts over water use. Despite huge quantities of water in the Zambezi Watercourse, water availability continues to be an issue, with many in the region still lacking adequate access to clean water and sanitation. In addition, several planned water transfer schemes put further water security at risk. There is also significant interest in developing the navigable stretches of the Zambezi.

3.1.2.2 Energy

The Zambezi Watercourse has enormous hydropower potential, with several large-scale projects both in operation and in planning stages. The installed hydropower capacity in the Watercourse is considerable, but, together with other modes of electricity production, is not yet capable of meeting the demands for electricity. While an upward trend in hydropower production has reduced the structural energy deficit, when aggregated for seven out of eight riparian states (excluding Botswana) the deficit still amounts to 4,045 GWh/year, with Zambia alone representing more than half of the energy deficit at 2,501 GWh/year (DAFNE, 2018). The historical operation of reservoirs to maximize hydropower significantly alters the natural discharge regime in Zambezi Watercourse, and therefore further development and operation towards energy production alone, without considering the objectives of other sectors (e.g., irrigation diversions and ecological flows), is expected to have negative implications on the water-energy nexus.

All countries in the Zambezi Watercourse are part of the South African Power Pool (SAPP). The SAPP's installed capacity mix is currently dominated by thermal (coal) with 60.67%. Other generation technologies available in SAPP are hydropower, solar, distillate, nuclear, wind, gas, and biomass. Several studies suggest that African countries must triple their current electricity generation by 2030 (Spalding-Fecher, Senatla, et al., 2017; Wu et al., 2017). But as reported by Gonzalez-Sanchez et al. Africa accounts for the lowest electricity access rate (54%) worldwide, which becomes significantly lower in Sub-Saharan Africa (47.7%).

Consequently, there is an urgent need for new deployment of power infrastructure to compensate for the lack of energy access. The high dependency of SAPP countries on hydropower – around 21% of the installed capacity and around 60% excluding South Africa (SAAP, 2017) – has been highlighted as a significant vulnerability (Conway et al., 2017; Spalding-Fecher, Joyce, et al., 2017). As their primary generation option and currently major rivers, such as the Zambezi, are subject to significant variability of their mean annual discharge, hydropower productivity is expected to drop by more than 10%.
Finally, since Africa is characterized by a very high solar potential with a yearly sum of solar irradiation exceeding 2000 kWh/m^2 (Gonzalez-Sanchez et al., 2021), a shift in the generation mix towards other renewables such as solar (ground photovoltaics or floating photovoltaics) in the longer term, other than hydropower, mostly of interest in the medium term, is predicted to happen, especially considering scenarios with a fast decline in capital costs for renewables (Spalding-Fecher, Senatla, et al., 2017). Moreover, results of Wu et al.'s (2017) multicriteria assessment of wind and solar potential for large regions of Africa shows how economically competitive and low-environmental-impact renewable resources can significantly contribute to meeting this demand.

3.1.2.3 Food

Although rainfed agriculture is ubiquitous, irrigation demand is high and increasing in areas of the Zambezi Watercourse where climate is unfavourable to rainfed agriculture. Major irrigation schemes are in Malawi, central Zambia, and north Zimbabwe and almost absent in the other parts of the Watercourse. Differences in food deficits among regions is correlated with the level of agricultural development (DAFNE, 2018). Areas with less agricultural development are not related to water scarcity, but rather to the dominance of natural landscapes and the remoteness of the region with respect to the major centres of development. In regions characterized by a surplus of food production, the available data do not establish whether the extent of irrigated area induces conditions of water stress. A precise quantification of water stress is possible only by simulation with an integrated, high-resolution water-energy-food nexus model.

3.1.2.4 Ecosystems

The Zambezi Watercourse includes 82 key biodiversity areas (DAFNE, 2018). Of those, 24 have been identified as most relevant for the hydrological cycle as water dependent ecosystems such as lakes, rivers, streams, waterfalls, gorges, wetlands (floodplain grasslands, deltas) and riparian forests, or water supplying ecosystems from the upper catchments such as forests and grasslands (DAFNE, 2018).
Natural beauty and wildlife are the most important drivers for tourism in the Zambezi Watercourse. For example, more than 50% of tourists primarily come to Zambia to see Victoria falls and an additional 30% to see wildlife in national parks (World Bank Group, 2010). Victoria Falls requires an estimated flow of 1000 m3/s for the most spectacular scenes for tourists (Shela, 2000). Due to natural seasonal variability, these flow values are only reached for about half of the year, from February to July. Therefore, various other activities have been added to the portfolio of the region, mostly related to adventure tourism. The gorges between Victoria falls and Lake Kariba have gained a reputation as the best place in the world for whitewater rafting. Given the high prices tourists are willing to pay for this activity, it generates an estimated US$10 million per year (World Bank Group, 2010). This activity can be carried out year-round as it requires a minimum flow of 500 m3/s; however, the Batoka

Gorge dam would lead to impoundment of the gorge and thus loss of the fast rapids and current on which this important part of the tourism industry is dependent (ERM, 2019). National parks are the other main tourist attraction in the Watercourse, the most visited being Chobe-Caprivi and Kafue National parks. Together with Victoria falls and other parks in the region they form part of the Kavango-Zambezi Trans-frontier conservation area. Other well visited national parks are Lower Zambezi, Middle Zambezi, and Luangwa, while Lake Malawi and Lower Shire are becoming increasingly popular. The Zambezi delta does not have a well-developed tourism infrastructure, but the potential is high due to large wildlife populations. Any upstream activity leading to a regulated flow in the delta may harm this potential.

About 15,000 km2 of cropped areas in the Zambezi Watercourse overlap with wetlands (DAFNE, 2018) whose seasonal and permanent inundation are important for agriculture. Hotspot areas include the Barotse plains, the Kafue flats, and the Lower Shire. Regular flooding provides fresh plant nutrients and can maintain high water tables, making these areas much more reliable for small-scale food production than rainfed agriculture, as irrigation schemes are often too expensive for smallholders. Seasonally inundated areas are therefore of high importance for food security in the Watercourse (Lautze et al., 2017). Dams typically reduce the occurrence of seasonal high and low flows and may thus lead to a loss of suitable areas for flood recession farming. Environmental flows therefore need to maintain seasonal, but also decadal variations in flow, to make sure inundation intervals are maintained or restored.

Fish is the main source of proteins for the majority of rural communities in riparian regions of the Zambezi Watercourse (DAFNE, 2018). The most important fishing ground is Lake Malawi with the highest fish species diversity in the world. Other important fishing grounds are the Barotse plains, the Kafue flats, the Lukanga wetlands, Chobe-Caprivi, Lower Shire, and the Delta as well as the three reservoirs Kariba, Cahora Bassa and Itezhi-Tezhi. Major population declines have been reported for larger, most valuable fish species (Tweddle et al., 2015). The main reasons for this are unsustainable fishing practices and overfishing. In addition to that, fish depend on seasonal variation in surface waters, as inundated wetlands provide food, shelter, and spawning habitats. Occasional high flows are also important to provide spawning cues to fishes. Streamflow regulation due to hydropower operation is therefore a direct competitor for this type of provisioning ecosystem service, especially in the Zambezi delta, the Kafue flats, the Lower Shire, and the middle Zambezi.

3.1.3 Stakeholders

Stakeholders present at the first GoNEXUS dialogues, represented several regional river basin organizations and authorities. These included: ZAMCOM; Ministry of Agriculture (Zambia); Ministry of Water, Development, and Sanitation (Zambia); SARDC (Zimbabwe); Ministry of Agriculture, water, and Land Reform (Namibia); SADC Groundwater Management Institute; Ministry of Water (Tanzania); Zambezi River Authority (Zambia); Department of Water and Sanitation (Botswana); HCB Hydropower, Cahora Bassa (Mozambique); Department of Water Resources (Zimbabwe); Zimbabwe National Water Authority; Department of Water Resources (Malawi); National Irrigation Institute (Mozambique); Directorate of Water Resources Management (Mozambique); Zimbabwe Parks and Wildlife Management Authority; Water Resources Management Authority

(Zambia); Department of Water Resources (Zimbabwe); Zimparks (Zimbabwe); Zimbabwe Gender Commission; Ministry of Energy Malawi; and Resilient Waters – Southern Africa.

3.2 Lake Como

3.2.1 Basin Setting

The Lake Como Basin (LCB) is in the Italian Alps near the border with Switzerland (Figure 12) and is the upstream part of the Adda River Basin with a catchment area of 4500 km². The LCB is a highly controlled water system, including a large, regulated lake with an operative storage capacity of 247 Mm³. The lake not only is one of Italy's most scenic and popular tourist spots, but its basin also provides water for irrigation to a wide cultivated area (1320 km²) and for energy production to 16 hydropower plants (13% of national hydropower). Most hydropower plants are in the northern upstream sub-basin, with smaller artificial lakes, operated to exploit the high terrain gradient for electricity production, but some run-of-the-river plants are also operated downstream of the lake.

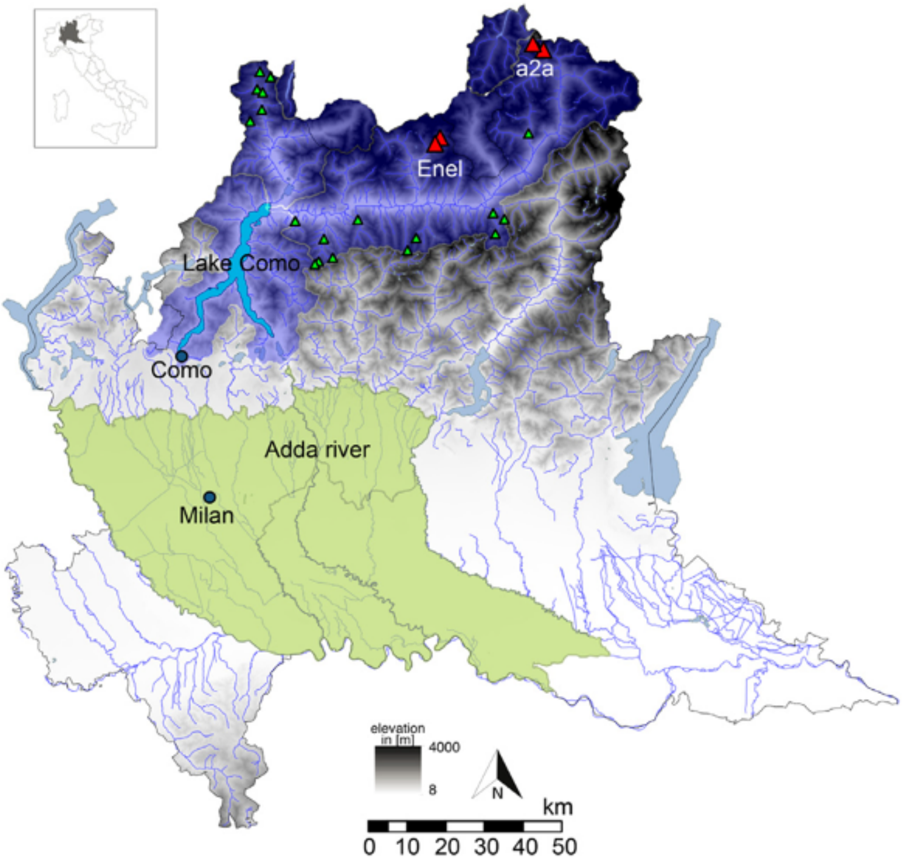

Figure 12. Map of the Lake Como basin: Lake Como, the catchment area (violet) and downstream agricultural districts (green). The triangles denote hydropower reservoirs with the red ones being the main ones (Denaro et al., 2017).

Like most sub-alpine regions, the river and lake levels alternate two dry seasons in winter and summer with wetter seasons in late spring and autumn when water level peaks are fed by snowmelt and rainfall, respectively. Snowmelt during May-July is the most important contribution to the accumulation of the seasonal storage of the lake, which is then used mainly for irrigation supply in the summer during the peak demand period (Figure 13). The water summer demand usually exceeds the natural water availability and makes the role of the lake operation paramount. The lake is in fact regulated since 1946 by a regional public authority, Consorzio dell'Adda, operating the dam located at Olginate (South-East branch of the lake). The regulation of the lake is driven by two primary competing objectives: water supply, mainly for irrigation but also for hydropower, and flood control along the lake shores (Giuliani, Li, et al., 2016). The agricultural districts downstream prefer to store the water from snowmelt in the lake to satisfy the peak summer water demands when the natural inflow is insufficient to meet irrigation requirements. Yet, storing such water increases the lake level and, consequently, the flood risk. Additional interests are related to navigation, fishing, tourism, and ecosystems, that further challenge the existing water management strategies and motivate the search for more efficient solutions relying on climate services, hydro-meteorological data and forecasts, and risk hedging tools. Climate services and forecasts can potentially inform farmers' agricultural practices (Y. Li et al., 2017) and contribute to improving the reliability of the irrigation supply (Giuliani et al., 2020), particularly in facing severe dry conditions, as well as to mitigating existing conflicts between competing sectors.

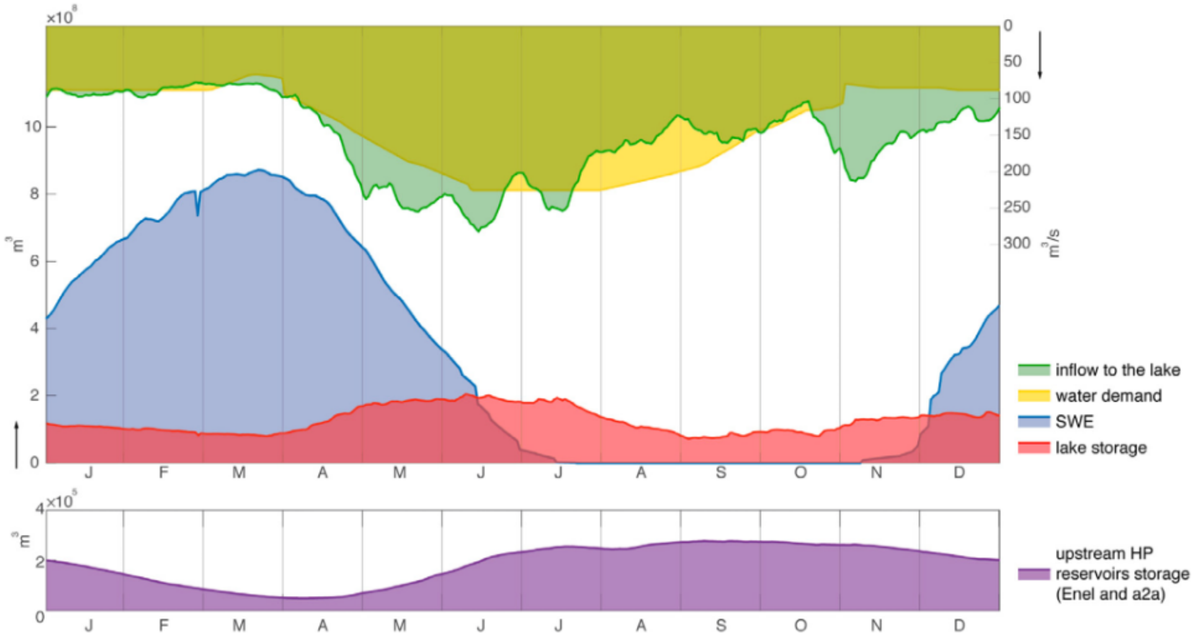

Figure 13. Main components of the hydrological cycle in the study area. The patterns represent moving averages computed from observed data over the period 2006–2013 (Denaro et al., 2017).

3.2.2 Nexus Challenges

The main Nexus challenges for Lake Como include:

- **Conflicts over seasonal allocation of water across the WEFE Nexus** sectors for food and energy production, flood control and irrigation supply, and ecosystem preservation. The main WEFE Nexus tradeoffs are:
    1. Water (flood and low levels) vs. food (irrigation supply): ensuring the downstream irrigation supply, while preventing floods along the lake shores and avoiding excessive lowering of water levels especially during the summer period.
    2. Energy (hydropower) vs. food (irrigation): meeting the irrigation demand requirements, while ensuring optimal hydropower generation.
    3. Two actions for WEFE adaptation that should reduce the conflicts across sectors are: (i) modification of the lake regulation space, and (ii) hydropower relicensing and coordination of the lake regulation with Alpine hydropower reservoirs.

- **Observed increase in drought events requiring new management strategies** to cope with water scarcity. Increasingly frequent and prolonged droughts are exacerbating the conflict among the LCB stakeholders and require new strategies and tools to satisfy the water demand. An action to adapt to changes is to take advantage of increasingly available hydro-meteorological data and forecasts to inform the lake operation.
- **Projected increase in climate change induced extreme events requiring the adoption of novel financial tools** (e.g., index-based insurances) to hedge the risk. The effect of climate change is expected to reduce water availability in summer in the Alpine catchment where snow and glacier dynamics play an important role. Lake inflows are projected to decrease by mid-century challenging the reliability of the irrigation supply (Giudici et al., 2021). Moreover, an increase in temperature and heat waves will contribute to crop failure risk.

3.2.2.1 Water

The flood control objective of the LCB system is related to the cities and towns lying along the lake shores. In particular, the City Center of Como (Piazza Cavour) is a very critical area. Como is the lowest city on the lake shoreline (Giuliani et al., 2019), moreover, its central area is suffering from a subsidence phenomenon which strongly affects the problem of flood control. The main causes of this phenomenon are the characteristics of the geological settings in the Como basin and anthropogenic activities, like the exploitation of water resources from the deep main aquifer and land reclamation (Nappo et al., 2020). The problem has been studied for more than 40 years (see *Relazione di sintesi della commissione per lo studio dei fenomeni di subsidenza. Documenti e Ricerche, 34, 1980*). The construction of the Olginate dam reduced the number of flood events, but flood control remains a crucial aspect of lake management. Due to the subsidence and consequent sinking of Piazza Cavour and the Como City Center, the flooding threshold for the lake level has been progressively reduced, it is now at 1.1 meters, while it was 1.24 m in 2017 (Denaro et al., 2017). No sluice gates are currently operational in Como, but this additional infrastructural solution is being considered to enhance the adaptive capacity of the system to the increase of extreme events expected with climate change. Building sluice gates would allow raising the flood level threshold in Como significantly, potentially up to about 2.9 meters according to the executive sluice gate project plan (see *Regione Lombardia Infrastrutture Lombarde 2019 Opere di difesa dalle esondazioni del lago nel comparto Piazza Cavour - Lungo Lago di Como – Progetto Esecutivo, Dettagli Tav. 2019*).

More recently, the lake management has been increasingly concerned with avoiding extremely low levels of the lake, which is becoming a new objective for the lake operation. Low lake levels have been achieved more and more frequently during dry seasons, when water is released to satisfy the demand, even when inflow in the long term is not sufficient. Low levels can occur sporadically even in other seasons, before expected extreme flood events when large amounts of water are released to create a buffer for the incoming inflows. Low levels are detrimental to all stakeholders: for the lake users, as low levels strongly affect navigation, as well as environmental and touristic aspects; for upstream hydropower companies, as they are required to release more water downstream at times of low levels which leads to a direct loss in energy production; for the irrigation consortia, as further release limitations due to low levels lead to disturbances to the crop cycle that require adaptation of the cropping practices and irrigation methods.

3.2.2.2 Energy

The LCB system has a great potential for hydropower energy production that is exploited through several hydropower reservoirs and run-of-river plants upstream and downstream of the lake. Upstream of the lake, there are 16 sub-alpine reservoirs with a total storage capacity of 545 Mm^3, approximately double the Lake Como's storage, contributing to roughly 12% of the national electricity demand (Denaro et al., 2017). Downstream of the lake, in addition to eleven small run-of-river hydropower plants, also two thermoelectric power plants operated by the Consorzio dell'Adda are relying on the water stream to function.

Some private hydropower companies manage the large storage and hydropower production capacity of the Adda River Basin, both upstream and downstream of Lake Como. Three main groups of managers and companies (ENEL, A2A and EDISON) operate 70% of the stored water in the upstream hydropower dams. The Regione Lombardia (local Italian region authority) regulates the license agreements between hydropower companies and other downstream users. Any revision in this regulation or new licenses will impact the hydropower generation and the associated tradeoffs with other sectors (e.g., food and water). Hydropower relicensing is an adaptation action based on revising license parameters (threshold) for the restitution of reservoirs introducing conditions to optimize their timing and characteristics in coordination with the lake regulation. Thus, the hydropower relicensing is aiming to reach hydropower reservoir operating policies that guarantee Pareto optimal for the system's objectives.

3.2.2.3 Food

The total cultivated area fed by the Adda River after exiting Lake Como is about 1350 km2, which is divided into four irrigation districts. The irrigated area is mostly cultivated with maize, rice, and soy. The crop irrigation is supported by seven main canals derived from the Adda river downstream of the lake. The natural requirement of the crops in the irrigation period leads to a peak of the total water demand (irrigation + hydropower) in summer.

The irrigation district governance is managed by twelve Consorzio di Bonifica e Irrigazione (Consortia for reclamation and irrigation). These Consortia are public economic entities of the regional system of Lombardia, which address multiple purposes, from environmental protection to governing the artificial waters of the irrigated plain. At a higher policy level, the EU's Common Agricultural Policy (CAP) strategy has logical influences on irrigation demand in the basin as it impacts on the agricultural activities of the irrigation district served by the lake operation. If the CAP is revised the farming and agricultural activities in the LCB would need to take this into account, and tradeoffs with other sectors (water and energy) and solutions may be impacted.

3.2.2.4 Ecosystems

An environmental constraint affecting the release of water downstream of the lake is the Minimum Environmental Flow (MEF), i.e., the minimum flow released from the lake, to protect the downstream environment and ecosystems. This amount of water is always required downstream whenever the natural inflow to the lake is sufficient to provide it and adds to the downstream stakeholders' demand. The MEF definition is regulated by Regione Lombardia (regional authority) but is an argument of debates and it changes over time as the compromise between environmental and economic needs is difficult to find. For the release from Lake Como and for the Adda catchment, the MEF is defined as the minimum between the legally defined value, which currently is 22 m3/s, and the available inflow to the lake.

3.2.3 Stakeholders

Stakeholders involved in the WEFE Nexus for the Lake Como Basin include irrigation districts and farmers, the lake shore community, hydropower companies (ENEL, A2A, EDISON), the Consorzio dell'Adda (Adda Consortium) (i.e., Lake operator), the ADBPO Water Authority of the Po river basin, and the Regione Lombardia government. The interests of these stakeholders range from avoiding water shortages, controlling flood, maximizing hydropower revenue, and protecting the basin environment and ecosystems.

3.3 Júcar

3.3.1 Basin Setting

The Júcar River Basin (JRB) is a semi-arid area that covers 22,261 km^{2}, with the Júcar stream (512 km long) being one of the most important rivers in Eastern Spain. It starts at the Iberica mountain range besides the San Felipe hill, at 1,585 m height. The river flows along the Cuenca, Albacete, and Valencia provinces until it meets the Mediterranean Sea. The annual precipitation ranges between 309 and 717 mm, averaging 473 mm. Its precipitation pattern is typically Mediterranean: high rainfall in autumn (especially in October), a second peak in April–May, and very little precipitation during summer. The combination of high water demand and hydrological variability forces adaptation by different management strategies, such as water storage infrastructures, conjunctive use of surface and ground waters, and institutional and legal development. The total average available water resources are 1,668 mm3 per year, mostly from groundwater; 75% of the average river flow is regulated through surface reservoirs, with Alarcon (1,118 mm3 of useful capacity; upper basin) and Tous (378 mm3, lower basin) the two largest along the main course of the river, together with Contreras (852 mm3) (Escriva-Bou et al., 2017). The most significant amount of water use is for agricultural use (89%), followed by urban (9%) and industrial uses (2%).
The Júcar River system also holds 31 hydropower plants (with a total installed capacity of 1,272 MW). There are permeable materials that allow rainfall infiltration into the aquifers of La Mancha Oriental (middle part of the basin, Molinar) and La Plana de Valencia (lower basin, Sueca), where groundwater is abstracted (Suárez-Almiñana et al., 2020).
The Júcar is the primary source of urban water supply to Valencia and its metropolitan area (about 1,500,000 inhabitants, third-largest municipality in Spain). These surface and groundwater resources are used conjointly to supply all users, particularly those of higher priorities, such as urban areas and agriculture, with the most consumptive demand. The main area of the irrigated crops is in the middle basin and the coastal plain, coinciding with the location of the aquifers, where the Albufera de Valencia, an important wetland (211.2 km^{2}), is located. The wetland is a lake surrounded by rice crops (Suárez-Almiñana et al., 2020). Water scarcity, irregular hydrology, and groundwater overdraft result in droughts with significant economic, social, and environmental consequences. This situation is expected to be exacerbated by the impacts of climate and socioeconomic (global) changes and increasing institutional impediments from political disputes among the two main riparian regions,

Castilla-La Mancha (upstream; mainly Albacete province) and Valencia (middle and downstream basin) (Rubio-Martin et al., 2020).
Gómez-Martínez et al. (2021) analyze the effects of climate change on the raw water quality. Concerning the future scenarios, the most significant change was found in the projected increase of conductivity for the station of the Júcar river, between 4 and 11% by 2100, respectively, under the medium (SSP2–4.5) and pessimistic (SSP5–8.5) emission scenarios.
Estrela-Segrelles et al. (2021) assesse the sea level rise (SLR) related risk in the JRB due to climate change. The risk analysis results show that 90% of the JRB area affected by SLR corresponds to coastal wetlands. Half of the affected area belongs to the L'Albufera wetland with 32.44 km^2 below sea level, which represents a water volume of 42.64 hm^3 (2026–2045) and a surface between 72.53 and 138.96 km^2 representing 118.36 to 289.70 hm^3 (2081–2100). In the case of L'Albufera de Valencia, the impact will be throughout the 21st century; the average rate of SLR will leap from 4 to 11 cm per decade.

3.3.2 Nexus Challenges

Climate change is expected to decrease water resources in the JRB. Depending on the source, they could be curtailed up to 40/50% of the level shown in the late 20th century in some areas. The most significant reductions are expected in the basin's headwaters, where most reservoirs are placed, which could reduce the over-year storage needed to deal with the interannual droughts.
Although the uncertainty in the decrease percentage is large, most of the CMIP5 projections agreed on pointing at a reduction, so the degree of confidence is high. Furthermore, future projections of drought indices indicate an increase in the frequency and severity of droughts, further challenging the sustainability of water use in the system.
This expected decrease will drive impacts on all water uses: urban supply, agriculture, hydropower, and environmental status. Among them, impacts on agriculture and the environment are expected to be the most important. With an 80% share of total water use and lower priority than urban supply, agriculture will suffer the largest curtailment in water deliveries among consumptive uses. On the other hand, the environmental status of water and dependent ecosystems will be challenged by decreasing streamflow and the competition against agriculture. Hydropower production may also suffer a significant decrease, but it is expected to be lower than the equivalent in the previously mentioned sectors.
According to the Júcar River Basin Management Plan of the JRB district, 53% of their natural river reaches will not reach a good status before 2027, as required by the WFD. Similarly, all heavily modified or artificial reaches will not reach a good status. The situation improves in the case of reservoirs, with 86% expected to show a good status by 2027. However, it drops for the case of natural lakes (63%) and even further for the case of heavily modified or artificial lakes (50%). The overall evaluation of surface bodies shows that 52% will not reach the good status by 2027 required by the WFD. The situation of groundwater bodies is similar since 46% will not reach a good status before the original deadline of the WFD. This situation is combined with a heavily committed basin concerning water resources since consumptive water demands account for 95% of the average surface water resources.
Improving the environmental status of the Júcar River to meet the standards of the WFD would necessarily imply a modification in the operation of the river combined with a

reduction (and/or substitution by non-conventional water resources) in the amount of water abstracted by consumptive uses in both surface and groundwater.
Our analysis reveals the existence of two main challenges in the JRB. First, water scarcity and the increasing extreme events due climate change (multi-annual droughts and heat waves). In turn, the alternative scenarios should incorporate the balance among the agriculturalwater demands, the hydropower production, and the environmental status. Second, energy transition towards sustainability impacts energy prices, the farmer's economy, and environmental pressures and impacts in the JRB.
Furthermore, there are two subbasin challenges regarding the sustainable management of the upper-lower conflicts in the JRB.. On the one hand, the sustainability of the Mancha Oriental aquifer water management should be improved due to the GW overexploitation and its impacts on the JRB. On the other hand, the research study must focus on the Albufera wetland and its environmental status related to the impact of irrigation modernization.
In summary, the main challenges in the Jucar basin are as follows:

- **Water scarcity:**
    - Contamination of aquifers by phytosanitary products and pesticides.
    - Significant and prolonged drought episodes and increasing demand.
- **Energy transition:**
    - Decarbonizing the electricity sector and reducing energy demand
    - Rising energy costs directly impact crop profitability
- **Food sustainability:**
    - Transitioning to a more efficient, ecological, sustainable, and profitable production model.
- **Environmental sustainability:**
    - Protection of the coastal wetlands and other ecosystems in the Jucar Basin
    - Establish an ecological flow adequate to maintain the environmental integrity of the basin.

3.3.3 Stakeholders

Stakeholders include the JRB authority, environmental NGOs, farmer's associations, the energy company responsible of hydropower production, local and regional governments, and the media. All of them are usually related to knowledge institutions such as universities or other R&D organisms. Below in Table 1 is a comprehensive list of the most relevant Júcar stakeholders who actively participated in the initial dialogue and subsequent participatory modelling activities. The table also provides a detailed description of the stakeholders' primary responsibilities within the system and their connections with various elements of the WEFE (Water-Energy-Food-Ecosystems) nexus.

Table 1. Jucar stakeholders

Stakeholder	Responsibilities related to the nexus challenge selected	Interests and perceptions related to the nexus challenge	Scale (local, regional, national)
Jucar Basin Agency (CHJ)	Preparation of the basin hydrological plan, as well as its monitoring and revision; administration and control of the Public	Achieve a sustainable water use, fulfil the WFD, reconcile all the water users and interests, ensure that dams are adequately operated	Regional

	Hydraulic Domain; Administration and control of the uses of hydric resources		
Jucar Users Union (USUJ)	Defend the interests of the 40,000 members of the entity.	Downstream farmers with elder rights and Iberdrola. Want to ensure the sustainability of their activities and preserve the elder-right position they currently hold. Legal owners of the main reservoir (Alarcon).	Local
Acequia Real Del Júcar (ARJ)	It ensures compliance with ordinances and good order in the use of water. It carries out the functions of policing, distribution, and administration of the assigned waters.	The most important farmer association among USUJ members. Want to ensure the sustainability of their farming activities and preserve the elder rights that they currently hold.	Local
Canal Jucar-Turia (CJT)	Regulates the general operation of the Jucar-Turia Canal in its two aspects: • Relations with irrigation users. • Relations with supply users.	Farmers without elder rights from the lower Jucar. They use surface and ground water, during droughts they are not allowed to use surface water unless they pay a financial compensation to USUJ. They want to ensure the sustainability of their farming activities and achieve a more equitable share of surface wate	Regional
Junta Central de Regantes de la Mancha Oriental (JCRMO)	Manage and supervise the coordinated use of groundwater and surface water for irrigation and other purposes to ensure that the resources are used in a sensible manner maintaining their sustainability and preventing overuse. The adoption of measures to preserve the environment and the good qualitative status of the bodies of water in their area.	Farmers without Elder rights from the middle Jucar. They use mostly groundwater, although lately they have been entitled to a small share of surface water. Due to the overexploitation of the aquifer from which they pump (Mancha Oriental) they are being pushed to reduce their pumping rates. They want to ensure the sustainability of their farming activities, stop, or at least reduce the pace of groundwater pumping curtailments and increase the share of surface water they currently have	Local?
Iberdrola (energy company responsible of hydropower production)	Member of USUJ and the owner of all the main hydropower facilities in the basin. They also own the hydropower reservoirs in the middle Jucar, which can be freely operated subject to some restrictions on their minimum and maximum storage levels, as well as environmental flows.	They want to preserve the statu-quo in terms of managing their own reservoirs	National
City of Valencia		75% of the water used by Valencia comes from the Jucar. Urban supply has priority over agriculture according to the Spanish law, so they do not expect curtailments. However, an expansion of their current share to cope with population increase is unclear. They are also worried about water quality issues.	Local
City of Albacete		It used ground water until they switched to surface water due to quality issues. During droughts it has to pay a financial compensation to USUJ. It would like to preserve and expand its surface use and avoid as much as possible the payment of financial compensations	Local
Government of the Valencian Region		The Jucar water supplies water to the main urban area of the region, some of the main farming sectors and the most known protected are in the region. It wants to preserve and improve, if possible, the economic activity of the farming districts and the ecological status of the protected areas.	Regional
Government of		It would like to increase the share of the surface water of the Jucar, which is currently allocated	Regional

Castille – La Manch		mostly to the lower basin, as surface water is cheaper and cleaner than the ground water from the Mancha Oriental aquifer	
Xúqer Viu (Environmental NGO)	Protection and preservation of the Xúquer River Basin. The main objectives of Xúquer Viu include raising awareness of the importance of the Xúquer River Basin, promoting sustainable water management practices, and advocating for the protection of the river and its ecosystems.	Platform made up of several environmental NGOs, municipalities, and other public and private entities. They would like to improve the environmental status of the river, in particularly increasing the minimum environmental flows and preventing water transfers from the Jucar to other basins (e.g., the Jucar – Vinalopó transfer)	Local
AEMS Ríos con Vida (environmental NGO)	Conservation and restoration of rivers as well as the promotion of sustainable management of fluvial fish resources based on scientific knowledge	Nationwide NGO founded by fishermen pursuing a sustainable fish population and fishing activity. They would like to improve the environmental status of the Jucar to enable a healthy habitat in its streams, favouring native species.	National
University of Valencia	Spanish public university	Research on WEFE	National
Polytechnic university of Valencia	Spanish public university	Research on WEFE	National

3.4 Tagus-Segura

3.4.1 Basin Setting

The Tagus-Segura system comprises two basins linked by an aqueduct through which the Tagus basin transfers water to the Segura basin (Figure 14).

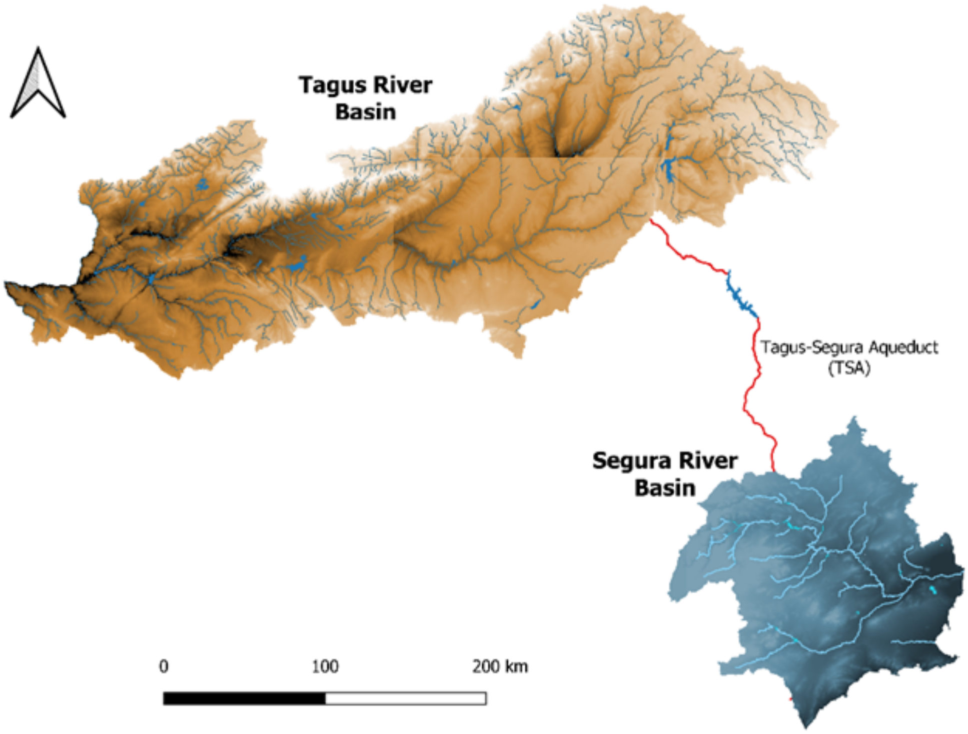

Figure 14. Section of the TRB and water transfer to the SRB

The Tagus River Basin (TRB) is the longest river in the Iberian Peninsula, stretching over 1092 km. Its basin covers an area of 83,680 km², of which 66.5% belongs to Spain and the

remaining 33.5% to Portugal. Its source is in the Universal mountains, in the Sierra de Albarracín (Teruel), and flows into the Atlantic Ocean in Lisbon. Its mouth forms an estuary. The water management challenge is particularly trying in transboundary basins, as any action must be accepted across the border by a larger number of stakeholders and different policy sectors. Significant variability in elevation, climate, and geology, leading to a heterogeneous landscape. The climate is Mediterranean with continental features. Annual average temperatures are irregularly distributed within the catchment, ranging from 8°C in the mountain peaks in the north to 17°C in the western area. The average annual precipitation is 648 mm, with a high variability with respect to season and elevation (Valerio et al., 2021). It is the most populated basin in Spain with almost 8 million inhabitants, and it is home to 11.8 million people and two European capitals (Madrid and Lisbon), which are important economic hubs. Forested areas cover 25% of the basin and are located mainly in the highlands. Cropland, found mainly on the plains close to the Tagus River, is the second most significant land use in terms of surface area (32% of the basin). Urban areas and bare soil account for less than 2%, while grassland covers 39% of the territory, this being the predominant land cover (Mezger et al., 2022).
Aquifers are mostly seen as a strategic water source during severe droughts or to meet local water needs. Moreover, they are key in the maintenance of the baseflow in rivers. The upper part of the TRB is the less populated and the major source of water transfers to the Segura River in the Mediterranean coast. Water is diverted from the Entrepeñas and Buendía reservoirs, with a total storage capacity of 2518 hm^3 (23% of the total reservoir capacity in the basin).

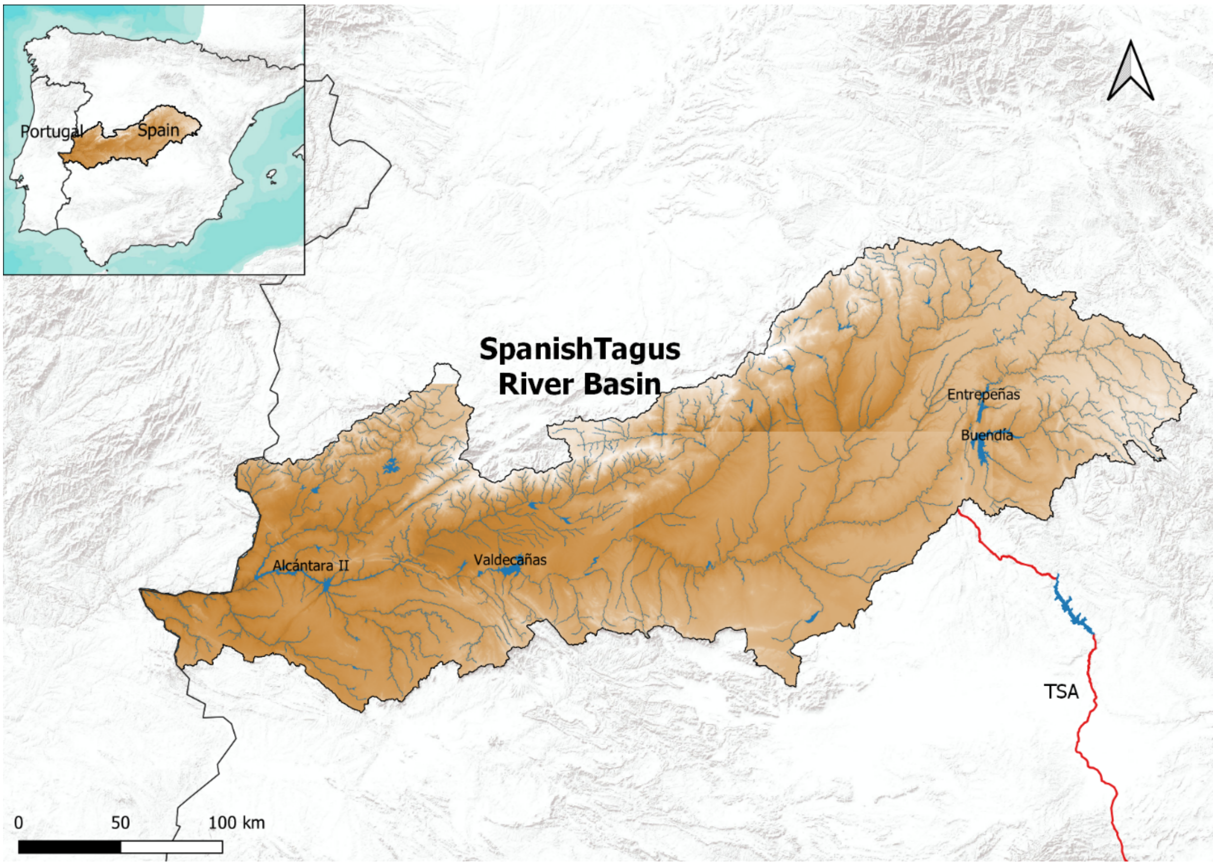

Figure 15. Spanish section of the TRB

The Segura River Basin (SRB) district is in south-eastern Spain and covers an area of 18740 km^2. The Segura River rises in Pontones (Jaén), located in the Sierra del Segura, in the heart of the Betic system. On its 325 km route, it crosses the provinces of Jaén, Albacete, and Murcia to flow into the Mediterranean coast in the province of Alicante. The co-existence of good-quality soils, a semi-arid climate and water resources, both surface and groundwater, has fostered the development of one of the most productive irrigated-agriculture systems in Europe (Martínez-Paz et al., 2015).

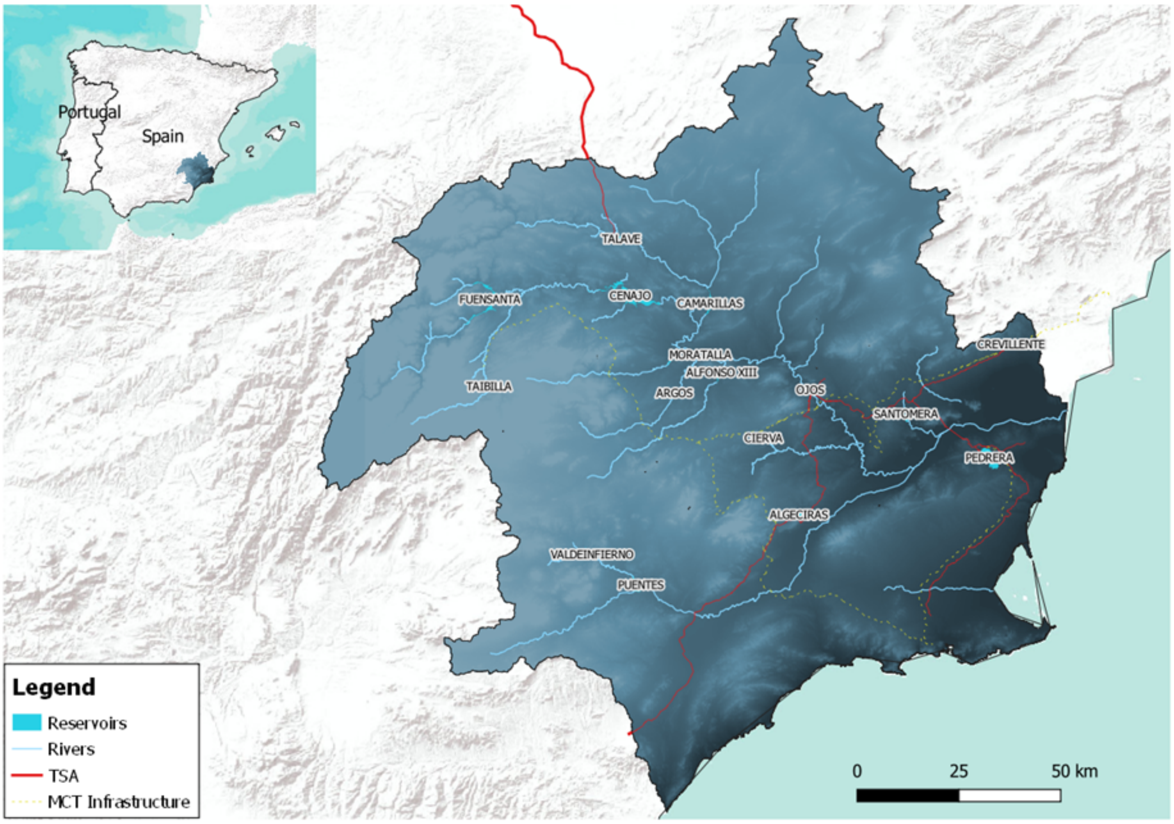

Figure 16. Segura River Basin

It has an average precipitation of 400 mm/year, although with a strong variability in space and time, it can be over 1000 mm/year in the North-western areas and under 200 mm/year on the coast. Mean annual temperatures are high, between 10 and 18 °C, which implies a high average potential evapotranspiration, around 700 mm/year, the runoff coefficient is low (0.15), and there are serious erosion problems (Almansa et al., 2012). The temperature and potential evapotranspiration show a distinctive seasonal pattern: values are lowest in winter and maximal in summer. On the other hand, precipitation is maximal in the winter and spring months but rare in the summer (Garcia Galiano et al., 2015). The co-existence of good-quality soils, a semi-arid climate, and water resources, both surface and groundwater, has fostered the development of one of Europe's most productive irrigated-agriculture systems (Martínez-Paz et al., 2015). Given the elevated participation of the agricultural and tourism sectors in the water-use activity of the basin, the water demands are highly seasonal, the summer being the period when greater volumes are required (Perni & Martínez-Paz, 2017). However, the natural water resources, mainly originating in winter and spring, are at their lowest levels in summer. This seasonal gap, together with the frequent droughts in the basin, has promoted the construction of important hydraulic infrastructures, such as channels and reservoirs since the beginning of the 20th century. Although the capacity of the reservoirs (over 1,100 Mm^3) is greater than the mean annual surface water resources (1,010 Mm^3), the supply problems have not yet been solved. Due to this , transfers from other basins (TRB) and a large group of coastal desalination are implemented at the SRB. According to Cañizares et al. (2022), the Tagus basin has suffered a significant reduction in rainfall, surface runoff, and volumes of reservoir-stored water in the subbasin of the Upper Tagus. There has not been a

reassessment or review of the operating calculations of the transfer to SRB in over 50 years. This research claims a new sustainable plan with a profound restructuring of hydrologic planning. It encourages the SRB to commit to using non-conventional sources (increase), such as treated wastewater and desalinated water.
García-López et al (2022) concluded that environmental impact is strongly related to energy consumption from fossil fuels, so the search for energy alternatives is also an activity that could bring major improvements to the functioning of the water transfer. In particular, introducing energy efficiency improvements or using alternative energy sources could contribute to reducing the environmental impact and the financial cost of the water transfer. The latter would also make it possible to reduce tariffs by reducing the variable costs associated with water conveyance.

3.4.2 Nexus Challenges

The Tagus-Segura water transfer moves water resources from the upper Tajo (Bolarque) to the upper Segura (Talave) basins, facilitating the development of irrigated agriculture areas in the SRB. Since the SRB is currently overexploited and suffering major quantitative and qualitative issues, the agricultural production in the SRB (one of the most important farming areas in Europe and one major driver of the economy in the Murcia region) depends on the water transfer. There is some potential for desalination, but it is yet far from being fully exploited due to energy costs preventing a sustainable use of desalinated water.
However, the transfer causes significant impacts on the TRB, since the water transferred is not allocated in the Tagus but in the Segura. These impacts include almost all uses, but the most important ones are the decline in the environmental status of the Tagus River (due to the reduction of streamflow challenging native habitats and the cleaning capacity of the river against the discharges of sewage treatment plants into it). The last news is that the Tagus River Basin Management Plan, currently under approval, foresees an increase in its minimum environmental flows that would decrease the amount of water transferred to the Segura, something that will be opposed by the farmers of the SRB and the associated regional governments (Región de Murcia and Comunitat Valenciana).
The main tradeoff occurs between the agricultural use in the Segura and the environmental status of the Tagus. Other direct tradeoffs of the transfer are caused by the reduction of water storage in the Tagus, with significant impacts on its agriculture and hydropower production, as well as recreation in the Entrepeñas and Buendia reservoirs (something that has caused a significant negative impact in the municipalities placed beside those reservoirs). There are also some tradeoffs associated with a reduction in the water transferred, which would force the Segura farmers to employ water alternative . Surface and groundwaters are already overexploited, and their use would imply potentially devastating impacts on the surface and groundwater status. Wastewater reuse is almost at maximum in the SRB, and the possibilities for a further increase are very low. The most suitable source, from a quantitative point of view, desalination, bears significant energy costs.
The main challenge in the Tagus-Segura case study is to improve the management of the Tagus-Segura water transfer to reconcile agriculture, energy production, and ecosystem status in both basins. It is closely related to water scarcity and the increasing of extreme events due to climate change (multi-annual droughts and heat waves). Furthermore, energy transition towards sustainability also impacts on hydromorphological and hydroelectric

pressures and environmental impacts in both basins. Mainly, these impacts provoke the bad environmental status in the Segura coastal water bodies (Mar Menor) and in the Tagus River due to urban sewage and farming/livestock pollution.
In summary, the main challenges in the Segura basin are as follows:

- Water Scarcity: Increase the availability of the resource to supply demands under climate change scenarios.
- Energy Transition: implementing efficient, profitable, and sustainable energy systems to promote the use of alternative sources of water.
- Food Sustainability: Adapt agricultural production to limited resource.
- Environmental Sustainability: Managing ecosystem pollution and overexploitation of aquifers.

From the First Dialogue in Madrid, regarding the TRB. Main challenges were identified:

- Water governance: Decrease in water availability due to climate change and water allocation issues among the different users.
- Urban Demand of Madrid and its pressure on TRB
- Energy Transition: Support greater renewable energy to meet TRB user´s demands.
- Environmental Sustainability: Adapting environmental flows to potential climate change effects in the basin and feasibility of the water transfer.
-

3.4.3 Stakeholders

Stakeholders include the TRB authority, SRB authority, the Farmers Union of the Tagus-Segura Water Transfer (SCRATS), the hydropower company which owns the main hydropower facilities of the TRB, the regional and local governments, the environmental NGOs from both basins and representatives for the Spanish Agency of Climate Change. Current media has a great influence and power. There are also small stakeholders related to water users and civil society. All of them are usually linked to knowledge institutions such as universities or other R&D organisms.
Below is a comprehensive list of the most relevant Tajo (Table 2) and Segura (Table 3) stakeholders who actively participated in the initial dialogue and subsequent participatory modelling activities.

Table 2. Tajo basin stakeholders

Stakeholder	Responsibilities related to the nexus challenge selected	Scale (local, regional, national)
Tagus Basin Agency - Confederación hidrográfica del Tajo (CHT)	Preparation of the basin hydrological plan, as well as its monitoring and revision; administration and control of Achieve a sustainable water use, fulfil the WFD, reconcile all the water users and Regional the Public Hydraulic Domain; Administration and control of the uses of hydric resources	Regional

Irrigation association - Federación de Comunidades de Regantes del Tajo (Fertajo)	Manage and supervise the coordinated use of groundwater and surface water for irrigation and other purposes to ensure that the resources are used in a sensible manner maintaining their sustainability and preventing overuse.	Local
Oficina Española de Cambio Climático (OECC)	This entity directs and coordinates the execution of the powers that correspond to the department concerning preventing pollution and climate change.	National
Energy company - Iberdrola	Iberdrola is the owner of all the main hydropower facilities in the basin. They also own the hydropower reservoirs, which can be freely operated subject to some restrictions on their minimum and maximum storage levels and environmental flows.	National
Water Observatory Botin Foundation	Contributes to current and emerging debates on managing water resources, both in Spain and the rest of the world, while working to promote and improve water-related policies.	National
Polytechnic university of Madrid	Spanish public university	Regional
NGO -Fundación Renovables	Its main objective is to raise awareness in society about the need to change the energy model with savings, efficiency, and renewables as fundamental principles.	National
NGO - Fundación Nueva Cultura del Agua (FNCA)	Collects, integrates, generates, and transmits knowledge to promote the adoption of the New Water Culture, focused on environmental, economic, social, and cultural sustainability.	National
WWF	Defense of nature and the environment	National
University of Valladolid	Spanish public university	Regional

Table 3. Segura basin stakeholders

Stakeholder	Responsibilities related to the nexus challenge selected	Scale (local, regional, national)
Irrigation association Las Fuentes de Letur	Manage and supervise the coordinated use of groundwater and surface water for irrigation and other purposes in Letur region, to ensure that the resources are used in a sensible manner maintaining their sustainability and preventing overuse.	Local

Segura Basin Agency - Confederación hidrográfica del Segura (CHS)	Preparation of the basin hydrological plan, as well as its monitoring and revision; administration and control of Achieve a sustainable water use, fulfil the WFD, reconcile all the water users and Regional the Public Hydraulic Domain; Administration and control of the uses of hydric resources	Regional
Irrigation Association - Comunidad de Regantes del Campo de Cartagena	Manage and supervise the coordinated use of groundwater and surface water for irrigation and other purposes Cartagena region to ensure that the resources are used in a sensible manner maintaining their sustainability and preventing overuse.	Local
Center for Edaphology and Applied Biology	improve agri-food development and the production of safe and quality food, within a sustainable use of natural resources in semi-arid environments.	National
NGO - Pacto por el mar menor	Inform and ensure the protection of the ecosystem associated with the Mar Menor	Local
University of Murcia	Spanish public university	National
Dirección General del Medio Natural	Plan and manage the protected natural areas of the Natura 2000 Network, natural habitats, wild fauna, and flora.	Regional
Irrigation association - Mancomunidad de los Canales del Taibilla (MCT)	Manage and supervise the coordinated use of surface water for irrigation and urban purposes to ensure that the resources are used in a sensible manner maintaining their sustainability and preventing overuse.	Regional

3.5 Senegal

3.5.1 Basin Setting

The Senegal River drains an area of 300,000 km^2 in western Africa (Figure 17). The basin is shared by four countries: Guinea, Mali, Mauritania, and Senegal. The headwaters are located in Guinea, the water tower of the Senegal River basin (SRB), where the Bafing River runs north until it merges with the Bakoye in Mali. From there, the Senegal River runs north-west through a series of falls and gorges before arriving in Kayes. Downstream of Kayes, the hydraulic gradient is much lower, and the river meanders through the plain while forming the boundary between Mauritania and Senegal until it discharges into the Atlantic Ocean.
At Bakel, the Senegal receives the flows from the Faleme River, the last major tributary from Guinea.

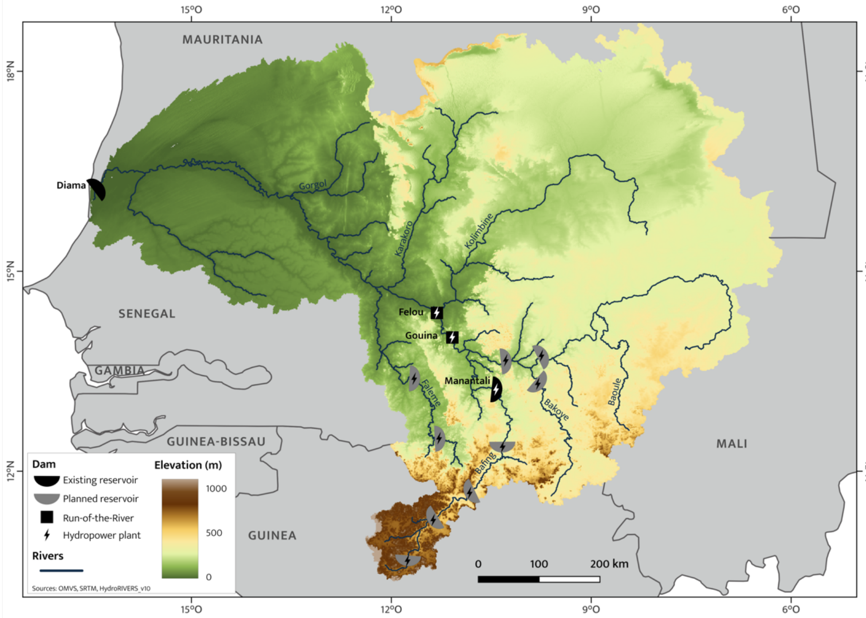

Figure 17. Map of the Senegal River basin.

Water in the SRB has been used by humans for transportation (navigation) and food production through flood recession agriculture. More recently, Senegal River flows have been used to generate hydroelectricity and three hydropower plants are now operational: (a) Manantali is a 200-MW power station supplied by an 11 km^3 multipurpose reservoir and (c) Gouina is 140-MW run-of-river power plant (b) Félou is a 62-MW run-of-river power plant located 60 km downstream of Gouina. Irrigated agriculture is mostly taking place downstream of Bakel, in Mauritania and Senegal, where the irrigation area is around 90 kha. Other hydroelectric power stations are planned on the main course and tributaries of the Senegal River. The next to be built in the coming decades are Koukoutamba (294 MW), Gourbassi (18 MW) and Boureya (161 MW).

The flow regime is characterized by two seasons: a high-flow season from July until November followed by a low-flow season during the rest of the year. The year-to-year variability of river discharges during the high flow season is significant and exposes water users to a high hydrological risk, especially subsistence farmers/herders whose livelihoods rely on the banks of the Senegal river.

During the high-flow season, flooding tends to occur primarily downstream of Bakel where the alluvial plain is about 10-20 km wide and in the delta. The floodplain covers a total of about 1 million ha and supports farmers, pastoralists, and fishing communities. According to Degeorges and Reilly (2006), up to half a million people depend on the flood-related cropping in the depressions along the river. Before the construction of the Manantali dam, the floods recharged the shallow aquifers, provided nutrients, and the retreating floodwaters enriched the soil permitting the development of flood recession agriculture while sustaining ecosystems.

During the dry season, navigation was possible up to Podor, 320 km upstream from the River Mouth at Saint-Louis. Moreover, during that season, the lower portion of the river became increasingly estuarine with saltwater intrusions moving as far upstream as Richard Toll.

The 1970-1980's were characterized by a sharp decline in runoff and by the construction of two major hydraulic infrastructure: the Manantali dam on the Bafing and the Diama dam close to the River Mouth. The main objective of the Manantali dam is to regulate the flows from Guinea to stock water during flood season and to increase dry season flows for navigation and irrigation purposes. At the same time, the hydropower plant is expected to generate 800 GWh of energy annually. Diama, on the other hand, prevents saltwater intrusion with the goal of boosting agricultural production in the lower valley. The construction of the Diama Dam in 1987 stopped the saline intrusion into the delta and the valley; the dam also contributed to the modification of hydrodynamic conditions in the estuary. The Langue de Barbarie sandy spit, whose extremity marks the position of the river mouth, has continued to extend southward, causing its gradual distancing from the city of St. Louis, with significant risks of flooding during rainy season. In October 2003, the Senegalese authorities decided to breach the sandy spit of the Langue de Barbarie to prevent flooding that would be disastrous for the city of St. Louis. The mouth was thus moved from 30 to 6.5 km south of the city. This is now a factor of increasing vulnerability for the whole of the lower estuary where some localities are under the double pressure of over-salination of water and land.

The Senegal River basin (SRB) is a good example where infrastructural developments and traditional uses are on a collision course (Kipping, 2009). The formers, advocated by the political elite, urbanites, and the private sector, aim at transforming the Senegal River into a major energy-food-transportation hub in West Africa. It involves the construction of several hydropower plants, modern irrigation schemes and river shipping infrastructure, and basically requires constant river discharges (Tilmant et al., 2020). It therefore directly threatens the livelihoods of riverine communities who rely on the banks of the river mostly for flood recession farming and fishing (Adams, 2000). The damming of the main tributary has already altered the flow regime, affecting farmers and herders in the low valley up to a point where it became a push factor for mass migration to the urban centers or abroad (Bruckmann, 2018). Among the environmental problems, the impacts of climate variability and change are felt with great intensity within the region, as in other Sahelian countries and even in the world. Indeed, developing countries like the Senegal River riparian states, with limited resources, are the most exposed to these impacts which compromise their development. In many river basins more rational water management seem necessary (Singh, 2012; Zhang et al., 2012). The management, thus, should integrate all other sector and be managed as a system.

Flooding has been a controversial topic for almost 40 years. In the management plans for the Manantali dam, a flood pulse was considered to maintain agricultural activities during the transition from flood-recession agriculture to irrigated farming. Depending on the growth rate of the irrigated areas, the artificial flood should have been maintained for 10 to 20 years after the construction of the Manantali dam. Since the 1970s, various artificial flooding hydrographs have been proposed to support flood-recession farming. For example, the latest scenario in 1999 was to supply 50,000 ha through flood pulse of 4,5 km^3 (Bader et al., 2003). Flood releases have been implemented for around ten years after the construction of the Manantali dam, then were abandoned in 2004 after the installation of all the dam's electric turbines. The evolution of flooding on the Senegal River is a striking example of the conflict between a modernist vision of river use (irrigation and hydroelectricity) and the maintenance of ecosystem services on flood plains. Like in other watersheds where it was planned (like the Zambezi at Kafue dam), the artificial flood has been abandoned due to difficulties in satisfying hydropower production.

3.5.1 Nexus Challenges

Our analysis of the tradeoff relationships reveals the existence of two coalitions of objectives (Tilmant et al., 2020): traditional food production (agriculture and floodplain fisheries) versus "modern" uses (hydropower, irrigated agriculture and river shipping). This tradeoff is characterized by a strong political asymmetry: the former coalition involves politically and economically marginal communities, whereas the political and economic elites advocate the second one. Contrasting vulnerabilities: The former coalition is particularly vulnerable to changes in allocation policies, whereas the latter is mostly affected by supply changes (e.g., climate change). Moreover, in terms of transboundary cooperation, a benefit sharing arrangement does exist for hydropower generation (riparian countries own shares of the power plants regardless of their location), but not for the agricultural sector.
Although the Senegal River basin is not yet approaching river basin closure, various alarming trends require the attention of water managers and policy makers: climate change and its impact on water demands and supply, increasing water demands due to sustained population growth, agriculture (irrigation and flood-recession agriculture), energy, navigation, etc.). The stakeholders responsible for managing water resources, and more generally those involved in the NEXUS, are faced with problems such as a lack of qualitative and quantitative information on water resources and water demands, and poor interaction between stakeholders within the basin, which complicate the identification of compromise solutions when managing tradeoffs.
Methodological support regarding hydrological, environmental as well as economic aspects for problem-solving processes in such contexts is lacking. The different priorities identified by the local stakeholders in the framework of the SDAGE are: (1) drinking water; (2) water for irrigated perimeters; (3) Hydroelectricity; (4) water for aquatic environments; (5) riverine transport; (6) floodplain agriculture. During first round of dialogues in the framework of GoNEXUS, we have identified same priorities with few differences: (1) drinking water; (2) water for irrigated perimeters; (3) water for aquatic environments; (4) floodplain agriculture (5) Hydroelectricity; (5) riverine transport.

3.5.2 Stakeholders

Stakeholders include the OMVS river basin authority, dam management companies, state departments in charge of rural development, NGOs and civil society organizations that are involved in the definition of scenarios and solutions, which will be tested and assessed by the hydroeconomic model.
OMVS is often credited for the peaceful management of the SRB. An important element of this success is the legal framework for cross-border water management, in which several conventions and tools determine effective cooperation and rational exploitation of the river's resources: the Water Charter (2002), the SDAGE (2011 and 2023), or the Permanent Commission on Water (CPE). These policy tools are usually funded by international donors and developed through various programs focusing on water management programs (PGIRE), on environmental problems (PAS), on irrigated areas (PARACI), on climate change (PIC), and so on.

3.6 Danube

3.6.1 Basin Setting

The Danube River Basin is the most international river basin on the Earth, shared by 19 countries and located in Central and SE Europe (Figure 18).

Figure 18. Location and countries sharing the Danube River Basin.

The Danube River Basin shows a tremendous diversity of habitats through which rivers and streams flow including glaciated high mountains, forested midland mountains and hills, upland plateaus and through plains and wet lowlands near sea level. Therefore, the basin is a challenging area from water management point of view. Due to its large extent from west to east (the total basin area is 801,463 km^2, while the total length of the Danube is 2,780 km), and diverse relief, the Danube River Basin also shows great differences in climate. The upper regions in the west show strong influence from the Atlantic climate with high precipitation, whereas the eastern regions are affected by Continental climate with lower precipitation and typical cold winters (ICPDR, 2004).

Climate change is the dominant factor driving a change in water resources in the Danube River Basin. The water, energy, food, and ecosystem nexus in the region is highly dependent on water, which is under significant pressures from pollutions by organic substances, pollutions by nutrients and hazardous substances, hydromorphological alterations, quality and quantity of sediment, invasive alien species as well as diffuse pollution on groundwater. Agriculture is the major water user in the basin, followed by domestic and industrial uses. Many small and medium size hydropower plants exist in the western part of the Danube Basin on both the main river as well as on smaller tributaries.

In addition to climate change, other drivers that influence the water nexus are demographic changes, changes in agriculture (CAP, Farm to Fork), and changes in energy production (Green Deal targets).

3.6.2 Nexus challenges

More and more studies underline that there will be significant annual average air-temperature increase globally and in Europe, as well. A European Environmental Agency (EEA) report presented that the annual average air-temperature change (increase) will vary from 0.34°C to 2.47°C in the European territory. Increasing air-temperature is predicted for the Danube Basin as well with higher than 1°C temperature increase in the Eastern and South-Eastern part of the basin.

The observed change in annual precipitation highlights that the southern part of Europe including the Danube Basin is significantly affected. The observed annual precipitation decreased in most part of the Danube Basin, especially in the Carpathian Mountains, which

are the dominant recharge area of the groundwater resources in the lower part of the Carpathian Basin.
Modelling simulation study results showed significant increasing trends in maximum number of consecutive dry days for three European regions when different climate scenarios were applied. For Central Europe, including the Danube Basin, approx. 60% increase is predicted in the maximum number of consecutive dry days.
The main impacts on water-related sectors are triggered by temperature and precipitation changes, including (a) an increase in air temperature with a gradient from northwest to southeast, particularly in summer in the south-eastern Danube region; (b) overall small annual precipitation changes for the whole basin on average, but major seasonal changes in the Danube River basin; (c) changes in the seasonal runoff pattern, triggered by changes in rainfall distribution and reduced snow storage; (d) the likelihood that droughts, low flow situations, and water scarcity will become longer, more intense, and more frequent; and (e) an increase in water temperature and increased pressures on water quality.
The climate change tendency would further impact the actual evapotranspiration of the soil. It will increase the frequency of agricultural droughts and increase the irrigation water demand, while decrease the flow in rivers and creeks, which are the dominant sources of irrigation. Century long meteorological observation highlights the negative tendency in drought situation in the middle part of the Danube Basin.
Warming trend in river water temperature also observed in the main rivers of the Danube Basin. Since 1950 average water temperature increased by more than 1 °C when considering the linear trend. The temperature of Danube River increased a bit faster than the Tisza River, largest tributary of the Danube by area.
The warming trend in river water temperature is highlighted by another observation as well. The date of ice formation on the river surface and the date of final disappearance of ice on the river surface have convergence in long term. This convergence is valid both for the linear trend and moving average line, as well. As water temperature has an increasing trend reflecting the climate change tendency, it can be considered as a scenario that there will be no ice formation during the winters on large parts of the Danube and some of the tributaries within the Danube Water Nexus modelling "near" future (2030-2050) period.
Time to time conflicts (such as water for irrigation and environment / water for irrigation and hydropower etc.) are already occurring even at the current climate situation. Consequently, three challenges were identified for the Danube River Basin Case Study:

1. Water scarcity and increased flood risk due to climate change, which may require changes in land management.
2. Water scarcity due to growing irrigation demand because of a warmer and drier climate.
3. Vulnerability of riverine and terrestrial ecosystems (biodiversity) due to water scarcity and land use changes driven by agriculture and energy.

3.6.3 Stakeholders

Stakeholders include the International Commission for the Protection of the Danube River (ICPDR) and the International Sava River Basin Commission (ISRBC) aka Sava Commission, which was established in June 2005. In 1948 the Danube Commission was established by seven countries to promote the maintenance and improvement of navigation conditions of the Danube River, from its source in Germany to its outlets in Romania and Ukraine, leading to the Black Sea. A subregional important stakeholder is the Carpathian Convention. This Convention is a subregional treaty to foster the sustainable development and the protection of the Carpathian region. It has been signed in May 2003 by seven Carpathian States (Czech Republic, Hungary, Poland, Romania, Serbia, Slovak Republic, and Ukraine). Other stakeholders to be considered in the dialogues of the DRB Case Study include: EU Strategy for Danube Region: Priority Area 4, 5 and 6; Global Water Partnership Central and Eastern Europe (GWP CEE); World Wildlife Fund Central and Eastern Europe (WWF-CEE); International Association of Water Service Companies in the Danube River Catchment Area (IAWD); European Centre for River Restoration (ECRR); Water management associations from the Danube countries; Chambers of Agriculture from the Danube countries; International Association for Danube Research (IAD); and the Nature Conservation Park National Associations from the Danube countries.

4 Applications and Model Development

4.1 High-resolution WEFE Modelling

4.1.1 Lake Como

4.1.1.1 Application Development

Stochastic climate downscaling

We develop the AWE-GEN-2d stochastic weather generator for the Como domain based on observed climate variables for the present/historical period. The AWE-GEN-2d model is configured at a spatial resolution of 1km² and hourly temporal resolution to ensure it can capture sub-daily dynamics in the simulated climate variables. Additionally, the climate scenarios developed in WP2 are analysed to develop factors of change to apply the Delta change method for generating AWE-GEN-2d future stochastic scenarios.

To calibrate the present climate precipitation, we considered two gridded rainfall products. The first a numerical model reanalysis product ERA5-Land (Muñoz-Sabater et al., 2021), while the second we evaluated is the satellite derived IMERG product (Huffman et al., 2020). Both have a spatial resolution of 0.1 degrees, while ERA5-Land has hourly and IMERGE half hourly temporal resolution.

Figure 19 and Figure 20 show a comparison of the mean annual precipitation totals for ERA5-Land and IMERG respectively. The mean annual total for these products is compared with the totals from the available station observations. The spatial pattern of the observations is best captured by ERA5-Land (however with a bias), while the spatial distribution of rainfall from IMERG is very homogeneous across the domain.

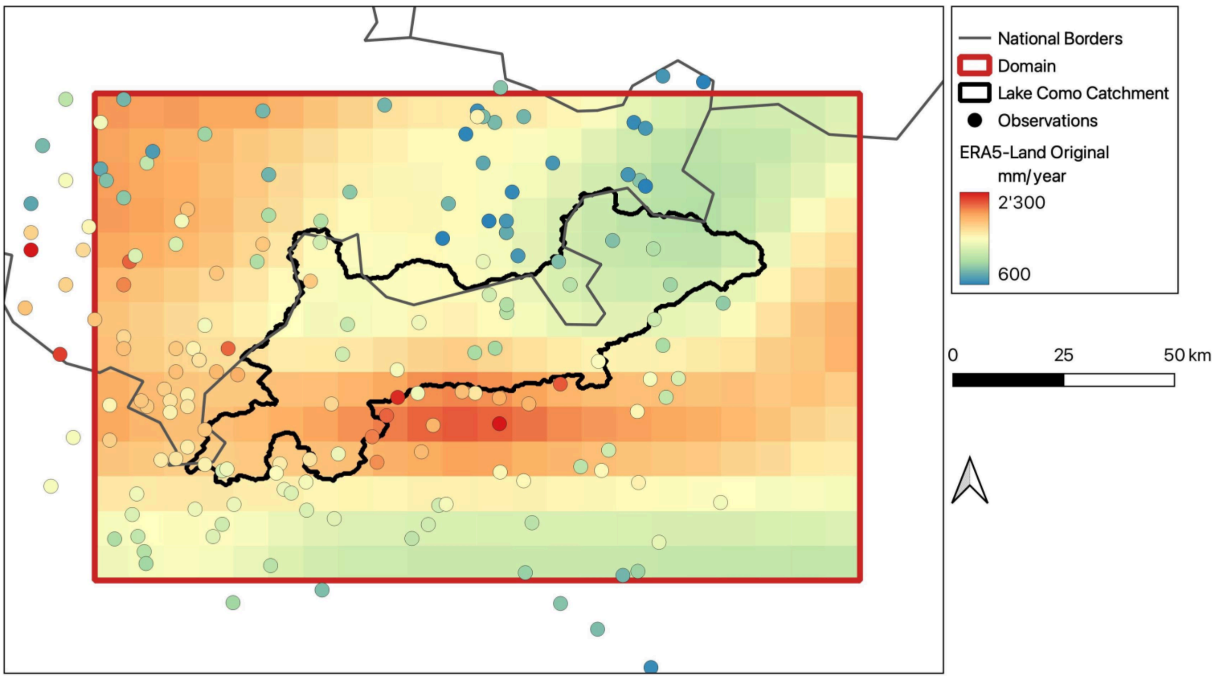

Figure 19. Comparison between the mean annual rainfall totals from ERA5-Land (gridded), and rainfall station observations (points). Note that the spatial pattern is well captured by ERA5-Land, but there is a bias in the magnitudes.

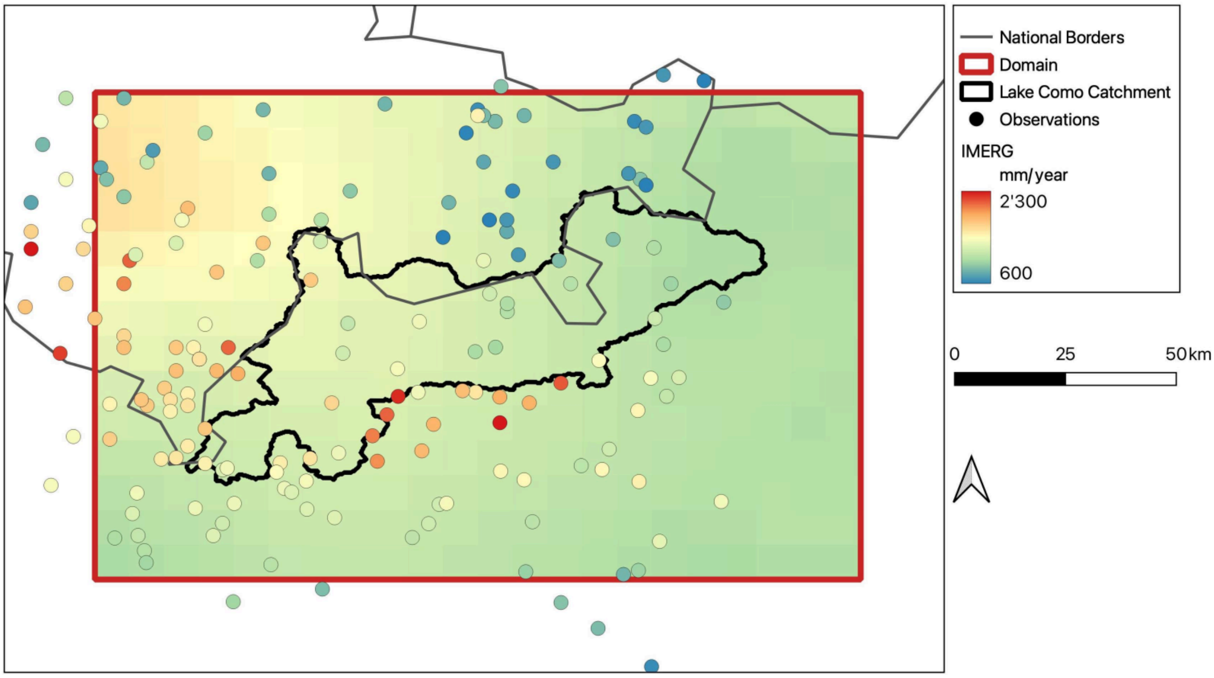

Figure 20. Comparison between the mean annual rainfall totals from IMERG (gridded), and rainfall station observations (points). Note that the spatial pattern is poorly captured by IMERG, in addition there is a bias in the magnitudes. However, as shown in Figure 21, the distribution of hourly rainfall amounts is captured well by IMERG compared to ERA5-Land.

On the other hand, the hourly distributions of rainfall from IMERG compare favourably with the observations (Figure 21), with ERA5-Land generating too high a frequency of low magnitude wet events. To maintain the spatial behaviour of ERA5-Land and the hourly scale distribution of IMERG, we applied a quantile mapping bias correction to ERA5-Land. We adjusted the ERA5-Land hourly distributions for each month of the year to match those of IMERG. The reason for adjusting to IMERG instead of directly to the observations was partly to avoid adding the extra uncertainty of interpolating the observed distributions at stations to unknown grid locations, and to maintain the stations as an independent source of model validation.

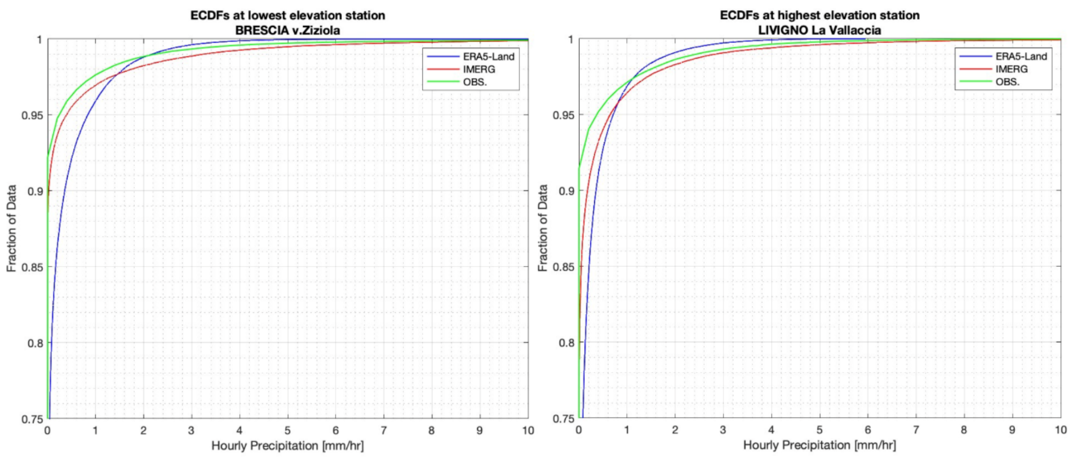

Figure 21. Empirical cumulative distribution functions of hourly rainfall derived from observations (green), IMERG (red) and ERA5-Land (blue). ERA5-Land exhibits a too high probability of low rainfall rates, while IMERG is able to capture the observed

distribution quite well. The behaviour shown in these two example stations is consistent for all the station analysed in the modelling domain.

The plot in Figure 22 shows that the spatial structure is maintained after the de-biasing exercise, while the bias is greatly reduced relative to the observations. In Figure 23 we give an example of the bias correction results for the month of April.

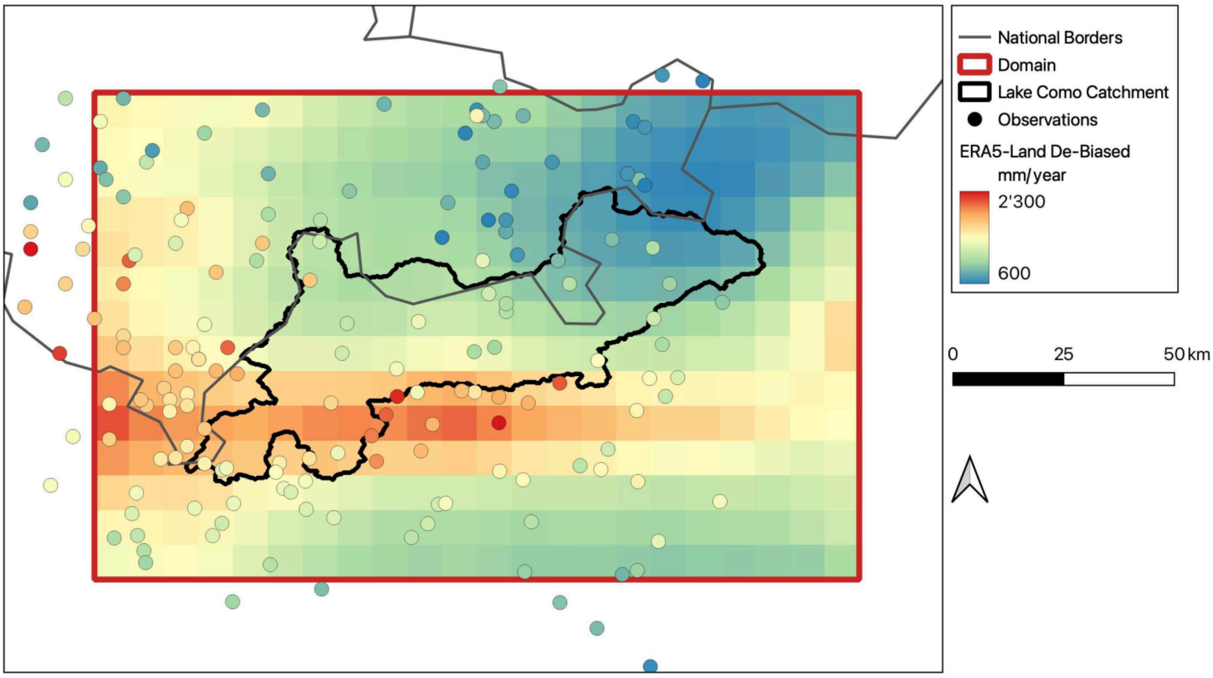

Figure 22. Mean annual rainfall totals from bias corrected ERA5-Land (gridded), and rainfall station observations (points). Note that both the spatial pattern and magnitudes of the station observations are captured well by the de-biased ERA5-Land.

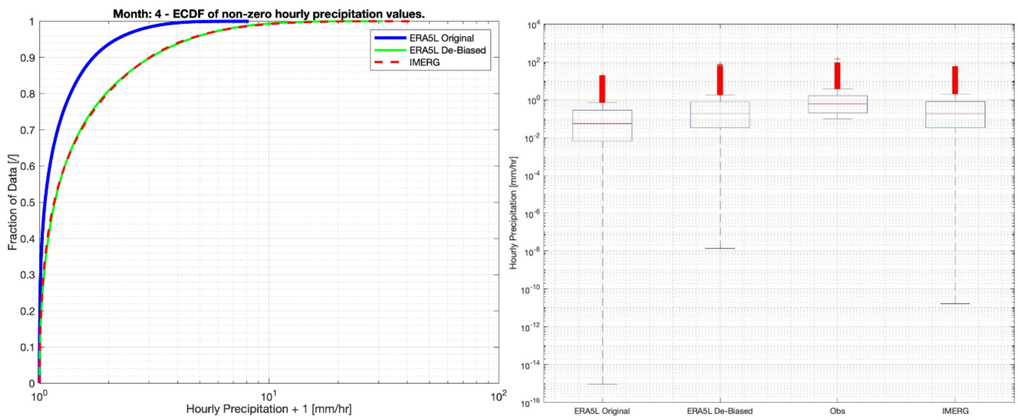

Figure 23. Example of the results of quantile transforming ERA5-Land hourly precipitation to match the distribution of IMERG. The de-biased ERA5-Land shows an improvement in the mean relative to observations, and a strong reduction in the number and range of low hourly precipitation.

To adapt the AWE-GEN-2d model of the present climate to the future climate scenarios of WP2, we extracted the lake Como domain from the global climate model projections, and computed factors of change for each grid cell in the domain. The change factors are based on a 30-year moving window, where the difference is relative to the present climate model simulations. We apply the factors of change to the AWE-GEN-2d model of present climate to develop simulations for the GoNEXUS future scenarios.

Figure 24 compares the trends for historical and future scenarios in the Como domain compared with the global mean. Generally, the temperature trajectories are consistent with the global average, with an expected larger deviation between models in the ensemble. However, for precipitation there is little to no trend evident in the case study domain, compared with the very distinct trends and differences among SSP scenarios at the global scale.

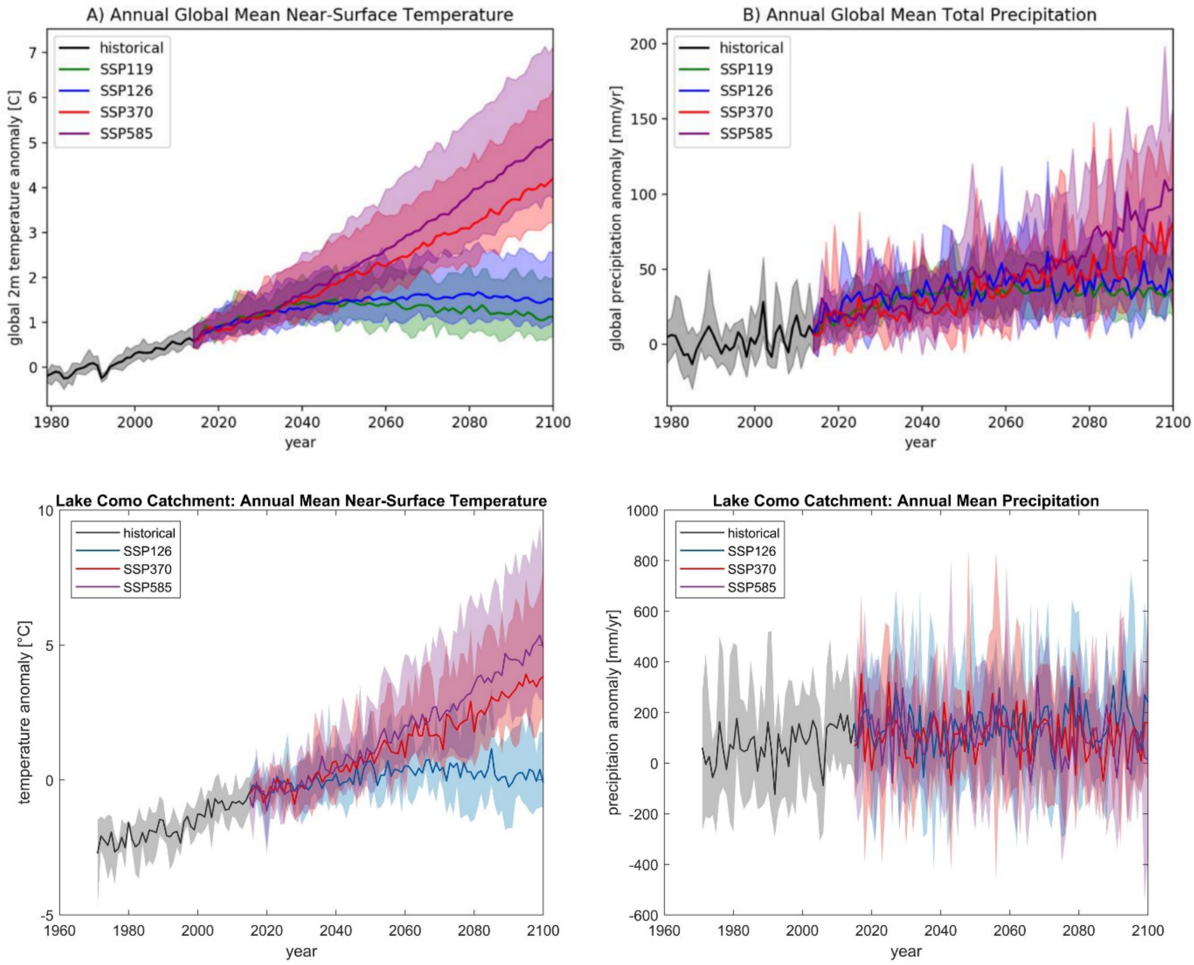

Figure 24. Comparison of the mean future trajectories for temperature and precipitation over the Como domain, compared to the global mean plots reported in D2.1. For temperature, the trends are consistent with the global trends; however, for precipitation there is no clear trend and even little difference indicated between the climate scenarios. The variability between model projections (shaded range) is greater in the Como domain compared to the global mean.

In Figure 25, Figure 26, and Figure 27 the seasonal behaviour of the factors of change is mapped at mid and late century. The temperature trends are as expected when considering Figure 24, a distinct increase in mean temperatures between mid and late century and the largest increase for SSP5-8.5. The range of differences between the models for each season also increases between mid and late century. The most significant increase in all scenarios is for the summer season JJA.

The models predict a small increase of precipitation during DJF and MAM, with a tendency towards decreasing precipitation in JJA, and more neutral changes in SON. The magnitude of the median change in all seasons is small compared with the model spread.

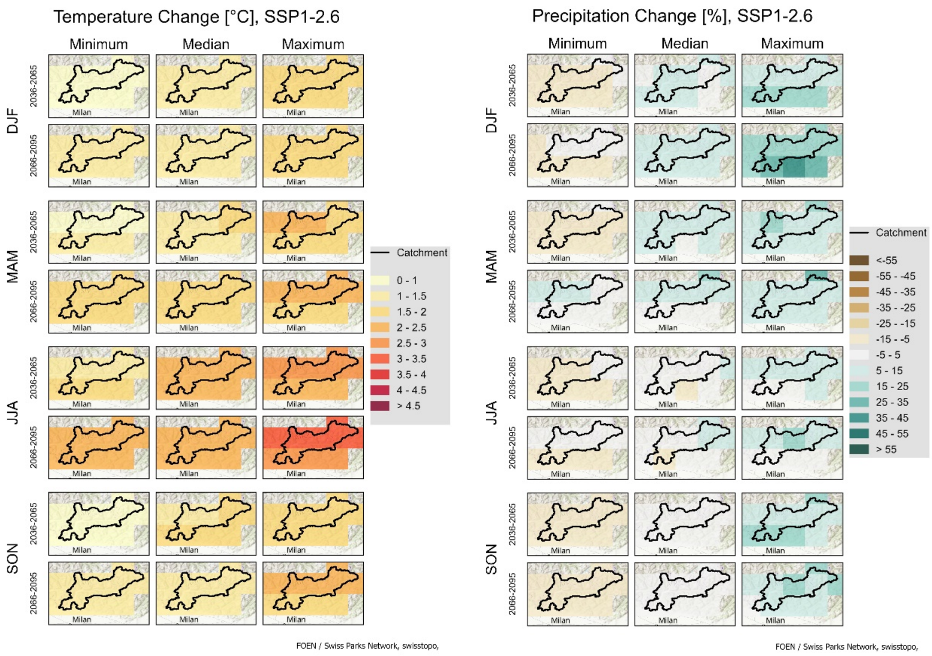

Figure 25. Seasonally projected changes in temperature (left panel) and precipitation (right panel) for mid (2036-2065) and late (2066-2095) century for climate scenario SSP1-2.6. The maps in each column show the minimum, median and maximum changes in the lake Como catchment among the model ensemble members for the scenario. Units of temperature change are the direct difference in °C between the historical scenario (1979-2014), and the relevant period in the future scenario. Units for precipitation are in percentage change relative to the historical scenario.

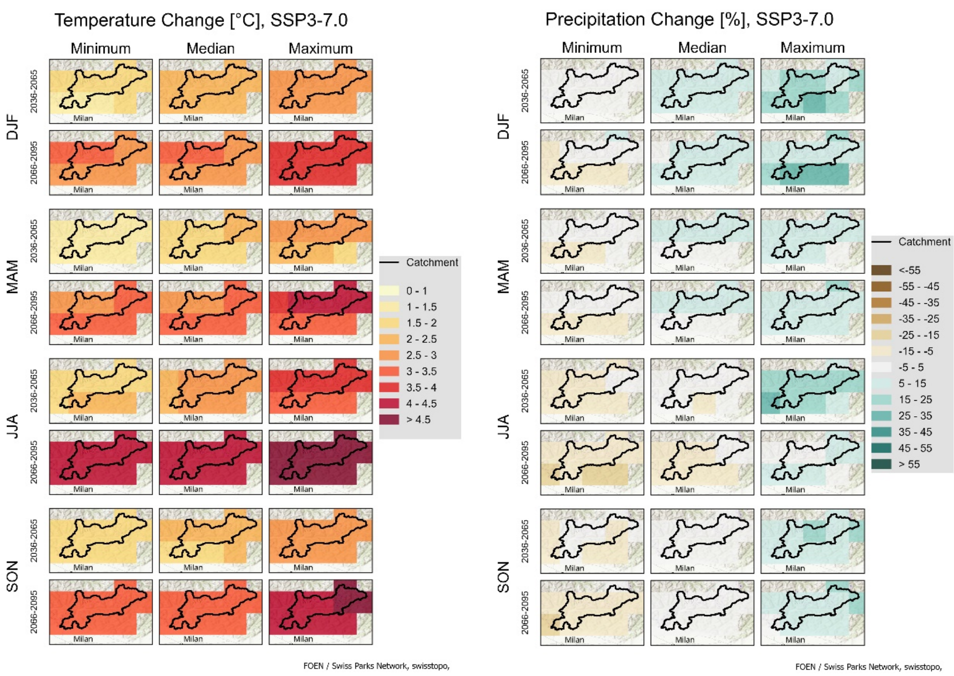

Figure 26. Seasonally projected changes in temperature (left panel) and precipitation (right panel) for mid (2036-2065) and late (2066-2095) century for climate scenario SSP3-7.0. The maps in each column show the minimum, median and maximum changes in the lake Como catchment among the model ensemble members for the scenario. Units of temperature change are

the direct difference in °C between the historical scenario (1979-2014), and the relevant period in the future scenario. Units for precipitation are in percentage change relative to the historical scenario.

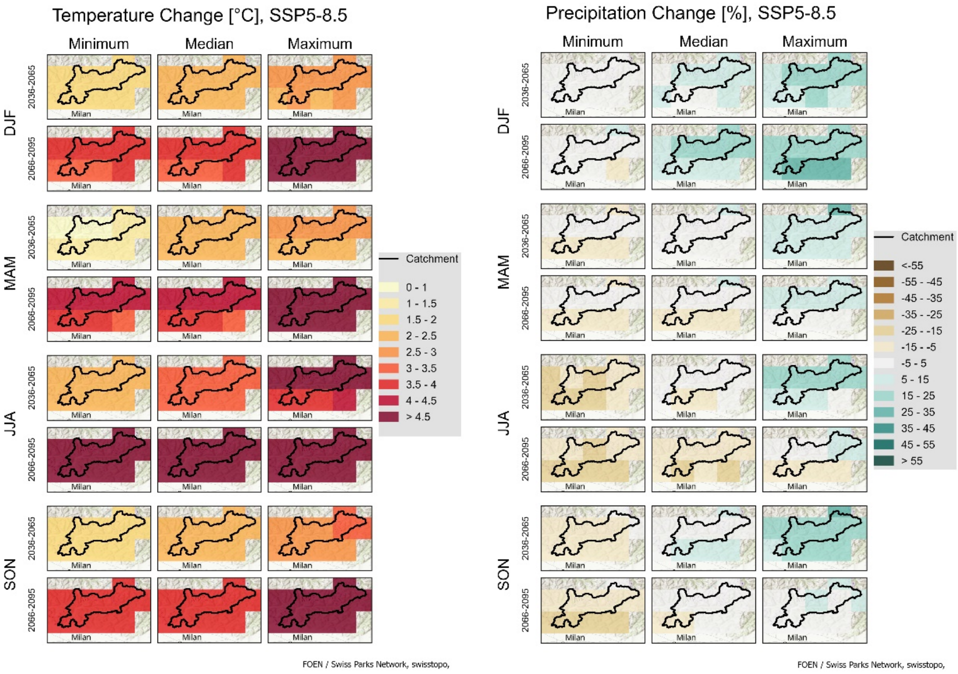

Figure 27. Seasonally projected changes in temperature (left panel) and precipitation (right panel) for mid (2036-2065) and late (2066-2095) century for climate scenario SSP5-8.5. The maps in each column show the minimum, median and maximum changes in the lake Como catchment among the model ensemble members for the scenario. Units of temperature change are the direct difference in °C between the historical scenario (1979-2014), and the relevant period in the future scenario. Units for precipitation are in percentage change relative to the historical scenario.

Hydrological modelling

The starting point for the hydrological modelling is a TOPKAPI-ETH configuration developed by Giudici et al. (2021). In GoNEXUS, we have adapted the TOPKAPI-ETH model configuration to run using the new TOPKAPI-ETH version 2. The change to the newer model version allows the possibility to analyse the WEFE challenges assessed from spatially distributed indicators, using the MORDM optimized reservoir operation policies for the three largest hydropower schemes (A2A, Enel, and Edison).

The model (depicted in Figure 28) covers an area of 4750km^2 and consists of 76196 inter-connected cells with a spatial resolution of 250m^2. The model has been configured to run at a daily time-step selected to match the daily time resolution of the climate scenario inputs from WP2, as well as the time resolution used in MORDM to maintain consistent reservoir operations according to the MORDM optimized policies.

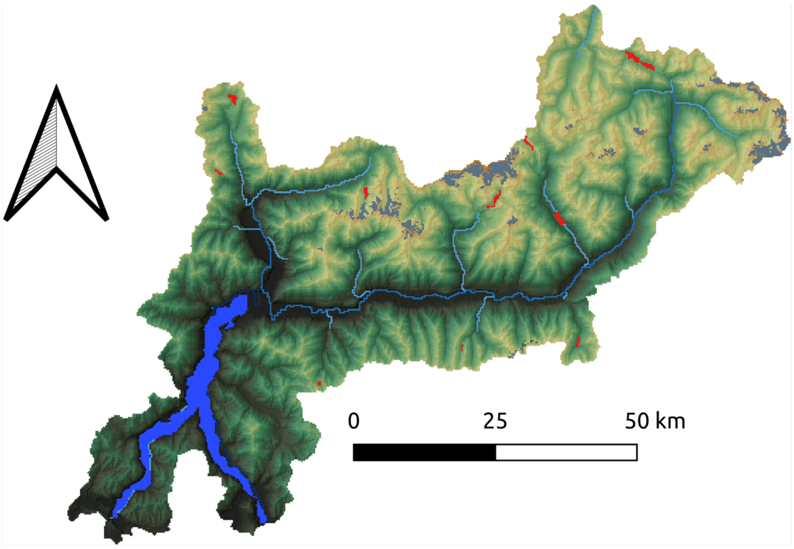

Figure 28. TOPKAPI-ETH model of the Lake Como catchment showing the mainstream network and Lake Como (blue), hydro-power reservoirs (red), and glaciated areas (grey). The background is the digital elevation model with elevation increasing from dark green to light brown.

The calibration fit achieved by Giudici et al., (2021) for net reservoir inflow during the historically observed period is reproduced in Figure 29. The model can satisfactorily reproduce the reservoir inflows. As described later in this section the model has been adapted in GoNEXUS to improve the parameterization of glaciated areas, and to operate reservoirs according to the MORDM operations policies.

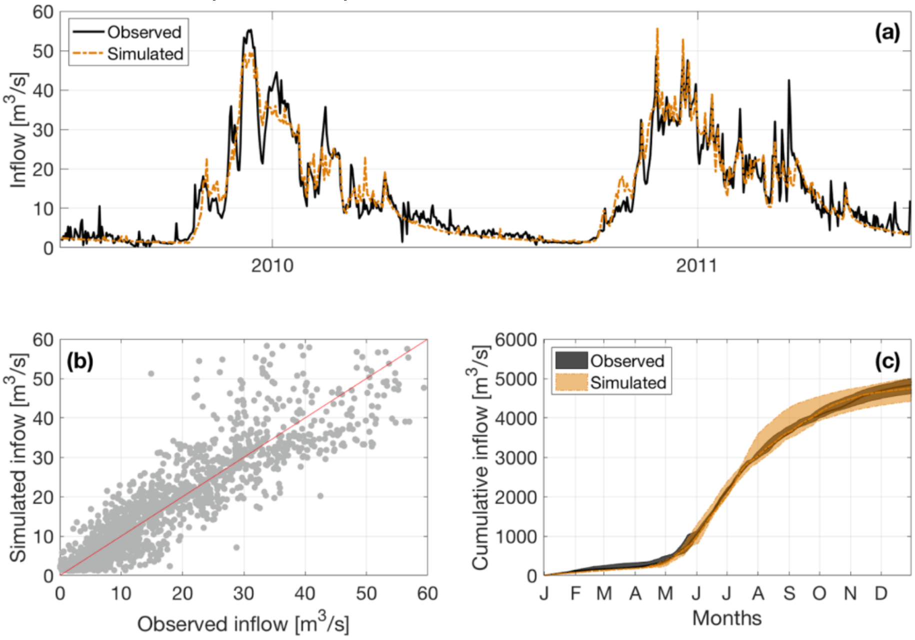

Figure 29. Calibrated model fit achieved by Giudici et al., (2021). Most of the streamflow character is well captured. However, the variability of the recession limbs is most likely attributable to hydro-power operations.

A particular aspect which we emphasize in the modelling work is the use of the glacier dynamics module in TOPKAPI-ETH to account for the impacts of the expected loss of glacier volume under a warming climate. The Lake Como catchment contains several glaciated areas, and the impact of glacier loss on streamflow has recently been studied by Fuso et al.,

(2021), using a spatially distributed model (Poli-Hydro). In GoNEXUS we include the reservoir regulations in the upstream part of the catchment and force the model with higher resolution climate inputs.
The glacier ice thickness in the Giudici et al., (2021) model was parameterized using an empirical relationship based on the spatial extent of each glacier. In this work we revised the distribution of ice thickness in the model according to the global glacier ice thickness inventory of Farinotti et al (2019). The database consists of multiple high-resolution tiles, which were merged into a single raster layer (Figure 30), and subsequently the ice thickness was assigned to TOPKAPI-ETH model cells containing sufficient ice coverage and volume (Figure 31).

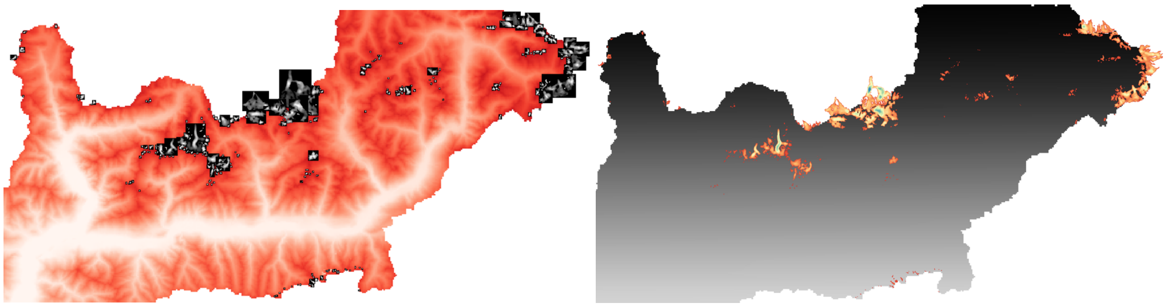

Figure 30. The Farinotti et al., (2019) *database in the left panel, consisting of many small independent tiles, was merged into a single layer (right panel).*

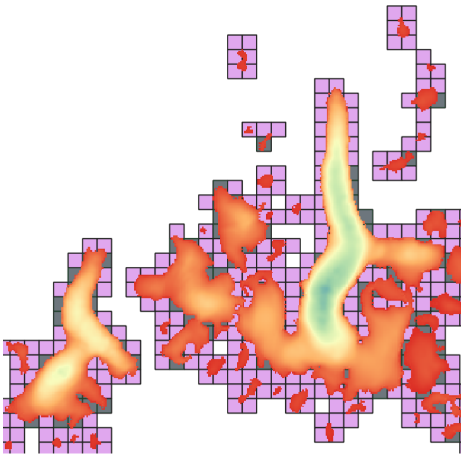

Figure 31. The merged glacier thickness dataset of Figure 30 was assigned to TOPKAPI-ETH grid cells according to the degree of spatial coverage, and the estimated volume of ice on a grid cell.

MORDM operation policies have been implemented in the TOPKAPI-ETH model of the lake Como catchment. Figure 32 and Figure 33 show the results of a test case during the historical period. They show that the release decisions based on current reservoir storage are almost identically equivalent for the MORDM and TOPKAPI-ETH policy implementations given the same input time-series.

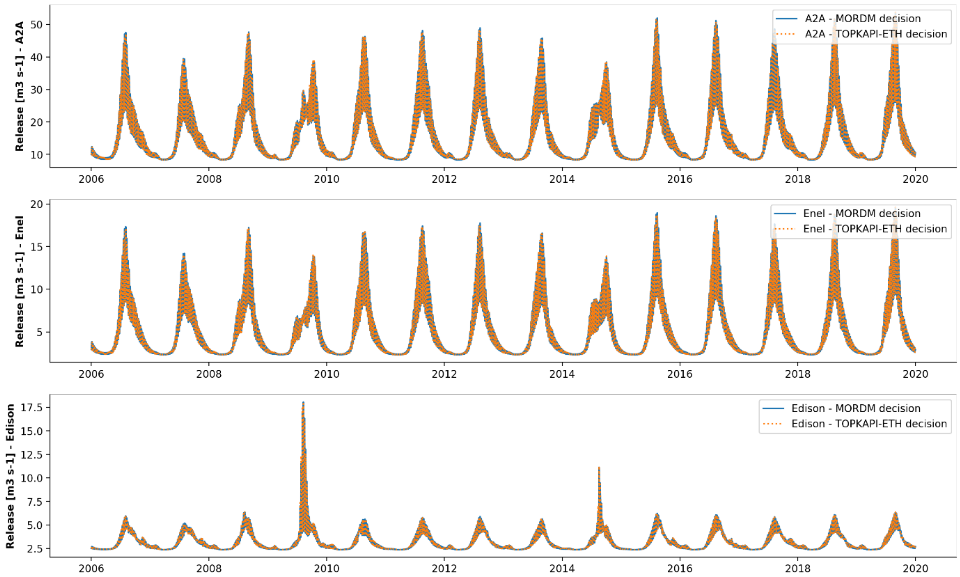

Figure 32. Time-series validation of the implementation of MORDM reservoir operations policies in TOPKAPI-ETH. The time-series illustrates the different operational release decisions, depending on the climate conditions during the observed historical period.

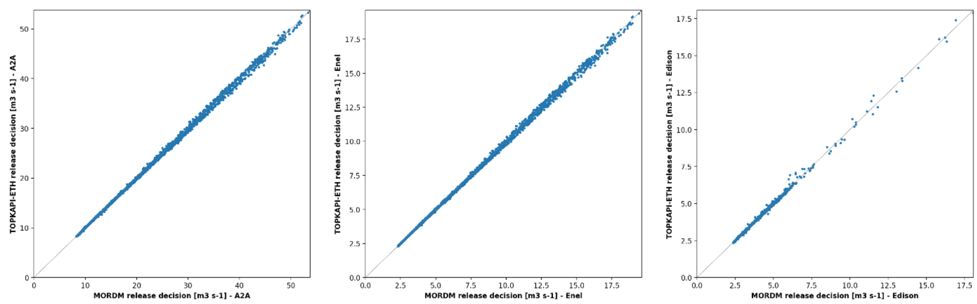

Figure 33. Scatter plot comparison of the operating decisions implementation in TOPKAPI-ETH. The plots compliment those of Figure 32 by giving a clearer indication of the density and spread across release rates.

4.1.1.2 Application Results

Due to the developmental nature of the methodology, and complexity of the high-resolution modelling effort, sufficiently mature application modelling results were not available at the time of this deliverable. Instead, the relevant modelling results are targeted for reporting in the WP5 WEFE evidence deliverables D5.6 and D5.7.

4.1.2 Zambezi Watercourse

4.1.2.1 Application Development

Stochastic climate downscaling

The starting point for the AWE-GEN-2d model of ZWC in GoNEXUS is based on the model calibrated to the present-day climate during the EU funded DAFNE project (DAFNE, 2018; Peleg et al., 2020). The model can simulate climate variables at 8km² spatial and hourly temporal resolution. Figure 34 shows a comparison between the mean annual precipitation simulated by AWE-GEN-2d, the satellite derived CMORPH rainfall product (Joyce et al., 2004) used in model calibration, and an independent estimate based on interpolation of rain gauge data by Gumindoga et al., (2019). The AWE-GEN-2d model is able to faithfully represent the spatial pattern, and the differences shown in the lower panel of Figure 34 are not large if expressed as a percentage of the observed annual precipitation, and are likely a result of the stochastic generation, since this comparison is for a single climate realization.

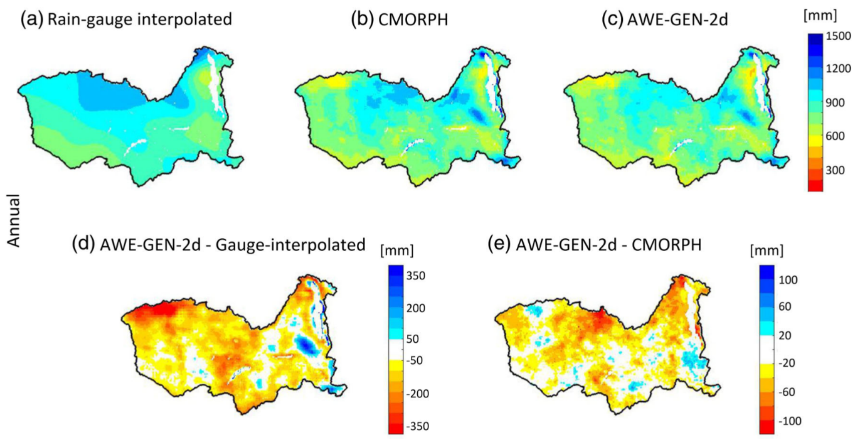

Figure 34. Annual rainfall maps for the present climate: (a) rain-gauge interpolated rainfall based on Gumindoga et al. (2019) *the period 1998–2013; (b) CMORPH (1998–2017) and (c) simulated using the AWE-GEN-2d model. Maps (d) and (e) are showing the differences between (c) and (a) and (c) and (b), respectively (note the different range on the colour scales—With AWE-GEN-2d being closer to CMORPH as expected, due to the calibration procedure). [Figure after Peleg et al. ((2020)]*

Figure 35 compares the model simulated climate variables with observations at the Lusaka meteorological station in Zambia. All the simulated variables are well captured when compared with the observed quantities.

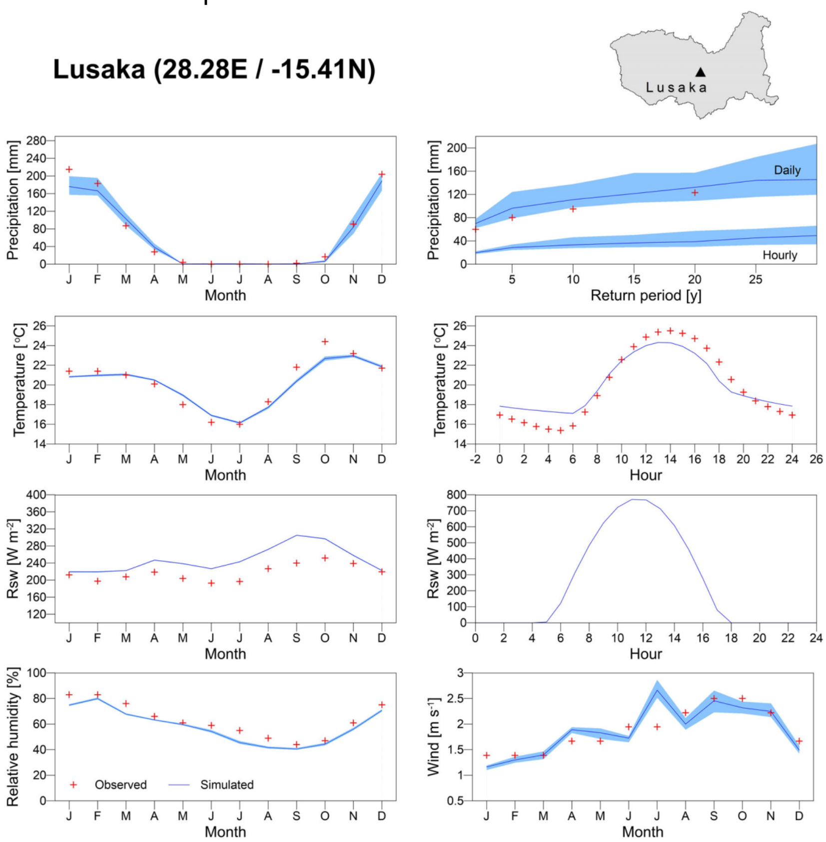

Figure 35. Observed (red) and simulated (blue) climate variables for Lusaka airport station, computed from 30 realizations of 30-year each. Solid lines represent the median and blue areas represent the 5-95th percentile range of the natural (stochastic)

climate variability. Values are reported for monthly rainfall (a), rainfall extremes at daily and hourly scales (b), monthly air temperature (c), air temperature daily cycle (d), monthly shortwave radiation (e), shortwave radiation daily cycle (f), monthly relative humidity (g), and monthly wind speed (h). [Figure after Peleg et al. (2020)*]*

The simulated seasonality over the entire basin is illustrated in Figure 36 (mean monthly temperature for present climate) and Figure 37 (mean monthly precipitation total for present climate). The southern hemisphere winter is evident in Figure 36, with June-August having distinctly lower temperatures. The well-known dry season during April-October () is clearly shown in Figure 37, with some regions of the basin consistently getting no rainfall in the Winter season of June-August for the AWE-GEN-2d realization depicted here.

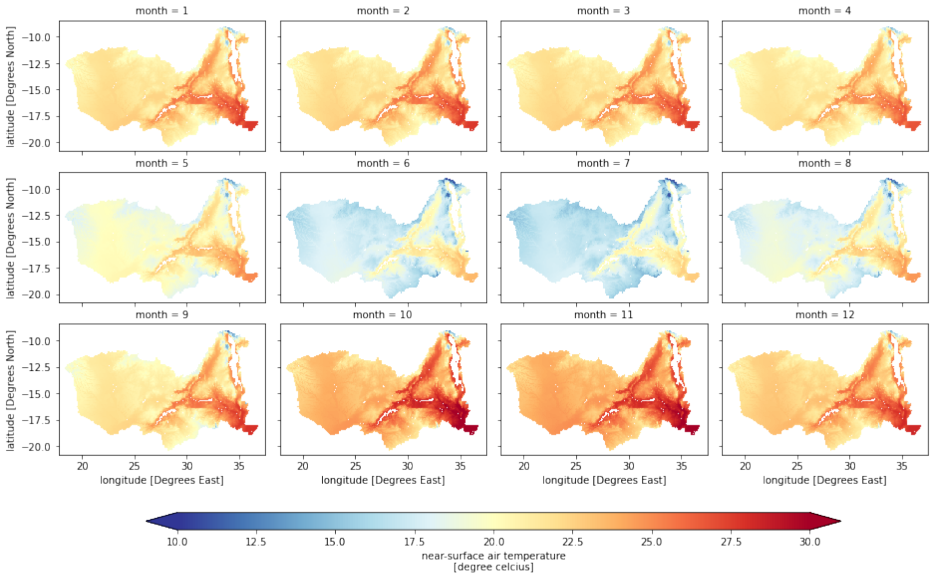

Figure 36 of the mean monthly temperature for a single present day climate realization simulated by the AWE-GEN-2d model for the ZWC. Note the level of spatial detail and the distinctly warmer low-lying regions of the main Zambezi valley during all months of the year.

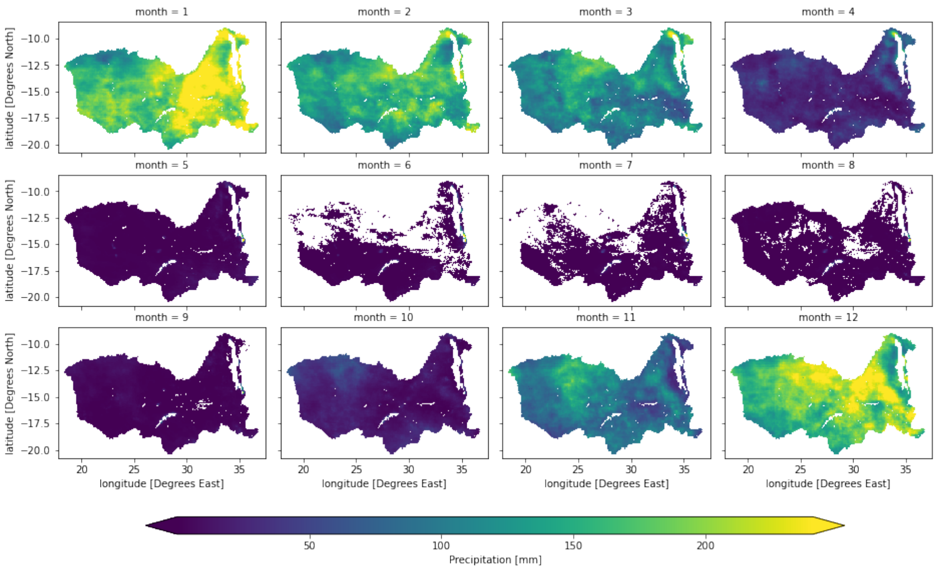

Figure 37. Example of the mean monthly precipitation totals for a single present day climate realization simulated by the AWE-GEN-2d model for the ZWC. Note the very distinct wet and dry seasons, with the April-October dry season showing regions with almost no precipitation on average.

The CMIP6 based climate scenarios developed in WP2 are different from the Africa CORDEX scenarios used in previous work during the DAFNE project. The new scenarios required us to derive Factors of Change for temperature and precipitation for the ensemble of climate projections. To do so we extracted the Zambezi domain from the global climate model projections, and computed factors of change for each grid cell in the domain. The change factors are based on a 30-year moving window, where the difference is relative to the historical climate model simulations. We apply the factors of change to the AWE-GEN-2d model of present climate to develop simulations for the GoNEXUS future scenarios.
Figure 38 compares the trends for historical and future scenarios in the Zambezi domain compared with the global mean. Generally, the temperature trajectories are consistent with the global average, with an expected larger deviation between models in the ensemble. However, for precipitation there is little to no trend evident in the case study domain, compared with the very distinct trends and differences among SSP scenarios at the global scale.

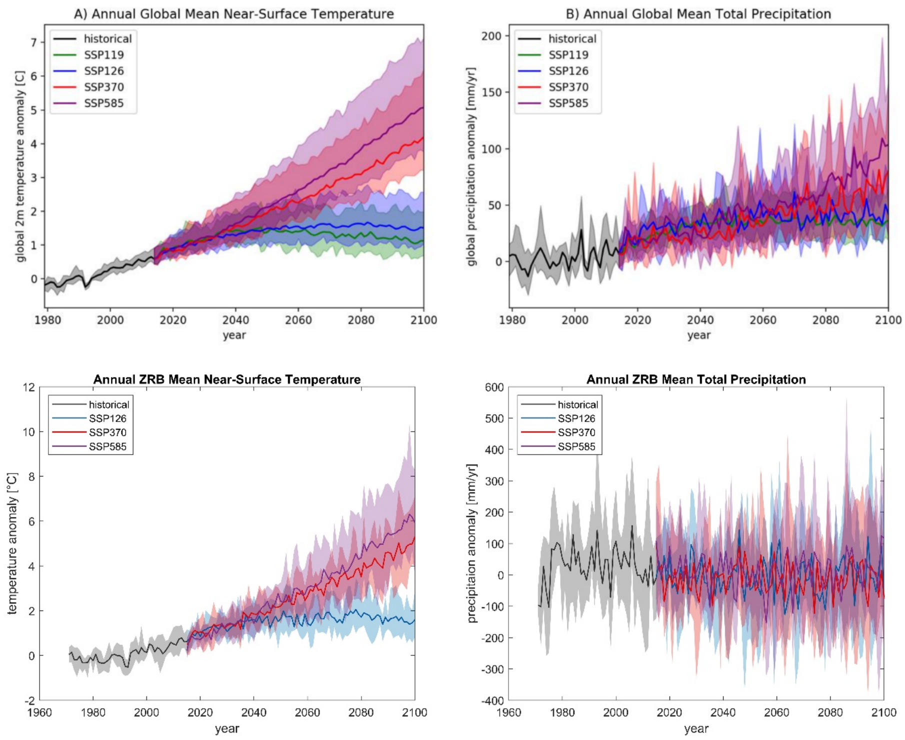

Figure 38. Comparison of the mean future trajectories for temperature and precipitation over the Zambezi watercourse, compared to theglobal mean plots reported in D2.1. For temperature, the trends are consistent with the global trends, however for precipitation there appears a biased reduction, but with no clear trend and very little clear difference indicated between the climate scenarios. The variability between model projections (shaded range) is greater in the Zambezi watercourse domain compared to the global mean.

In Figure 39, Figure 40, and Figure 41 the seasonal behaviour of the factors of change is mapped at mid and late century. The temperature trends are as expected when considering Figure 38, a distinct increase in mean temperatures between mid and late century and the largest increase for SSP5-8.5. The range of differences between the models increases between mid and late century. The most significant increase in all scenarios is for SON, and a general decrease in mean precipitation is also predicted for this season.
For precipitation the median change is neutral across the SSP scenarios for DJF and MAM with some models wet and others dry. For SON all models predict a reduction in rainfall for

all the scenarios. Note that the behaviour in JJA is very likely attributable to model noise because this season typically has almost no rainfall, and the factors of precipitation change are reported as a percentage value.

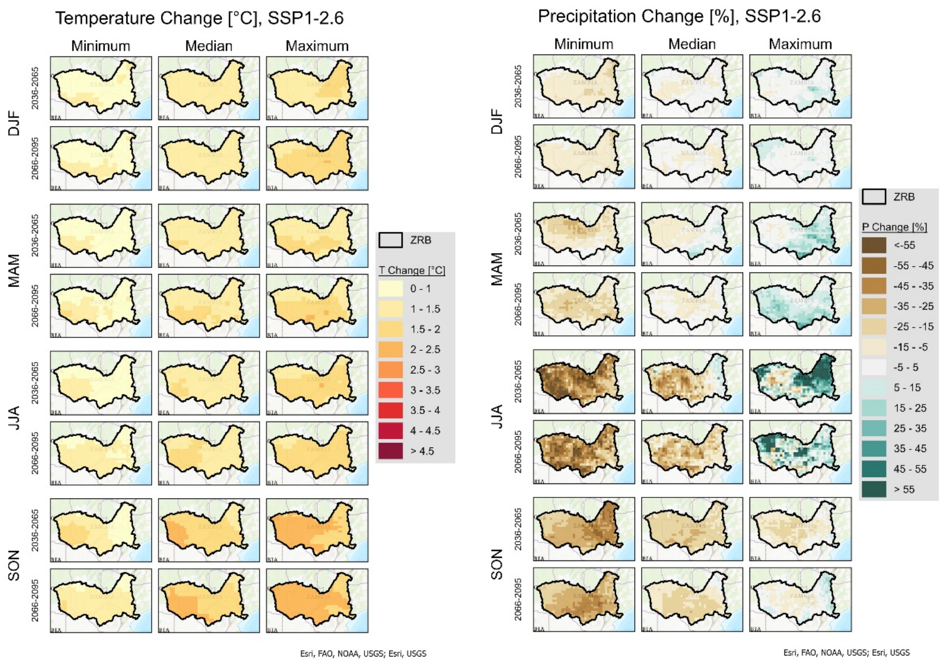

Figure 39. Seasonally projected changes in temperature (left panel) and precipitation (right panel) for mid (2036-2065) and late (2066-2095) century for climate scenario SSP1-2.6. The maps in each column show the minimum, median and maximum changes in the Zambezi watercourse among the model ensemble members for the scenario. Units of temperature change are the direct difference in °C between the historical scenario (1979-2014), and the relevant period in the future scenario. Units for precipitation are in percentage change relative to the historical scenario.

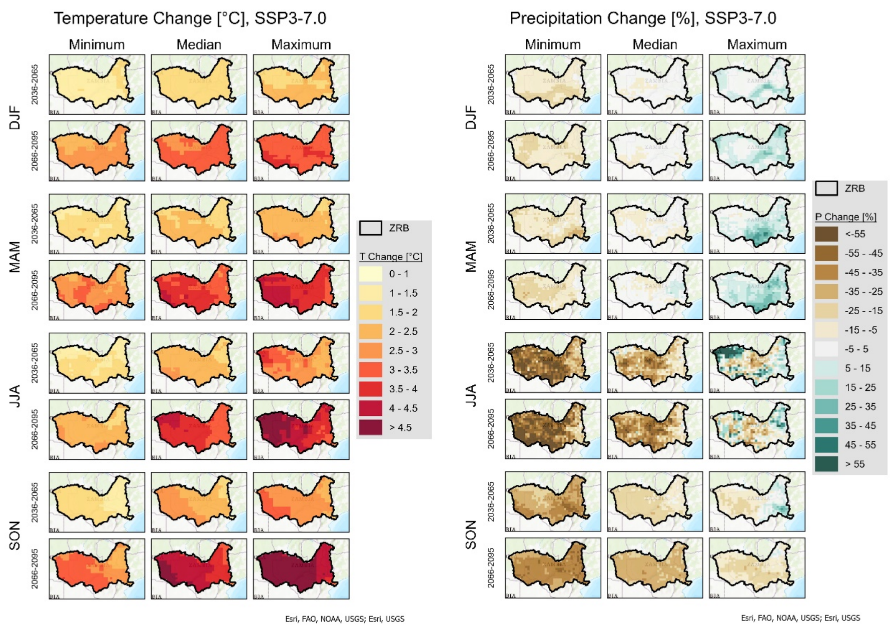

Figure 40. Seasonally projected changes in temperature (left panel) and precipitation (right panel) for mid (2036-2065) and late (2066-2095) century for climate scenario SSP3-7.0. The maps in each column show the minimum, median and maximum changes in the Zambezi watercourse among the model ensemble members for the scenario. Units of temperature change are

the direct difference in °C between the historical scenario (1979-2014), and the relevant period in the future scenario. Units for precipitation are in percentage change relative to the historical scenario.

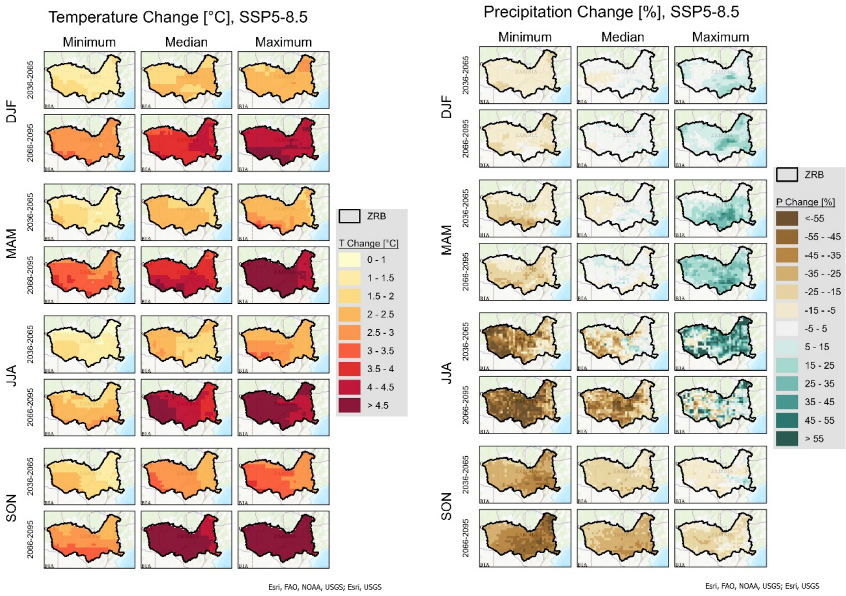

Figure 41. Seasonally projected changes in temperature (left panel) and precipitation (right panel) for mid (2036-2065) and late (2066-2095) century for climate scenario SSP5-8.5. The maps in each column show the minimum, median and maximum changes in the Zambezi watercourse among the model ensemble members for the scenario. Units of temperature change are the direct difference in °C between the historical scenario (1979-2014), and the relevant period in the future scenario. Units for precipitation are in percentage change relative to the historical scenario.

Hydrological modelling

The high-resolution model of ZWC (depicted in Figure 42) covers a total extent of approximately 1,400,000km^2 and consists of 1,661,000 inter-connected cells with a spatial resolution of 1km^2. The model has been configured to run at a daily time-step selected to match the daily time resolution of the climate scenario inputs from WP2.

There are four sub-models that are forced only by the WP2 climate and socio-economic scenarios (Upper ZWC, Kafue, Shire, Luangwa). The simulated streamflow from these sub-models enters the Core ZWC sub-model at distinct single-entry points defined according to the watersheds obtained from the HydroSHEDS v1 1km^2 DEM (Lehner et al., 2006). The sub-basin connection points were selected based on the location of flow observation stations with relatively long and complete historical records.

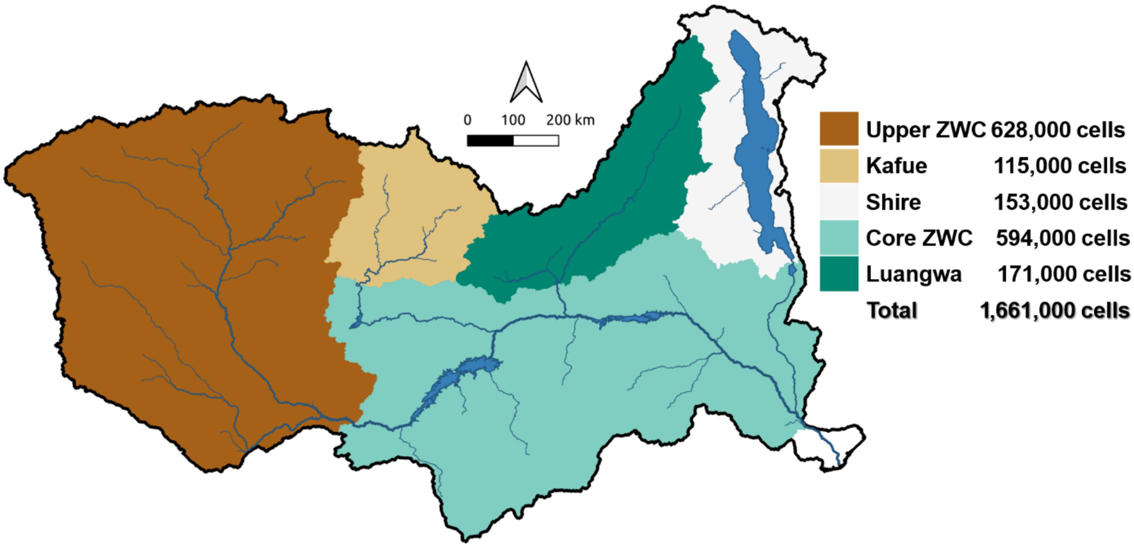

Figure 42. Spatial extent and number of model grid cells for each of the five sub-models comprising the high-resolution hydrological model of ZWC. The connection points of each sub-model domain approximately coincide with flow gauges that have the longest and most complete records of streamflow in the basin.

The Core ZWC sub-model (Figure 43) contains the major existing and planned reservoirs, which are large enough to shift the seasonal flow regime depending on their operation policies. This sub-model has 8 structural configurations of the main reservoirs matching the MORDM reservoir operation policies.

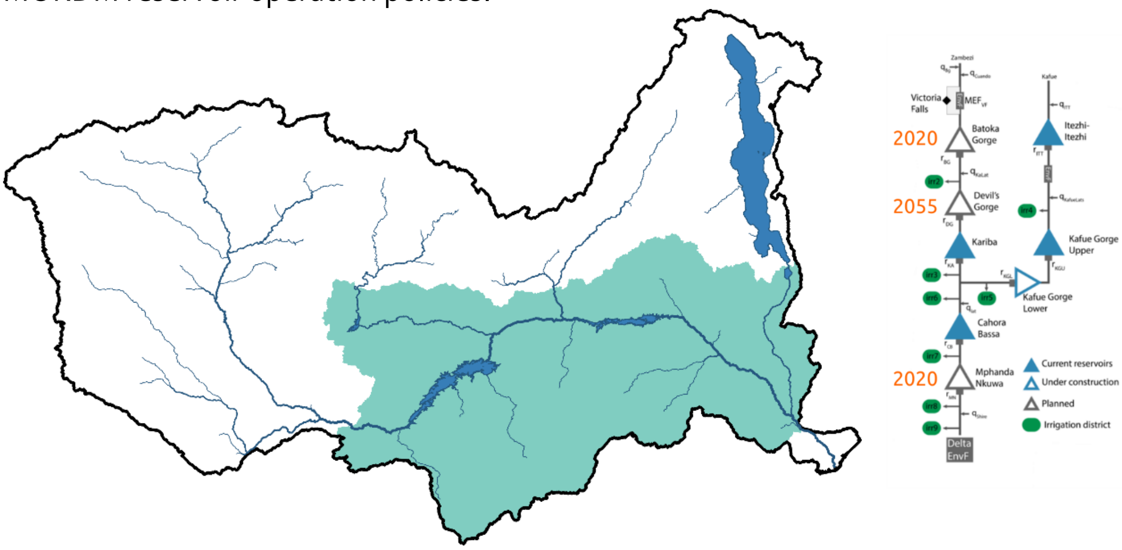

Figure 43. An illustration of the implementation of MORDM designed infrastructure timing into the TOPKAPI-ETH model of the Zambezi watercourse (ZWC).

MORDM operation policies have been implemented in the TOPKAPI-ETH model of Zambezi watercourse for several configurations of existing and planned reservoirs, matching the MORDM configurations described elsewhere in this report. 4445444544

4.1.2.2 Application Results

Due to the developmental nature of the methodology, and complexity of the high-resolution modelling effort, sufficiently mature application modelling results were not available at the time of this deliverable. Instead, the relevant modelling results are targeted for reporting in the WP5 WEFE evidence deliverables D5.6 and D5.7.

4.2 Many-objective Robust Decision Making

4.2.1 Lake Como

4.2.1.1 Application Development

4.2.1.1.1 Overview

A simulation model of the reservoir operations at the daily time step, the Lake Como Design Model, has been developed to conduct MORDM for the Lake Como Basin. The model receives as input the water flow drained by the lake and computes its dynamics. The water released from the lake is distributed to the agricultural districts for irrigation and to same existing hydropower plants. These processes have been modelled by means of a water distribution model of the main river steam and the canals that actually divert the flow to the districts and plants. In addition, the crop yield and production have been estimated by IdrAgra (Gandolfi et al., 2011), a conceptual model for the simulation of irrigation and crop production of irrigated areas.
The Lake Como Design Model allows to develop Pareto-optimal sets that jointly consider planning and management actions, evaluating the robustness of each combination against present and future climate. The planning action here considered is the definition of the Lake Como operating space, i.e., the range of level within which the operator can actually decide the daily amount of water to be released. If the level is higher than the range upper bound, the legislation requires to completely open the dam gates. Conversely, below the lower bound, the gates must be closed. A redefinition of the operating space is necessary due to the positioning of new barriers in the city of Como, which have significantly risen the flooding threshold. In addition, for a given operating space, the lake management has to be defined.
Three WEFE objectives are considered for the Lake Como Basin, namely the water deficit of the downstream users and the frequency of flooding events in Como as well as that of the lake low levels.

4.2.1.1.2 Lake Como Design Model

To derive the Pareto-optimal set of planning and management actions a widely used simulation-optimization framework is adopted: Evolutionary Multi-Objective Direct Policy Search (EMODPS) (Giuliani, Castelletti, et al., 2016). First, it requires to define a simulation model that computes the value of some objectives (representative of the stakeholders interests) starting from an initial state of the system (lake level), the trajectories of deterministic (water demand) and stochastic (lake inflow) disturbances. Then, an evolutionary (usually genetic) algorithm is used to iteratively search an optimal planning decision or management strategy.
System simulation
The dynamics of Lake Como are described through the water balance:

$$s_{t+1} = s_t + i_{t+1} - r_{t+1}$$

being s_t and s_{t+1} the lake storage at time t and $t+1$, $i_{t+1}$the net inflow (it already includes losses such as those due to evaporation and infiltration) into the lake between time t and $t+1$, and r_{t+1} the release in the same time interval. The actual release r_{t+1} is modeled through a stochastic and nonlinear relationship of the release decision u_t. The releases from the Olginate dam are indeed constrained by the minimum (N^{min}) and maximum (N^{max}) release functions, which respectively define the minimum and maximum outflow from the lake for each possible level. These functions are mathematically defined as follows:

$$N^{min} = \begin{cases} 0 & se\ h_t < h^{lb} \\ q_t^e & se\ h^{lb} \leq h_t < h^{ub} \\ 3.37\,(h_t + 2.5)^{2.015} & se\ h_t \geq h^{ub} \end{cases}$$

$$N^{max} = \begin{cases} 0 & se\ h_t < h^{lb} \\ 1534\,h_t + 623.37 & se\ h^{lb} \leq h_t < h^{lb} + 0.1\,m \\ 3.37\,(h_t + 2.5)^{2.015} & se\ h_t \geq h^{lb} + 0.1\,m \end{cases}$$

being h_t the lake level on day t at 8 am and q_t^e the minimum environmental flow. h^{lb} and h^{ub} defines the lower and upper bound of the operating range, respectively. Below h^{lb} the dam gates must be closed, while above h^{ub} they must be completely opened. In between h^{lb} and h^{ub} decisions on the release can be made, however they cannot be lower than N^{min} or higher than N^{max}:

$$r_t = \min\,(N^{max}, \max\,(N^{min}, u_t))\Delta t$$

The decision on the release u_t is the output of the so-called operating policy, a function that takes in input the lake level h_t and two periodic signals that provide information on the time of the year:

$$u_t = p_\theta\big(h_t, sin(2\pi t/365), cos(2\pi t/365)\big)$$

θ is a vector of parameters that define the shape of the policy, which is specifically selected to be highly flexible. In this case, a network of radial basis functions has been used, as suggested in Giuliani et al. (2016).
Under the assumption to have available the policy parameters θ and the operating space limits (h^{lb} and h^{ub}), the system can be simulated starting from an initial level to generate the level and release trajectories for a time horizon of length H. From them, the numerical values of the objectives can be computed:

- Flood control - number of days per year with an exceedance of the flooding threshold (h^f) in Como,

  $$J^{flo} = \frac{1}{N_y}\sum_{t=1}^{H} \Gamma\,(h_t > h^f)$$

  where N_y is the number of years of the simulation horizon and

  $$\Gamma(h_t > h^f) = \begin{cases} 1 & if\ h_t > h^f \\ 0 & otherwise \end{cases}$$

- Low level prevention - number of days per year with lake level below low-level threshold ($h^l = -0.2\ m$),

  $$J^{low} = \frac{1}{N_y}\sum_{t=1}^{H} \Gamma\,(h_t < h^l)$$

where

$$\Gamma(h_t < h^l) = \begin{cases} 1 & if\ h_t < h^l \\ 0 & otherwise \end{cases}$$

- Downstream deficit minimization:

$$J^{def} = \frac{1}{H}\sum_{t=1}^{H} \max\left(\left(w_t - (r_t - q_t^e)\right)^n, 0\right)$$

where w_t is the downstream water demand that represents both the needs of the agricultural districts and of the hydropower plants. The exponent n is equal to 2 during the irrigation season (conventionally from Aprile, 1st to October, 10th) and equal to 1 for the rest of the year. In this way, deficits (especially the most critical) are weighted more during the irrigation season, when many mild shortages are preferred to few severe ones.

Depending on the width of the operating space (defined by h^{lb} and h^{ub}) and on the flooding threshold (h^f) we can distinguish between 3 alternative actions:

- Alternative 0 (A0), that represents the current situation with $h^{lb} = -0.4\ m$ and $h^{ub} = h^f = 1.1\ m$;
- Alternative 1 (A1), that considers the new flooding threshold ($h^f = 1.73\ m$) established after the installation of the barriers in Como. This allows to restore the operating space ($h^{lb} = -0.4\ m, h^{ub} = 1.3\ m$) set by the legislation, which have been lowered in the past decades due to the subsidence affecting some areas in the city of Como;
- Alternative 2 (A2), that takes advantage of the new barriers in Como to increase the flooding threshold as in A1 and does not fix h^{lb} and h^{ub} a priori but optimize them as two additional parameters to be added to those defining the policy (vector θ).

Optimization

The EMODPS problem has been solved using Borg (Hadka & Reed, 2013), an adaptive genetic algorithm that represent the state of the art in the field (Al-Jawad & Tanyimboh, 2017; Liu & He, 2023). Practically speaking the optimization problem is defined as follows:

$$\theta^* = \arg\min_{\theta}\left[J^{flo}, J^{low}, J^{def}\right]$$

where θ^* represent the optimal set of policy parameters θ. This formulation can be used to solve the problem adopting A0 as well as A1, because the only variables to be optimized are the policy parameters.

As said, the larger operating space resulting from the presence of barriers opens up the possibility of revising the regulation range with respect to that of A0 and A1. In this case, the management problem can be solved together with the planning problem, meaning that the lower and upper bounds of the operating space must be added to the optimization vector $\bar{\theta} = [\theta,\ h^{lb},\ h^{ub}]$ (A2):

$$\bar{\theta}^* = \arg\min_{\bar{\theta}}\left[J^{flo}, J^{low}, J^{def}\right]$$

4.2.1.2 Application Results

4.2.1.2.1 Historical Horizon

The optimization problem produced the Pareto fronts for the historical period 2000-2021, with the configurations presented as A0, A1 and A2 (Figure 46). The figure show that A1 and A2 clearly dominate A0: both allow to obtain better solutions in terms of flooding (left), downstream deficit (bottom), and low levels (dark blue).
The increase of the operating range upper bound to 1.3 m and of the flooding threshold to 1.73 m (A1) strongly reduce the conflict between the objectives (they span a relatively small range of values considering each objective). A2 is almost equivalent to A1. The main difference is that it is able to decrease the deficit indicator of about 10% with respect to A1, but with a concurrent increase of the frequency of the flooding occurrence.

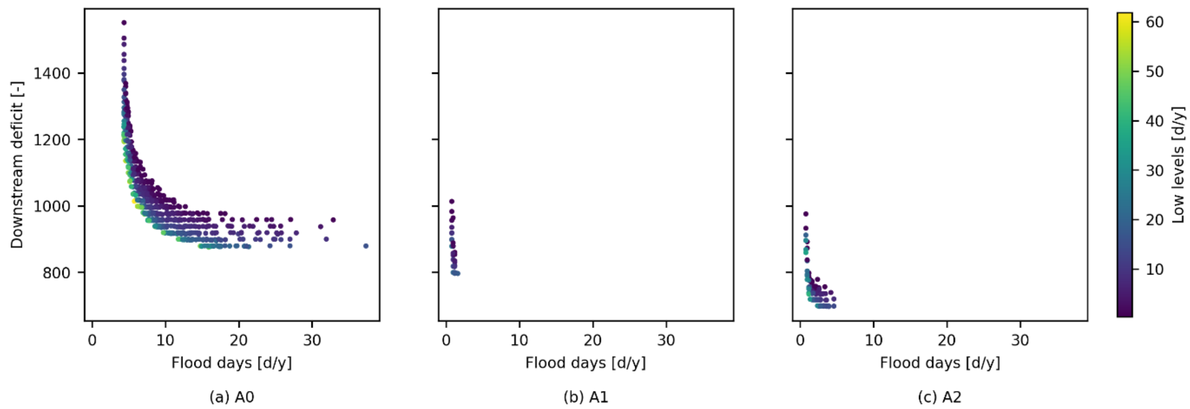

Figure 46. Comparison of the Pareto fronts obtained for the three alternatives A0 (a), A1 (b), and A2 (c) on the historical horizon (2000-2021).

The comparison between the three alternatives can be performed also considering single compromise solutions (Figure 47) instead of the whole set of Pareto efficient solutions. The results reported in Figure 47 confirms the insights discussed before. The objective values obtained with A1 and A2 are substantially equivalent unless some numerical difference. The same goes for the optimized values of h^{lb} (+ 0.016 cm with respect to A1) and h^{ub} (+ 6.78 cm with respect to A1).

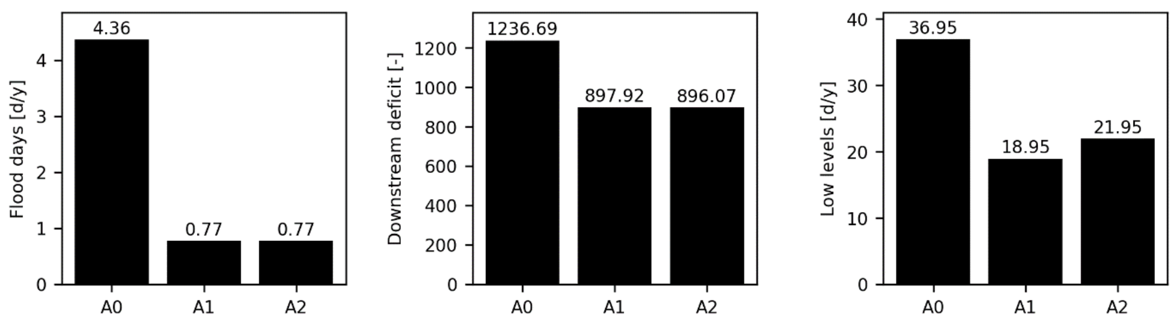

Figure 47. Comparison of the performance of three compromise operating policies: A0 (a), A1 (b), and A2 (c) on the historical horizon (2000-2021).

4.2.1.2.2 Future scenarios

The solutions found for the historical horizon must be evaluated on future scenarios to test their robustness to the variations of the hydro-meteorological regime caused by the climate change. A schematic representation of the future scenarios' features is reported in Figure 48. We specifically considered the following features to allow meaningful comparisons between the combinations:

- two horizons, one representative of the mid-term future (2039-2060), the other at the end of the century (2079-2100).
- three RCPs. A very stringent mitigation scenario (RCP2.6), an intermediate scenario (RCP4.5), and the one usually considered as a worst-case scenario (RCP8.5).
- three combinations of global and regional circulation models (ICHEC+RACM, ICHEC+RCA4 and MPI+RCA4). Comparing ICHEC+RACM and ICHEC+RCA4 we can isolate the contribution of the regional model, while the comparison between ICHEC+RCA4 and MPI+RCA4 quantifies the contribution of the global model.
- three planning and management alternatives (A0, A1 and A2).

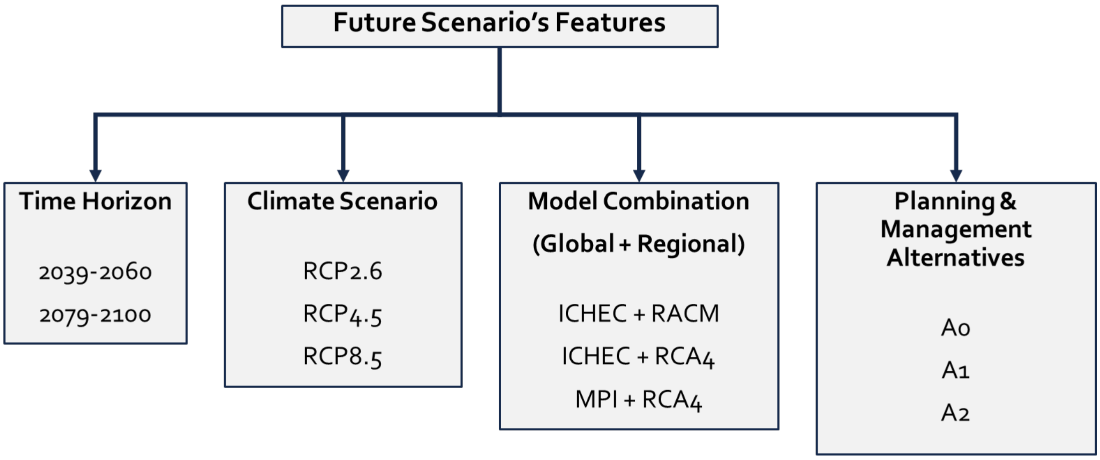

Figure 48. Aspects of the future scenarios considered in the study: two horizons, three RCPs, three combinations of global and regional circulation models, three planning and management alternatives.

Figure 49 shows the average temperature and precipitation of historical data (2006-2013) and of the 18 future scenarios considered.

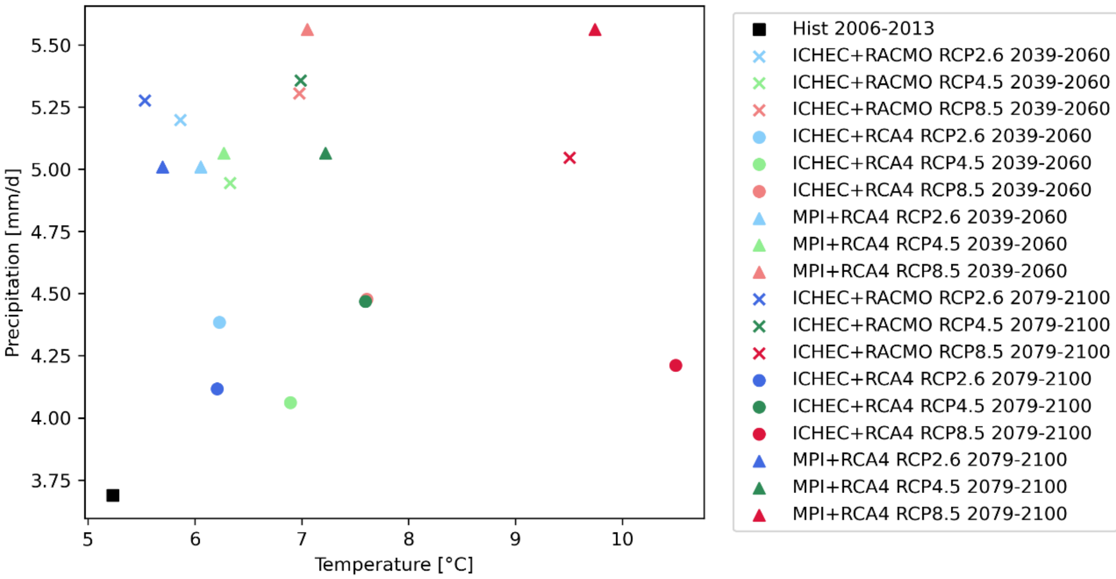

Figure 49. Average temperature and precipitation of the 18 future scenarios considered (3 combinations of global and regional climate models, 3 RCPs, and 2 time horizons). The historical averages for the period 2006-2013 are reported for comparison. Mid-term horizon is represented in lighter tones, long-term in darker tones. RCP2.6 is in blue, RCP4.5 in green, and RCP8.5 in

red. Each combination of global and regional climate models has a different symbol (cross for ICHEC+RACMO, circle for ICHEC+RCA4, and triangle for MPI+RCA4).

All the combinations produce warmer and wetter climates with respect to the historical data. The range of temperature and rainfall covered is quite broad. Temperature spans from around 5.5 to 10.5 °C, while precipitation is expected to be in the range from 4 to 5.5 mm/d. As expected, temperature is primarily influenced by the combination of RCP and time horizon. RCP2.6 and RCP4.5 has similar temperature in the period 2039-60 and exhibit opposite trends in the longer term (2079-2100). The temperature slightly decreases in RCP2.6 as effect of the emissions decline (for instance, CO_2 projected emission goes to zero by 2100), while there is a small increase in RCP4.5. RCP8.5 is the most critical scenario, with a temperature increasing to 7°C by mid-century and to around 10°C in 2079-2100. The combination of global and regional climate model does not seem to affect the temperature variation significantly. However, ICHEC+RACMO is usually a little cooler than MPI+RCA4, and ICHEC+RCA4 turns out to be the warmer case. The regional model has thus a stronger influence on temperature (RCA4 is warmer than RACMO) than the global model.
Repeating the same analysis for the precipitation, the combination of global and regional climate models is much more relevant than the RCP and time horizon. ICHEC+RCA4 is by far the drier case, while ICHEC+RACMO and MPI+RCA4 are essentially equivalent. It is thus the combination of global and regional model that affects the rainfall rates, and our analysis does not allow to identify which of the two has a more relevant role. Analysing the effect of different RCPs and time horizons, no significant patterns emerge.
To evaluate the performance of the planning and management strategies found with the optimization in the historical period, we can simulate them on the future scenarios. The results obtained for the climate model combination ICHEC+RCA4 for the horizon 2039-2060, considering the three RCPs are reported in Figure 50 (RCP2.6), Figure 51 (RCP4.5), and Figure 52 (RCP8.5).
The comparison between the panels of each figure shows the same pattern obtained for the historical period 2020-2021 (Figure 46). A1 and A2 are almost equivalent and clearly dominate A0, proving that the enlargement of the operating space and the flooding threshold elevation to 1.73 m strongly improve the situation. However, the future hydro-

meteorological regimes are expected to exacerbate the conflict between the three objectives.

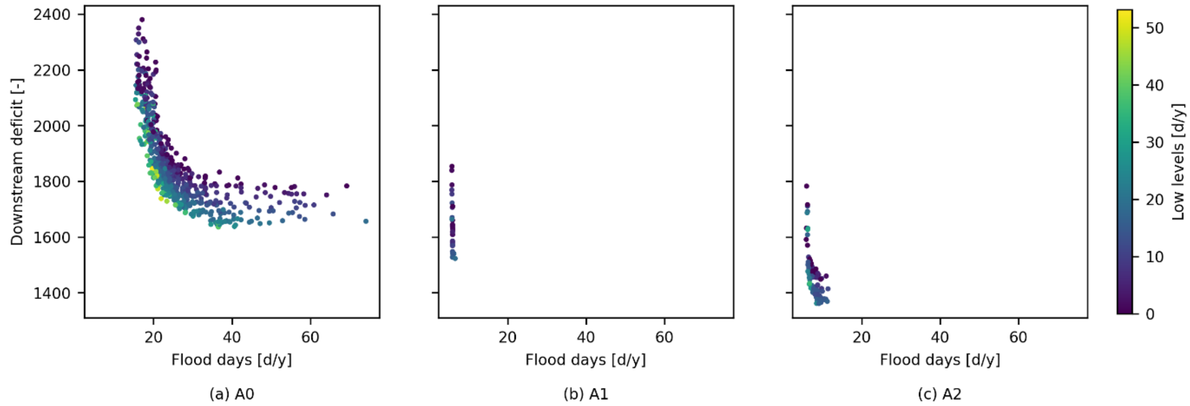

Figure 50. Comparison of the Pareto fronts obtained for the three alternatives A0 (a), A1 (b), and A2 (c) on the future horizon (2039-2060) with the climate model combination ICHEC+RCA4 and RCP2.6.

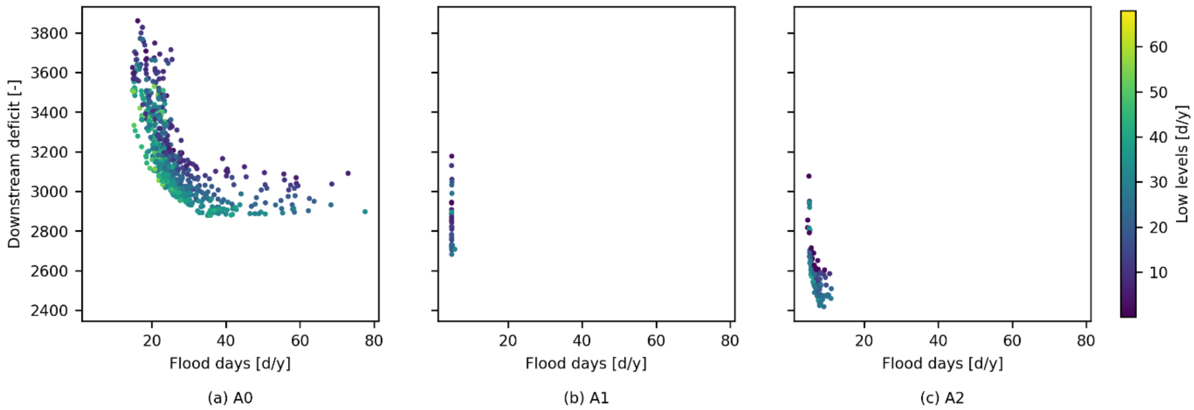

Figure 51. Comparison of the Pareto fronts obtained for the three alternatives A0 (a), A1 (b), and A2 (c) on the future horizon (2039-2060) with the climate model combination ICHEC+RCA4 and RCP4.5.

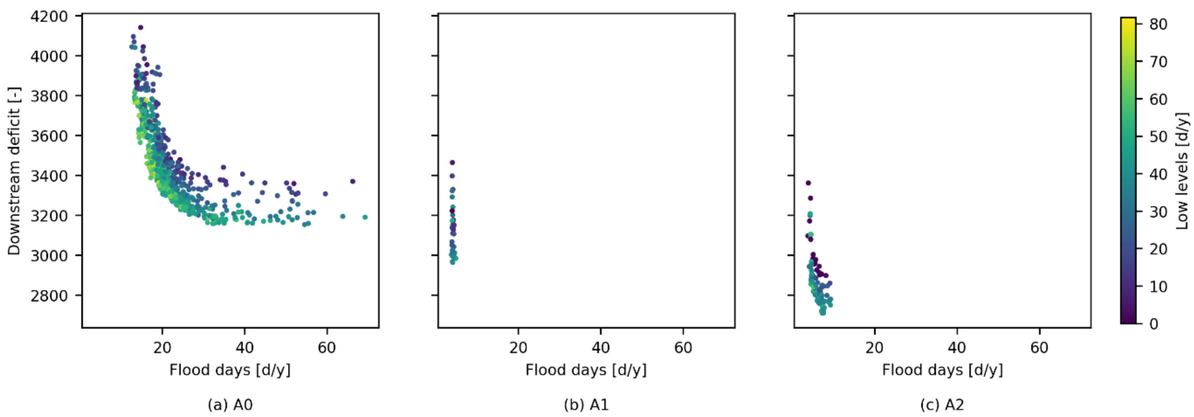

Figure 52. Comparison of the Pareto fronts obtained for the three alternatives A0 (a), A1 (b), and A2 (c) on the future horizon (2039-2060) with the climate model combination ICHEC+RCA4 and RCP8.5.

A more extensive comparison including all the future scenarios presented (see Figure 48) is reported in Figure 53, where the objectives' values obtained by the compromise solution for A0 are reported. The top panel shows a dramatic increase of the floodings in all the

considered scenarios, spanning the range from 13.36 d/y (+206 % wrt the historical horizon) to more than 2 months per year (63.59 d/y in the most critical scenario, RCP8.5 at the end of the century). The high frequency of flood events is probably due to the increase of extreme rainfall events that produce large inflow into the lake in relatively short time periods. In the scenarios characterized by mild changes, these water flows have a positive effect for at least one of the other objectives (see downstream deficit in the middle panel and low levels in the bottom panel). Conversely, in the most critical scenarios (see, for instance, ICHEC+RCA4 with RCP8.5 at the end of the century), all the three objectives are much worse: flood days per year increase from 4.36 to 22.91, downstream deficit from 12.37 to 7727, and low level from 36.95 to 96.59 d/y.
The results reported in Figure 53 thus show that there is a high uncertainty on the future system conditions. However, despite this uncertainty, the effect of all the considered future projections is expected to be critical.

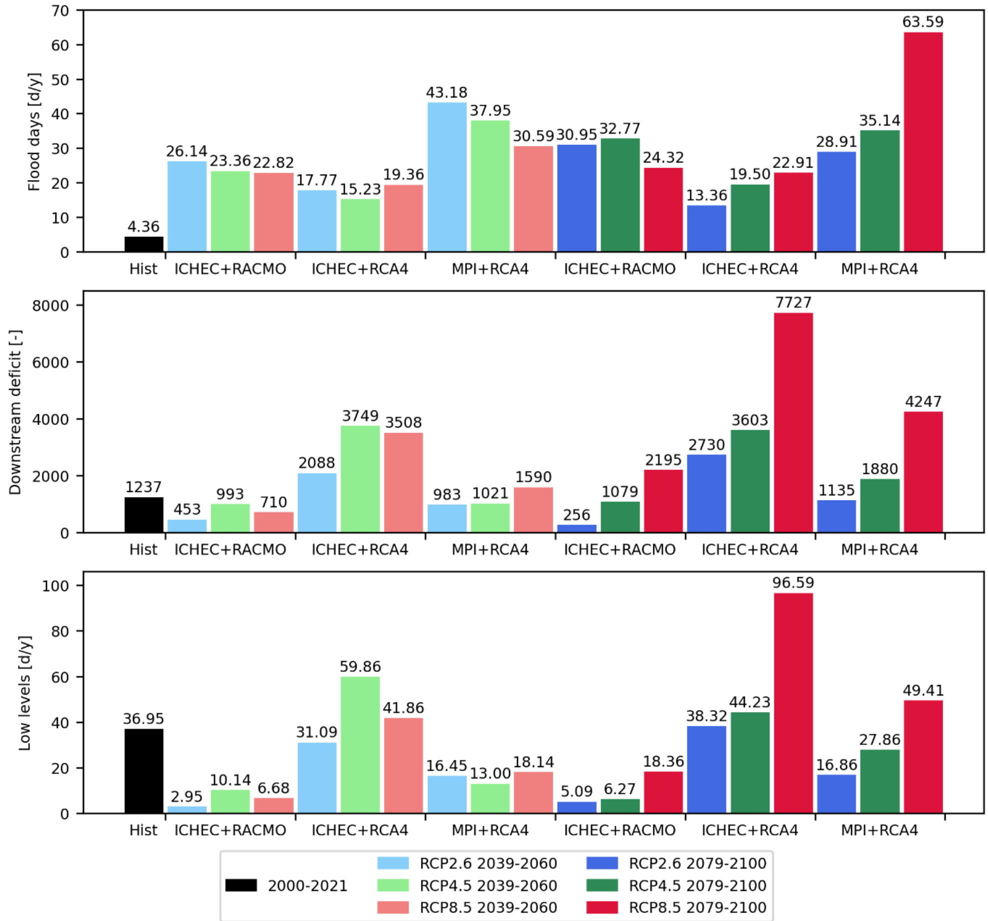

Figure 53. Flood days, downstream deficit and low levels obtained with a compromise policy for the alternative A0. The objectives are evaluated on the historical horizon and on the 18 future scenarios.

The same analysis can be repeated for the compromise solution relative to A1 (see Figure 54, where the A0 performance are reported as diagonal hatched bars for comparison). The effect of the infrastructural ($h^f = 1.73\ m$) and normative ($h^{ub} = 1.3\ m$) changes is significant for all the three objectives. In particular, the flooding events are strongly reduced with respect to the corresponding scenario with alternative A0: from 13.36 to 2.73 d/y in the best case, from 63.59 to 14.45 d/y in the worst case. As for the results of Figure 24, there is a high uncertainty related to all the features of the future scenario.

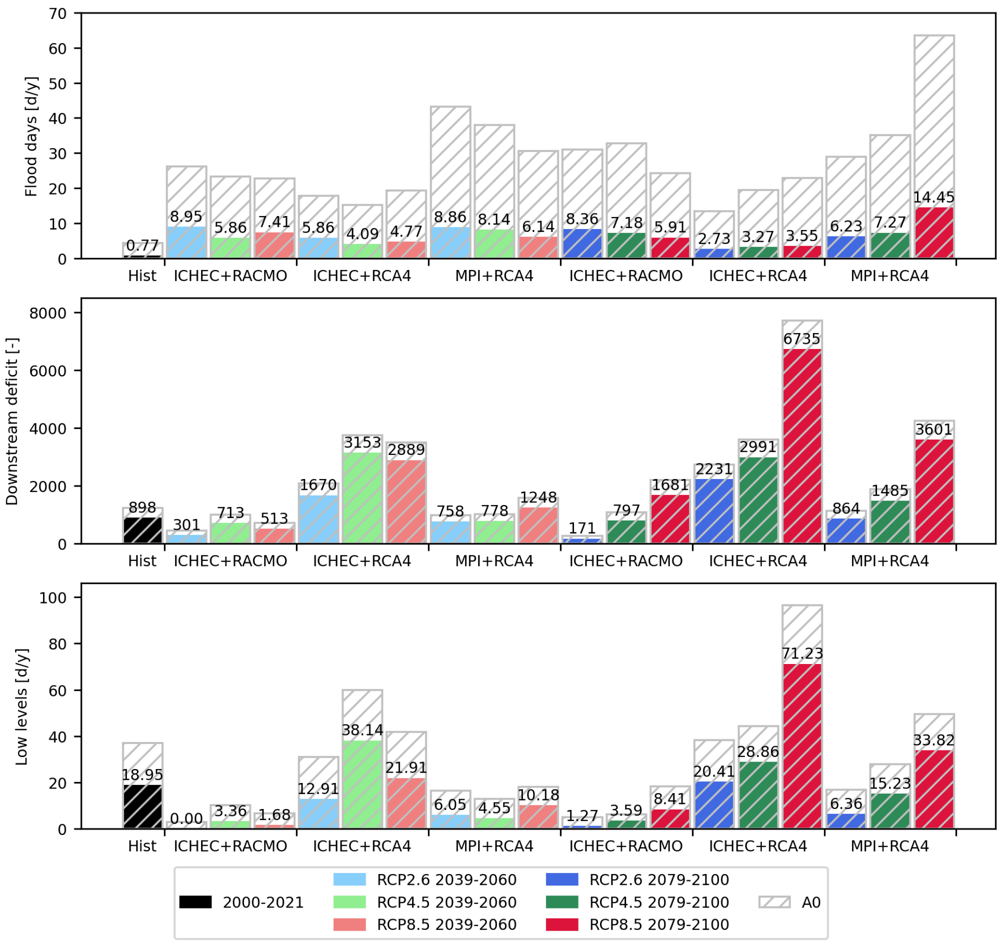

Figure 54. Flood days, downstream deficit and low levels obtained with a compromise policy for the alternative A1. The objectives are evaluated on the historical horizon and on the 18 future scenarios. A0 performance (diagonal hatched bars) is reported for comparison.

Figure 55 reports the comparison between the compromise solution for A2 (colored bars) and A1 (diagonal hatched bars). Again, the two alternatives are almost equivalent. The small operative space extension of A2 ($h^{ub} = 1.3678\ m$, thus 6.78 cm higher than in A1) allows to reduce the frequency of low levels but slightly increases the number of flood events.

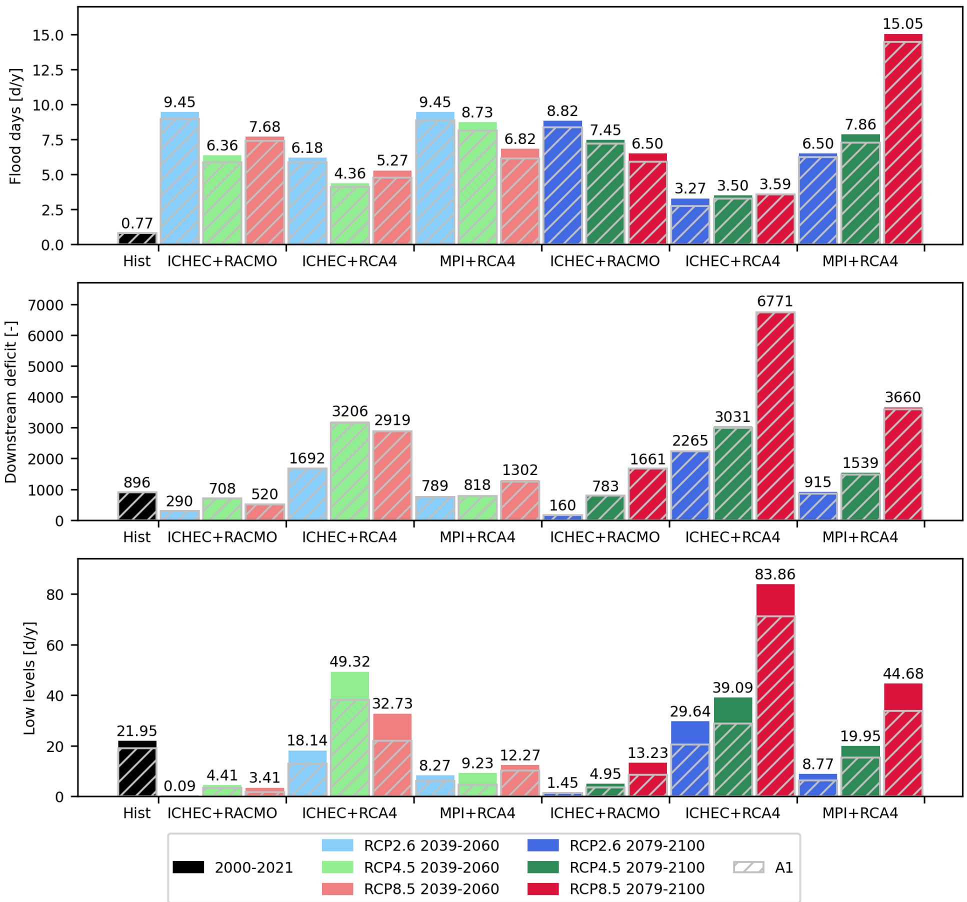

Figure 55. Flood days, downstream deficit and low levels obtained with a compromise policy for the alternative A2. The objectives are evaluated on the historical horizon and on the 18 future scenarios. A1 performance (diagonal hatched bars) is reported for comparison.

4.2.1.2.3 Robustness against drought events

To further investigate the capacity of the system to deal with future hydro-meteorological regimes, we perform a robustness analysis by perturbing the historical inflow to Lake Como following the approach presented in Zaniolo et al (2023). It allows to generate scenarios of arbitrary length with controlled statistical features following a two-step procedure. First, we extract a random time series from a desired statistical distribution of streamflow (e.g., fitted from historical streamflow data), and then use Simulated-Annealing (Kirkpatrick et al., 1983) to refine such time series until it matches some user-specified parameters.

The definition of these parameters is based on the Standardized Runoff Index (SRI), a drought index computed on a runoff trajectory where each value is the standardized deviation in the streamflow magnitude of a certain time step with respect to the average (Amin Zargar et al., 2011). Zaniolo et al (2023) identified the following key properties:

- persistence, the total duration of a dry spell.
- intensity, the mean value of the SRI during a drought.
- frequency, the number of droughts in the considered period.

We identify a drought as a period of 2 months or longer where SRI is negative (meaning that the streamflow is lower than average). The drought persistence is then defined as the total duration (in months) of a dry spell.

Figure 56 shows the SRI time series computed for the historical horizon 2000-2021. Four relevant droughts have been identified, with average persistence and intensity equal to 12.75 months per drought and -0.902, respectively.

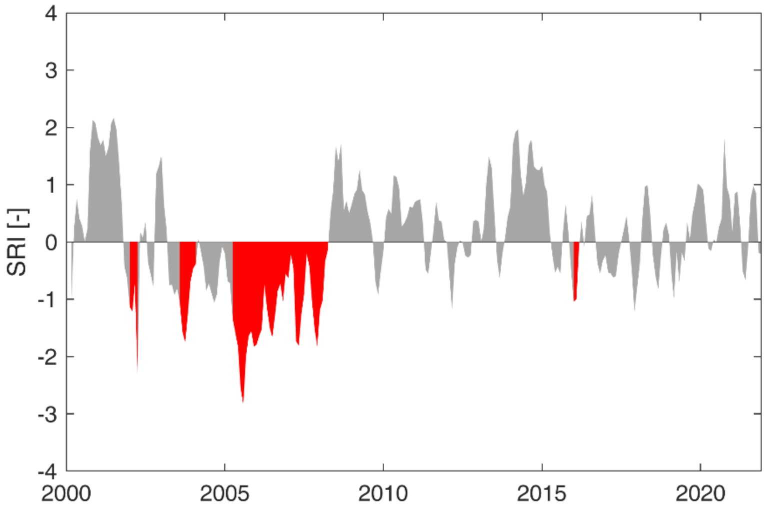

Figure 56. SRI drought index computed for inflow into Lake Como in the historical period 2000-2021. The hydrological droughts are highlighted in red. Drought features: 12.75 (persistence), -0.902 (intensity) and 4.0 (frequency)

Based on the historical drought characteristics, we defined the variability range of the three parameters. The duration is varied from 11.48 (0.9 times the average historical duration) and 40.70 (1.1 times the maximum observed value). The intensity from -1.328 (1.1 times the historical minimum) and -0.812 (0.9 times the observation average). The number of droughts from 3.2 and 4.8 (0.8 and 1.2 times the number of droughts from 2020 to 2021). Latin Hypercube Sampling (LHS) is used to obtain evenly distributed samples in the parameter space define above. The results of 100 LHS is reported in Figure 57.

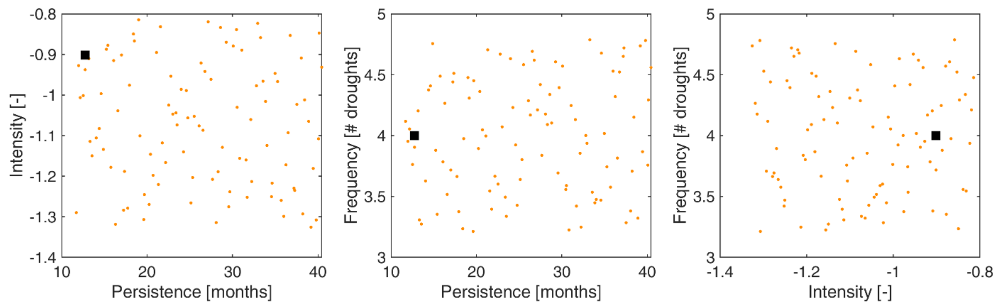

Figure 57. One hundred LHS samples (orange points) in the 3-dimensional space (intensity; persistence; frequency). The value representative of the historical period 2000-2021 is reported for comparison (black square).

In this way, it is possible to produce 100 synthetic scenarios with desired parameters. Each inflow trajectory is then fed into the simulation model replacing the historical inflow to compute the indicators for floods, downstream deficit, and low levels under the alternatives A0, A1 and A2. The results obtained from these simulations are reported in Figure 58 using the same visualization of Figure 54. It is worth stressing the main difference between the two approaches. In Figure 54 scenarios from future climatic projections (downscaled to the area of interest), while in Figure 58 they are synthetically generated perturbing the historical inflow time series.

Considering the alternative A0 (diagonal hatched bars in Figure 58), the situation is more critical with respect to the historical simulation in 73 scenarios over 100 for the downstream deficit and in 80 scenarios considering the low levels. There is also a remarkable number of scenarios where the indicators values increase of more than 50% with respect to history (18 for the deficit, 16 for low levels). As expected, the number of flood days generally lower than the historical value (it happens in 59 scenarios over 100). However, there are many scenarios characterized by critical regimes in terms of floods: in 36 scenarios over 100 are more than 5 flood days per year, and in 3 of them the limits of 10 flood days per year is exceeded. This last point has a high impact on the lake operation since it suggests that an overall reduction of the water volumes drained by the basin does always imply a decrease of the risk associated to inundations and floods. In Fact, in 22 synthetic scenarios over 100, both the downstream deficit and the frequency of floods increase. Similar insights can be derived for the alternative A1 (orange bars in Figure 58).

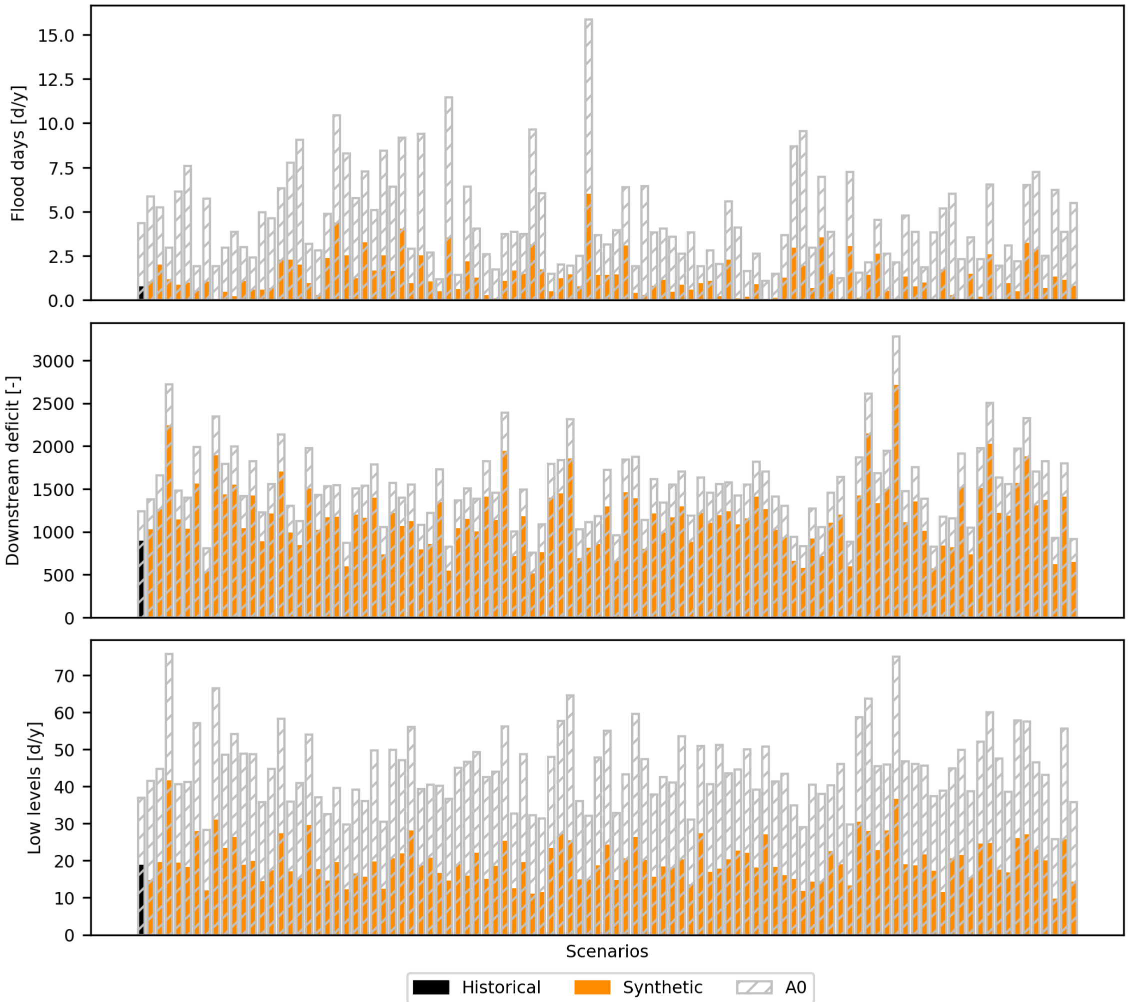

Figure 58. Flood days, downstream deficit and low levels obtained with a compromise policy for the alternative A1. The objectives are evaluated on the historical horizon and on 100 synthetic scenarios. A0 performance (diagonal hatched bars) is reported for comparison.

The comparison between the three alternatives (A0, A1 and A2) confirms the insights already derived with historical inflow and future projections. A1 provides a remarkable improvement in terms of floods, downstream deficit, and low levels with respect to A0 for all the 100 synthetic scenarios (orange bars are always lower than hatched bars in Figure 58). A1 and A2 are substantially equivalent in all the synthetic scenarios (figure not reported here for the sake of brevity).
To conclude the robustness analysis, we investigate the relationship between the features of a drought and the corresponding objectives obtained through the system simulation. The first scenario considered is that producing the higher number of flood events. Its SRI trajectory (see Figure 59) shows that it is characterized by an alternance of strongly wet and dry periods. The intensity of both wet and dry period is much higher than in the historical period (compare Figure 59 and Figure 56). The average intensity of the dry spells is more critical (-1.143) if compared to that of the observed inflow (-0.902). The other two drought features (persistence is equal to 13.00 and frequency to 4) are almost identical to the historical (12.75 and 4, respectively).
Simulating the system with the synthetic inflow scenario, it is possible to compute the corresponding objectives. For instance, under A1, the frequency of floods dramatically increases to 6.00 days per year (against 0.77 with the historical inflow). The strong increase of the peaks in the inflow allows to store water which contrasts the 4 dry spells: The downstream deficit decreases to 811.99 (from the historical value of 897.92) and the low-level indicator is to 14.95 days/year (from 18.95).

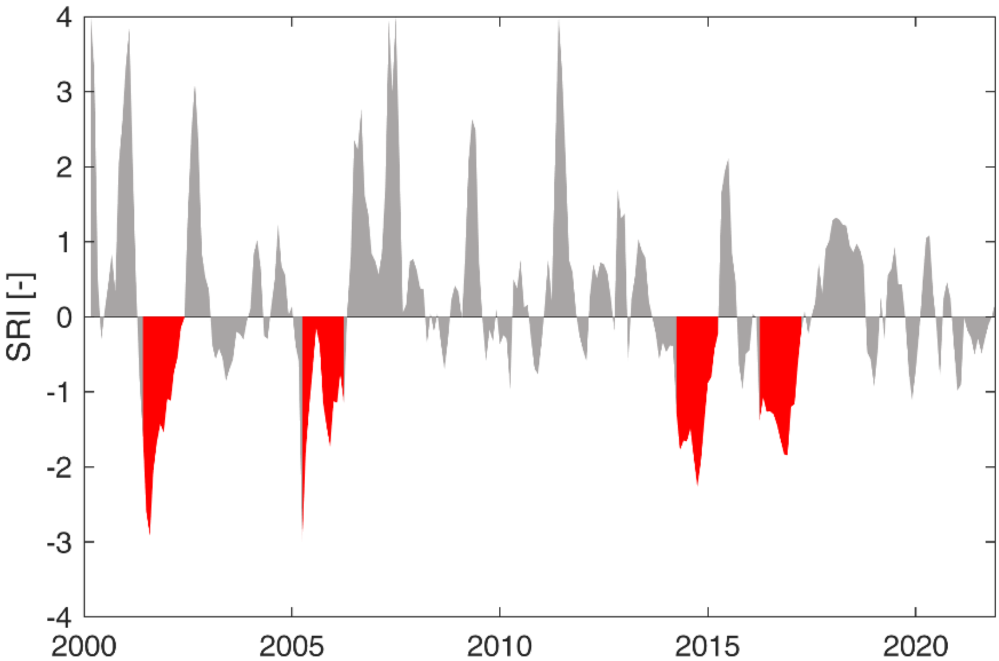

Figure 59. SRI drought index computed of the scenario that generates the most critical value of the floods indicator. The hydrological droughts are highlighted in red. Drought features: 13.0 (persistence), -1.143 (intensity) and 4.0 (frequency).

The scenarios that generate the most critical situation for downstream deficit (Figure 60) and low levels (Figure 61) are characterized by extreme values of persistence (around 3 years, three times the historical value), intensity (around -1.3) and frequency (5 droughts in the 22-year period). In both the scenarios, 3 of the 5 dry spells are so close that could be also considered as a single long-lasting event with a couple of relaxed months in between. Even when under A1, the hydrological regimes of these scenarios are so critical that the downstream deficit reaches a value of 2714.04 (+200% of the historical value) and the frequency of low levels increases to 41.73 days/year (+120%).

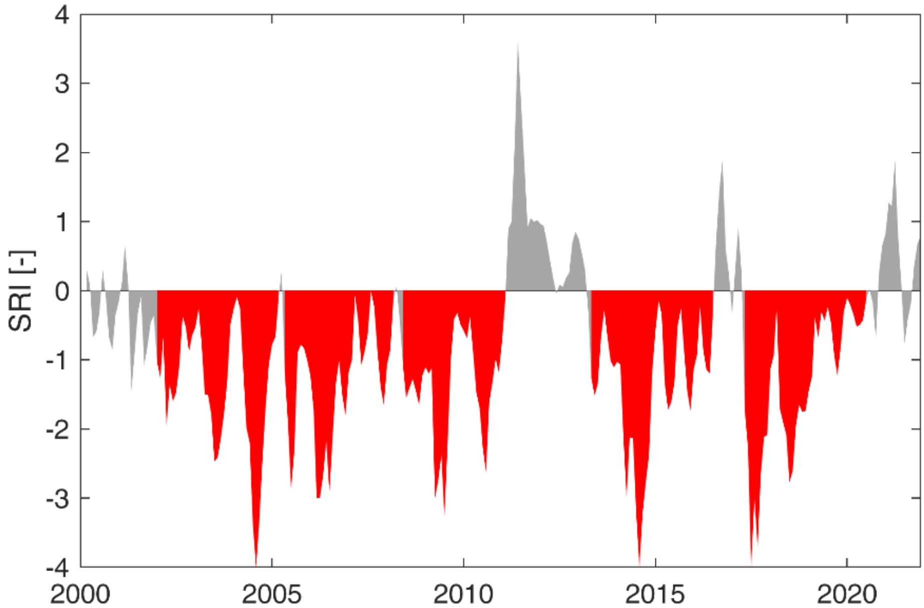

Figure 60. SRI drought index computed of the scenario that generates the most critical value of the downstream deficit indicator. The hydrological droughts are highlighted in red. Drought features: 37.0 (persistence), -1.321 (intensity) and 5.0 (frequency).

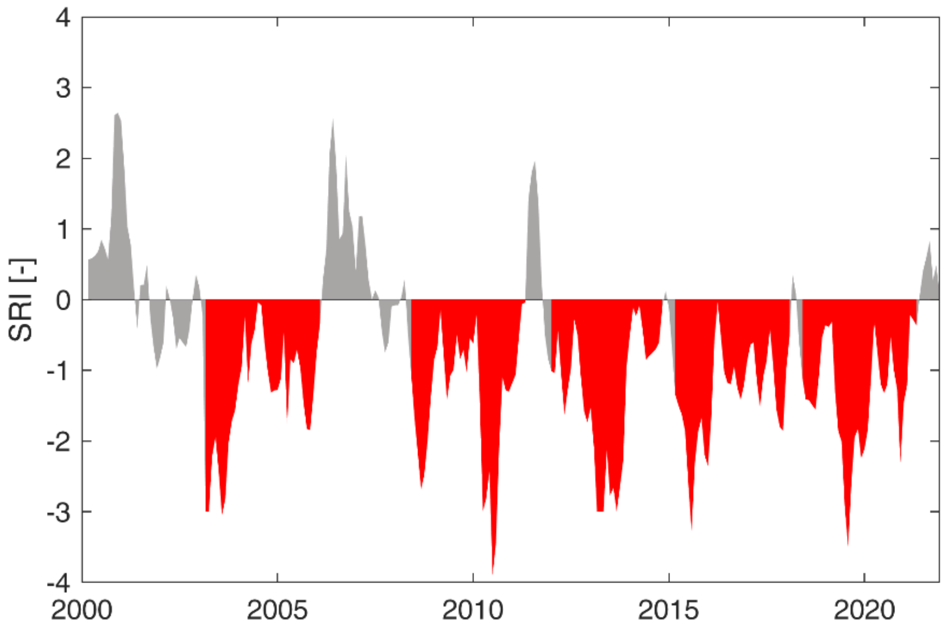

Figure 61. SRI drought index computed of the scenario that generates the most critical value of the low-levels indicator. The hydrological droughts are highlighted in red. Drought features: 35.0 (persistence), -1.300 (intensity) and 5.0 (frequency).

The proposed framework allows to quantify the response of the system (in terms of stakeholders' satisfaction) considering a comprehensive set of future hydroclimatic conditions (combining different temporal horizons, RCPs, global and regional circulation models) as well as synthetically generated scenarios spanning a wide range of droughts features.

4.2.2 Zambezi Watercourse

4.2.2.1 Application Development

4.2.2.1.1 Overview

A monthly reservoir operations simulation model, the Zambezi Design Model, has been developed to conduct MORDM for the Zambezi Watercourse. In addition, an electricity system operations model of the South African Power Pool has been soft linked to the Zambezi Design Model to better capture the response of the energy sector to hydropower and solar power generation in the Watercourse. An overview of the decisions and policies, objectives, and exogenous drivers included and related between the two models is shown in Figure 62. The Zambezi Design Model is used to develop Pareto-optimal sets of operating policies with new solar installation capacities at the existing reservoirs as well as one or more of the planned reservoirs incorporated into the reservoir network. Five WEFE objectives are evaluated at the Zambezi Watercourse basin-wide level, with energy system operational cost (OPEX) acting as the soft-linked response of the larger regional SAPP energy system to hydropower and solar production in the Watercourse. The main exogenous drivers of the Zambezi Design Model and SAPP energy model are monthly hydrology and hourly, country-level electricity demand, respectively. Both models use nominal monthly or hourly time scale solar generation potential developed from 20 years of historical gridded meteorological and solar radiation data (European Commission Joint Research Centre, 2022).

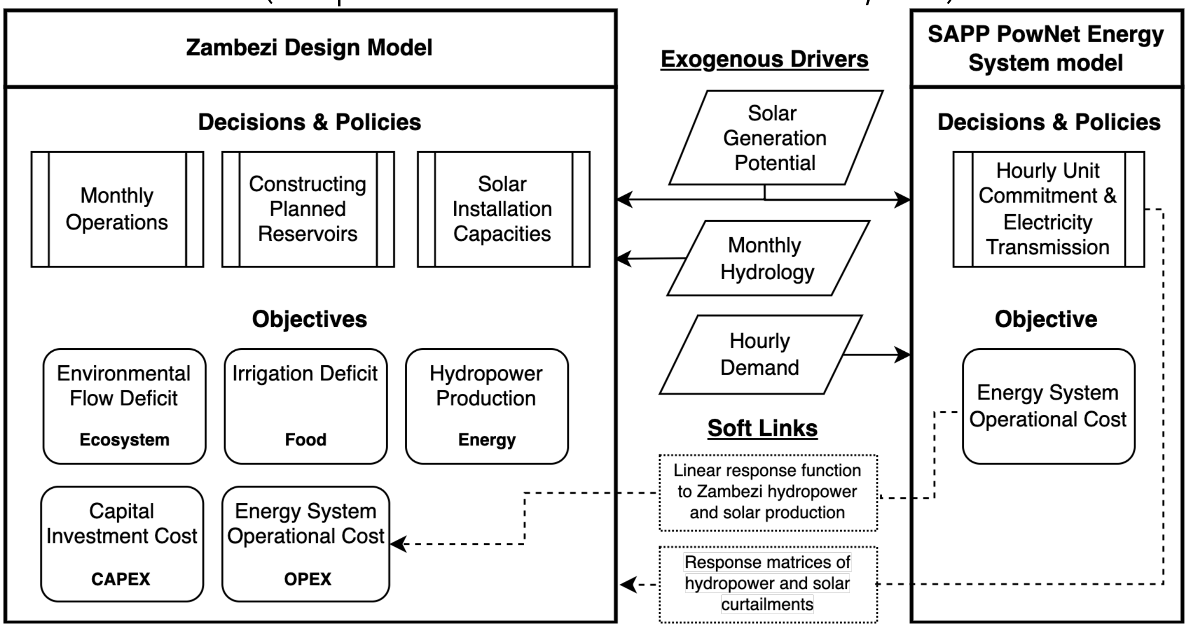

Figure 62. Overview of decisions and policies, objectives, and exogenous drivers of the soft-linked Zambezi Design and SAPP PowNet Energy System models.

4.2.2.1.2 Zambezi Design Model

4.2.2.1.2.1 Water System Model

The Zambezi Design Model includes five existing reservoirs (Kariba, Itezhi-Tezhi, Kafue Gorge Upper and Lower, and Cahora Bassa), three planned reservoirs (Batoka Gorge, Devils

Gorge, and Mphanda Nkuwa), one run-of-the-river hydropower plant in Victoria Falls, and eight irrigation districts (see system network schematic in Figure 63). A monthly modelling time-step is used to capture the reservoir network's dynamics with the following fundamental mass balance equation:

$$s_{t+1}^{r} = s_{t}^{r} + \sum_{i,r,id}\left(q_{t+1}^{i} + r_{t+1}^{r_{above}} - \omega_{t+1}^{id}\right) - e_{t}^{r} S_{t}^{r} - r_{t+1}^{r} \quad (8)$$

where s_t^r is the storage of the r-th reservoir at the beginning of month, $e_t^r S_t^r$ is the water evaporated, r_{t+1}^r is the volume of water released, q_{t+1}^i and $r_{t+1}^{r_{above}}$ are inflow to the reservoir from the i-th tributary and the r-th reservoir directly upstream, respectively, and $\omega_{t+1}^{id}$is the water abstracted by the id-th irrigation district. In particular, e_t^r is the mean monthly evaporation rate, while S_t^r is the reservoir surface area defined by a non-linear relation given s_t^r. To account for the significant evaporation losses in the Kafue Flats, the evaporation at Kafue Gorge Upper has been calibrated accordingly (Gandolfi et al., 1997). The actual release of the r-th reservoir is defined as $r_{t+1}^r = f(s_t^r, u_t^r, q_{t+1}^r, e_t^r)$ where $f(\cdot)$ describes the nonlinear, stochastic relation between the release decision determined by the operating policy, i.e. $u_t^r = p(\cdot)$, and the actual release r_{t+1}^r (Piccardi & Soncini-Sessa, 1991). The actual release at the end of the time step interval is generally equal to the release decision unless physical constraints prohibit it (e.g., if the prescribed release lies outside the minimum and maximum allowable releases, if there is insufficient water to meet the prescribed release, or if the prescribed release would result in the reservoir storage capacity being exceeded, and thus spillages occur).

There are three environmentally vulnerable river stretches included in the Zambezi Design Model. Two areas are protected by Minimum Environmental Flow (MEF) constraints: at Victoria Falls, 250 m^3/s are left in the river every month and cannot be thus diverted to the run-of-the-river hydropower plant; at Kafue Flats, Itezhi-Tezhi reservoir releases must be above 40 m^3/s every month, except for March when 315 m^3/s are needed to maintain the natural flooding pattern. Since no environmental protection of the delta is already in place, the delta environmental flow is implemented as an objective function used in the operating policy design.

According to the monthly time-step adopted in the model, the river reaches are modeled as plug-flow canals with negligible travel time, in which the velocity and direction of flow are constant everywhere, without any lamination effect. An exception is made for the river reach between Itezhi-Tezhi and Kafue Gorge Upper reservoirs, which requires two months travel time due to the presence of the Kafue Flats.

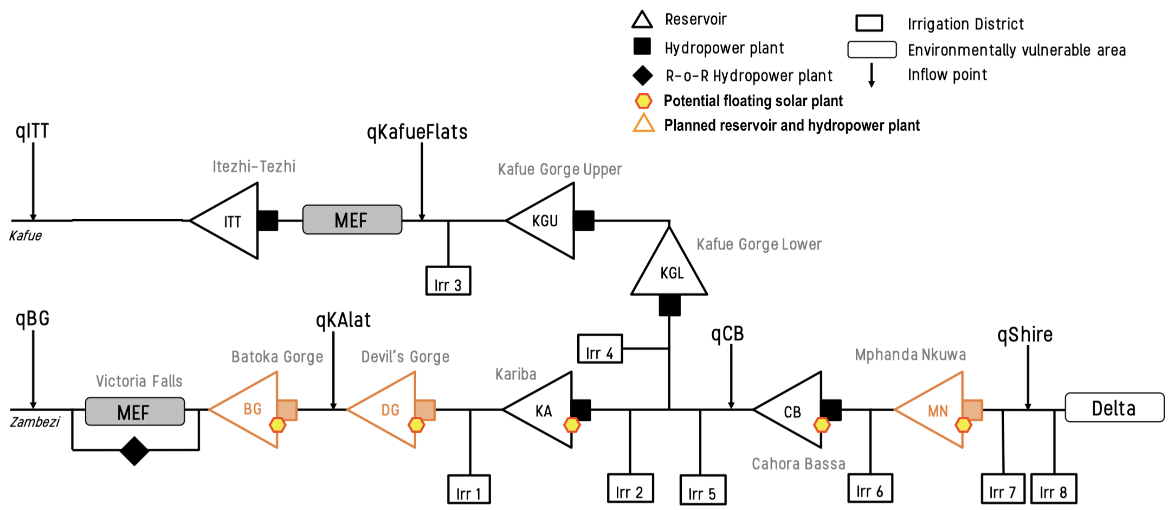

Figure 63. Schematic of Zambezi Design Simulation-Optimization Model including the three planned reservoirs and potential floating solar installations. Minimum environmental flows (MEF) are enforced at Victoria Falls and below Itezhi-Tezhi reservoir at Kafue Flats.

4.2.2.1.2.2 *Operating Policies*

Because EMODPS resolves a problem of parameter optimization for a given policy structure, the best possible solution is limited by the chosen class of functions. The greater the flexibility of the class of functions increases the possibility of approximating the optimal solution. Radial basis functions (RBFs) have been proven as an effective, case study-independent option for solving EMODPS problems for reservoir operations (Giuliani, Castelletti, et al., 2016). RBFs are thus adopted as the functional form of the closed-loop operating policy $\boldsymbol{u_t} = p(t, \boldsymbol{s_t})$, where t is time, and $\boldsymbol{s_t}$ is the vector representing the current state of the system (reservoir storages and total basin inflow).

As for the eight irrigation districts (*id*= 1, ..., 8), they can abstract water from the river through a regulated water diversion channel. The volume of water ω_{t+1}^{id} abstracted is calculated according to a non-linear hedging rule (Celeste & Billib, 2009):

$$\omega_{t+1}^{id} = \min\left(q_{t+1}, T_t^{irr,id} * \left[\frac{q_{t+1}}{h^{id}}\right]^{m^{id}}\right) \quad if \quad q_{t+1} \leq h^{id} \quad else \; \min\left(q_{t+1}, T_t^{irr,id}\right) \qquad (9)$$

where q_{t+1} is the volume of water available in the river and h^{id} and m^{id} are the parameters regulating the diversion channel. The diversion rules allow hedging water abstractions to account for downstream users.

4.2.2.1.3 SAPP PowNet Energy System Model

PowNet is a freely available, open-source modelling tool for simulating the operations of large-scale power systems (Chowdhury et al., 2020). The model solves a unit commitment/economic dispatch (UC/ED) optimization problem (Conejo & Baringo, 2018) to schedule least-cost operations that balance supply and demand over a 24-hr period. The electricity system is represented by a set of nodes that include demand units, power generating units, and substations. Intermittent renewable energy is represented as an externally pre-processed time-series of available power, while the optimization algorithm determines the actual renewable power dispatched to satisfy demand. Thus, PowNet's computed generation mix accounts for the technical and economical constraints of power plants and transmission lines that can limit penetration of renewable energy generation into the grid. Furthermore, a 'slack' generator, also called the backstop technology, allows simulating shortage of electricity demand by dispatching electricity as needed to prevent a shortfall (program crash), but with a production cost that is orders of magnitude larger than any other generation source.

4.2.2.1.3.1 Inputs and Grid Configuration

In addition to the hourly availability of hydropower, solar, and wind, PowNet requires economic and technical input data of the following types:

- **Power plants**: maximum and minimum capacity, rate of fixed cost ($US/MW), start-up costs ($US/MW), variable O&M cost ($USD/MW), fuel price ($US/MMBtu), minimum up and down time (hour), ramping limits (hour) and heat rate (MMBtu/MWh).
- **Load**: hourly demand (MW) for each node
- **Transmission lines**: electrical transmission network line capacity (MW) and line susceptance (S, Siemens)

These specifications have been gathered from available public data to build a simplified representation of the existing country-level interconnections of the SAPP power grid with potential expansion of reservoirs and floating solar installations in the Zambezi Watercourse as depicted in Figure 64. Because only one connection between two nodes is permitted in PowNet and usually lines between countries are more than one, capacity of multiple country interconnections is summed, and an arithmetical mean applied for line susceptance. Hourly power demand time series for each country were built with different load curves representative of different typical days of the year (e.g., winter and summer days or weekday and weekend day). These daily profiles were scaled along the year and calibrated to match 2018 demand data.

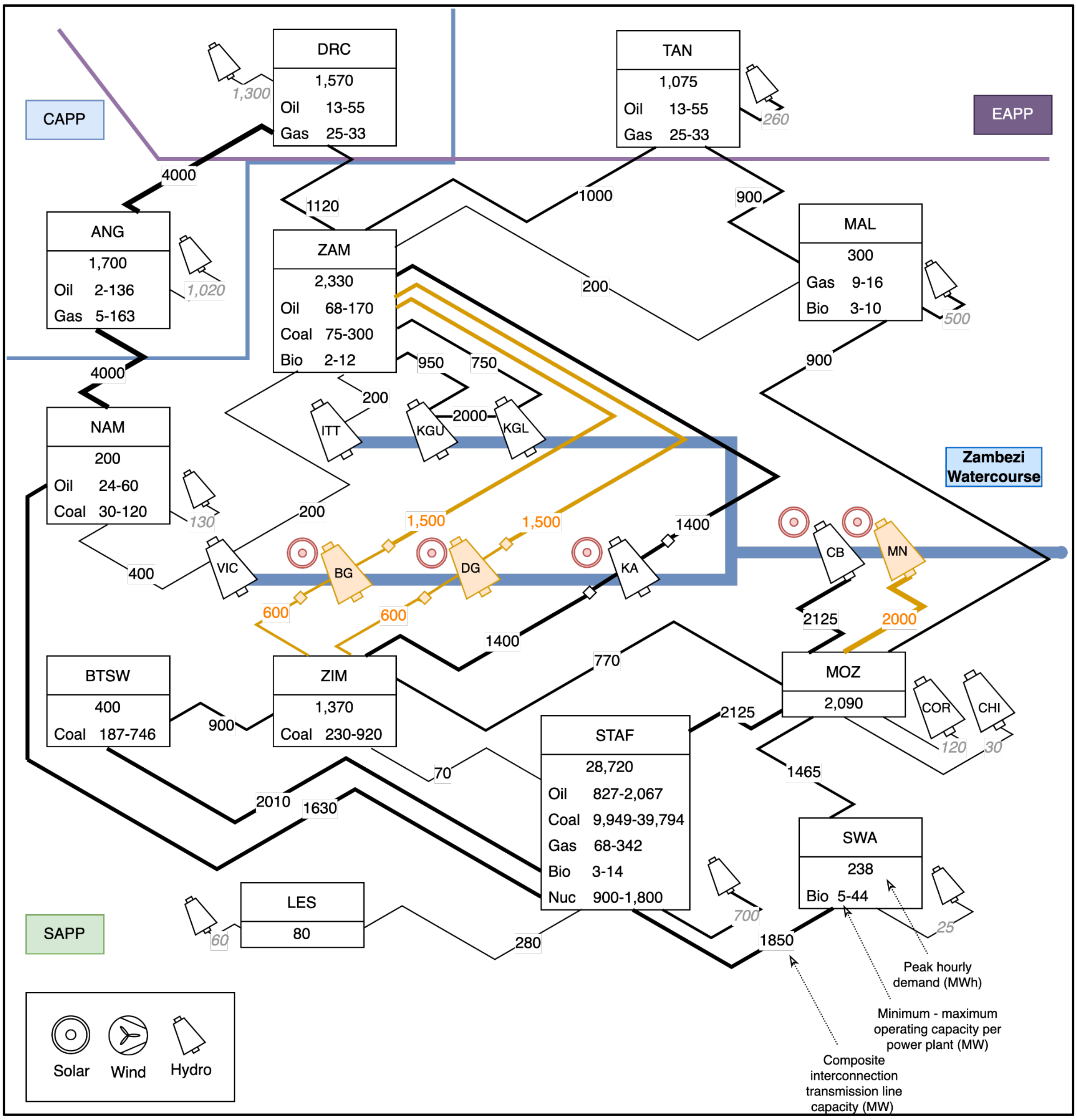

Figure 64. Configuration of SAPP PowNet Energy System model country-level peak annual demand, thermo-generation capacity, country-to-county (node-to-node) transmission capacity, and interconnections with existing and planned hydropower plants with potential floating solar installations in the Zambezi Watercourse.

4.2.2.1.3.2 *Floating Solar Representation*

Floating solar photovoltaic (FPV) generation is released on the same transmission line connecting hydropower generation to the demand node(s). Parameters for the transmission line connecting the FPV unit to the hydropower generation unit are set to permit a capacity an order of magnitude higher than any considered FPV capacity so that the transmission between FPV and hydropower units is not a limiting constraint. The driving constraint is thus focused on the transmission lines connecting hydropower units to country demand nodes, and the congestion created by the dual use of these lines for FPV and hydropower dispatch.
In addition, a small "persuasion" penalty has been placed on hydropower dispatch so that PowNet prioritizes FPV generation first. This results in a 24-hour dispatch curve that curtails hydropower when the total available solar and hydropower generation is greater than the

transmission capacity of the line connecting the hydropower unit to the country demand node(s). Thus, PowNet determines the optimal scheduling of hydropower over a 24-hour period as a function of the demand and available FPV generation.

4.2.2.1.3.3 Floating Solar Capacity Constraints

The range of feasible floating solar installation capacities at five candidate reservoirs was initially determined in PowNet by sampling solar dispatch as a function of the solar peak-capacity and the hydropower unit's outgoing transmission line capacity. Figure 65 shows how the nominal solar dispatch scales directly with peak-capacity until transmission line capacity begins to sharply constrain the dispatchable solar generation. The initial range of peak solar capacities was set on a 0-2 multiplier scale where a multiplier of 1 corresponded to the point where existing transmission line capacity begins to severely constrain dispatchable solar.

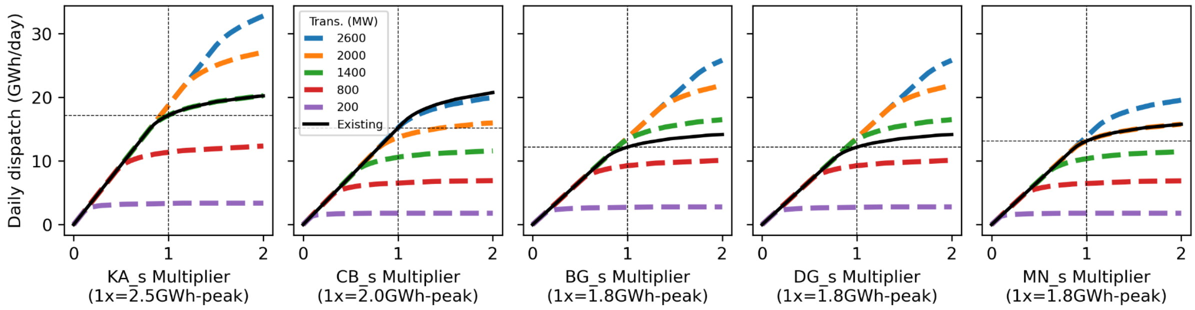

Figure 65. Solar dispatch as a fraction of maximum daily potential for different transmission line capacities and solar capacity multipliers at the five potential reservoir floating solar sites.

The second feasibility check for floating solar peak capacity was based on the size of the solar panel area required to achieve the specified peak-capacity. The required area was determined by accounting for nominal crystalline PV system efficiencies (~20%) as well as average angle-of-incidence, ambient condition (e.g., temperature and irradiation), and system losses. For the existing reservoirs of Kariba and Cahora Bassa where even the minimum operating storage volumes correspond to large surface areas (4,400 km^2 and 1,000 km^2 respectively), a solar panel footprint area of up to 35 km^2 was considered feasible (see Table 4 for a crosswalk of peak capacities and panel footprints). For the planned reservoirs of Batoka Gorge and Mphanda Nkuwa, whose minimum operating volumes correspond to a surface area of ~20km^2, a maximum panel footprint area of 6 km^2 was considered feasible. For the planned reservoir of Devils Gorge, whose minimum operating volume corresponds to ~120km^2, a maximum panel footprint area of 12 km^2 was considered feasible.

Table 4. Possible floating solar installation peak capacities and approximate area of panel footprint.

Reservoir	Capacity (GWp)	Feasible Panel Footprint (km^2)
Kariba	5.0	35
Cahora Bassa	4.0	28
Batoka Gorge	0.9	6
Devils Gorge	1.8	12
Mphanda Nkuwa	0.9	6

4.2.2.1.4 Linkage of the Zambezi Design Model with the SAPP Energy System

The purpose of soft-linking the Zambezi Design Model with the SAPP PowNet Energy System model is two-fold: 1) to include an objective in the Zambezi Design Model that represents the economic value of solar and hydropower generation at the regional energy market scale, and 2) to include a more realistic representation of solar and hydropower grid penetration in the Zambezi Design Model, especially given the constraints of existing hydropower plant transmission lines to which new floating solar installations would connect. The soft-linkage was developed using a single 24-hour period based on the day of the year with peak demand to sample the response of the SAPP PowNet Energy System Model to a large sample of daily hydropower (8 reservoirs) and solar generation (5 installations) in the Zambezi Watercourse. Hourly solar generation availability during the 24-hour period was based on a nominal solar power output curve determined from the PVGIS v5.2 (2022) historical dataset.

Three SAPP PowNet model responses were developed for the Zambezi Design Model:

1) A linear regression model predicting energy system operation cost (OPEX) from combined daily hydropower and solar dispatched to the grid (i.e., actual production).
2) A lookup table mapping a solar installation's peak-capacity to the total daily solar dispatched to the grid.
3) A lookup matrix mapping a hydropower plant's daily hydropower availability and solar installation peak-capacity to the total daily hydropower dispatch.

4.2.2.1.4.1 Linear Response of Energy System Operation Cost

Figure 66 shows the 24-hour SAPP PowNet energy system operation cost objective (OPEX) for 25,000 random latin hypercube samples of a 14-dimensional input matrix corresponding to the power availability of 9 hydropower units and 5 floating solar units in the Zambezi Watercourse. A linear model was fit to this input-output response and scaled to the annual level so that SAPP energy system operation cost could be estimated based on hydropower and solar production calculated within the Zambezi Design Model. Residuals of the linear model are normally distributed, with a maximum underestimation error of ~0.6%, although >99% of the 25,000 predicted values are within ±0.1% of the PowNet modelled cost.

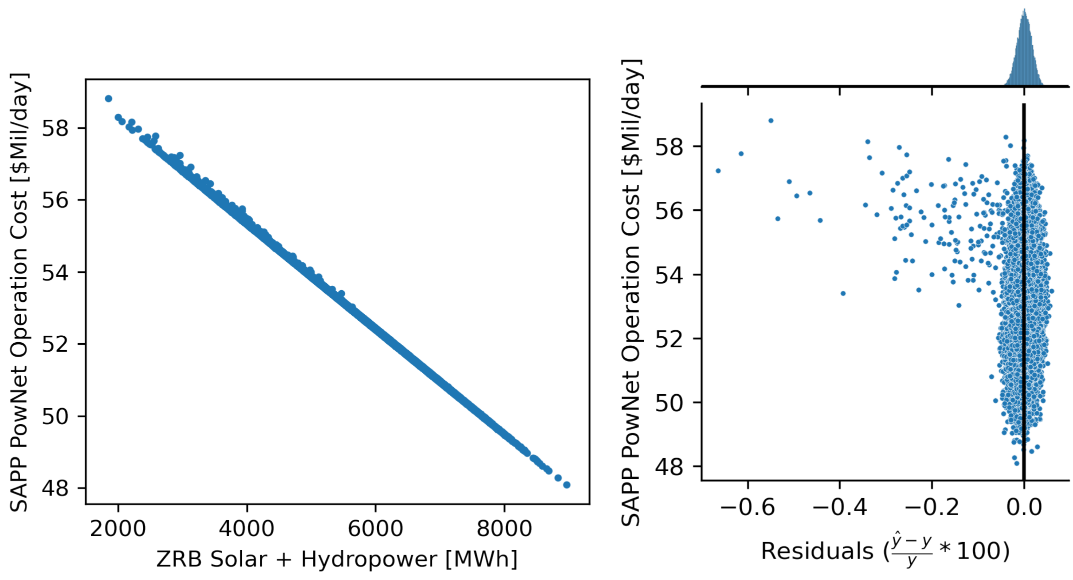

*Figure 66. **(a)** Total SAPP PowNet energy system operation cost for 25,000 random Latin hypercube samples of ZRB hydropower and solar multipliers (n=14 dimensions). **(b)** Residuals with histograms of predicted SAPP PowNet cost using linear regression on total Zambezi Watercourse solar and hydropower production.*

4.2.2.1.4.2 Solar Dispatch Lookup Table

Since solar peak capacity is one of the design variables in the Zambezi Design Model and energy system operation cost is estimated using the linear relationship with total solar and hydropower production, a PowNet response of daily total solar dispatch was developed as a function of the solar peak capacity input. The results of this input-output relationship were converted into lookup tables for use in the Zambezi Design Model at runtime. Figure 67 shows the lookup table plotted for the Kariba reservoir unit where total solar production scales linearly with peak capacity until transmission line capacity constraints begin to sharply reduce the amount of solar power output that can be dispatched to the grid.

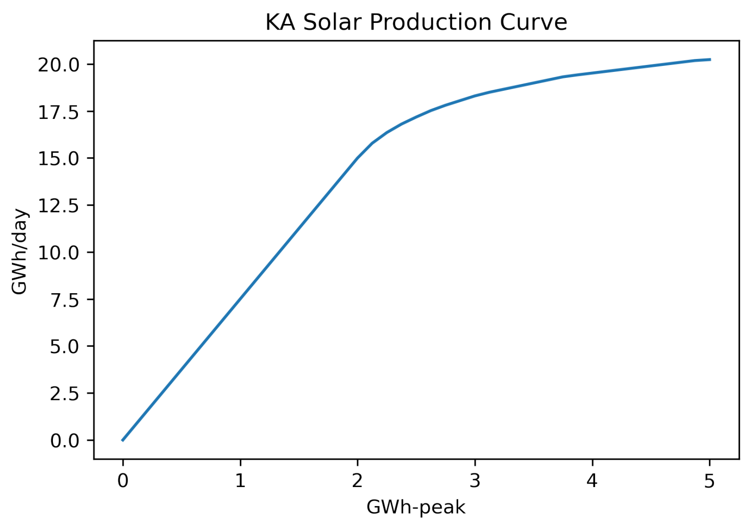

Figure 67. Daily solar production (dispatch to grid) in SAPP PowNet as a function of floating solar peak capacity installation at the Kariba reservoir unit.

4.2.2.1.4.3 Hydropower Curtailment Lookup Matrix

A second lookup matrix is needed to account for PowNet's curtailment of hydropower due to transmission line congestion with solar power dispatch. The PowNet response of hydropower curtailment is developed as a function of daily hydropower availability (a function of the monthly reservoir release in the Zambezi Design Model) and daily solar production. The results of this input-output relationship are converted into lookup matrices for use in the Zambezi Design Model at runtime. As shown in Figure 68 for the Kariba hydropower unit, hydropower curtailment never occurs below 7.5 GWh/day of solar production (i.e., there is sufficient line capacity to dispatch 100% of the available hydropower and solar production at each hour); however, as solar production increases, curtailment of daily hydropower production can reach over 30% of the available hydropower generation.

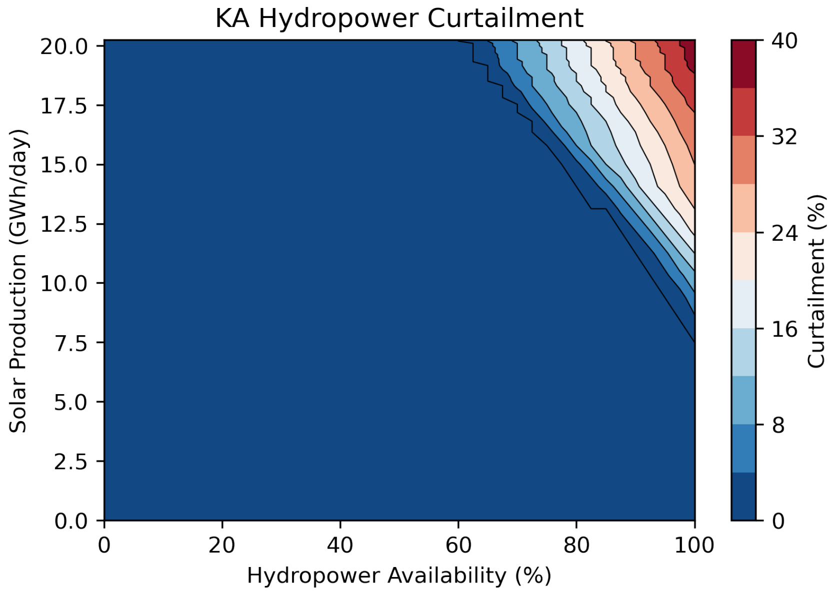

Figure 68. Response matrix of hydropower curtailment (hydropower dispatched as a fraction of hydropower availability) as a function of daily solar production and hydropower availability.

4.2.2.1.5 Validation

Validation of the soft-linked Zambezi Design Model and SAPP PowNet Energy System Operation was performed by simulating PowNet with solutions developed from the Zambezi Design Model. 14 solutions were randomly selected from the non-dominated sets of each possible reservoir configuration (n=8; a total of 112 solutions). The solutions specify the solar peak capacity and monthly hydropower availability over the 20-yr historical simulation period where monthly hydropower production is disaggregated evenly across the month to create 24-hour period hydropower availability in PowNet. In addition, solar power output was constrained to the actual hourly power output given the specified peak capacity developed from a world-wide dataset of historical hourly solar radiation and ambient conditions (European Commission Joint Research Centre, 2022).

As shown in Figure 69, the annual OPEX calculated in the ZRB Design Model has a \$2.04Bil-yr^{-1} positive bias from annual OPEX determined in the daily PowNet simulation. As shown by the near unit-slope and limited residual spread, the positive bias varies little over the wide range of ZRB Design Model operational policies, reservoir network configurations, and year-to-year hydrologic conditions. The consistent bias indicates a robust soft linking of the OPEX objective, with adjustment to actual PowNet simulated conditions a function of the lower power demands seen over a full year.

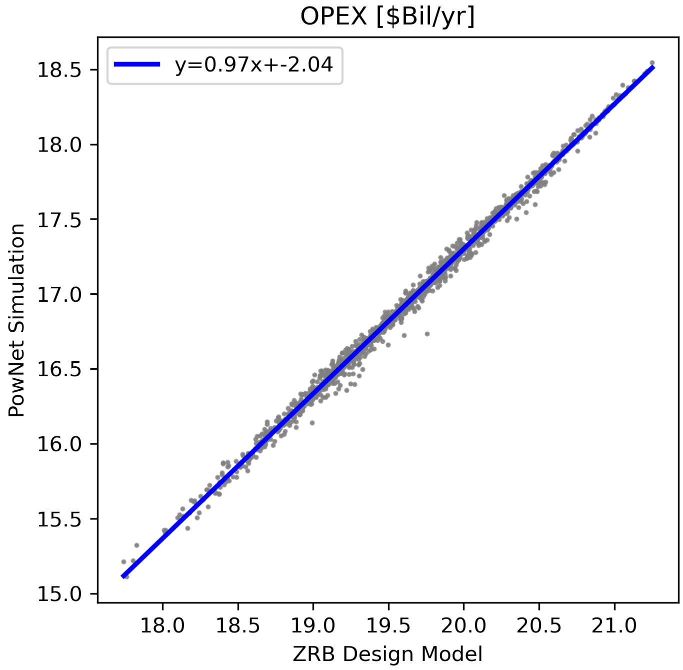

Figure 69. Annual energy system operation cost (OPEX) for 14 randomly chosen solutions from each possible reservoir network configuration (n=8) simulated in the Zambezi Design Model and re-validated with a 20yr daily simulation of the SAPP PowNet model (each point represents one year of simulation in both models for one possible design solution).

4.2.2.1.6 Optimization Framework

The Zambezi Design Simulation-Optimization Model is coupled with an optimization engine to design alternative reservoir operating rules, irrigation diversion policies, and floating solar installation capacities for each possible reservoir network. The optimization is performed using multiobjective evolutionary algorithms (MOEAs, for a review see (Maier et al., 2014)), which generate a set of solutions representing tradeoffs across objectives constructed to represent different WEFE components. Technically, an alternative solution developed in this way is defined as Pareto-optimal (or nondominated) if no other solution gives a better value for one objective without degrading the performance in at least one other objective. The advantage of this a-posteriori approach with respect to traditional a-priori methods, such as cost-benefit analysis or multi attribute value theory, is that decision makers do not have to state what is preferred in absence of their understanding of what is attainable (Cohon & Marks, 1975). In addition, it allows considering heterogeneous and incommensurable utility functions without going through any monetization process.

The Watercourse operational design problem requires determining optimal sequential reservoir release and irrigation decisions at each time step that produce an immediate benefit/cost and affect the next system state, thereby affecting all the subsequent benefits/costs. In particular, the vector of release decisions (e.g., release from a dam, diverted flow at a diversion point) $\boldsymbol{u}_t$ is determined at each time step by an operating policy, i.e., $\boldsymbol{u}_t = p(t, \boldsymbol{x}_t)$. The state of the system (e.g., the reservoir storage) is then altered according to a transition function $\boldsymbol{x}_{t+1} = f_t(\boldsymbol{x}_t, \boldsymbol{u}_t, \boldsymbol{\varepsilon}_{t+1})$ affected by a vector of stochastic external drivers $\boldsymbol{\varepsilon}_{t+1}$, (e.g., reservoir inflows). In the adopted notation, the time subscript of a variable indicates the instant when its value is deterministically known. The storage is observed at time t, whereas the inflow has subscript $t+1$, denoting the realization of the inflow stochastic process in the time interval $[t; t+1)$. The sequence of states over the time horizon defines a system trajectory, which allows the evaluation of the performance of the operating policy p by means of the different objective functions J^i (with $i = 1, \ldots, M$) capturing the interest of different stakeholders. Each objective function is hence formulated as a functional of the trajectory τ over the evaluation horizon $[0, h]$ and across an ensemble of K realizations of system disturbances. The optimal policy is then obtained by solving the following multi-objective problem:

$$p^* = arg\min \boldsymbol{J} = | J^1, \ldots, J^M | \qquad (1)$$

This problem is solved by using Multi-Objective Evolutionary Algorithms (MOEAs), and in particular evolutionary multi-objective direct policy search (EMODPS) following the approach of Bertoni et al. (2019) and Arnold et al. (2022 under review), which replaces the traditional stochastic dynamic programing approach with a simulation-based optimization that directly operates in the policy space. EMODPS parameterizes the operating policy p_θ within a given family of functions and then explores the parameter space Θ seeking the best parameterization of the operating policy with respect to the expected long-term cost defined by the objectives of the problem, i.e.

$$p_\theta^* = arg\min \boldsymbol{J} \qquad \text{s.t. } \theta \in \Theta; \qquad s_{t+1} = f_t(s_t, u_t, q_{t+1}) \qquad (2)$$

Finding p_θ^* corresponds to finding the best parameters θ^* for the class of policy p_θ, measured by the objectives $\boldsymbol{J}$. A schematization of the EMODPS algorithm is reported in Figure 70.

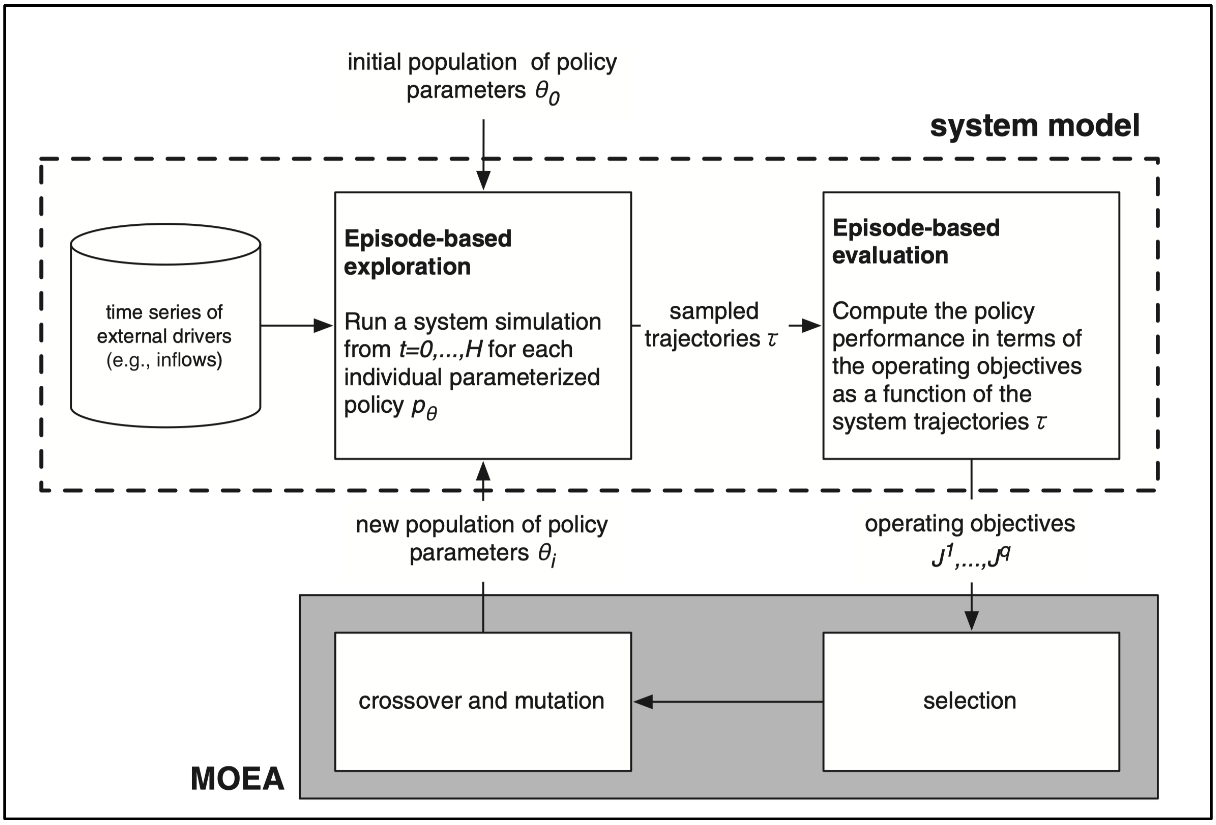

Figure 70. Schematization of the evolutionary multiobjective direct policy search (EMODPS) approach; dashed line represents the model of the system and the gray box represents the MOEA algorithm (Giuliani, Castelletti, et al., 2016).

4.2.2.1.7 WEFE Objectives

Several stakeholders are affected by the operations of the Zambezi Watercourse reservoirs and irrigation diversions. A preliminary subset of indicators was developed to represent the main components of the WEFE nexus based on the previous Zambezi Watercourse nexus assessment (DAFNE, 2018). These indicators are used as the vector of operating objectives ***J*** in the optimization:

1. **Environmental flow deficit (ecosystem):**

   $J^E = \frac{1}{h}\sum_{t=0}^{h-1}\left[max\left(Q_{e_t} - q_{t+1}, 0\right)\right]^2$

   where Q_e = 7,000 m^3/s is the specified monthly environmental flow in the river delta to be met in February and March, and q_{t+1} is the amount of water entering the ecosystem in the Zambezi River delta. The squared environmental deficit, which penalizes severe deficits more than smaller deficits, is averaged across all the months of the evaluation horizon *h*.

2. **Hydropower Production (energy):**

   $J^H = \frac{1}{h}\sum_{t=0}^{h-1}\sum_{r=1}^{R} hp_t^r - hp_{t,curtail}^r$

   where hp_t^r is the hydropower production of the *r*-th reservoir and $hp_{t,curtail}^r$ is the curtailment of hydropower production due to transmission capacity constraints. The total hydropower production is computed at the Zambezi Watercourse scale by summing all operating power plants and averaged across all time steps in the evaluation horizon.

3. **Energy System Operation Cost (OPEX):**

   $J^{OPEX} = \frac{1}{h}\sum_{t=0}^{h-1}[OPEX_0 - OPEX_{ZRB}(\sum_r^R hp_t^r + sp_t^r)]$

   where hp_t^r is the hydropower production of the *r*-th reservoir, sp_t^r is the solar production of the floating panel installation at the *r*-th reservoir, $OPEX_{ZRB}$ is the change in the SAPP-level energy system operations cost from one unit of hydroelectric or solar energy production in the Zambezi Watercourse, and $OPEX_0$ is the SAPP-level energy system operations cost when there is no hydroelectric or solar energy production in the Zambezi Watercourse. The total OPEX is averaged across all time steps in the evaluation horizon.

4. **Capital Investment Cost (CAPEX):**

   $J^{CAPEX} = \sum_r^R \iota^r + \sum_s^S[\kappa^s * W^s]$

   where ι^i is the the capital expenditure of the *i*-th candidate reservoir, κ^s is the peak capacity of the s-th floating solar installation, and W is the estimated capital expenditure per unit capacity.

5. **Normalized Irrigation Deficit (food):**

   $J^F = \frac{1}{h}\sum_{t=0}^{h-1}\left[\frac{max\left(T_t^{irr,id} - \omega_{t+1}^{irr,id}, 0\right)}{T_t^{irr,id}}\right]_{id=1,\ldots,ID}^2$

   where $T_t^{irr,id}$ and $\omega_{t+1}^{irr,id}$ are irrigation water demand and actual abstraction for the *id*-th irrigation district, respectively. The normalized formulation weighs irrigation district deficits equally regardless of the magnitude of their demands which allows districts to be grouped within the same design indicator without favouring one district over another.

4.2.2.2 Application Results

4.2.2.2.1 Alternatives

Optimization of the reservoir release and irrigation diversion policy together with floating solar capacity sizing was performed for the existing and each possible reservoir network configuration in the Zambezi Watercourse (i.e., "pathways", including one or more of the three planned reservoirs) over a historical period of hydrology (1986-2005). A final Pareto-sorting of the combined Pareto reference sets of the eight pathways yielded 1,324 non-dominated alternatives with the following relative contributions from each pathway:

- Pathway 1: Existing (7%)
- Pathway 2: Mphanda Nkuwa (10%)
- Pathway 3: Devils Gorge (8%)
- Pathway 4: Batoka Gorge (5%)
- Pathway 5: Devils Gorge + Mphanda Nkuwa (14%)
- Pathway 6: Batoka Gorge + Mphanda Nkuwa (9%)
- Pathway 7: Batoka Gorge + Devils Gorge (9%)
- Pathway 8: All three reservoirs (37%)

Figure 71 shows a parallel plot of the 1,324 alternatives' performance for the five WEFE objectives. Overall, a clear tradeoff develops between CAPEX and OPEX which is expected given the increase in total basin power production realized with greater capital expenditure on new reservoirs and floating solar. A second clear tradeoff develops between hydropower and the environmental deficit; however, this occurs mostly on a pathway-by-pathway basis. Pathway 8 has many solutions with higher solar production (reaching up to 18 TWh-yr^{-1}). Pathways 2 and 5 also tend to have more solar production, indicating that Mphanda Nkuwa and Devils Gorge are particularly good candidates for solar installations. This partially indicates why Pathways 2, 5 and 8 together make up more than 60% of the non-dominated solutions.

In addition to the five WEFE objectives, two post-calculated metrics are reported:

- **Change in net present value (ΔNPV [$Bil])**. This is calculated by using the solution from the existing network (Pathway 1) with no solar capacity and the minimum OPEX value (i.e., the highest hydropower production) as the reference point - also referred to as the "base" solution. The "base" solution's OPEX is subtracted from the OPEX of all other solutions, thus yielding positive annual "savings" for alternatives with lower OPEX, and negative annual "costs" for alternatives with higher OPEX. Finally, this value is repeated over a 100-year horizon, discounted at a 10% rate, and subtracted from the CAPEX of the solution to produce ΔNPV.
- 5th percentile of total annual energy production (ZRB TWh-5%).

The results of the ΔNPV metric show that, overall, a large proportion of alternatives from more capital-intensive pathways 5 and 8 tend to have greater positive ΔNPV due to their ability to produce comparatively more energy per dollar invested. Indeed, when Pareto sorting is performed on ΔNPV and environmental and irrigation deficits alone, pathways 5 and 8 represent nearly 80% of the non-dominated alternatives.

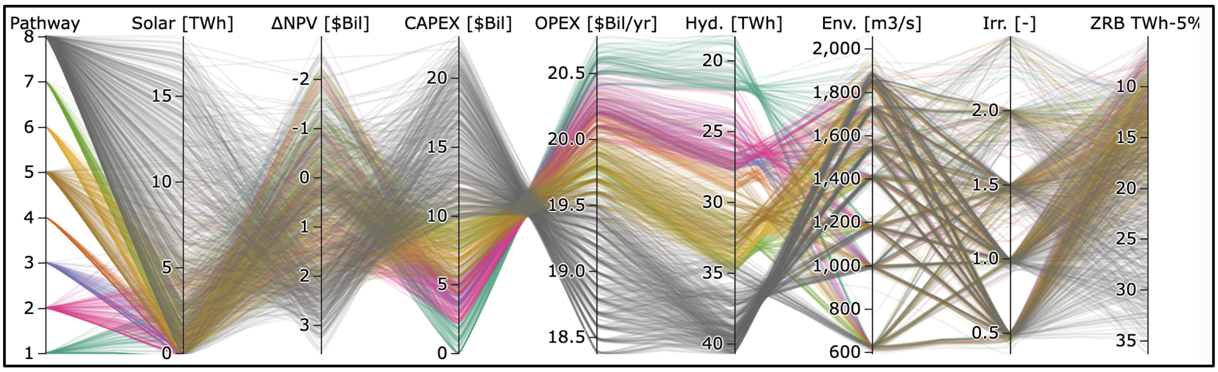

Figure 71. Pareto optimal alternatives of reservoir and irrigation management and floating solar capacity for the existing Zambezi Watercourse reservoir network and networks that include up to 1 (pathways 2, 3, and 4), 2 (pathways 5, 6, and 7) and 3 new reservoirs (pathway 8). The direction of preference is points downwards for the five WEFE objectives.

Example Selection of Alternatives

An alternative selection narrative is constructed to highlight some key results and demonstrate a robustness evaluation of the chosen alternatives. Five solutions are chosen by "brushing" to filter on one or more of the WEFE objectives following the sequential procedure listed below and shown in Figure 72:

- **Solution 1: Reference "Base":** This solution is found by restricting new reservoirs (pathway 1) and solar capacity. The solution with the best hydropower among these is chosen. As described above, this solution is the reference solution for developing the ΔNPV metric.
- **Solution 2: "Hydropower"**: This solution is found by continuing to restrict any solar capacity but allows any combination of the three new reservoirs. The solution with the best hydropower among these is chosen. The chosen solution includes all planned reservoirs (pathway 8), performs poorly on environmental and irrigation deficits, and has the absolute best hydropower solution among all alternatives.
- **Solution 3: "Solar w/ Budget"**: This solution is found by restricting CAPEX to less than $10Bil (Solution 2 CAPEX) while lifting the restriction on new floating solar capacity. The solution with the minimum OPEX among these is selected. The chosen solution includes the planned Devils Gorge and Mphanda Nkuwa reservoirs and produces ~7 TWh/yr of solar power, effectively substituting the hydropower production produced by Batoka Gorge in Solution 2.
- **Solution 4a: "Solar w/ Compromise w/ Budget (2 new reservoirs)"**: This solution is also found by restricting CAPEX to less than $10Bil (Solution 2) while allowing solar investment, however, seeks compromise with environmental and irrigation deficits by brushing solutions in the 80th percentile range of performance. Finally, the solution is restricted to a maximum of two new reservoirs. The solution with the lowest OPEX among these is chosen.
- **Solution 4b: "Solar w/ Compromise w/ Budget (3 new reservoirs)":** This solution follows the same restrictions of Solution 4a, however limits the selection to three new reservoirs (pathway 8). The solution with the lowest OPEX among these is chosen.

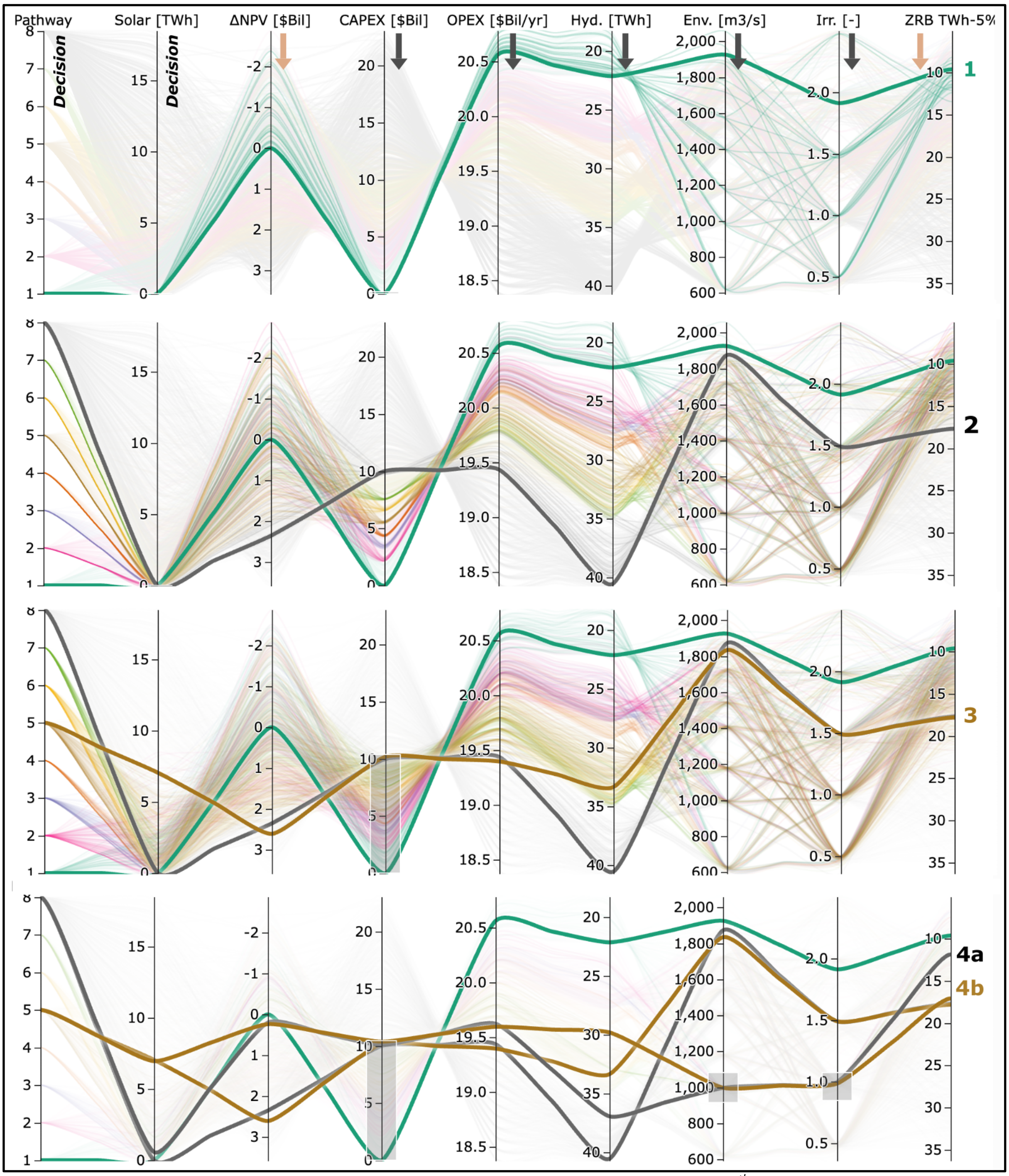

Figure 72. Pathway, total solar capacity (Solar [TWh]), change in net present value (ΔNPV), 5th percentile power production (ZRB TWh-5%), and performance over the 5 WEFE objectives for the example narrative selection of Zambezi Watercourse alternatives (1, 2, 3, 4a and 4b) for infrastructure and reservoir operational design.

4.2.2.2.2 States of the World

The chosen alternatives are re-evaluated under plausible climate conditions outside of what they were optimized to using a 450-member synthetic stochastic streamflow ensemble developed from climate model-driven hydrologic simulations. Figure 73 shows the average annual streamflow and trends determined for each inflow location and model-RCP combination as emboldened larger symbols and the corresponding synthetic ensemble as lighter, smaller symbols. Across all locations, average annual trends range from below -4%/yr to nearly +2%/yr. There is evidence of model uncertainty dominating RCP scenario uncertainty as shown by the clustering of models along average annual streamflow and the lack of a strong relationship to RCP across the models. A tendency towards positive or negative streamflow trends is not seen for the RCPs (although there are too few to draw any conclusion). However, nearly all model-RCP simulations show a negative trend for Shire River streamflow.

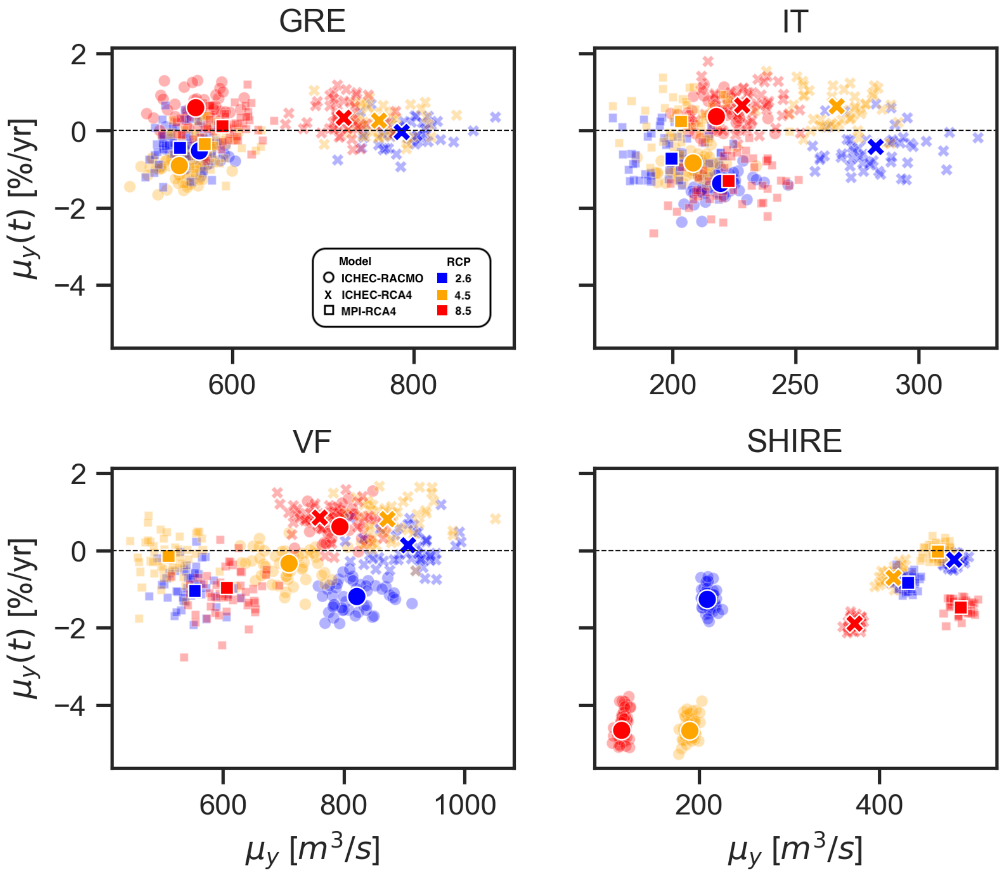

Figure 73. For each streamflow location ("GRE" = Great East (Luangwa River), "IT" = Itezhi-Tezhi (Kafue river), "VF" = Victoria Falls (Zambezi river), and "SHIRE" = Shire river) this plot shows the average annual streamflow and annual trend normalized to the average annual streamflow for each model-RCP combination as emboldened larger symbols and for the corresponding synthetic ensemble of as lighter, smaller symbols.

4.2.2.2.3 Robustness Evaluation

Robustness is most closely defined here as "the insensitivity of system design to errors, random or otherwise, in the estimates of those parameters affecting design choice" (Matalas & Fiering, 1977). The quantification of robustness is performed by visualizing the performance of the selected alternatives across all sampled states of the world outside which they were optimized to. This approach allows decision makers to determine the acceptable system performance a-posteriori, based on the level of robustness attained over the considered ensemble (Bertoni et al., 2019).

The objective performances of solutions 2, 3, and 4 a/b re-simulated over the 450-member stochastic hydrology ensemble are shown in Figure 74. Compared to solution 2 ("Hydropower"), solution 3 ("Solar w/ Budget") produces less hydropower over all sampled hydrology which is expected given the lack of Batoka Gorge reservoir in solution 3; however, under drier conditions, the OPEX, environment deficit, irrigation deficit, and 5th percentile of power production of solution 2 degrades compared to solution 3, suggesting solution 3 a more robust alternative. A similar result is also shown in comparing solutions 4 a/b. The robustness evaluation exercise thus shows how two alternatives may be equivalent under the deterministic condition they were optimized for but can diverge significantly when evaluated over the uncertain range of plausible states of the world. This is especially the case when considering multiple objectives, where certain objectives can show greater robustness for certain alternatives.

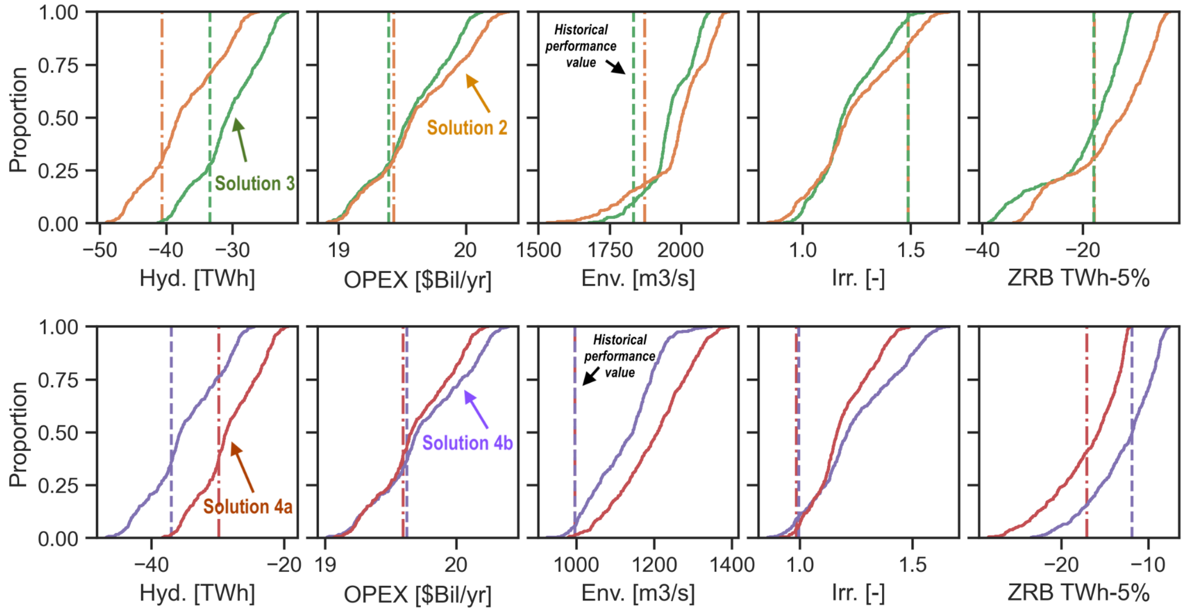

Figure 74. Performance of example narrative selected alternatives 2, 3, 4a and 4b over the 450-member stochastic streamflow ensemble. "Proportion" corresponds to the percentage of the450 alternative streamflow members for which the selected alternative performs better than the value crossing the x-axis (performance preference is leftward for each plotted objective).

4.2.3 Danube

4.2.3.1 Application Development

For the Danube Case Study, the large-scale hydrological model PCR-GLOBWB 2 (Sutanudjaja et al., 2018) has been applied. PCR-GLOBWB2 is a water resource model combining the physical part of the hydrological cycle with human demands and the resulting withdrawals from the available water resources (Figure 75). Additional human interactions are the inclusion of desalinated water as a possible water source, the operation of reservoirs for hydropower generation, water supply and flood prevention, and an energy balance to simulate the surface water temperature. Furthermore, a module to include the environmental flow requirements was added that potentially cap water withdrawals for human use. This makes PCR-GLOBWB 2 a suitable hydrological model to evaluate WEFE nexus challenges for the Danube River at the different intended scale (river basin, subbasin, local) that can be linked to models considering other aspects of the WEFE nexus.

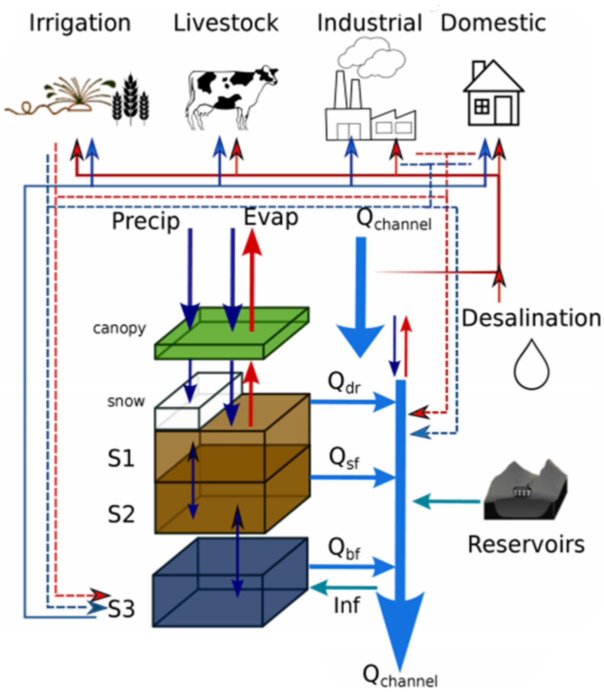

Figure 75 Model structure of the large-scale water resources model PCR-GLOBWB. The arrows between the sectors of human water demand and the different parts of the hydrological cycle (notably, the surface water and the renewable and renewable groundwater) are indicated, with withdrawals shown as solid lines, return flows as broken lines.

The current application of PCR-GLOBWB 2 is implemented at a spatial resolution at 5 arc minutes and covers the Danube River Basin in its entirety. The temporal resolution of the model is daily and the model period covers the historical period 1979-2014 and future projections covering 2015-2100 (considering the GCM input for three projections of climate and socio-economic conditions in the GoNEXUS project: SSP1 – RCP 2.6, SSP3 - RCP 7.0 and SSP3 - RCP8.5). In order to avoid any bias in the future projections, PCR-GLOBWB is not calibrated, and its parameterization based on the application of a priori global estimates.
PCR-GLOBWB generates a wide range of outputs that are aggregated to daily, monthly, or annual values and from which downscaled values can be derived. Here, two derived variables are used to evaluate the consequences of future climate and socio-economic conditions, being the water exploitation index (WEI; (Casadei et al., 2020)and the index of hydrological alteration (IHA, based on the IAHRIS model of (Martinez Santa-Maria et al., 2008); Figure 76). For the computation of the WEI, the net total water demand was used (gross demand minus return flows) and an estimate of the environmental flow requirements based on the Variable Monthly Flow Method (Pastor et al., 2014), which was explored in addition to an approach based on the monthly discharges that were exceeded 90% of the time.

Hydrological Status Martinez Santa-Maria and Fernandez Yuste (2010a,b)					
	Category I	Category II	Category III	Category IV	Category V
IHA	0.8<IHA≤1	0.6<IHA≤0.8	0.4<IHA≤0.6	0.2<IHA≤0.4	0≤IHA≤0.2

Overview	
Indicator	**Description**
IHA 1	The annual average discharge.
IHA 1b	The average monthly discharge.
IHA 2	The difference between the annual maximum and minimum discharge values.
IHA 4	The difference between the 90th and 10th discharge percentile.
IHA 5	The average of the maximum daily discharge.
IHA 8	The 5th exceedance percentile for discharge, related to floods.
IHA 9	Coefficient of variability for the maximum daily discharge.
IHA 10	Coefficient of variability of the 5th exceedance percentile for discharge.

Overview	
Indicator	**Description**
IHA 12	The amount of days the 5th exceedance percentile is exceeded within a month.
IHA 13	The average of the minimum daily discharge.
IHA 14	The 95th exceedance percentile for discharge, related to drought.
IHA 15	Coefficient of variability for the minimum daily discharge.
IHA 16	Coefficient of variability of the 95th exceedance percentile for discharge.
IHA 18	The amount of days without any flow (Q=0).
IHA 19	The amount of days discharge is lower than the 95th exceedance percentile.

Figure 76 Components included in the computation of the Index of Hydrological Alteration (IHA) and its ranking, from low (1) to high impact (0). Adapted from Martinez Santa-Maria et al. (2010)

4.2.3.2 Application Results

For a preliminary overview of the modelling capacities of PCR-GLOBWB 2 for the Danube, the WEI and the IHA were computed (see below), as well as the model validated.

Validation

The model performance of the uncalibrated version of PCR-GLOBWB 2 has been validated against observed discharge from the Global Data Runoff Centre (GRDC) for two rivers on the main stem of the Danube, one more upstream, one more downstream, and one downstream on the Tisza. The upstream area on the most downstream discharge station is about 7 times larger than those of the other two stations (Table 5). The validation period covers 20 years (1979-1999) for which the GRDC data are available. Model performance, expressed by the Kling-Gupta Efficiency (Gupta et al., 2009) and the modification to centre the naïve model at 0 by Knoben et al. (2019).

The model performance is similar for the three stations, with the Danube having slightly better performances, but all are skilful. Overall, the discharge of PCR-GLOBWB 2 is slightly higher for all stations, the greatest bias occurring on the Tisza. The standard deviation is more varied, with the simulated discharge underestimating the observed value at the most downstream station near the mouth of the Danube. This station has also the lowest correlation coefficient compared to the upstream stations on the Danube and the Tisza. As a result, the KGEs are quite comparable, with the most upstream station on the Danube (Bratislava) having the best performance. Also, the discharge hydrograph of the most downstream station on the Danube is shown (Figure 77).

Table 5 Summary statistics and model performance of PCR-GLOBWB 2 at 5 arc minutes over the period 1979-1999 for three stations on the Danube and the Tisza. Model performance is computed on the basis of the reported observations and the simulated values at the monthly resolution.

				Average Discharge [m3/s]		Standard deviation Discharge [m3/s]		Correlation coefficient	Kling-Gupta efficiency [-]	
River	Station	Area [km2]	GRDC code	Simulated	Observed	Simulated	Observed	[-]	Original	Corrected
Danube	Bratislava (SK)	131331	6142200	2529	2067	816	688	0.921	0.698	0.787
	Ceatal Izmail (RO)	807000	6742900	7179	5976	2392	2699	0.683	0.608	0.723
Tisza	Szeged (HU)	138408	6444100	1182	860	554	528	0.841	0.590	0.710

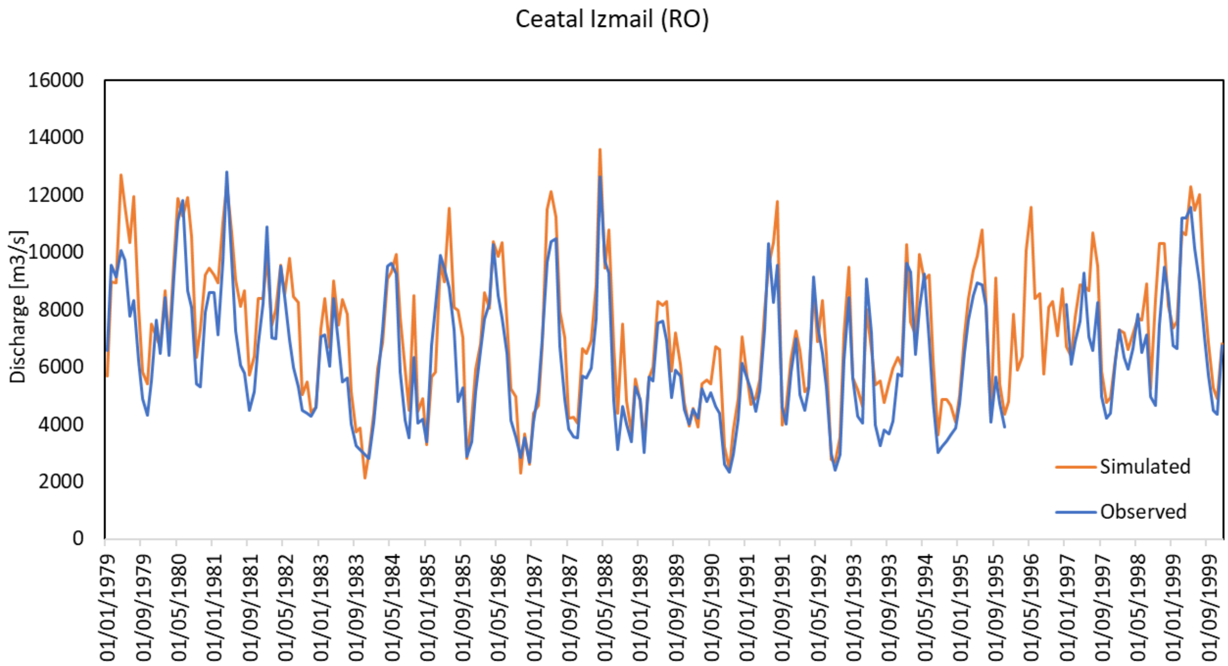

Figure 77 Hydrograph of the monthly discharges at Ceata Izmail (Romania) on the Danube

Environmental Flow Requirements

Environmental Flow Requirements (EFR) were defined in terms of the Variable Monthly Flow (VMF) and on the basis of the Q90, the monthly amounts exceeded 90% of the time. For the Q90 approach, the lowest overall monthly value was set as a hard limit whereas the actual monthly amount was considered to be a soft limit. Surface water withdrawals were only curtailed if the available water fell below the hard limit (Q90 – lower or VMF). If it fell between the two Q90 limits, withdrawals were reduced while all demand could be withdrawn without problem if sufficient surface water was available. In the preliminary analysis of the model, the VMF gave more constant values for the EFR and this method has been included in the following evaluations (Figure 78).

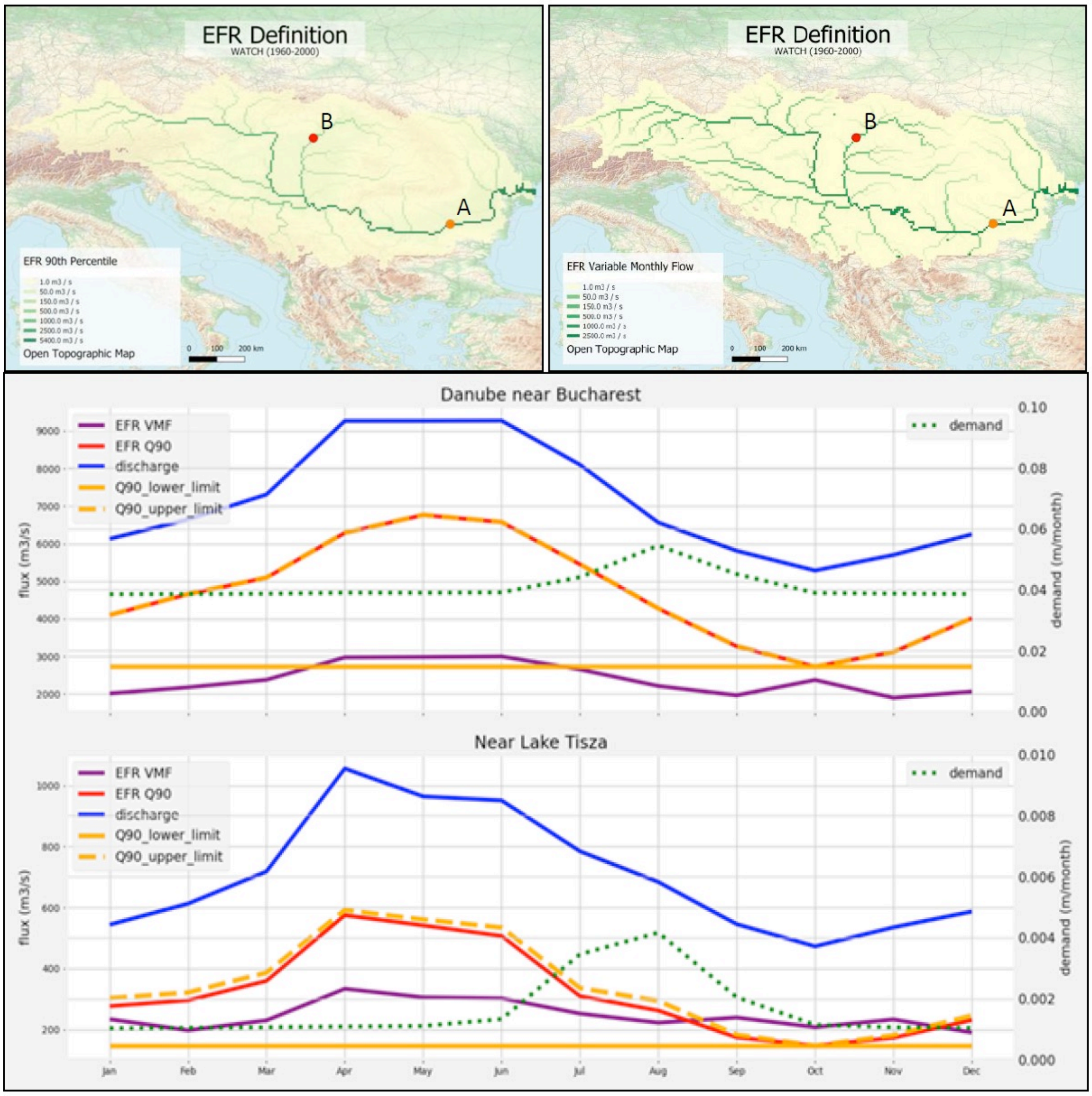

Figure 78 Maps pf the Q90 EFR (upper left) and VMF EFR (upper right) for the Danube River Basin. The bottom panel shows the average monthly climatology of the EFR at the monthly resolution, as well as the demand. Please note that the discharges and the demands are plotted on separate and distinct y-axes

A first evaluation shows that there is sufficient water on average in most of the months but that water shortages can occur frequently in the period from July to September on the Tisza and from August to October on the downstream part of the Danube (Figure 78). Relatively speaking, the availability of water is lower for the Tisza and here water shortages are hence more likely than for the Danube, where the discharge well exceeds the demand on average.

Water Exploitation Index

The water exploitation index (WEI) was computed for the SSP3-RCP7.0 scenario for all GCMs and for all environmental flow conditions. In this case, the Business-as-Usual scenario (no environmental flow requirements) is shown as well as the one based on the Variable Monthly Flow (VMF) for the observed, historical climate (W5E5) over the reference period (Figure 79). Values are shown on a scale from 0 to 1, the first indicating no to little exploitation, a value of

1 or higher over-exploitation. A comparison of the two scenarios of the EFR for the historical period show an increase in competition between water withdrawals and EFRs (higher WEI) when the EFR is included over the entire Danube River basin but in the lower course where irrigation demand is high in particular.

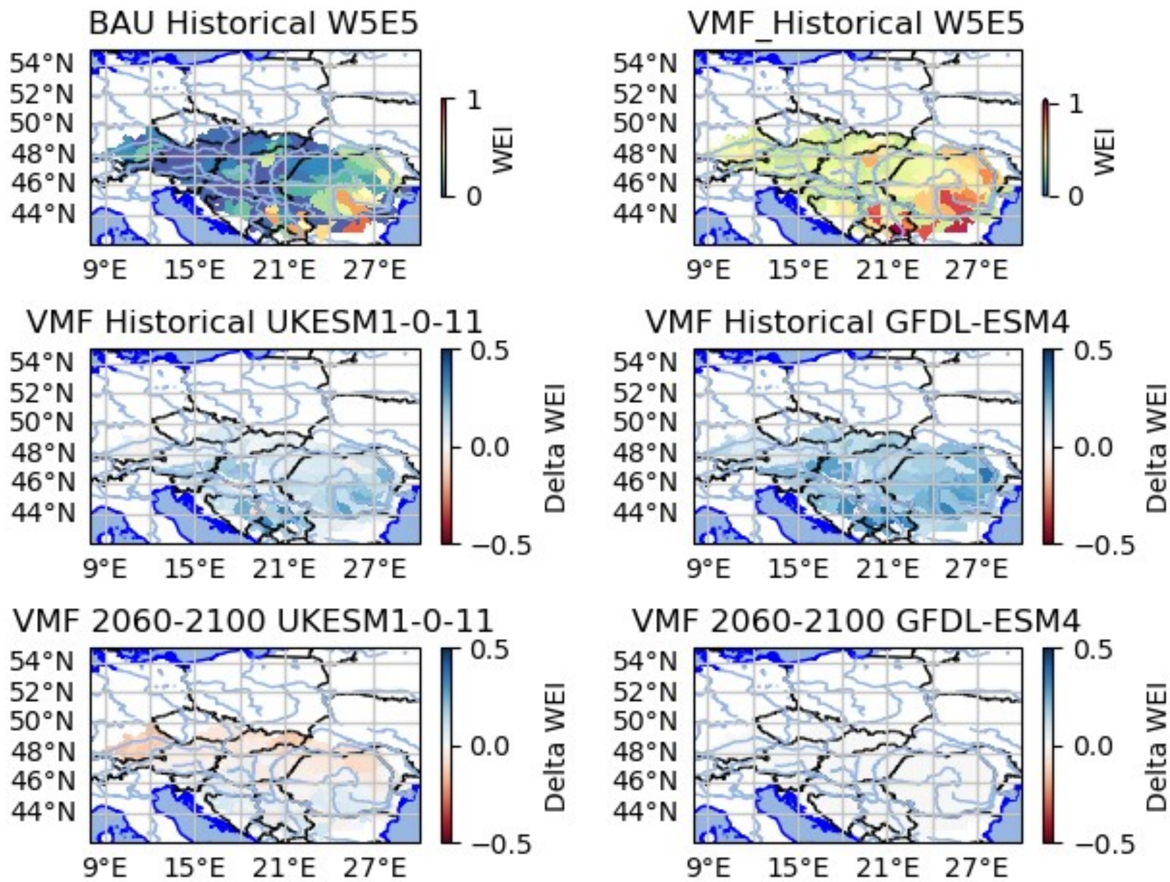

Figure 79 : Water Exploitation Index (WEI). The top row shows the WEI for the historical period using the W5E5 dataset of observed weather conditions over the reference period for the BAU (no EFRs imposed) and the VMF (EFRs based on the Variable Flow Method); used hereafter as reference. The two lower two rows show the differences between two GCMs (GFDL, UKESM) for the historical period and future period between 2060-2100 based on SSP3 – RCP 7.0. These fields have been subtracted from the WEI for the VMF of the historical period with W5E5. Positive values therefore indicate lower water exploitation compared to the reference.

The two selected GCMs are wetter than the observed climate of the W5E5 for the historical period. This is evident by the positive differences (GCMs having lower WEIs). Of the two GCMs, UKESM is slightly drier than GFDL-ESM4. For the future conditions, the UKESM GCM results show a decrease, i.e., higher WEIs in the future, in particular in areas currently not affected by water scarcity. If only the shift in the WEI within the GCMs is considered, future conditions show a strong increase in water scarcity, as expressed by the WEI, in the future.

Index of Hydrological Alteration

The Index of Hydrological Alteration was represented in a similar fashion. Again, higher values represent conditions that deviate more from the desired natural condition (Figure 80). The IHA under the historical conditions is large, particularly in the tributaries to the larger rivers .Along the rivers (Danube, Tisza) the values are lower, but still around 0.5. The improvement due to the inclusion of the EFRs (VMF) is small, which is the result that the EFRs only protect the low flows and these are more influential with respect to the withdrawals (e.g., the WEI) than to the overall discharge (IHA).

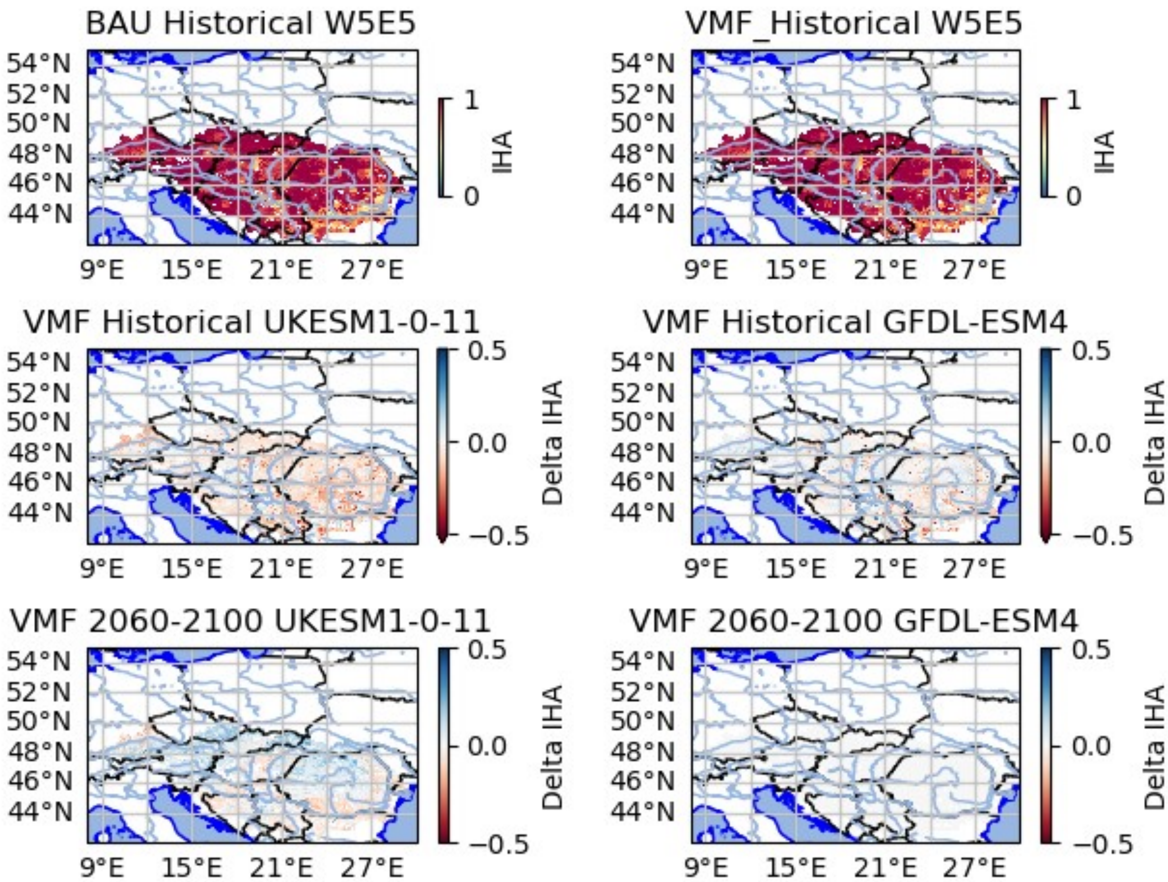

Figure 80 Index of Hydrological Alteration. The top row shows the IHAI for the historical period using the W5E5 dataset of observed weather conditions over the reference period for the BAU (no EFRs imposed) and the VMF (EFRs based on the Variable Flow Method); used hereafter as reference. The two lower two rows show the differences between two GCMs (GFDL, UKESM) for the historical period and future period between 2060-2100 based on SSP3 – RCP 7.0. These fields have been subtracted from the IHA for the VMF of the historical period with W5E5. Positive values therefore indicate less modification of the discharge relative to the reference (i.e., naturalized run).

The GCMs show larger IHAs and this arises partly because of the more even distribution of rain over the year and this negatively impacts the IHA for the historical period. For the future conditions, lower discharges lead to an improvement in the IHA but this is partly the result of the overall wetter conditions. Hence, for both the WEI and IHA an evaluation of the changes between the different periods of the GCM makes more sense than a comparison to the historical period of the observed climatological conditions. While this will give a more consistent overview of the changes due to climate change, the assessment of the relative changes per GCM prevent mutual comparison and a clear and direct condition to the present-day situation. This is an important limitation that one should address in the analysis of any non-calibrated model results as they cannot be readily compared.

4.2.4 Jucar

4.2.4.1 Application Development

4.2.4.1.1 Overview

The hydro-economic developed by Macián Sorribes (2017) has been evolved to conduct MORDM for the Júcar river basin. The structure of the model is made of 27 nodes, 8 surface reservoirs, 5 Embedded Multi-reservoir Models (EMMs) (i.e. model's components able to represent the stream-aquifer interactions, formulated by Pulido-Velazquez et al. (2005)), 7 sub-basins, 18 consumptive demands, 9 hydropower plants and 6 environmental flows. The scheme of the model is represented in Figure 81.

Figure 81. Hydroeconomic model schematic for the Júcar River.

Specifically, the model is composed of an optimization and a simulation module. The optimization component is a hydroeconomic conjunctive use model that has been developed to explore strategies to improve the operation of the Júcar river system considering the stream-aquifer interactions, with the goal of maximising the net total benefits. The optimization method, called Combined Surface-Groundwater Stochastic Dual Dynamic Programming (CSG-SDDP), is able to provide optimal decisions under hydrologic uncertainty considering influential stream-aquifers interactions.

The simulation component is a module developed to compare the CSG-SDDP optimization results with the simulation of the current operating rules. In this case, the water resources are not allocated according to economic benefits, as in the optimization component, but it's delivered based on different priorities attached to different demands and uses, calibrated to reproduce the historical operation of the system.

For the purpose of this work, only the simulation component of the model has been used to stress-test the system under a wide range of plausible futures, considering both the IPCC projections and an ensemble of synthetically generated scenarios.

4.2.4.1.2 WEFE indicators

In order to assess synergies and tradeoffs across the different components of the Water-Energy-Food-Ecosystem Nexus, different evaluation indicators were used for representing the interests of the agricultural sector, hydropower energy sector, and ecological sector.
The indicator representing the agricultural sector has been formulated as the yearly total agricultural benefit derived from the fulfilment of the agricultural water demand, excluding the rice cultivation districts. In these latter, the model was forced to maintain the same level of supply as under historical conditions (Macian-Sorribes et al., 2017). This constraint is motivated by the fact that rice constitutes one of the most important cultivation in the region, which is primarily cultivated in wetlands (Albufera lake). The monthly benefits of the agricultural districts are obtained by using the traditional hydro-economic model to compute the integral of the water supply function in terms of million euros per month. The same procedure is applied to the hydropower benefits, which are associated with the demands of nine hydropower plants: Alarcon, El Picazo, El Bosque, El Tranco del Lobo, Cofrentes, Contreras II, Cortes II, Millares II, Antella-Escalona.
The formulation of an indicator for the ecological sector is more challenging than for the other sectors. Every river has its own flow regime with peculiar hydrological characteristics, like flow volume, seasonal changes, temporal intervals, frequency, probability, and other factors (Nikghalb et al., 2016). Each of these characteristics influences river ecosystems: river flow is the driving force affecting not only the physical habitat for aquatic species, but also water temperature, water quality, biotic interactions, riparian vegetation, and terrestrial habitat interdependent on the aquatic one (Jowett, 1997).
Environmental flow is therefore defined as the required quality, quantity, and timing of water flows for sustaining freshwater and human livelihood and well-being (Poff and Zimmerman, 2010). The last Management Plan drafted by the Confederación Hidrográfica del Júcar (CHJ) defines environmental flow regimes for several river stretches, specifying minimum and maximum flows in normal conditions and during drought conditions (CHJ, 2023). In particular, the Júcar hydro-economic model includes in the modelling structure 6 river stretches subjected to environmental flow regime (highlighted in green in Figure 81). In this work, the stretch located into the Albufera was disregarded, since the water demand in this area was already prioritized and considered always satisfied. The remaining five stretches subjected to environmental flow constraints were taken into account for the formulation of the ecological indicator based on streamflow-habitat curves, i.e. curves relating flows and the habitat that a certain flow can provide for a target aquatic species.
The considered streamflow-habitat curves are taken from Annex 5 of the CHJ Management Plan 2022-2027 (CHJ, 2022), where they were defined according to the following procedure. The first step consists on the selection of the target species for which suitability conditions of habitat will be considered. The selection was carried out considering the native species, and giving priority to those categorized as "Endangered", "Vulnerable", "Sensitive" and "Of Special Interest" in the Catalogs of Threatened Species of the Júcar river basin. For the 5 river stretches of the analysis, the considered species are Trout (Salmo trutta), Chub (Squalius pyrenaicus) and Loina (Parachondrostoma arrigonis).
For each of the selected species, experts made available curves that relate the preference for different age classes (young, young adult and adult) towards different physical variables of environment, as average speed in the water column, depth, bed substrate. These curves are able to express suitability conditions for the species (of each age class) and thus indicate which is the preferred habitat in terms of optimal physical parameters.

Crossing hydraulic model's information and suitability habitat curves, it's possible to obtain a curve that indicates how the habitat (for a certain species and age class) varies depending on the flow. In order to compare curves of different species and stages, they are converted into dimensionless. The Potential Useful Habitat (HPU) that the given stretch of river can offer is thus identified on the original curves as the maximum of the curve or, in case the curve doesn't show a maximum, as the 25th percentile of the series in the natural regime. The curves are therefore normalized with respect to the maximum HPU, so that they show the relation between the flow and the percentage of HPU that the flow provides (with respect to the maxHPU). These curves are called streamflow-habitat curves (see an example in Figure 82).

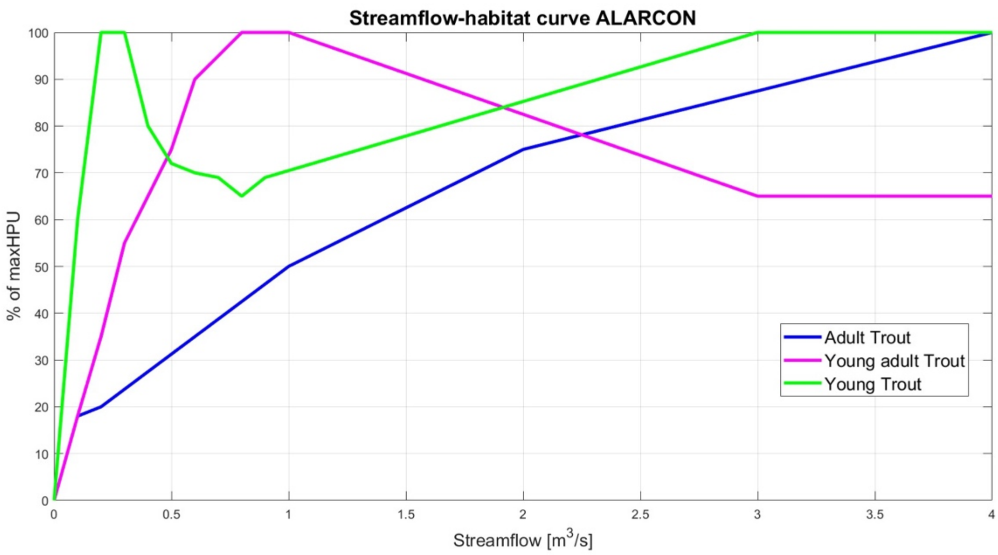

Figure 82: Example of streamflow-habitat curve of the Alarcon stretch for the 3 age classes of the Trout specie.

Finally, all the annual indicators are further aggregated over the considered 85-years simulation period (H) to obtain an overall evaluation of the performance. The aggregated indicators of both the agricultural and hydropower sectors are formulated as the average of the annual indicators (benefit values) over the simulation period. For the ecological sector, a hybrid approach was implemented by combining both the average and the minimum values. Aggregating the yearly spatial average habitat time series using the minimum highlights the importance of preserving a minimum percentage of habitat during the simulation period: the application of the simple average on the whole annual dataset would lead to a "smoothing effect" which causes that extremely negative events, very critical for the ecosystems' preservation, would not be captured by the analysis. On the other side, the average operator should not be completely excluded, due to the fact that the single worst-case event captured by the minimum value would not be completely representative of the long-term simulation. For these reasons, the formulation adopted in this work aggregates the two criteria with a weighted sum where weights of the average and minimum performance are equal to 0.2 and 0.8, respectively.

4.2.4.1.3 Climate projections

In order to perform the robustness analysis over the Júcar basin case study, projected climate data are needed as starting point for the subsequent analyses. The data used has been selected among those in the framework of the Climate Model Intercomparison Project

(CMIP), in particular the 6th phase of the project (CMIP6). For this work, the data used are temperature and precipitation data obtained by the model GFDL-ESM4, for the period 2016-2100 at a monthly scale, for each combination of RCP-SSP. The ESM4 model is one of the global circulation models developed by the US Geophysical Fluid Dynamics Laboratory (GFDL), based on an atmospheric component, an ocean component, land and vegetation dynamics components, sea ice dynamics components, biogeochemical and ecological interactions components, dust, and iron cycling components (Krasting et al., 2018). The GFDL-ESM4 data has been processed with a downscaling step using the quantile-mapping method and using the ERA5 reanalysis data (Hersbach et al., 2020) as local observations.

4.2.4.2 Application Results

4.2.4.2.1 Historical simulation and IPCC scenarios

The first step of the work consisted of the analysis of the historical performance of the current operating policy and the simulation of the latter over the 5 RCP-SSPs scenarios (Figure 83). The agricultural historical benefit (top panel) remains almost constant during the years reaching a value close to 200 Me/year, except for some low peaks in 1990, 1999 and 2001, probably due to water scarcity conditions. The trajectory of the hydropower benefit (middle panel) is instead more variable during the historical years, oscillating between 15 and 35 Me/year. A different pattern characterizes the habitat indicator (bottom panel), which keeps a constant value of 50% of maxHPU from 1980 to 2004 and decreases right after this year, fluctuating around 40% of maxHPU.

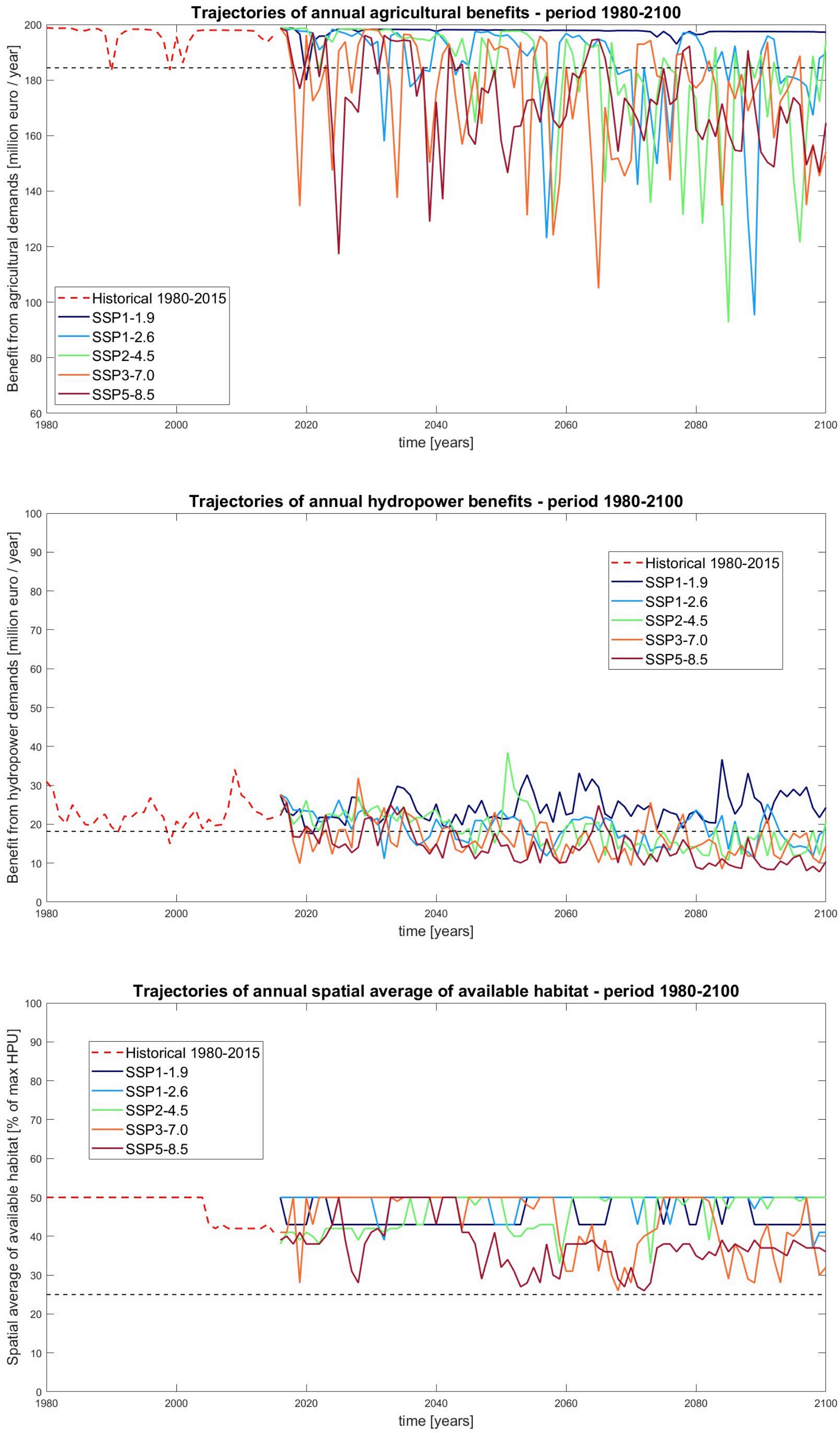

Figure 83: Trajectories of historical and projected performance over different RCP-SSP scenarios, for each of the 3 competitive sectors. The black dashed line represents the historical reference performance for each indicator.

The figure also includes a black dashed horizontal line that represents a reference value supporting the analysis of the projected performance. For the agricultural and hydropower sectors, the line represents the 5th percentile of the historical distribution of annual indicators. This low percentile has been chosen to represent critical conditions that rarely happened during the historical period for these two sectors. For the habitat sector, the Júcar Hydrological Management plan formulated by CHJ (2023) classifies the conditions to maintain into river reaches as follows:

- 80% of maxHPU in not hydrologically altered reaches;
- from 50% to 30% of maxHPU in already hydrologically altered reaches, according to the specific case;
- 25% of maxHPU only in severe drought conditions and only if the reach is not inside a protected area.

The 25% of maxHPU was then selected as it represents the minimum percentage of HPU that should be preserved even in critical drought conditions.

Focusing on the projected indicators' trajectories, different results are obtained across the RCP-SSP scenarios. Under SSP1-1.9 the performance of all the 3 indicators is similar to the historical one and it is the best performance among the considered scenarios. The situation changes under scenarios SSP1-2.6 and SSP2-4.5. In the short term (2016- 2030), the performance of all the 3 indicators is in line with the historical one and with scenario SSP1-1.9. For agricultural and hydropower indicators, while the performance remains still acceptable almost until mid-century, after 2050 it starts declining for many years below the historical reference line. Particular low peaks are registered under SSP1- 2.6 and SSP2-4.5 for the agricultural indicator in the very long term (2085 and 2089), with values of agricultural benefit below 50% of the historical average. For the habitat indicator, scenario SSP1-2.6 performs almost equal to SSP1-1.9 until the end of the century, while SSP2-4.5 shows lower peaks of available habitat under the 40% of maxHPU especially in the second half of the century.

The overall performance decreases further under SSP3-7.0 or SSP5-8.5. For the agricultural indicator, very low peaks of performance are associated with these scenarios especially from 2016 to 2065. From 2065 to 2100, instead, the trajectories of all the scenarios (except SSP1-1.9) are oscillating in a wide range of variability and the performance of SSP3-7.0 and SSP5-8.5 is not evidently worse than the other scenarios. However, it has to be noticed that during the whole century, the agricultural trajectory under SSP5-8.5 is most of the years below the historical reference line, with only a few years above this threshold. Similar considerations apply to the hydropower benefit trajectory. Habitat trajectories are the ones that show the largest difference in performance under SSP3-7.0 and SSP5-8.5 with respect to the other scenarios. The available habitat under SSP3-7.0 is almost in line with the one provided by the other scenarios until mid-century, but it presents several significant falls after 2050. Scenario SSP5-8.5 further anticipates these low peaks of available habitat before 2050. The lowest peaks under these scenarios reach values very close to the line of 25% of maxHPU, representing the minimum fraction of habitat to preserve even in cases of strong droughts. This condition is therefore crucial for the ecosystem's integrity and preservation.

4.2.4.2.2 States of the World

In this section, the results obtained considering the ensembles of synthetically generated states of the world are discussed. Figure 84 shows the distributions of the simulated performance measured by the annual indicators over the synthetic ensembles associated with each RCP-SSP scenario.

The synthetic ensembles of agricultural indicators and hydropower indicators have median values that are almost equal to the medians of the corresponding historical vales. However, large differences emerge when looking at the shape of the distribution and, particularly, at the worst-case performance.

In the agricultural sector (top panel), this difference clearly emerges for the SSP1-1.9 ensemble: while the minimum annual value in the baseline projection was equal to 179 Me/year, in the synthetic ensemble it drops to 87 Me/year. Similarly, the lowest benefit for the SSP5-8.5 ensemble (i.e. 78 Me/year), is lower than under the baseline SSP5-8.5 scenario. Moreover, we can observe that the shape of the violins for SSP3-7.0 and SSP5-8.5 suggests that a consistent number of scenarios is associated with performance values well lower than the median.

The widest sections of the hydropower violins (middle panel) are almost at the same performance level as the baseline ones for all the scenarios. However, we can notice a second wide section, containing a consistent fraction of annual indicators whose performance is lower than the ensemble mean.

Lastly, the violin plots of the habitat sector (bottom panel) show that a large fraction of the generated scenarios is located in the lower part of the violins (below the 50% maxHPU line). The lowest value of available habitat across all the ensembles is obtained under SSP3-7.0 and it is below the critical line of 25% maxHPU. In the ensembles of SSP3-7.0 and SSP5-8.5 a significant number of scenarios is also located below the level of 30% maxHPU.

To synthesize the results discussed so far, we aggregated the simulated performance over time. Figure 85 shows the distributions of 100 aggregated indicator values, one for each synthetic scenario. The same aggregated indicators relative to the RCP-SSP trajectories have also been computed and superimposed on the violins of the correspondent scenario using diamond markers. This visualization allows exploring how the performance simulated over the synthetically generated ensembles spread around the nominal scenarios. The historical indicators computed over the period (1980-2015) are also reported in the figure as black circles.

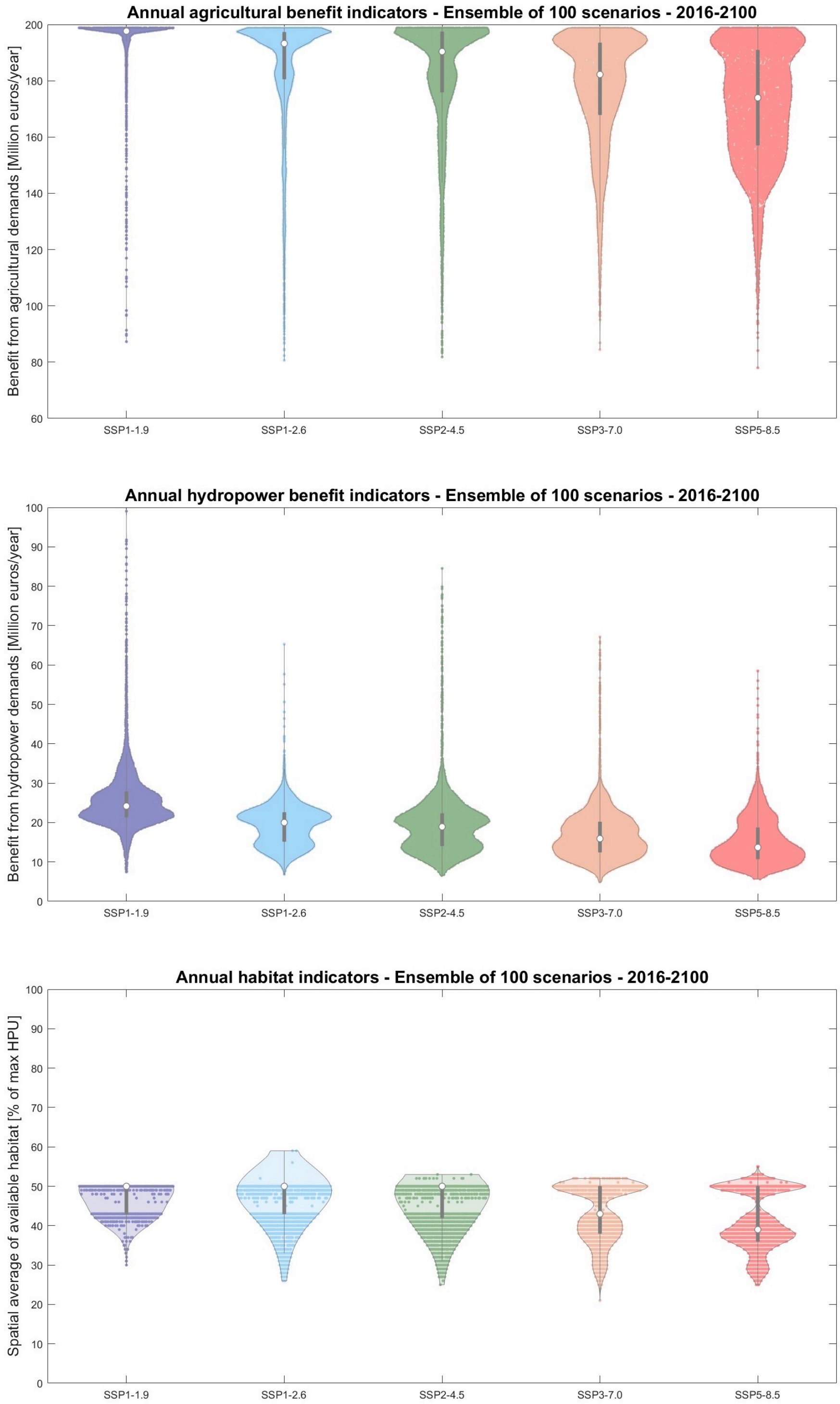

Figure 84: Violin plots showing the distributions of the of the annual WEFE indicators over the simulation period (2016-2100) for different future scenarios.

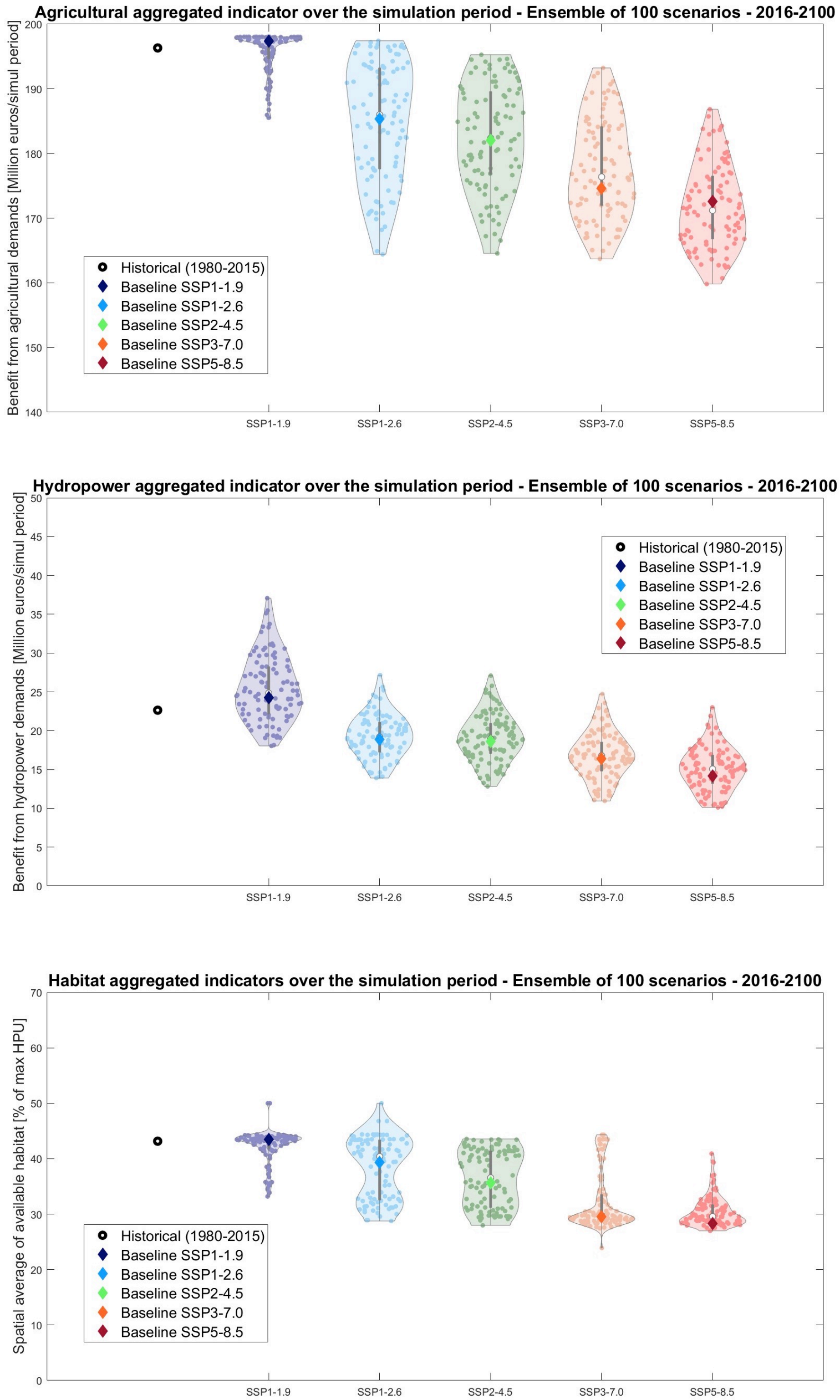

Figure 85: Violin plots showing the distributions of the WEFE indicators aggregated over the simulation period (2016-2100) for different future scenarios.

The five violins for both the agricultural and hydropower sectors show an overall decreasing performance moving from SSP1-1.9 to SSP5-8.5. In terms of agricultural benefit (top panel), the ensemble of SSP1-1.9 is the only one where the majority of the indicator values is higher than the historical performance. The ensemble of SSP1-2.6 also shows some scenarios having indicators in line with the historical performance, while SSP2-4.5, SSP3-7.0 and SSP5-8.5 have the violins distributed below the historical performance. A similar pattern is visible in the ensembles of hydropower objectives (middle panel). The violin of SSP1-1.9 is again the only one having the widest section at a level of performance slightly higher than the historical performance. The distributions of the habitat indicators (lower panel) are more interesting to analyse because the widest section of each violin is now not necessarily aligned with the ensemble median around a value of 50% maxHPU. For SSP1-1.9, SSP1- 2.6 and SSP2-4.5 the widest section is located around the 40% maxHPU, at the same level where the historical objective is located. For scenarios SSP3-7.0 and SSP5-8.5, it is instead shifted down up to 30% maxHPU.

4.2.4.2.3 Robustness Evaluation

This section presents the robustness assessment of the current operating policy of the Júcar river system building on the outputs of the Monte Carlo simulations discussed in the previous sections. For each sector, five Cumulative Density Functions are computed by analyzing separately the synthetic ensemble associated to each IPCC scenario. Each of these CDFs is thus computed over 8500 data points (100 synthetic trajectories of 85-years). The distribution of the indicators illustrated by the CDFs can be then compared with the reference values of performance identified in Figure 83 and represented here as vertical lines.

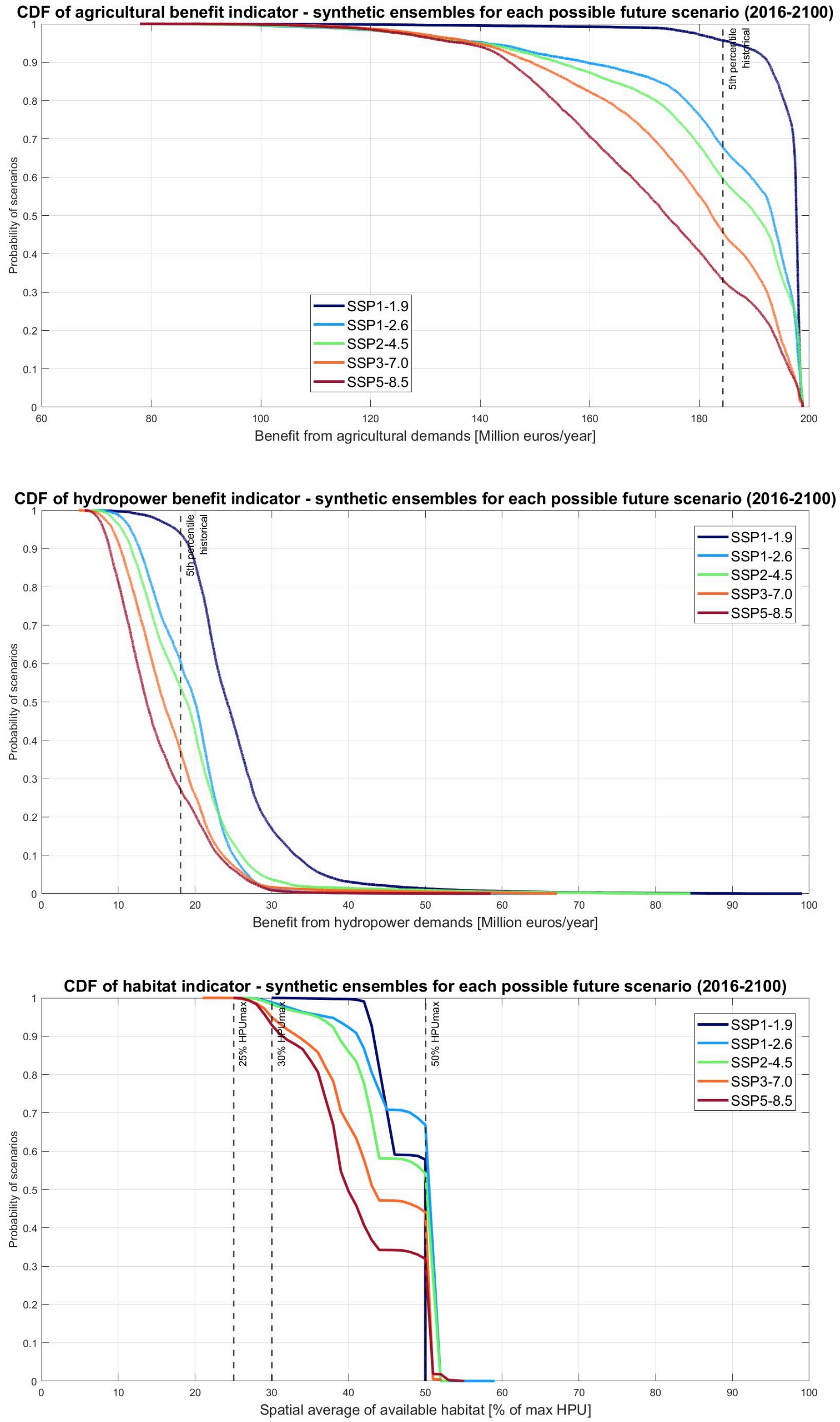

Figure 86: Performance of the current operating policy of the Júcar river system over the five 100-member stochastic ensembles.

Results reported in Figure 86 (top panel) show that the percentage of scenarios that guarantees the historical agricultural benefit varies substantially with the different SSP-RCP scenarios. The difference between the percentages associated to the ensemble of SSP1-1.9

and of SSP5-8.5 is important, especially if we consider that the 5th percentile of the historical performance is already a critical condition for the system, which is currently facing allocation problems and conflicts due to water scarcity conditions. A future where this (already low) performance might be guaranteed only with a probability of 30% under SSP5-8.5 clarifies the urgency of implementing climate change mitigation efforts.

In the case of the hydropower benefit (middle panel), the reference benefit will be guaranteed by about 50% of the generated scenarios for SSP1-1.9, SSP1-2.6, and SSP2-4.5. However, the fraction of scenarios ensuring the historical performance decreases to 28% under the pessimistic SSP5-8.5 scenario.

Finally, the CDFs for the habitat indicator (bottom panel) show that more than 90% of the explored scenarios guarantee an available habitat of 30% maxHPU, while the fraction of scenarios guaranteeing an available habitat of 50% maxHPU varies across the different SSP-RCP projections. Under the SSP3-7.0 scenarios, a few simulations return a habitat lower than 25% of maxHPU, which would correspond to very critical stress for the riverine ecosystems, with the risk of creating irreversible damages to the aquatic species. Results also suggest it will be very unlikely that the current operation of the Jucar system will ensure a spatial average habitat higher than 50% of maxHPU.

4.3 Hydroeconomic Modeling

4.3.1 Júcar

4.3.1.1 Application Development

Three hydroeconomic models with the same system representation have been developed for the Júcar River using the Explicit Stochastic Programming Advanced Tool (ESPAT) developed by (Macian-Sorribes et al., 2017). These models work at the monthly time scale and follow a simulation, stochastic optimization, and deterministic optimization approach respectively. The Júcar River system is represented by 27 nodes, 8 surface reservoirs, 5 groundwater bodies modeled using the Embedded Multireservoir Model (Pulido-Velazquez et al., 2005), 7 sub-basins, 18 consumptive demands, 9 hydropower plants and 6 minimum environmental flows (5 set according to habitat suitability curves of native fish species and 1 correspond to the minimum discharge to the sea committed). The system representation of all models is in the process of being updated to incorporate the last available data (Figure 87). The features described below correspond to the currently available version, which provides a coherent picture of the system representing the 1998-2020 period and may suffer modifications in the future.

Figure 87. Hydroeconomic model schematic for the Júcar River.

The physical features of the model (hydrological sub-basins; reservoir capacity, minimum level, storage-head, and storage-surface curves; groundwater models; river reach and canal capacity; minimum streamflow prescribed; water demands and returns; and fish habitat curves) were obtained from the Júcar River Basin Agency (RBA). The economic features of water uses (urban demand curves; energy prices; and pumping costs) were obtained from CHJ (2013) and updated from previous efforts (Pulido-Velázquez et al., 2006) in the context of the DMA implementation in the Júcar as part of the EU AQUAMONEY project, being successfully contrasted with other hydroeconomic models (Kahil et al., 2016). Urban demand was modelled using demand functions that link the amount of water supply to the marginal value of water for the user (Figure 88).

On the other hand, agricultural demand benefits for citrus, orchards and perennial crops were modelled using a revised version of the crop yield calculation included in the FAO33 methodologies (FAO, 2012). In this modified methodology, a yearly crop yield is calculated as a function of the supply-demand ratio. Then, the total food production is calculated from the product between the estimated crop yield and a reference production value extracted from historical statistics. Finally, the yearly total benefits are calculated trough the total food production and the crop price. Rice crops play a crucial role in maintaining the l'Albufera Lake, one of the most relevant protected areas in the region, and their supply has been considered as a constraint.

The only industrial demand using surface water is the Cofrentes Nuclear power plant, whose benefits per unit of water consumption have been evaluated using the alternative cost method, the cost of providing the same amount of energy by gas less the operation costs of the plant, obtained from Pereira-Cardenal et al. (2014).

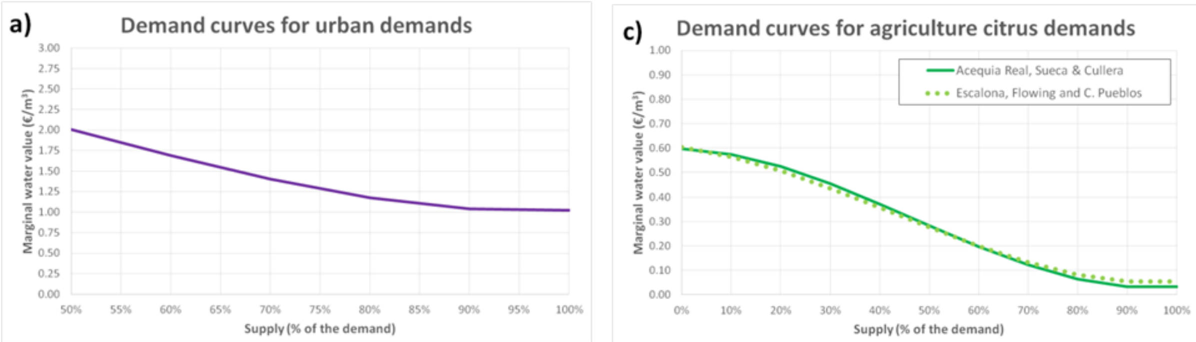

Figure 88. Demand functions that link the amount of water supply to the marginal value of water.

Since both stochastic optimization and deterministic optimization implement optimal rules that are not applied in practice, the calibration and validation of the system representation has been performed using the simulation model, which implements the reservoir operating rules currently applied by the Júcar RBA. The calibration and validation strategy involved the following variables and performance levels, showing an adequate overall performance:

- **Storage and releases from reservoirs:** the model successfully represents them for the main reservoirs (Alarcon, Contreas and Tous), while the minor reservoirs of Forata and Bellus so adequate storage levels but a so-so adjustment of releases that, in any case, does not play a distinct role in the systemwide operation (Figure 89).

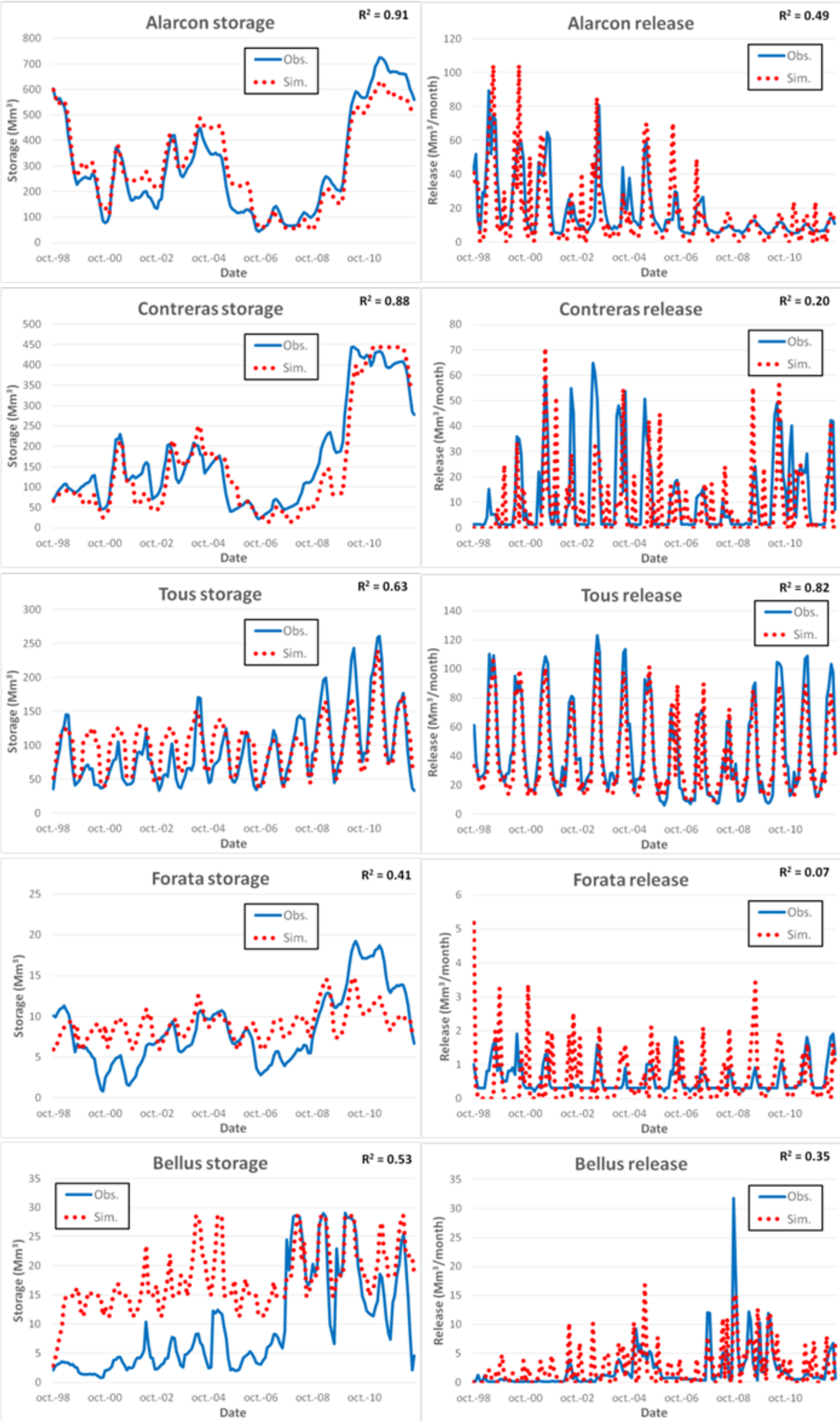

Figure 89. Storage and releases from reservoirs.

- **Annual production (GWh), water use intensity (m3/Kwh) and water use productivity (€/ m3) in hydropower plants:** the model slightly underestimates water use intensity and overestimates water use productivity in the main hydropower plants (Cofrentes, Cortes II and Millares II) and shows the opposite behavior for the rest, although deviations are not significant in most cases (see Table 6). Considering hydropower production (only available in the main plants), the model matches very well the annual production of Cortes II and Millares II and slightly underestimates Cofrentes.

Table 6. Observed and modeled energy production, water use intensity, and water use productivity for hydropower plants.

Powerplant	**Production (Gwh/year)**		**Water use intensity (m3/Kwh)**		**Water use productivity (€/m3)**	
	Observed (Iberdrola)	**Model**	**Observed (CHJ)**	**Model**	**Observed (CHJ)**	**Model**
Alarcon	-	14.34	9.00	13.01	0.008	0.004
El Picazo	-	24.16	-	9.26	-	0.006
El Bosque	-	8.91	20.00	17.99	0.004	0.003
El T. del Lobo	-	4.09	33.00	39.18	0.003	0.002
Cofrentes	51	33.49	4.00	3.13	0.015	0.009
Contreras II	-	13.47	6.00	7.00	0.009	0.014
Cortes II	120	119.26	5.00	4.27	0.013	
Millares II	141	148.64	4.00	3.06	0.015	0.020
Ant. - Esc.	-	5.85	-	55.66	-	0.001

- **Streamflows in gauge stations:** the model successfully reproduces the streamflow recorded in the lower basin and the most upper parts of the middle basin, together with the stream-aquifer interaction between the Júcar river and the Mancha Oriental aquifer (Figure 90). However, the records in some of the middle streams of the river could be improved. Nevertheless, this has not been considered as a major drawback, since is mainly caused by the fact that the Mancha Oriental aquifer is modeled as a lumped element whose interaction with the river is considered to take place in a single point rather than along tenths of kilometers along the river, as would be obtained by a distributed groundwater model, whose detail would be excessive for the formulation and the purpose of the model.

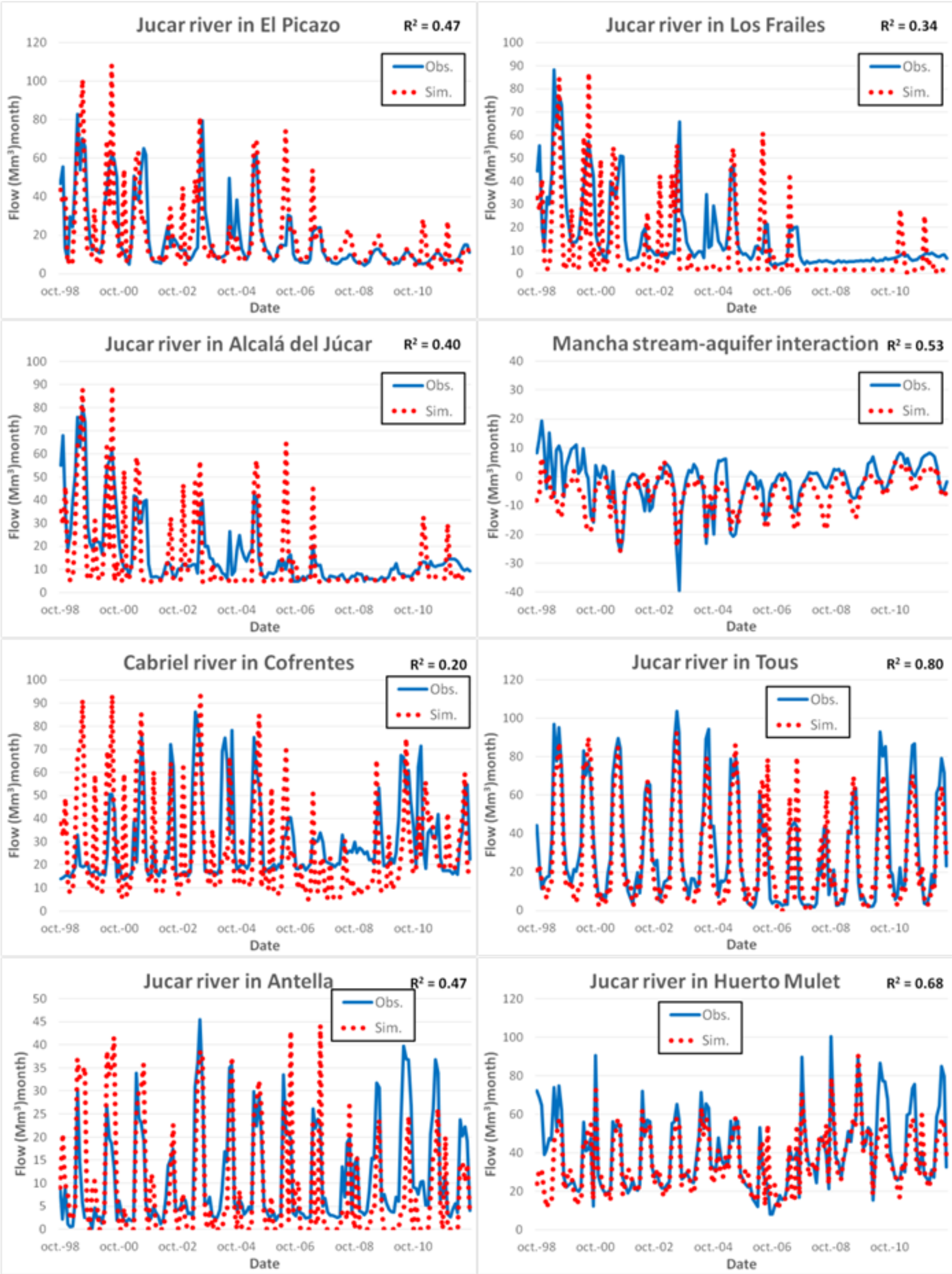

Figure 90. Observed and simulated streamflow.

- **Deliveries to consumptive demands:** the model reproduces in an adequate way the deliveries to the surface demands, in particular the largest ones (Acequia Real, Escalona, Sueca, Cullera and Canal Júcar-Turia) (Figure 91).

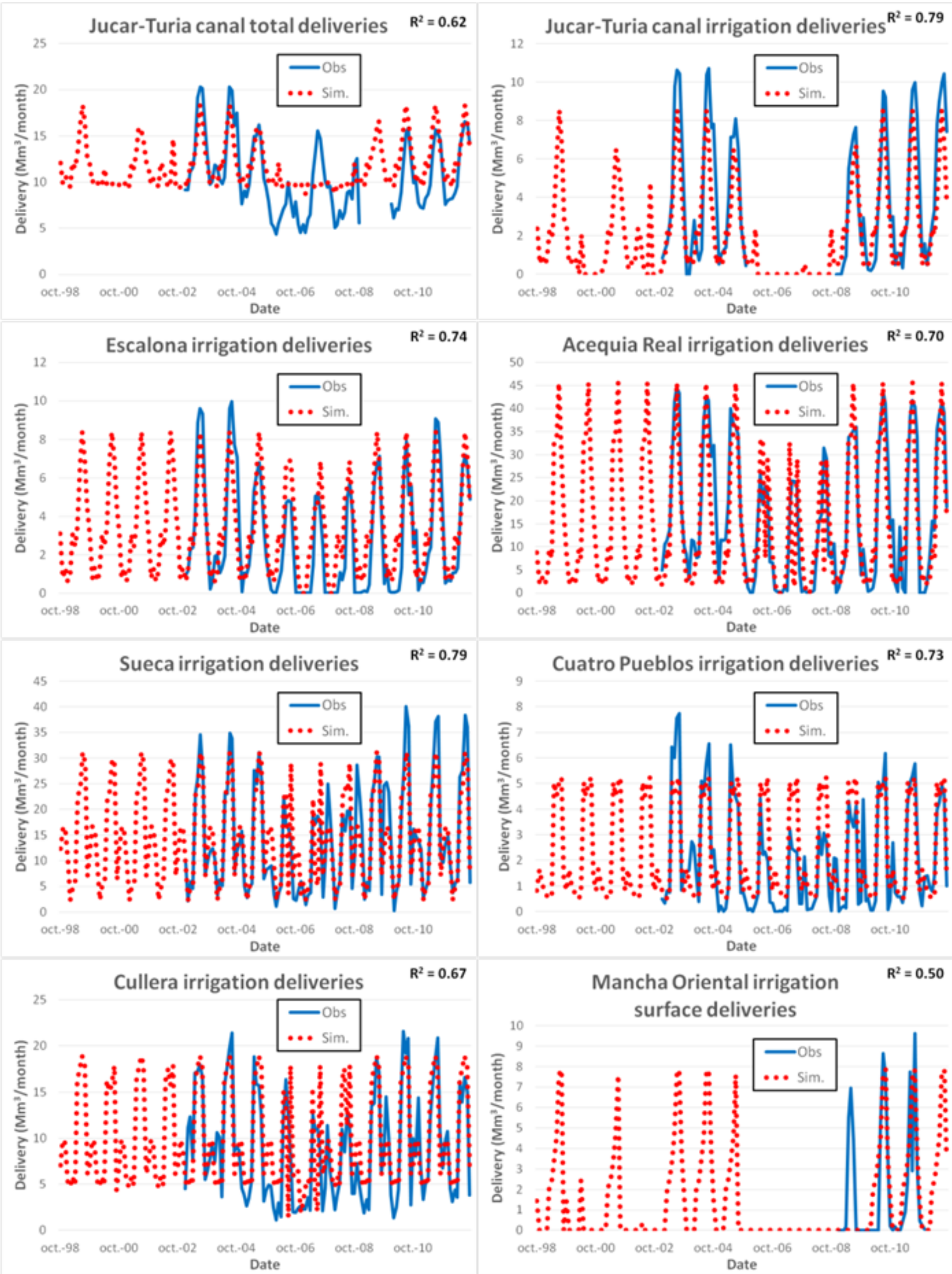

Figure 91. Observed and simulated surface water deliveries.

4.3.1.2 Application results

4.3.1.2.1 Economic performance

Preliminary results obtained for the historical period refer to how the current operating rules of the Júcar could be modified to increase their economic revenues while complying with the minimum streamflow prescribed and the requirements of the l'Albufera lake. A comparison between the current system operation and the stochastic hydroeconomic optimization is shown in Table 7 below:

Table 7. Comparison between the current system operation and the stochastic hydroeconomic optimization.

	Category	Consumptive uses					Energy	Aquifer	Systemwide level	
	Type	Urban		Agricultural			Totals	Mancha Oriental aquifer discharge	Urban	Agriculture
	Variable	Mancha	Valencia	Mancha	USUJ	Jucar-Turia & Magro				
Current system management	Surface deliveries (Mm³)	14.33	114.51	16.96	540.60	29.49	-	-	128.84	587.05
	Groundwater deliveries (Mm³)	16.10	0.00	315.45	0.00	73.10	-	-	16.10	388.55
	Energy produced (GWh)	-	-	-	-	-	372.20	-	-	-
	Economic benefits (M€)	60.26	228.78	78.89	63.37	51.65	22.26	-	289.04	193.91
	Groundwater discharge (Mm³)	-	-	-	-	-	-	-63.31	-	-
Stochastic programming	Surface deliveries (Mm³)	13.64	114.51	29.13	556.73	42.13	-	-	128.15	623.17
	Groundwater deliveries (Mm³)	16.79	0.00	238.30	0.00	59.99	-	-	16.79	303.11
	Energy produced (GWh)	-	-	-	-	-	414.03	-	-	-
	Economic benefits (M€)	60.36	228.78	78.34	65.83	52.21	25.00	-	289.14	196.38
	Groundwater discharge (Mm³)	-	-	-	-	-	-	-29.91	-	-
Differences	Surface deliveries (Mm³)	-0.70	0.00	12.17	16.14	12.64	-	-	-0.70	36.13
	Groundwater deliveries (Mm³)	0.70	0.00	-77.14	0.00	-13.11	-	-	0.70	-85.44
	Energy produced (GWh)	-	-	-	-	-	41.83	-	-	-
	Economic benefits (M€)	0.10	0.00	-0.55	2.45	0.56	2.73	-	0.10	2.46
	Groundwater discharge (Mm³)	-	-	-	-	-	-	33.40	-	-

The hydroeconomic model considers the recovery of the aquifer levels in the Mancha Oriental, and its subsequent increase of the Júcar streamflow due to stream-aquifer interaction, the most efficient option to achieve an economically optimal water use. Consequently, it curtails pumping from the Mancha Oriental aquifer by 80 Mm³/year (from 330 to 250 Mm3), which turns into an increase of 33 Mm³/year of discharge in the Júcar river that can be used to both produce energy in the most relevant hydropower plants and supply the downstream agricultural demands, which for the period of analysis show larger revenue margins than the ones in the middle basin. The decrease of groundwater pumping lowers the revenues of the Mancha Oriental, but this is compensated by a larger increase of economic profit in the lower basin. Despite depicting a basinwide increase in economic benefits, the hydroeconomic model enlarges the difference between the lower and the middle Júcar basin farmers, which would require further instruments to re-distribute this increase in a more equitable way.

4.3.1.2.2 Reservoir operation

The monthly storages in the main reservoirs (Alarcon, Contreras, and Tous) have been compared to establish how the hydroeconomic stochastic programming suggests improved operating rules compared to the status-quo. The rest of the reservoirs play a very minor role in water management due to a low live storage, since they are small reservoirs (Molinar, Forata and Bellus) or have strict level limits due to hydropower production (Cortes II, El Naranjero). The comparison of the records for the analysis period (Figure 92) shows that the Alarcon reservoir is operated similarly between both alternatives, although stochastic programming shows a clearer refill-drawdown cycle between winter and summer periods.

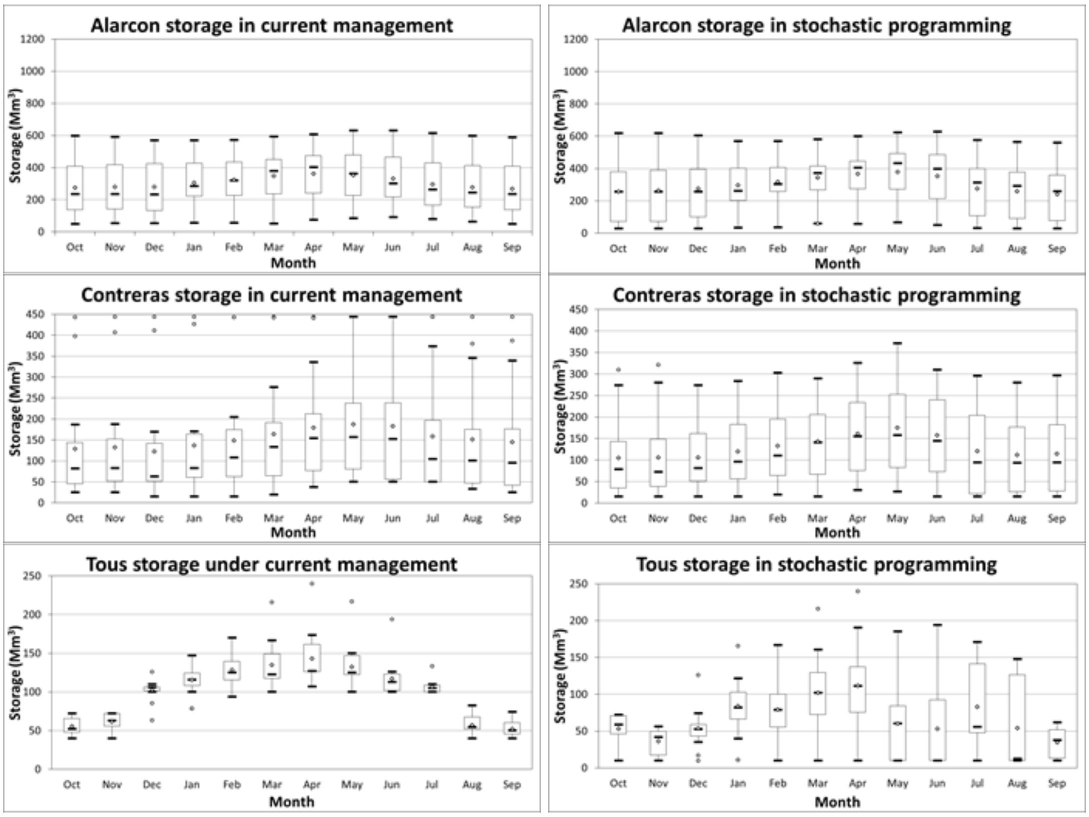

Figure 92. Reservoir storage in current management and solution determined with stochastic programming.

The results for Contreras also show a similar behavior on a broader view, but in this case the changes are opposite than for Alarcon: the refill-drawdown cycle shown by the current operation is clearer than the one provided by stochastic programming, which operates the reservoirs more in parallel than they are today. The strongest differences are found, however, in the Tous reservoir, which is placed at the tail of the system. While the current operation shows a strict refill-drawdown cycle regardless of the year, stochastic optimization depicts a more flexible operation strategy, in which Tous is perceived as the tail reservoir of the hydropower system, minding the energy prices in its refill-drawdown cycles rather than solely the consumptive demands in the lower basin.

4.3.1.2.3 Conjunctive use optimization

The surface and groundwater deliveries to the two agricultural demands that have the possibility to use both sources (Mancha Oriental and Júcar-Turia) are modified by stochastic programming compared to the current operation. As expected, the differences focus on the summer months, in which water demands are the largest of the year. As shown in Figure 93, stochastic programming curtails the groundwater deliveries to both demands while increases the surface deliveries. In case of the Mancha Oriental demand, the decrease of groundwater pumping maintains or slightly recovers (depending on the year) the aquifer levels, which results in a lower pumping cost and an increased discharge from the aquifer into the Júcar river due to stream-aquifer interaction. This discharge is the main reason why pumping rates are lower than the current operation, since increasing the streamflow in the middle Júcar reaches means higher water availability for hydropower production and agricultural supply in the lower basin, which turns to be more profitable than a direct allocation of groundwater resource into the Mancha Oriental agricultural districts. However, the increase of surface deliveries is lower than the pumping curtailment since, as found for increased groundwater discharges, the model finds it more profitable to mainly use these resources to produce energy and supply the downstream arable lands.

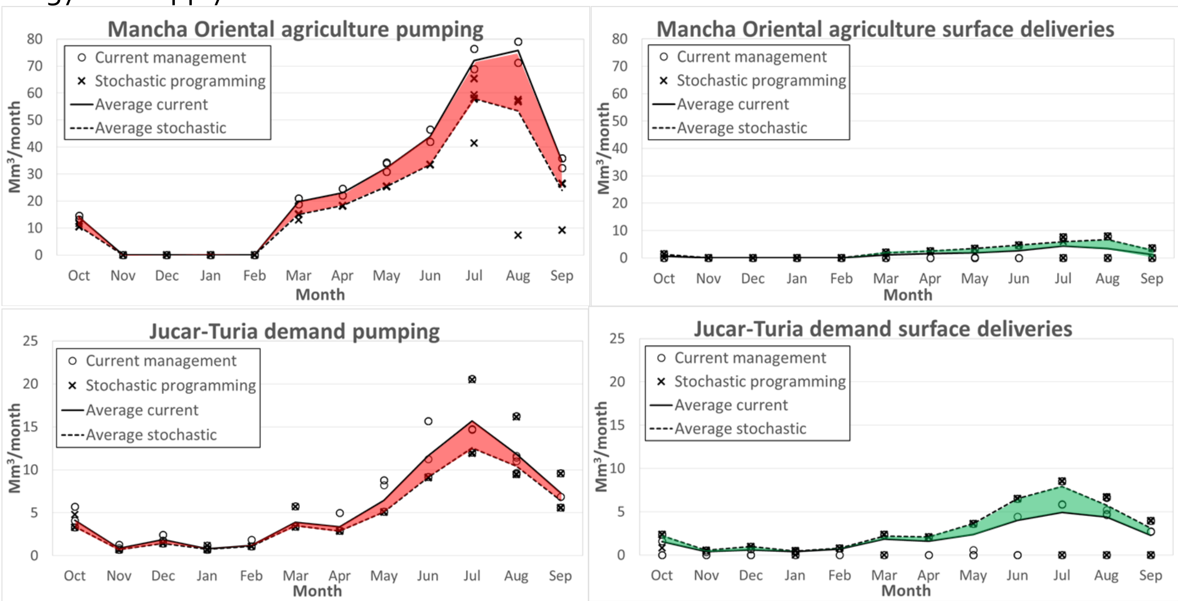

Figure 93. Groundwater pumping and surface deliveries with current management and solution determined with stochastic programming.

As shown in the economic performance subsection, the monetary tradeoff greatly favors the downstream areas due to the synergy between energy and agricultural use (water allocated to the lowlands can be employed for both uses since water allocated to the Mancha cannot be used to produce energy in the most profitable hydropower facilities). Nonetheless, the decrease in the Mancha Oriental revenues is small compared to the amount of water curtailed due to two factors: the aquifer level recovery decreases pumping costs and the surface water allocated, although less than the pumping curtailment, is distinctly cheaper.

On the contrary, the Júcar-Turia agricultural demand receives more or less the same amount of surface water as the pumping reduction. This is because the opportunity cost of water allocated to the Júcar-Turia canal is distinctly lower than the Mancha Oriental one, since the intake is downstream of the main hydropower plants (water allocated has been already used to produce energy) and the economic profitability of the crops is similar to the rest of the lower basin areas. Consequently, the Júcar-Turia canal substitutes groundwater pumping by surface resources when water availability is enough, while increases pumping in water scarcity events due to being the only agricultural demand that regularly uses this resource in the lower basin.

4.3.1.3 Food production

According to the results obtained from the hydroeconomic model (Figure 94), in a simulation base scenario the crops whose total annual production is most sensitive to the availability of resources in the system are vegetables, citrus fruits, and fruit trees.

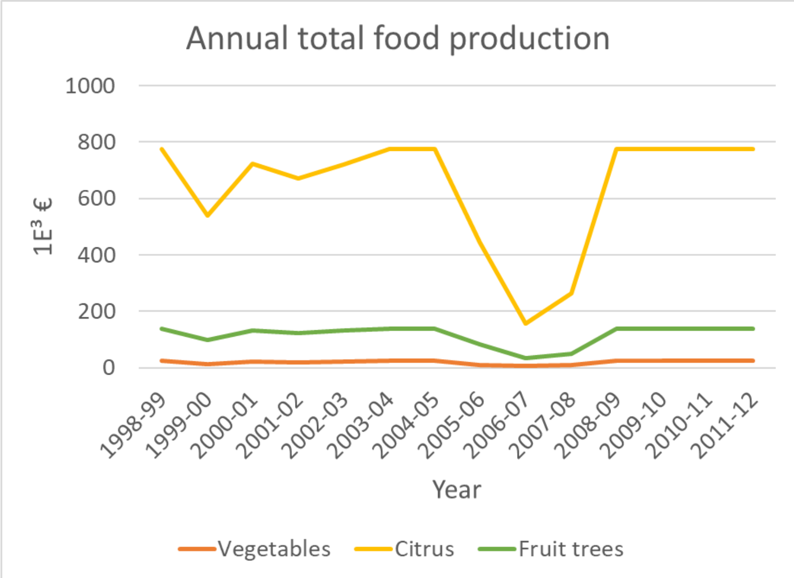

Figure 94. Annual total food production

As evidenced by the sensitivity of citrus crops to water availability, it becomes clear that targeted efforts are required to ensure the viability of these agricultural activities.

4.3.2 Tagus-Segura

4.3.2.1 Application Development

Due to the Segura River Basin (SRB) complexity (Figure 95), three robust deterministic models were developed to determine optimal water allocation policies for three scenarios at the monthly time scale. The first one is a system operation optimization model under current operating rules, and the other two scenarios look for economic-efficiency operation, i.e., minimization of operational costs and maximization of net agricultural benefits.

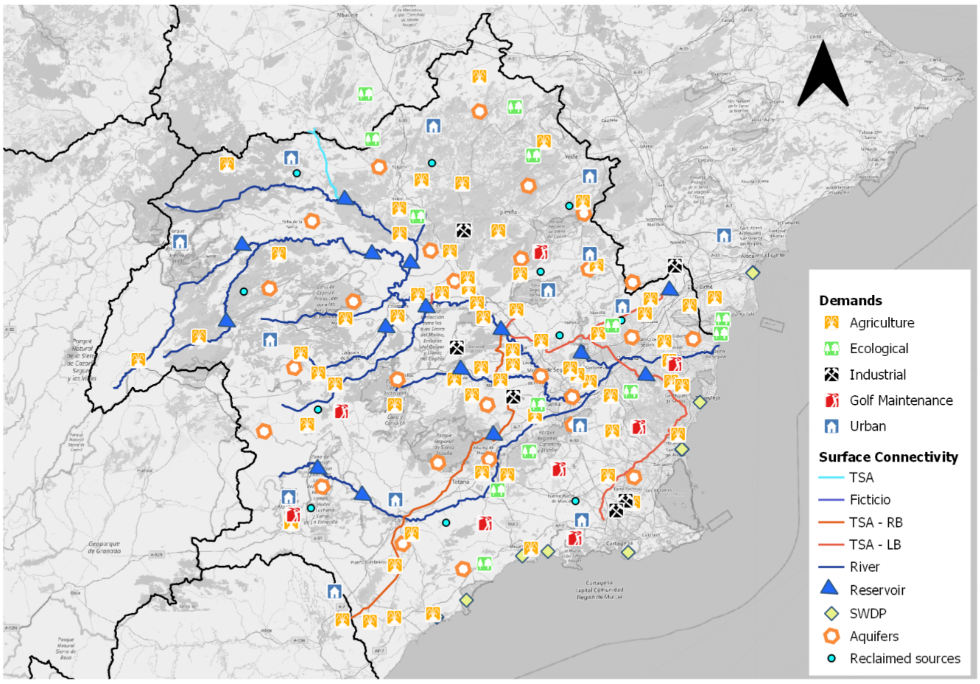

Figure 95. Hydroeconomic model schematic for Tagus-Segura system

The linked Tagus-Segura system is represented in the numerical models through the Tagus-Segura Aqueduct (TSA) water transfer. In this way, evaluating the economic impact on the system's WEFE nexus components for variations in the volume of water transferred is possible.

Table 8. Modelled elements

<table>
<tr><th colspan="2">Element</th><th colspan="2">Amount</th></tr>
<tr><td colspan="2">Nodes</td><td colspan="2">160</td></tr>
<tr><td colspan="2">Reservoirs</td><td colspan="2">15</td></tr>
<tr><td rowspan="2">Consumptive demands</td><td>Agriculture</td><td>64</td><td rowspan="2">105</td></tr>
<tr><td>Other</td><td>41</td></tr>
<tr><td colspan="2">Aggregated aquifers</td><td colspan="2">26</td></tr>
<tr><td colspan="2">Groundwater pumping facilities (GPF)</td><td colspan="2">140</td></tr>
<tr><td colspan="2">Surface water pumping facilities (SPF)</td><td colspan="2">8</td></tr>
<tr><td colspan="2">Hydroelectric Power Plants (HPP)</td><td colspan="2">6</td></tr>
<tr><td colspan="2">Sea Water Desalination Plants (SWDP)</td><td colspan="2">13</td></tr>
<tr><td colspan="2">Reclaimed water sources (RWS)</td><td colspan="2">10</td></tr>
</table>

The modelled system is defined by the elements presented in Table 8. These elements allow the evaluation of the main challenging WEFE nexus components in the system as follows:

Water: Optimal water allocation

Energy: Hydroelectric energy generation and operational energy consumption

Food: Net benefits from food production

Ecosystem: Minimum environmental flows accomplishing and aquifers overexploitation

The physical features of the model were obtained from the Segura River Basin Agency (SRBA) and adapted for the WEFE nexus modelling.

In all three scenarios, a deterministic optimization approach is followed where the water allocation in the system is formulated as an optimization problem where the objective function is set according to the objective pursued in each scenario. The characteristics of each of the models are summarized below.

4.3.2.1.1 Base scenario

In this scenario, the objective function is based on the sum of penalties or unit costs that condition the distribution of the resource subject to the priority orders established by the SRBA for the system.
The system of equations and penalties that define the objective function is based on the work of Andreu et al. (1996). It includes additional modifications to consider nexus elements such as electricity generation.

$$OP = \sum_{n=1}^{N} EFDP_n + DDP_n + AEP_n + HDP_n - MSAR_n$$

Where OP is the total operational penalties, N is the total simulation timesteps, $EFDP_n$ is the environmental flow deficit penalty, DDP_n is the demand deficit penalty, AEP_n is the aquifer exploitation penalty, HDP_n is the hydropower generation water supply deficit penalty and $MSAR_n$ is the minimum storage in reservoirs accomplishment reward.
With this optimization approach, the model allows knowing relevant aspects of the system against which comparisons can be made with the two scenarios of hydroeconomic efficiency. Therefore, as a result of the model, detailed results can be obtained regarding the storage volume in the system, the production of desalinated water, energy consumption, compliance with ecological flows, the deficit of the system's demands, operational costs and other variables.

4.3.2.1.2 Operational costs minimization

In the hydroeconomic efficiency scenario of minimum operational cost, the objective function is based on the sum of the most relevant operational costs of the system. For the Tagus-Segura system, the operational costs of water desalination, groundwater pumping, and surface water pumping along the infrastructure of the inter-basin transfer were included. The operational costs were included in the model as a function of the energy consumption rate per water volume pumped or desalinated and the energy mix used in each case (see equation).

$$OC = (EP_{mix} * EC_{rate} + AOC) * W_{vol}$$

Where OC is the total operational costs, EP_{mix} is the energy price (€/kW.h), EC_{rate} is the energy consumption rate (kW.h/m^3), AOC is the additional non-energy dependent operation cost (€/m^3) and W_{vol} is the water volume desalinated or pumped (m^3).
To ensure that during cost minimization, the system does not overexploit sources with lower operational costs while still achieving a minimum level of satisfaction for water demands and environmental flows requirements, it is necessary to establish a set of hard constraints that guarantee a maximum deficit in consumptive demands and ecological flows equal to the one achieved under the previous base optimization scenario.

4.3.2.1.3 Agricultural net benefits maximization

For the maximization of net benefits in irrigated demands scenario, the objective function is based on the sum of the annual net benefits obtained for each crop. These net benefits are calculated from crop yield curves concerning the amount of water supplied to meet the water demand. These curves were calculated through a modification made to the crop yield calculation recommended by the FAO33 method (FAO, 2012). The modification seeks to represent the variation in crop yield not as a function of evapotranspiration but as a function of the supply-demand ratio. Finally, a yearly net benefit is calculated through the product between the crop yield percentage and a reference total net benefit value extracted from the information established by the y the SRBA.
Similarly to the constraints imposed in the cost minimization scenario, for this scenario, a set of hard constraints was defined to ensure that the supply of all non-agricultural demands is at least as high as the one achieved in the base scenario.

4.3.2.2 Application Results

4.3.2.2.1 Base scenario

The results of the base scenario allow for analyzing the relevance of desalinated water in the system's operation. According to the results (Figure 96), it can be observed that with an optimized system operation, the water produced in the SWDP could represent approximately 25% of the total water that incurs operational costs. However, it is also observed that its high energy consumption implies a monthly average participation of 66% within the total operational cost. This fact highlights the importance of addressing energy policies that enable desalination in the basin to be more competitive than other sources.

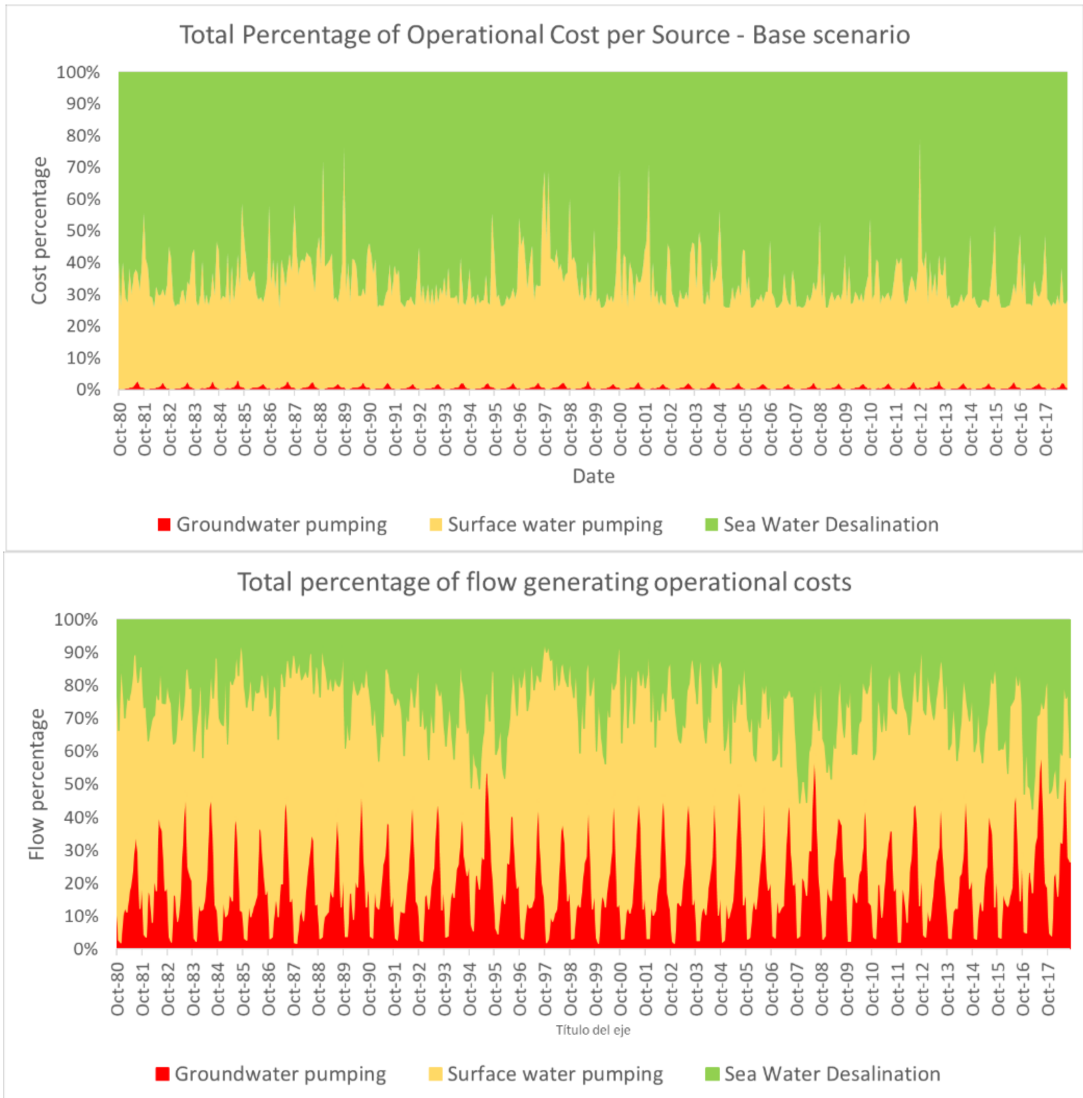

Figure 96. Total percentage of flows and operational costs per source

In comparison, resources from the TSA show the opposite behavior. Within the volume of sources that generate operational costs, the water pumped monthly along the TSA transfer would represent an average of 50% of the total. However, regarding operational costs, the TSA only accounts for 33%. This fact highlights the significant gap in the operational cost of desalination compared to TSA resources. This gap must be minimized if a more competitive position for desalination is desired compared to TSA resources as feasible solutions to address the scarcity in the system.

Regarding groundwater pumping, the results show that among the analyzed sources, this is the one that implies the lowest operational cost. However, the overexploitation of aquifers in the Segura system represents a strong restriction for the expansion of its use.

4.3.2.2.2 Operational costs minimization

Due to the deterministic nature of the optimization, this cost minimization scenario allows analyzing, even in an idealized manner, the most significant opportunities within the system and on which progress can be made to achieve better governance of the nexus.

The results of this scenario show that more intensive exploitation of natural surface resources and a change in how transferred water for irrigation is distributed in the Ojós dam can help reduce the system's operational costs. In Figure 97 it can be seen that for the historical period, this optimization proposes a scenario where the storage in the system's reservoirs is reallocated throughout historical time. According to the results obtained, a more economically efficient operation in terms of costs would entail a reduction in the monthly stored volume of approximately 1%.

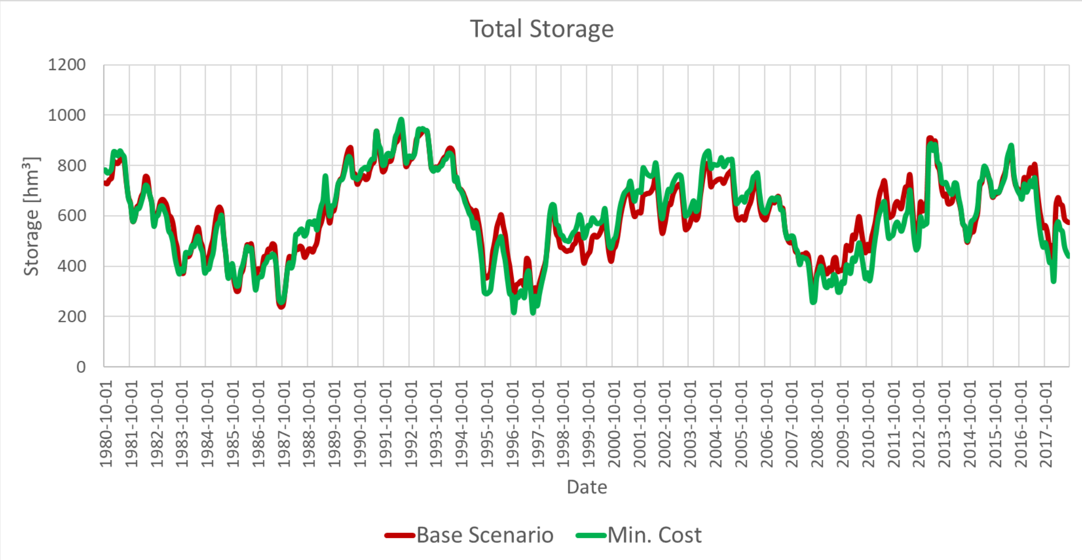

Figure 97. Total storage comparison

As seen in Figure 98, under both scenarios, the average monthly behaviour of the storage in the system remains consistent. However, the cost-minimization scenario shows slight reductions in the volumes of some specific reservoirs, such as the "La Pedrera" reservoir, which regulates part of the water transferred through the TSA.

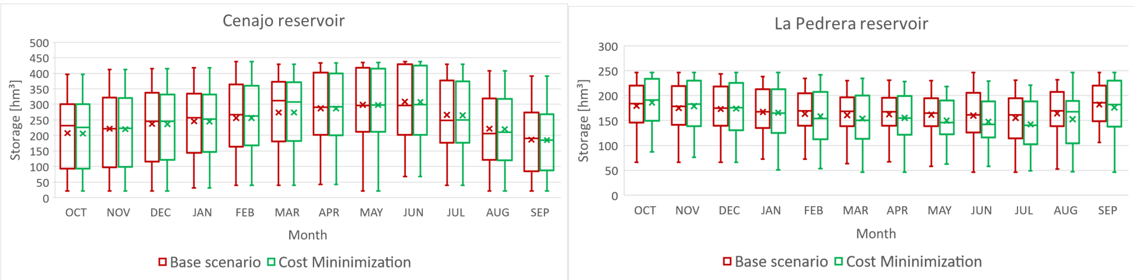

Figure 98. Mean monthly storage comparison

As observed in Figure 99, the additional use of natural surface resources leads to a decrease in the use of desalinated water, which impacts the system's energy consumption and operational costs. This reduction would be more pronounced in those SWDPs with higher energy consumption rates that supply urban demands, for example, Torrevieja, Alicante I, and San Pedro el Pinatar I.

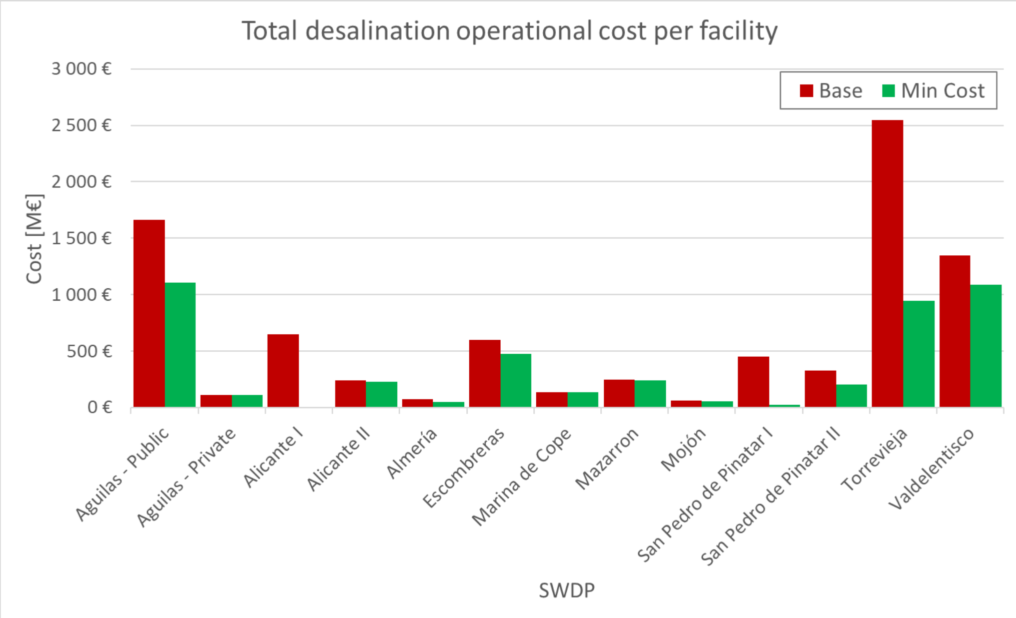

Figure 99. Tagus-Segura total desalination operational costs comparison

In summary, it is found that under an ideal cost-minimization scenario, the operational management cost could be reduced by approximately 1,5% resulting in mean monthly savings of 5-10 million (Figure 100).

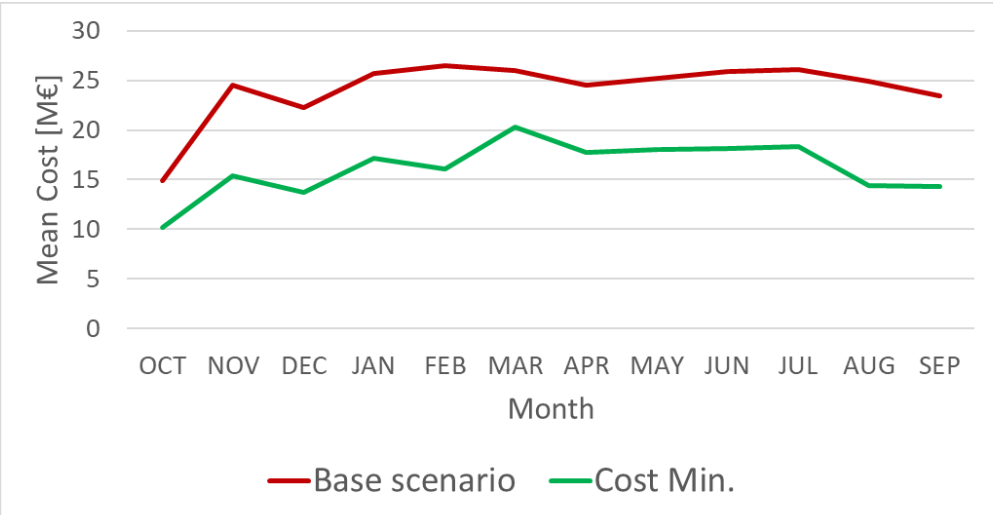

Figure 100. Mean monthly operational costs comparison

The preceding results indicate that the Tajo-Segura system presents opportunities where an enhanced governance of the WEFE nexus can lead to positive economic impacts. As observed, optimizing energy consumption in desalination, and implementing improved spatial and temporal management of the TSA resources can result in a more economically efficient operation. By identifying and capitalizing on these opportunities, stakeholders can not only bolster the sustainability of the Tajo-Segura system but also foster economic benefits through resource optimization and cost-effectiveness. Embracing a holistic approach to the WEFE management in the region will be key to unlocking the full potential of these opportunities.

4.3.2.2.3 Agricultural net benefits maximization

In this optimization scenario, as the algorithm seeks to maximize net profit in agricultural demands, it also reduces and relocates its potential deficit. For a historical reference period, it is found that the algorithm compensates for the deficit obtained in the base scenario and relocates it towards those demands with lower net benefit.
As shown in Figure 101, the optimization reduces the deficit in demands with higher net production, such as UDA08, UDA03, and UDA69, while at the same time, it increases the deficit in less profitable demands, such as UDA37, UDA10, and UDA54.

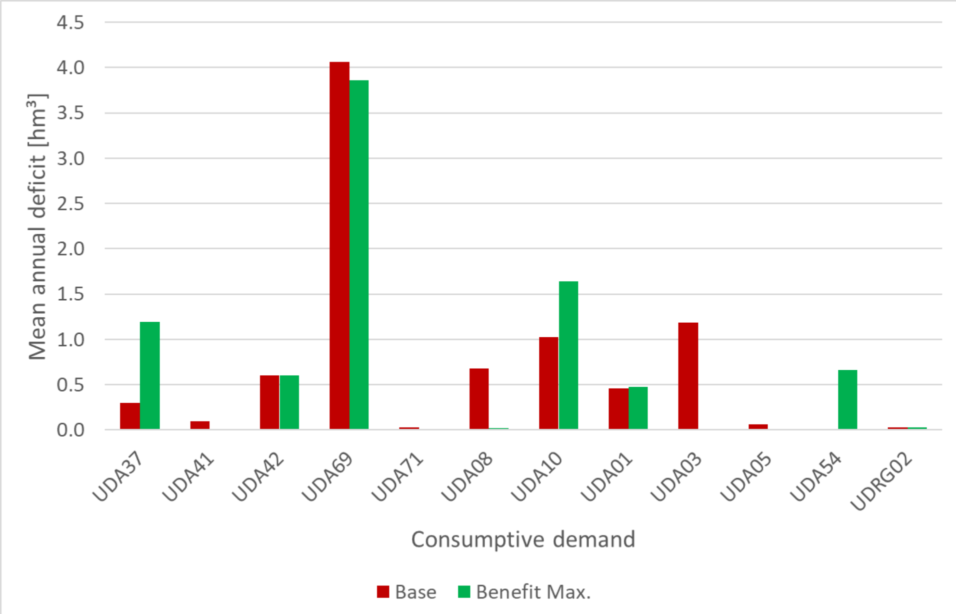

Figure 101. Mean annual deficit comparison

Additionally, as seen in Figure 102, the algorithm not only relocates the deficit but also reduces it over time. Notice how, for the reference period, there is only one year (hydrological year 2016-2017) where a deficit greater than the one reached in the base scenario is observed. As a result, it is found that the net benefit of agriculture could potentially increase annually by up to 1%, with an average annual increase of 0.4%.

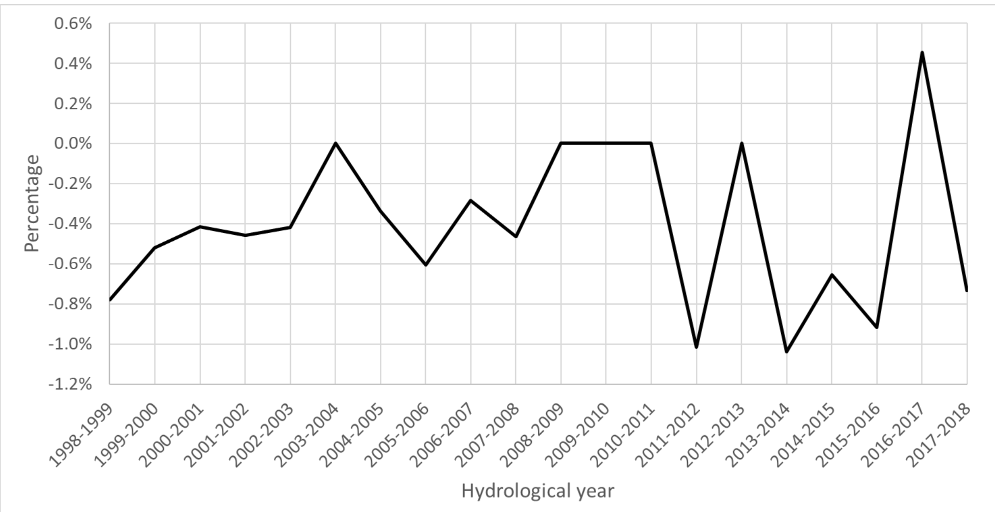

Figure 102. Change in mean yearly deficit between the analysed scenarios

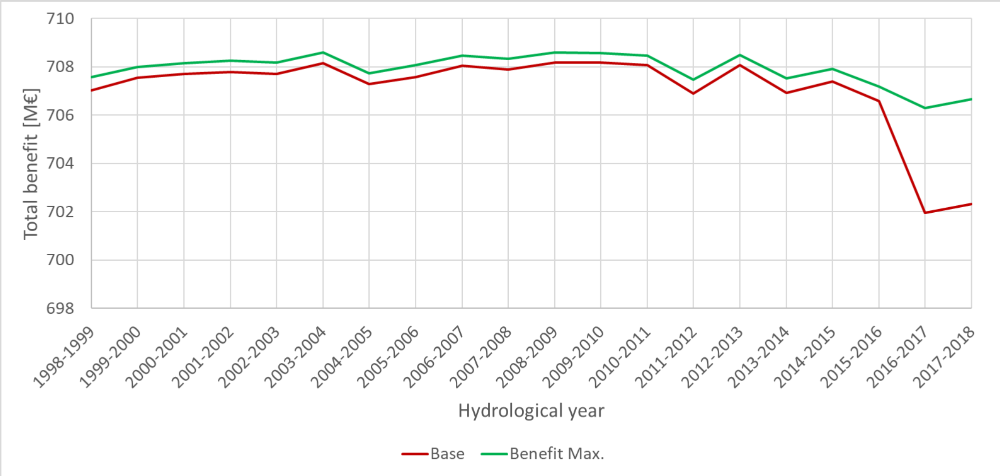

Figure 103. Total yearly net agricultural benefit comparison between the analysed scenarios

In summary, under an ideal management scenario aimed at maximizing benefits, the annual net agricultural benefit could be increased by an average of 0.12%, reaching potential benefit increases of up to 0.62% (Figure 103). Once again, these results indicate that the governance of the Water-Energy-Food-Ecosystem (WEFE) nexus in the Tajo-Segura system provides opportunities for improvement, and the developed hydroeconomic models can accurately capture these opportunities and facilitate the evaluation of their practical implementation within the nexus.

4.3.3 Senegal

4.3.3.1 Application Development

The hydroeconomic model of the Senegal River basin (SRB) seeks to determine optimal allocation policies, e.g., reservoir releases, water withdrawals for offstream uses, throughout the system schematized in Figure 104.

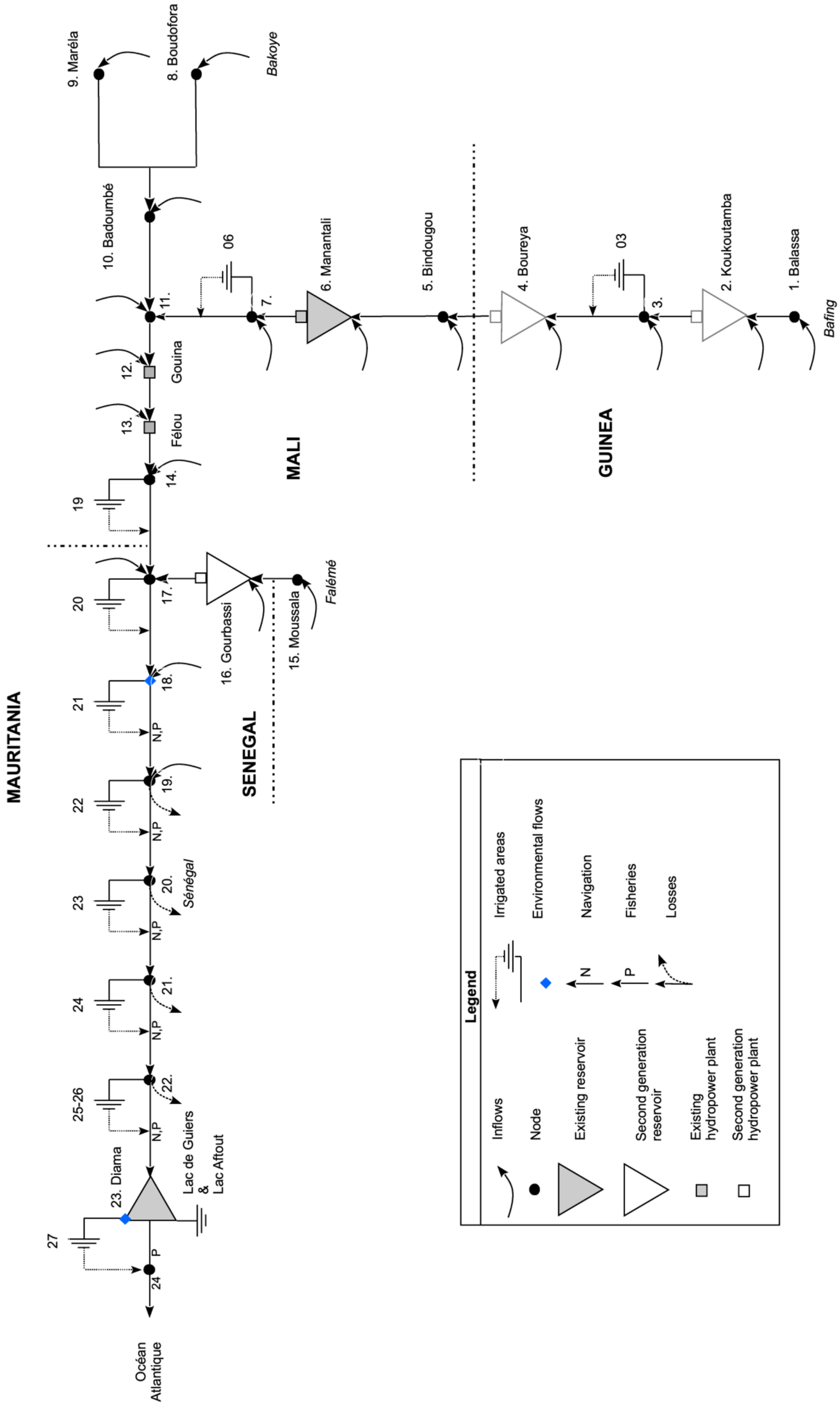

Figure 104. Schematization of the Senegal River basin

This system mainly comprises 24 nodes, up to 6 power plants, up to 5 reservoirs, 33 crops spread over 10 irrigation schemes. Since both supplies and demands are highly seasonal, the

allocation decisions are determined on a monthly time step, preferably over a period of several years.
Water allocation in the SRB is formulated as an optimization problem where the objective function corresponds to the expected sum of net benefits from water allocation subject to physical, operational, and legal constraints. The main economic activities are irrigated agriculture, hydropower generation, flood recession agriculture and fisheries. The development of river shipping is still in an early planning stage and economic appraisals have not yet been produced.
The hydroeconomic model formulation captures the long-term persistence that characterizes the flow regime of the Senegal River (Figure 105). Because those multiyear dry and wet periods are particularly challenging when it comes to sharing water between competing uses, the allocation policies are tailored to a limited number of climate state (e.g., dry, normal, or wet).

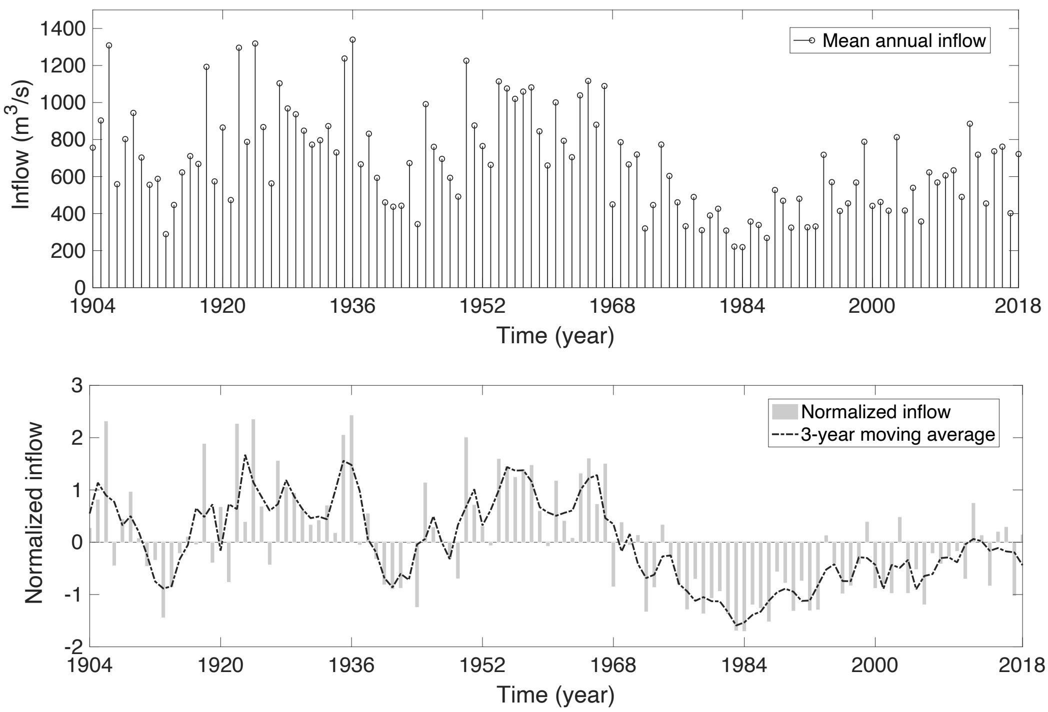

Figure 105. Long-term persistence in the SRB

The optimization problem is solved using the SDDP algorithm (Stochastic Dual Dynamic Programming). Like other Dynamic Programming methods, SDDP solves multi-stage decision problems based on the Bellman's principle of optimality, which states that the maximum return associated to a given state at a given stage is the sum of the immediate and future returns. Generally speaking, SDDP uses a multisite periodic autoregressive model (MPAR) to capture the hydrologic uncertainty. This model can represent serial and spatial correlations within a river basin and between different basins as well as seasonality, but it cannot capture the long-term persistence. To address this limitation, the SDDP algorithm was modified, and a new climate variable was added to the formulation (Espanmanesh & Tilmant, 2022). In a sense, this new climate variable labels the observations, giving rise to a new time series of (hidden) climate states whose statistical analysis reveals the long-term temporal persistence of the underlying hydroclimatic processes.

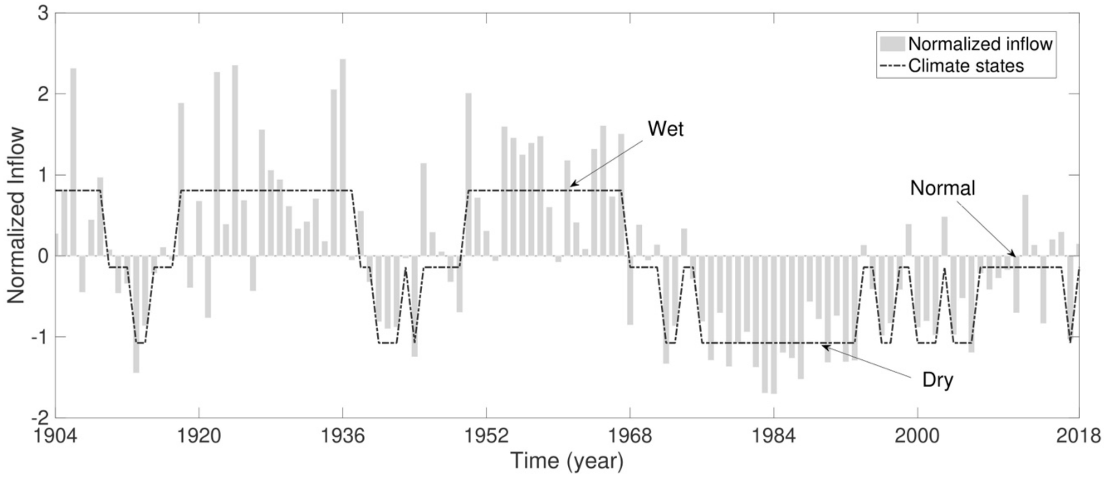

Figure 106. Time series of dry, normal, and wet states

Once climate-tailored allocation policies are determined, they are reoptimized (simulated) over the entire streamflow record, which can consist of observations (current climate) or hydrologic projections associated to climate change scenarios. WEFE indicators are quantified from those reoptimization results.

4.3.3.2 Application results

4.3.3.2.1 Current situation in the basin

Preliminary results are presented for the current situation in the basin, i.e., with two dams (Manantali and Diama), one storage hydropower plant (Manantali) and two run-of-river power stations (Félou and Gouina), 121 kha equipped for irrigation, water diversions to Nouakchott and Dakar (180 hm3/yr). Note that water withdrawals for municipal uses in the valley are considered negligible.
The amount of energy generated by each power station is a direct output of the hydroeconomic model based on their physical characteristics and on allocation decisions determined by the model.
Irrigated agriculture is mostly located in the delta and the floodplain downstream of Bakel (node 17 on Figure 104). Water withdrawals, consumptive uses, returns flows and gross margins are also directly computed by the hydroeconomic model.
Flood recession agriculture is still an important activity in the SRB. Areas available for flood recession agriculture are assessed using a logarithmic relationship between September flows at Matam (node 19 on Figure 104) and the cultivated area in the floodplain (IRD, 1999).
Annual fish catches in the floodplain are determined after regressing historical fish catch data with relevant hydrologic attributes such as September flows and annual flows. Historical fish catches in the floodplain are given in Diouf (1993) for a period extending before the construction of the dams (Manantali and Diama), i.e. under pristine hydrologic conditions. Fishing is also possible in the Manantali reservoir where the average yield is 25 kg/ha/y (Kantoussan et al., 2014).

As explained above, the allocation policies are first optimized using the hydroeconomic model and then used in simulation over the entire streamflow record (114 years). This procedure is repeated twice: with and without the artificial flood. The characteristics of the artificial flood come from Lamagat and Bader (2003). A 4,5 km^3 flood pulse is required at Bakel in September to sustain both flood recession agriculture over 55000 ha and aquatic ecosystems throughout the valley. The comparison of these two variants reveals the trade-off between two coalitions discussed in 3.5.1: traditional food production (agriculture and floodplain fisheries) versus "modern" uses (hydropower, irrigated agriculture, and river shipping).

4.3.3.2.2 Water resources

Annual natural runoff in the SRB amounts to 23 km^3, the majority being generated in Guinea. On average, total consumptive use is about 11 km^3/y, which corresponds to a water depletion of 49%. Table 9 lists the water depletion at key points in the basin: along the Bafing River in Guinea and Mali, upstream Bakel which marks the entrance of the Senegal floodplain, and for the entire river basin. As we can see much of the consumptive uses take place in Senegal, Mauritania and to a less extent in Mali. In the first two countries, the dominant process is evapotranspiration from irrigated lands whereas in Mali it mostly comes from the evaporation losses from Manantali as well as evaporation and infiltration in the riverbed.

Table 9. Average annual water depletion

	Water depletion (%)
Bafing	3.52
Upstream Bakel	2.61
Basin	49.04

The flow composition at Bakel with and without the artificial flood illustrates the importance of managed flood releases from the Manantali reservoir to sustain flood recession agriculture and fisheries in the floodplain. Figure 107 shows the average monthly discharge at Bakel and the contribution of the main sources (Manantali reservoir on the Bafing, the Bakoye river and the Faleme river). As we can see, managed flood releases from the Manantali dam on the Bafing almost double the contribution of that tributary in September. We can also see that the Bafing is the main contributor during the rest of the year and that the Bafing outflows are fairly constants due to the large carry-over capacity of Manantali reservoir, something beneficial not only for hydropower generation, but also for river shipping and irrigated agriculture.

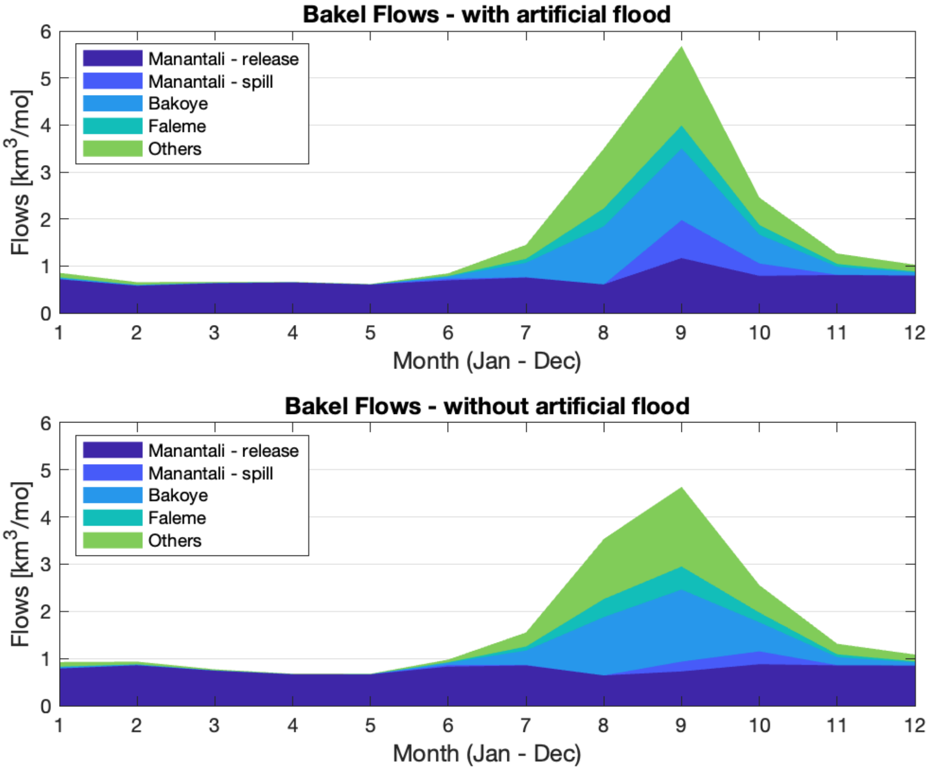

Figure 107. Flow decomposition at Bakel

To assess the hydrological alteration at Bakel Station, we employ the IHA method, focusing on metrics that can be derived from monthly data. These metrics provide a statistical assessment of the hydrological regime on a seasonal (monthly) time step. Specifically, we calculate the following IHA metrics: Median, Standard Deviation, Monthly minimum inflow, Monthly maximum inflow. In this analysis, we examine the IHA indicators for three different periods: pre-dam construction, post-dam construction without artificial flood (Post-WO), and post-dam construction with artificial flood (Post-W). These statistics are displayed as boxplots in Figure 108. The examination reveals the traditional impacts of large dams on downstream flow regime: low flow augmentation during the dry season combined with a larger year-to-year variability, reduction of peak flows during the high flow season combined with a slightly smaller year-to-year variability due to the contribution of free-flowing tributaries between Manantali and Bakel. If managed flood releases from Manantali do increase river flows during dry years, the year-to-year variability is significantly reduced in September (the interquartile range is about 350 m^3/s).

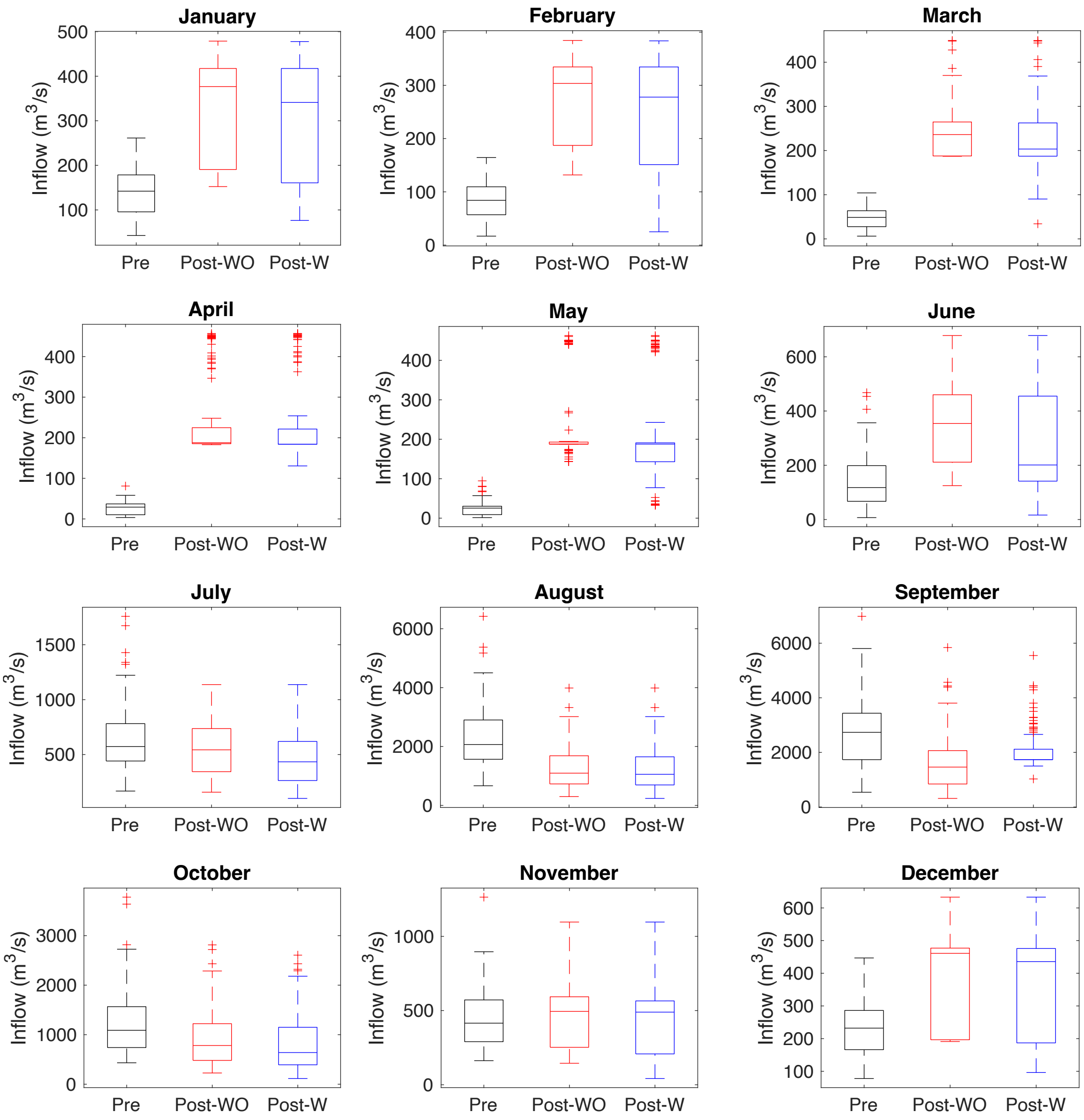

Figure 108. Flow alteration at Bakel

4.3.3.2.3 Energy generation

Figure 109 shows the statistical distributions of the annual energy output with and without the artificial flood. For a given energy output, it gives the non-exceedance probability, i.e., the probability that the energy output might be lower. The median production is around 1800 GWh when managed flood releases are implemented or 2000 GWh without, which correspond to a load factor between 50 and 56%. Almost 80% of the time, the artificial flood causes a reduction in energy generation, that difference being exacerbated by dry hydrologic conditions. During wet years, however, the difference between both variants is negligible because the contribution of free-flowing tributaries is enough to provide a 4.5 km^3 flood pulse.

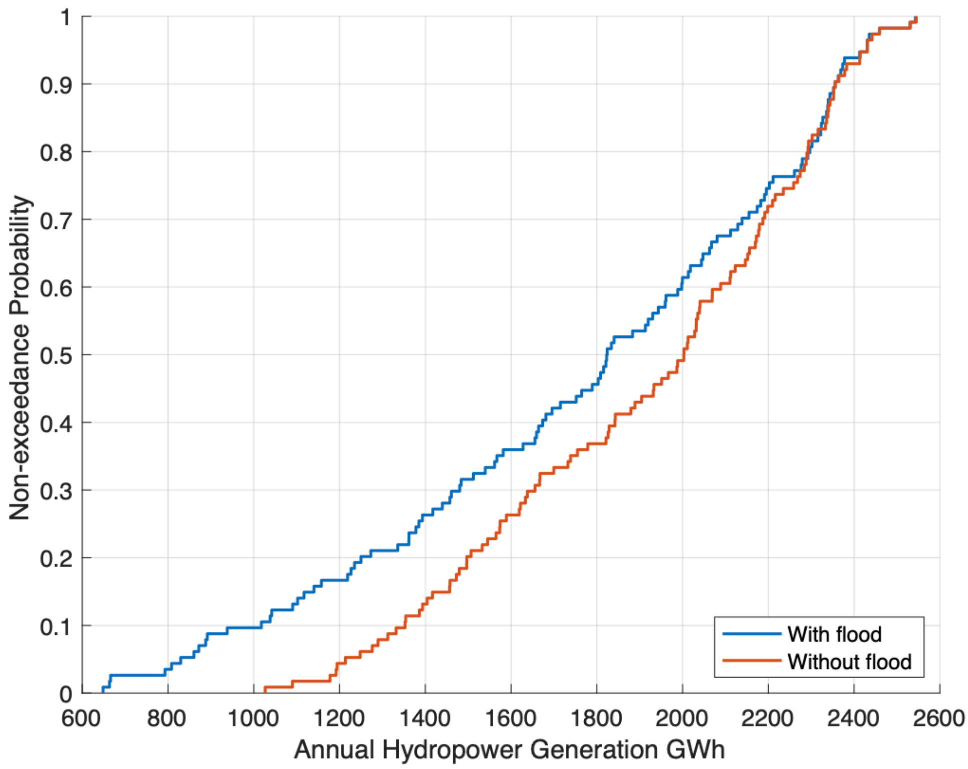

Figure 109. Statistical distribution - annual hydropower generation

4.3.3.2.4 Agriculture and fisheries

Under current supply and demand conditions, water demands in the irrigation sector are met with a reliability of 100% provided no artificial flood is implemented. If the Manantali reservoir must contribute to the September flood pulse, the probability of irrigation deficits increases to 10%. In other words, irrigation deficits are only observed under the driest hydrologic conditions, i.e., drought with a return period of ten years. Note that the deficits are small as they do not exceed 20kha 95% of the time.

Compared to flood recession agriculture, irrigation is more energy intensive. From the simulation results, we estimated the amount of energy needed to supply the irrigation schemes to about 80 GWh/y, which is roughly 4-5% of the energy generated by the three power stations.

Figure 110 shows the statistical distribution of the cultivated area for flood recession farming under the two management scenarios: with or without the artificial flood. As we can see, flood recession farming over 50kha is guaranteed 99% of the time thanks to the artificial flood. However, without the flood, that reliability falls under 45%, meaning that roughly one year out of two flood recession farming would only be possible on a smaller area.

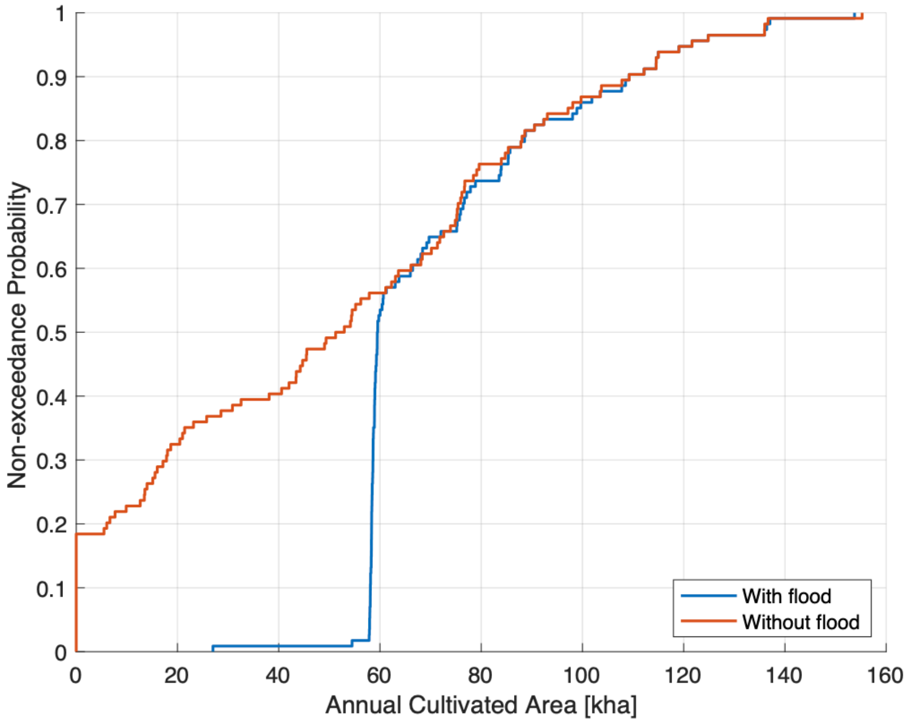

Figure 110. Statistical distribution - area for flood recession agriculture

Various authors have mentioned the adverse impacts of dams on the productivity of fisheries in the SRB. As pointed out by DeGeorges and Reilly (2006) during the wet season, from August through December, the flood plain exhibits characteristics of a freshwater fishery, relying upon inundation of the floodplains to replenish the fish stock by providing habitat for breeding and a nursery for various species. During the dry season, the river waters gradually subside, forcing the fish populations to leave the floodplain and concentrate in the main channel. By regulating the flow regime, the Manantali dam has altered this process, negatively impacting the productivity of fisheries. If the difference between the average productivity with and without managed flood releases is not significant (from 22,8 to 18,6 kT/y), the gap widens significantly as the hydroclimatic conditions get drier: one year out of five (non-exceedance probability = 0,2), the productivity is reduced by half without the artificial flood (Figure 111).

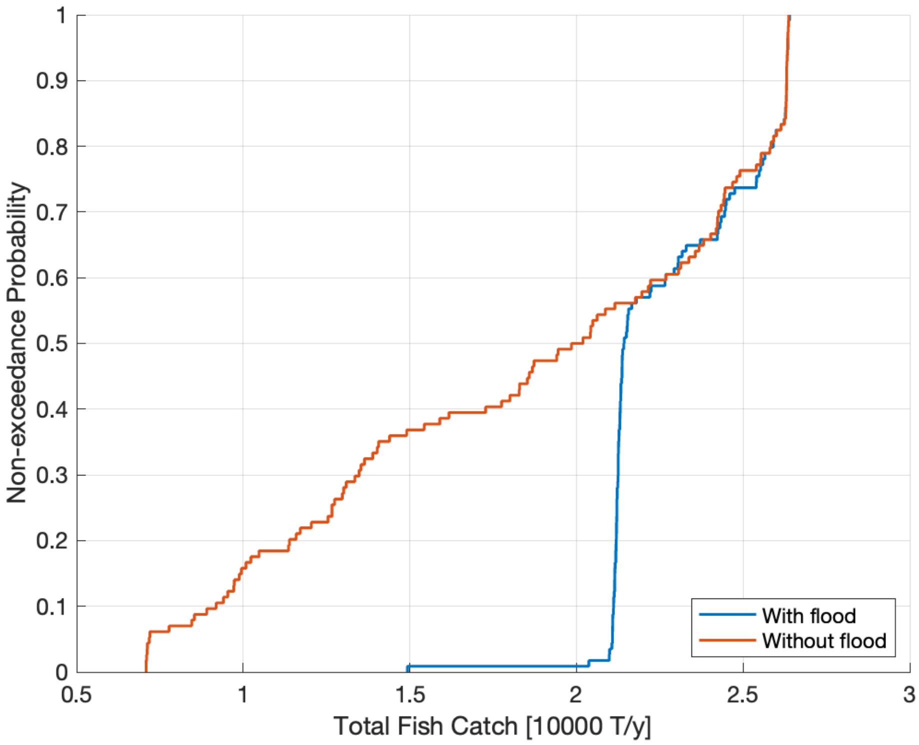

Figure 111. Statistical distribution - annual fish catch

4.3.3.2.5 Navigation

Various reports highlight the potentially important role that navigation could play to open up regions that are otherwise isolated and to provide a vehicle to export agricultural products as well as minerals extracted from mines. However, despite its apparent importance, little information is available to assess a relationship between the flow regime and economic indicators related to navigation. In this report, we consider that navigation is possible if the river discharge at Diama (node 24 on Figure 104) exceeds 200 m^3/s. The main performance indicator is therefore the reliability of meeting the target flow of 200 m^3/s.

Table 10 lists the reliability of river shipping under the two management scenarios, i.e. the probability that navigation is possible over a given period (number of months/year). The artificial flood tend to degrade the river's navigability. River shipping would be possible over 10 months only 20% of the time, i.e. one year out of five. For a shorter duration, e.g. seven months, the probability increases to 52% with managed flood releases and up to 68% without. Again, the difference between both variants of the baseline scenario is more pronounced under dry hydrologic conditions.

Table 10. River shipping reliability (%)

	10 months	7 months	6 months	5 months
With flood	19	52	66	76
Without flood	20	68	79	89

4.3.3.2.6 Basin-wide tradeoffs

Various visualization techniques are available to discover tradeoffs between multiple objectives. Here tradeoffs are explored using parallel-coordinate plots drawn for the two management scenarios: with and without the artificial flood. Economic activities and their performance indicators are thus listed on the X-axis, while the Y-axis indicates the direction of increasing preference. Hence, the ideal - but infeasible - solution corresponds to the top horizontal axis. To facilitate the comparison between both scenarios, the scale of the vertical axis associated with an indicator corresponds to the min and max values of that indicator across all scenarios. The average performance of a particular management scenario over the entire simulation period (114 years) is represented by a bold dotted line, while the variability of the performance is captured by a limited number of percentile ranges: 0-5%, 5-25%, 25-75%, 75-95%, and 95-100%. The first range therefore corresponds to the driest hydrologic conditions with a non-exceedance probability of 5%, i.e. when 95% of the time the river flows will actually be higher. In other words, the upper limit of this first range is the performance level that can be guaranteed 95% of the time. The first and second ranges include the 25% lowest values taken by the performance indicators. The third range is the interquartile range and includes 50% of the values around the mean, between the 25th and 75th percentile. Finally, the two remaining ranges comprises the highest scores, above the 75th percentile, which are observed under favorable hydrologic conditions. The larger the ranges are, the more vulnerable are the sectors to the hydrologic uncertainty.

The examination of Figure 112 reveals the presence of two coalitions of objectives, which are at the core of the WEFE nexus in the Senegal River basin: traditional food production based on flood recession farming and fisheries versus "modern" uses, which include hydropower generation, river shipping and irrigated agriculture. The former flourishes under a natural flow regime while the latter requires more or less constant river discharges all year long. With the impoundment of the Bafing river, the former can only be sustained through managed flood releases from the Manantali reservoir, which automatically reduces the energy output by increasing spillages losses (Figure 107) and by lowering the water level in the reservoir.

We can also see that the hydrological risk exposure of both flood recession farming and fisheries is significant but can be mitigated through managed flood releases from the Manantali dam. In contrast, irrigation water demands are almost always met, indicating that the river basin is not yet approaching closure. Not surprisingly, hydropower generation and navigation are also quite exposed to the hydrological risk, which increases with the artificial flood.

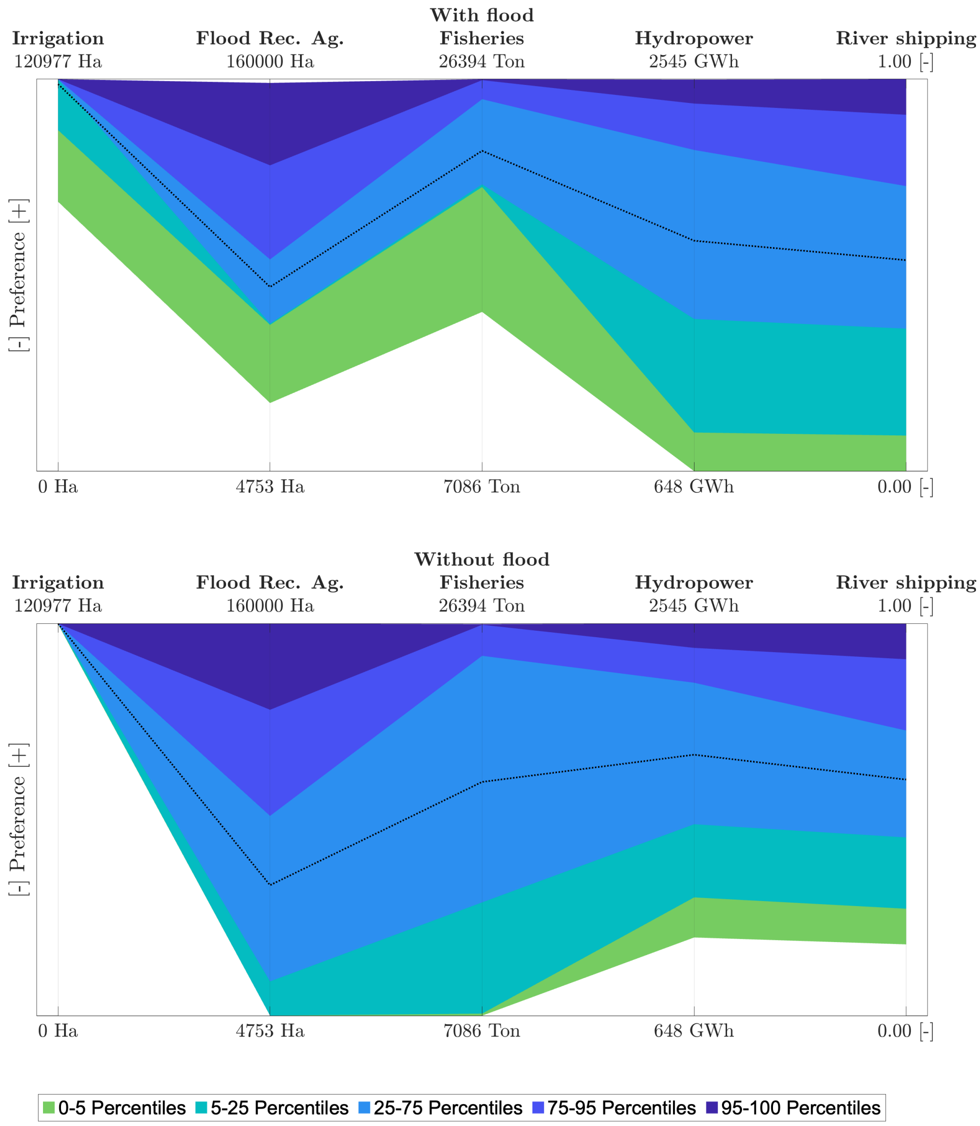

Figure 112. Probabilistic tradeoffs in the SRB: with the artificial flood (panel a) and without the artificial flood (panel b)

4.3.3.2.7 Marginal water values

As indicated above, the Senegal River basin is not yet approaching or exceeding the amount of renewable water available, indicating that there is still room for development. Economic indicators like the marginal value of water can also be used to characterize river basin closure. The marginal value of water indicates what society would be willing to pay to get an additional unit of water in the basin. Because water availability varies in space and time, so does the marginal value of water. At the optimal solution, a hydroeconomic model provides allocation decisions but also the marginal value of water at each time step and location where a mass balance equation must be computed (a reservoir, a junction, a confluence, a water diversion). The hydroeconomic model of the SRB comprises 24 nodes, each draining a portion of the river basin to which a marginal water value can be assigned. Figure 113 displays the average marginal water value in the SRB for the current level of development of the basin. We can see that the value increases as we move from downstream to upstream, indicating that water is more valuable in Guinea than in the floodplain. This is because the same unit of water generated in Guinea will be used several times as it flows through the turbines of the three power stations. Once, it reaches the floodplain, it becomes valueless (<1$/1000m^3) because the aggregated water demand does not yet approach the amount of water available. In other words, the higher value in Guinea reflects a "relative" economic scarcity, while the value (or lack thereof) in the floodplain indicates no physical scarcity.

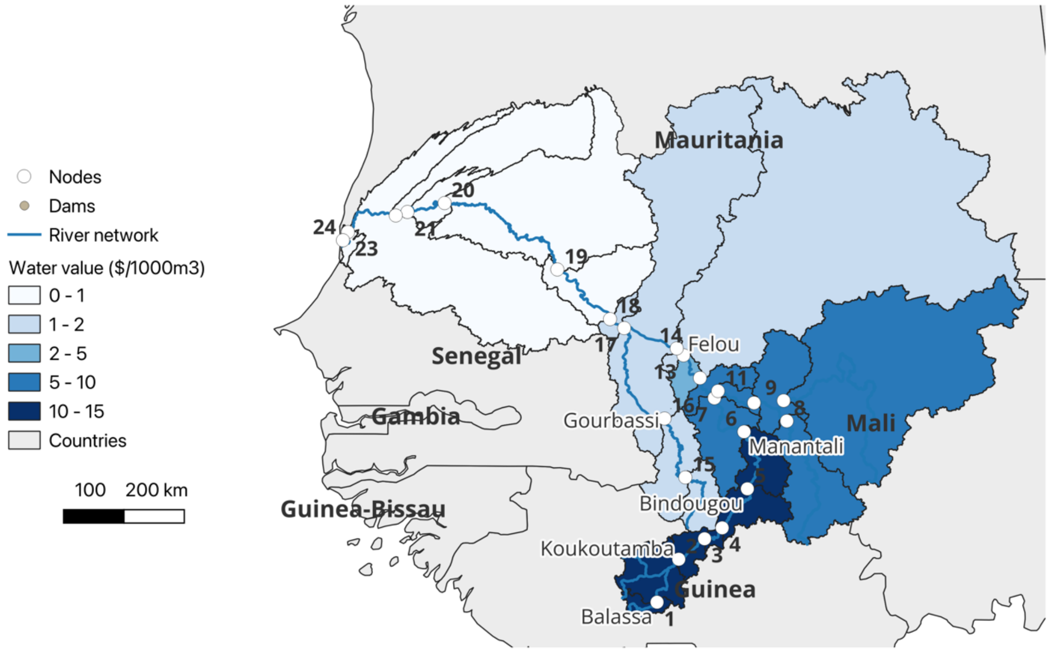

Figure 113. Marginal value of water ($/1000m^3)

4.3.3.2.8 Ecological indicators

The floodplain provides essential ecological services such as carbon storage, groundwater storage, water buffering, fish, and wildlife habitat. In particular, rivers with connected floodplains and an unaltered flood pulse generally have a higher yield of fish per area than do rivers lacking a flood pulse, known as the "flood pulse advantage". The annually flooded areas are therefore an important ecological indicator. Figure 114 shows the distribution of annually flooded areas for both variants: with or without an artificial flood. With an artificial flood, the median level of the flooded area is close to 100 kha, compared to 50 kha without managed flood releases. Small, flooded areas are really influenced by the operation of the Manantali dam. Flooded areas guaranteed with a reliability of 90% is 43 kha in the scenario without the artificial flood and reach 96 kha in the scenario with the artificial flood.

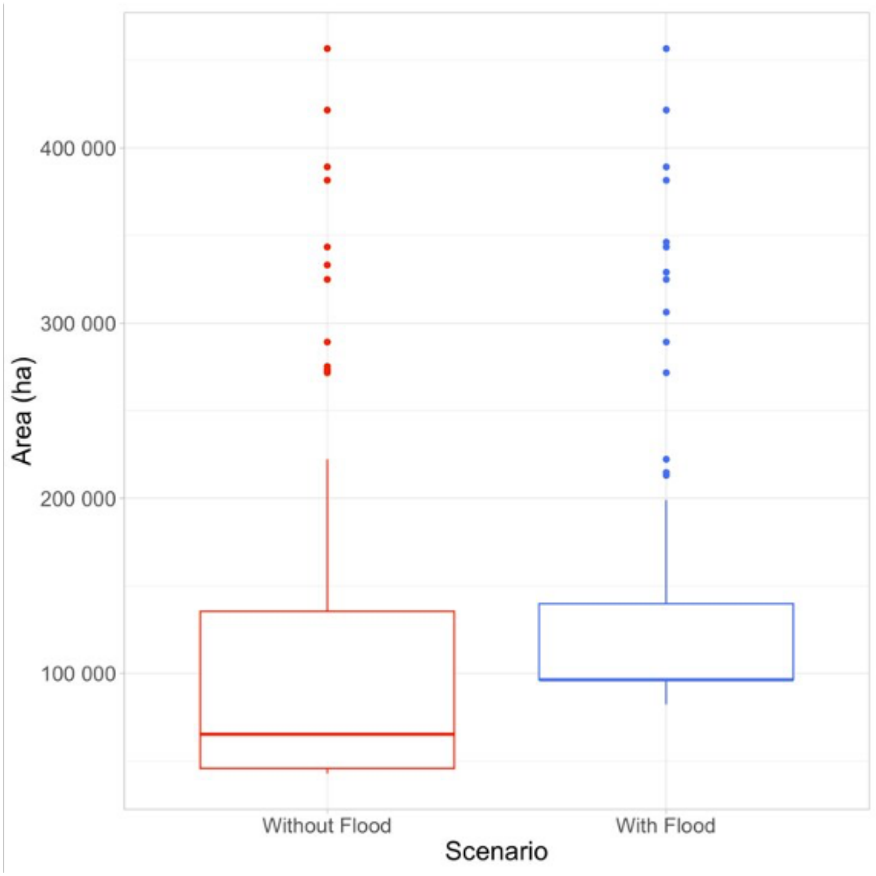

Figure 114. Annually flooded areas in Senegal river basin without artificial flood (red) and with artificial flood (blue)

The flooded areas are directly linked to the discharge at Bakel, which marks the entrance of the floodplain. The average monthly discharge is strongly correlated with the flooded area. Figure 109 shows the mapping of the flooded area as a function of the monthly discharge at Bakel. Certain large depressions in the floodplain are frequently flooded and require an average discharge of less than 1000 m3/s to be flooded, while others require a discharge three times greater. The map also shows a gradient from upstream to downstream as the downstream areas require higher river discharges at Bakel to be flooded. This situation is logical, since as the flood propagates downstream, it spills over into the floodplain and the volumes available are reduced from upstream to downstream.

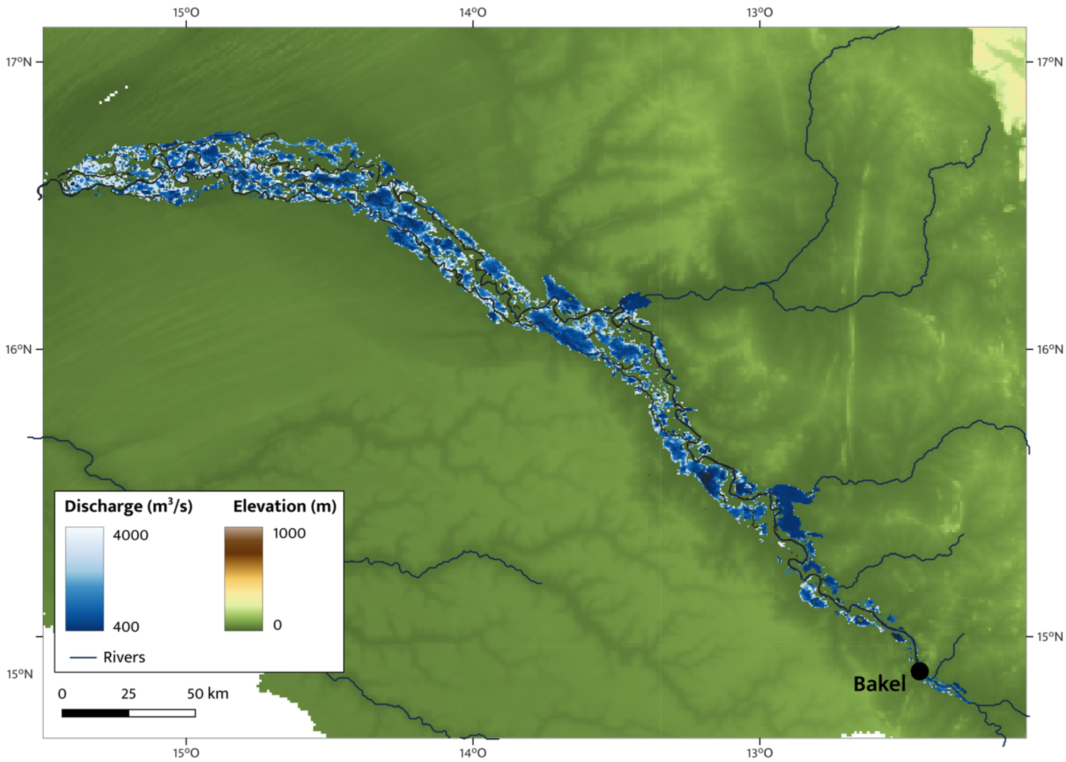

Figure 115. Flooded areas per monthly discharge at Bakel. Data are derived from an analysis using MODIS Imagery and MNDWI water indice.

4.4 System Dynamics Modelling

4.4.1 Júcar

4.4.1.1 Application Development

The system dynamics model developed for the Júcar River system represents its management with a monthly time step. It includes the management of the system based on the real operating rules of the reservoir and the drought management plan applied in the basin. It is divided in 5 subsystems that interact with each other within the same modelling framework. The brain of the model is the operating rules subsystem in which the monthly operating rules of the three main reservoirs of the Júcar River basin are defined. The development of quantitative system dynamics models requires the use of a large volume of data coming from different fields (from hydrological to economic and reservoir data) as well as a deep understanding of the system structure and behaviour. Very often, the most complex issue of this type of model is the development of the monthly operating rules for the reservoirs. The operating rules for the reservoirs were obtained using fuzzy rule-based systems (FRB), co-developed with the experts from the Operation Office of the Júcar River Basin Authority (Macian-Sorribes and Pulido-Velazquez, 2017), and adapted to the system dynamics model using piece-wise linear functions. The water demands considered by the model are divided into urban and agricultural demands and were located and compiled from the public information provided by the CHJ (CHJ, 2022). The water demands are updated to the current Hydrological Plan for the Júcar Demarcation for the 2022-2027 period, approved on the 24th of January 2023. Figure 116 shows the main view of the model capturing the water flowing through the Júcar system, including water infrastructures and stream-aquifer interaction with the Mancha Oriental aquifer.

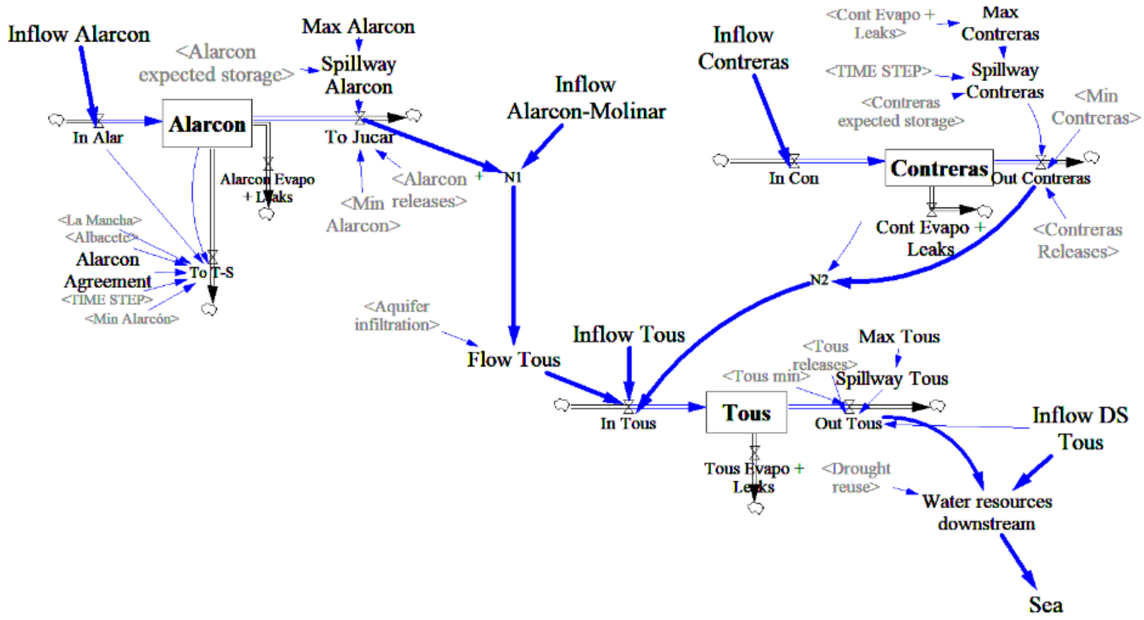

Figure 116. Overview of the model.

It provides a general framework to visualize the system's network and to allow the integration of other sub-models. The model simulates stream-aquifer interaction between the Mancha Oriental aquifer and the Júcar River using a two-cell Embedded Multi-reservoir Model (Pulido-Velazquez et al., 2005). The model also implements a state index subsystem that checks the state of the system each time-step during the simulation. The equations defining the relationship between past and present system states are taken from the Júcar drought management plan (CHJ, 2021). The state index subsystem is able to trigger drought management measures depending on the current state of the system.

The model simulates the relationship between irrigation return and the coastal lake of the Albufera of Valencia. This coastal lake covers an area of 2320 ha, most of the water reaching the Albufera comes from irrigation channels. Therefore, a reduction in irrigation returns as a result of a decrease in agricultural demand or due to the modernisation of irrigation would lead to a reduction in inflows.

Using data from the new basin hydrological plan (cycle 2022-2027) irrigation demand has been calculated for the main crops of the area (rice, citrus fruit, vegetables, persimmons). This allows for the simulation of scenarios of land use change. Additionally, the model takes into account the variable of irrigation efficiency when calculating demand, thereby enabling the acquisition of irrigation return values contingent upon different modernization levels. Consequently, this integrated approach harmonizes the agricultural and environmental components of the model, thereby linking the influence of agricultural practices with the dynamics of the Albufera lagoon.

4.4.1.1 Application Results

The system dynamics model for the Júcar River basin is able to reproduce the real operation of the system with adequate performance. Results from the updated version of the model are shown in the figures below. The comparison between simulation results and observed data for the 2003 to 2013 period at a monthly timescale show good results for Tous (Figure 117), Alarcon (Figure 118) and Contreras (Figure 120).

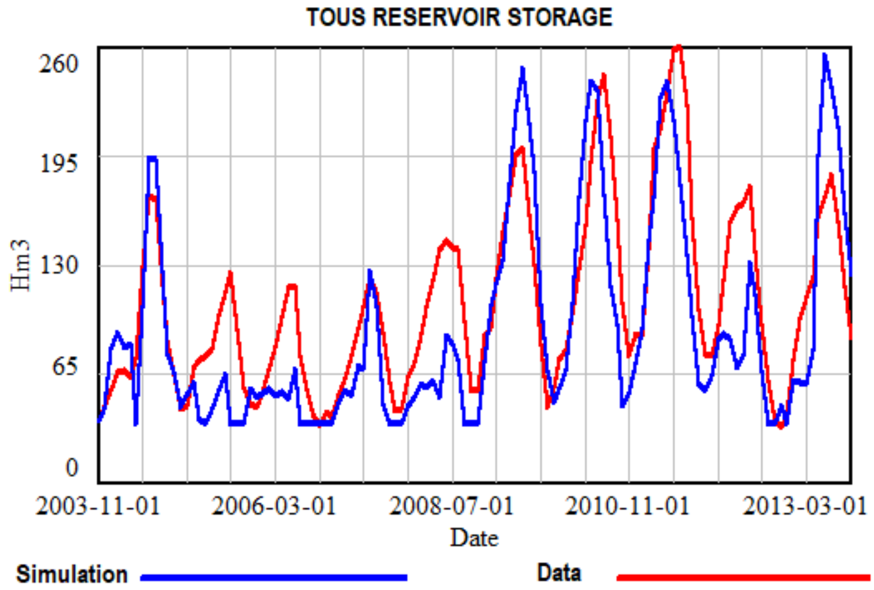

Figure 117. Model performance for Tous reservoir.

Tous, as the downstream reservoir of the system has a more dynamic and complex management when compared to the upstream reservoirs. This results in a more complex definition of its operating rules and a more controlled management, as the reservoir is emptied during autumn to keep a buffer for flood lamination.

In comparison, Alarcon, and Contreras reservoirs (Figure 118 and Figure 120) are bigger and have a momentum-based behaviour highly influenced by the inflows to the reservoirs. Water releases from both reservoirs are mainly depending of the irrigation water demands in the lower and middle basin, and the defined environmental flows.

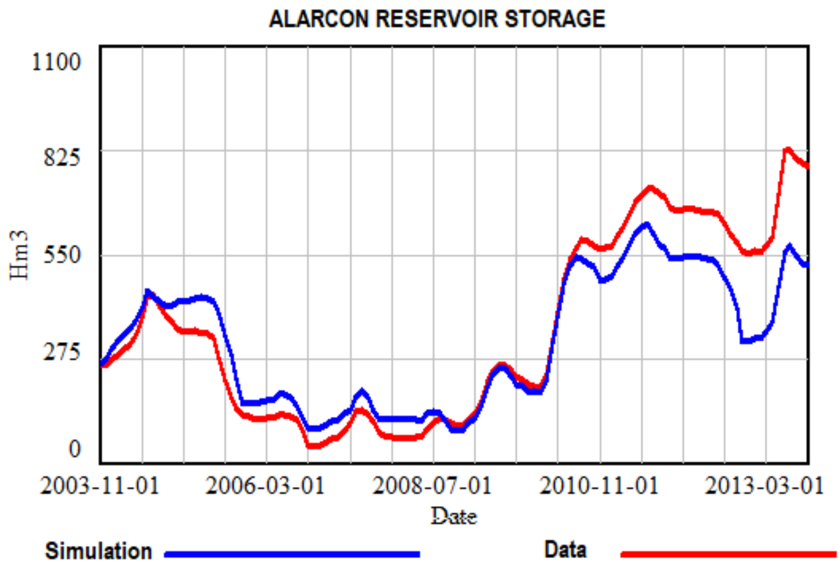

Figure 118. Model performance for Alarcon reservoir.

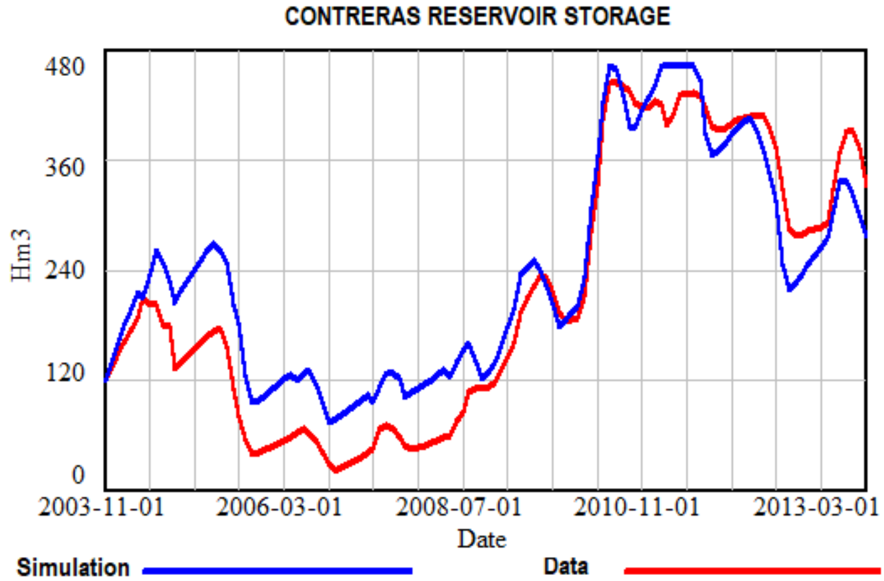

Figure 119. Model performance for Contreras reservoir.

The system state index takes values that range from 0 to 1. Each month, the model transforms the system state index (a floating-point number) to the corresponding integer state (normal, pre-alert, alert, and emergency) applying the thresholds defined by the water authority. A comparison between simulations with and without the drought management strategies introduced into the management in 2007 was performed. Results obtained when applying the drought management measures show improvements for the state index of the system and for the system's total water storage (Figure 120).

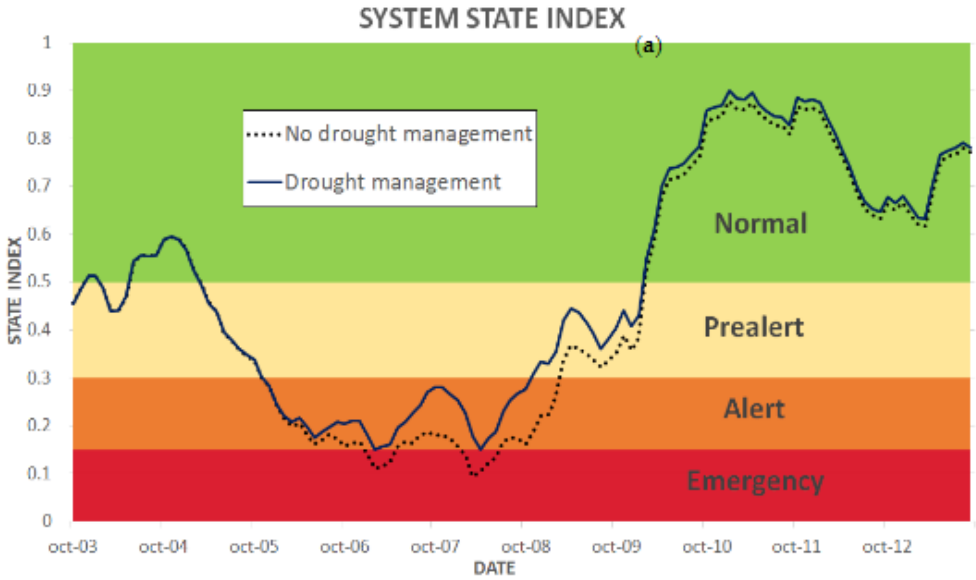

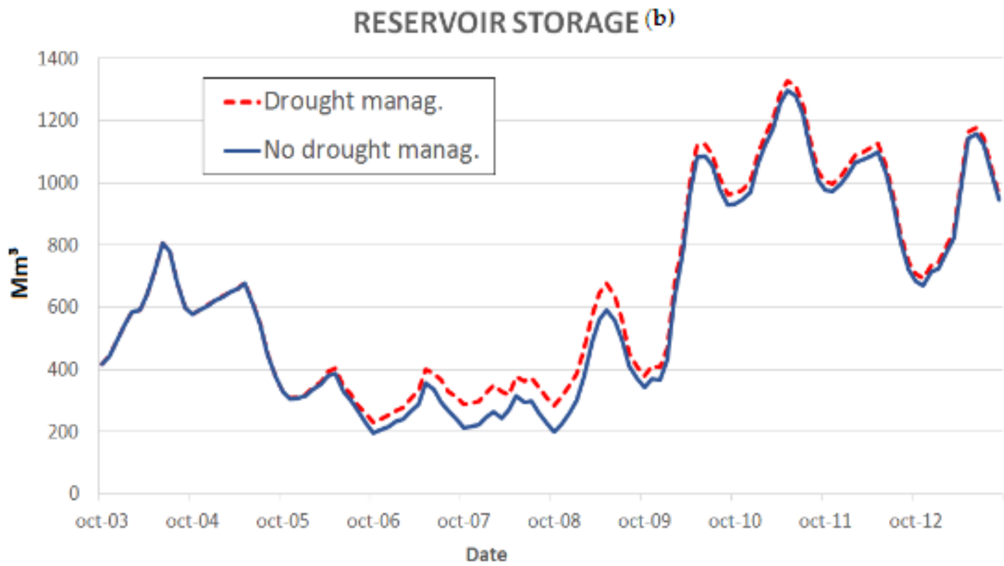

Figure 120. Comparison of simulation with and without drought management.

The system state index benefits from applying the drought management strategies defined in the state index subsystem. Thanks to them, the system state does not drop into an emergency state during the 2005–2008 drought.

The model has been improved with a new subsystem for the Albufera lagoon (Figure 121). Within the Albufera subsystem, the ecological status of the coastal lagoon is encapsulated by two key components.

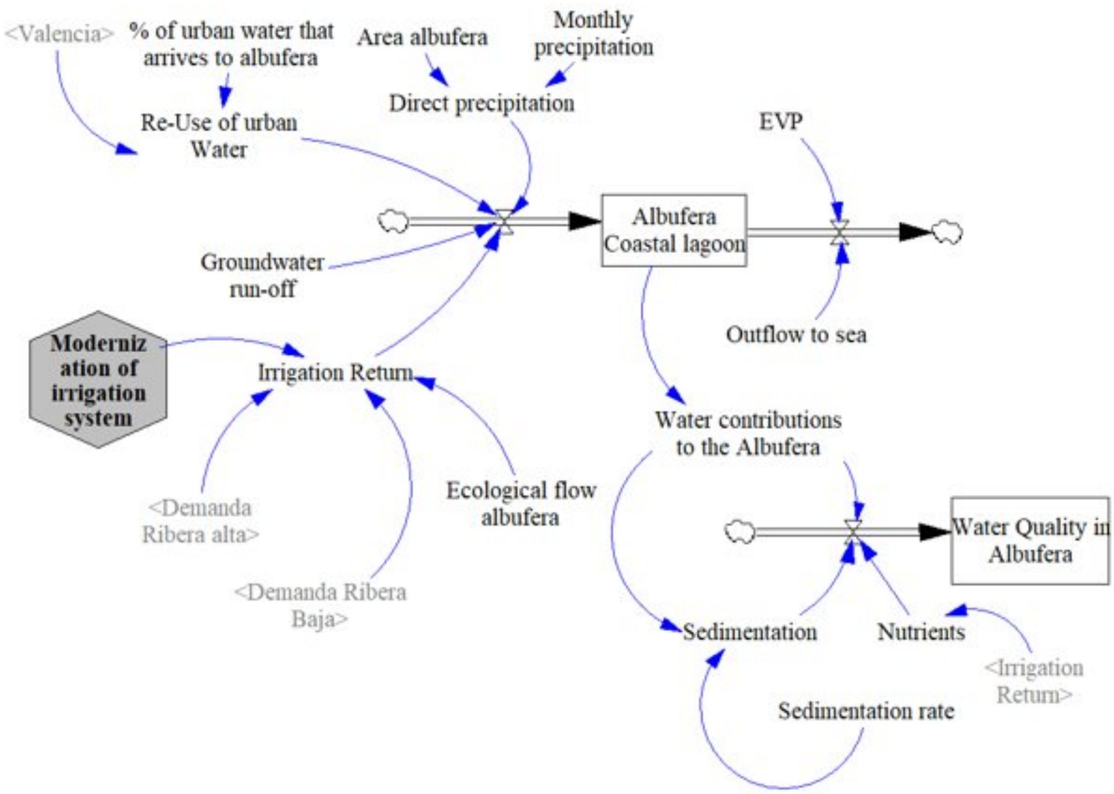

Figure 121. Albufera lagoon subsystem

Firstly, the monthly volume of water entering the lake plays a pivotal role in this context. The primary contributors to this water inflow are the irrigation returns, while factors such as direct precipitation, urban water re-use, and groundwater run-off also contribute to a lesser extent. In the model, the irrigation returns are calculated by incorporating agricultural demand and the specific irrigation system utilized.

The second component characterizing the ecological status of the lagoon is the water quality. This aspect is quantified through the consideration of both sedimentation rate and nutrient concentration.

Figure 122 illustrates the irrigated crops subsystem, which calculates agricultural water demand by considering both the irrigation requirements of primary crops in the region and the crop area. This subsystem is closely interconnected with the environmental subsystem. The water needs and crop area data for calculating agricultural demand are sourced from the new basin hydrological plan (Cycle 2022-2027). The subsystem allows for dynamic changes in crop patterns and water needs adequate for simulating different adaptation pathways to the future global scenarios.

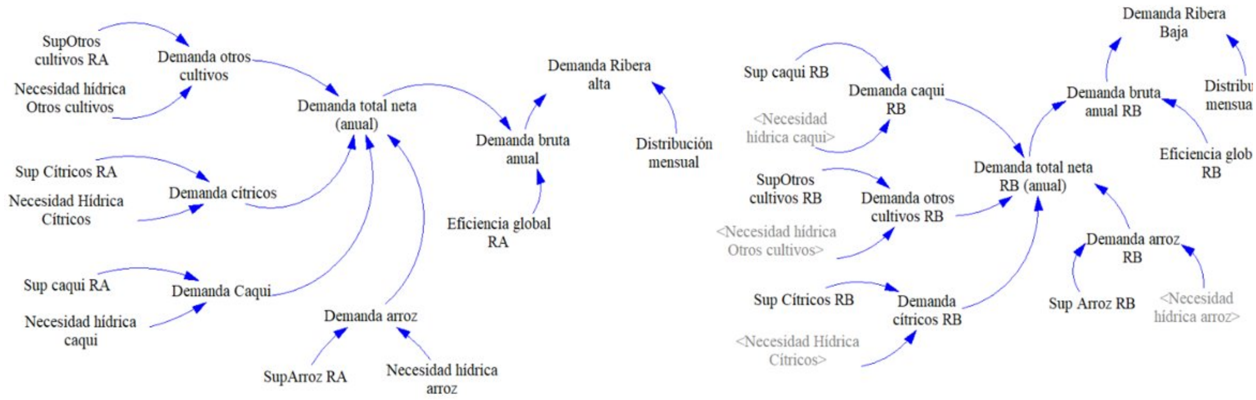

Figure 122. Irrigation demand subsystem

4.4.2 Tagus-Segura

4.4.2.1 Application Development

The development of quantitative system dynamics models in the Tagus-Segura case study commenced with a participatory phase. In this regard, the theoretical framework and methodology described in section 2.4 were applied. Two causal loop diagrams were subsequently created: one for the Tagus basin and another for the Segura basin. The co-creation process took place during two two-hour workshops. The first workshop held in Madrid involved key stakeholders and experts from the Tagus basin, while the second workshop in Murcia included key stakeholders from the Segura system. For further reference, Table 11 provides a list of stakeholders who actively participated in each workshop.

Table 11. Tagus-Segura Basin Stakeholder Participation

Segura Basin		Tagus Basin	
Organization	Category	Organization	Category
Acuamed	State-owned company	WWF-España	NGO
UCAM	Academia	Confederación Hidrológica del Tajo (Tagus river Basin authority)	River Basin authority
Geological and Mining Institute of Spain	Research organization	CEIGRAM-UPM	Academia
Fundación Nueva Cultura del Agua	NGO	Fundación Renovables	Research institute
Euro-Medirerraneam Water Institute	Research organization	Fundación Nueva Cultura del Agua	NGO
Future Water	NGO		

To prevent stakeholder fatigue and ensure effective moderation during the participatory process, a select group of stakeholders was chosen for both workshops. Despite the smaller number of participants, representatives from each WEFE sector were included. The main goal of these workshops was to identify key system components for inclusion in the quantitative system dynamics model, along with the primary relationships between these components. The resulting causal loop diagrams laid the foundation for the stock and flow model's development.

A syntactic rule was implemented during the Madrid workshop (Tagus system) to aid the moderation process. Different-colored cards were utilized to categorize system elements based on their respective WEFE sectors. Figure 123 shows the stakeholders during the Group Model Building exercise.

Figure 123. Madrid and Murcia workshop

The system dynamics model is developed once the main variables and components representing the system and their interconnections have been identified. This model consists of different subsystems, each representing one of the components of the water-energy-food nexus and an economic component.

The system dynamics model is developed once the main variables and components representing the system and their interconnections have been identified. This model consists of different subsystems, each representing one of the components of the water-energy-food nexus and an economic component.

The causal loop of the Segura River Basin shown in Figure 124 represents the interaction between the management of available water resources, agricultural production, energy consumption, the ecosystems within this system and different economic components.

For the development of the quantitative system dynamics model, a large amount of data from various fields is used, including hydrometeorological data, economic data, management data, and reservoir characteristics, among others.

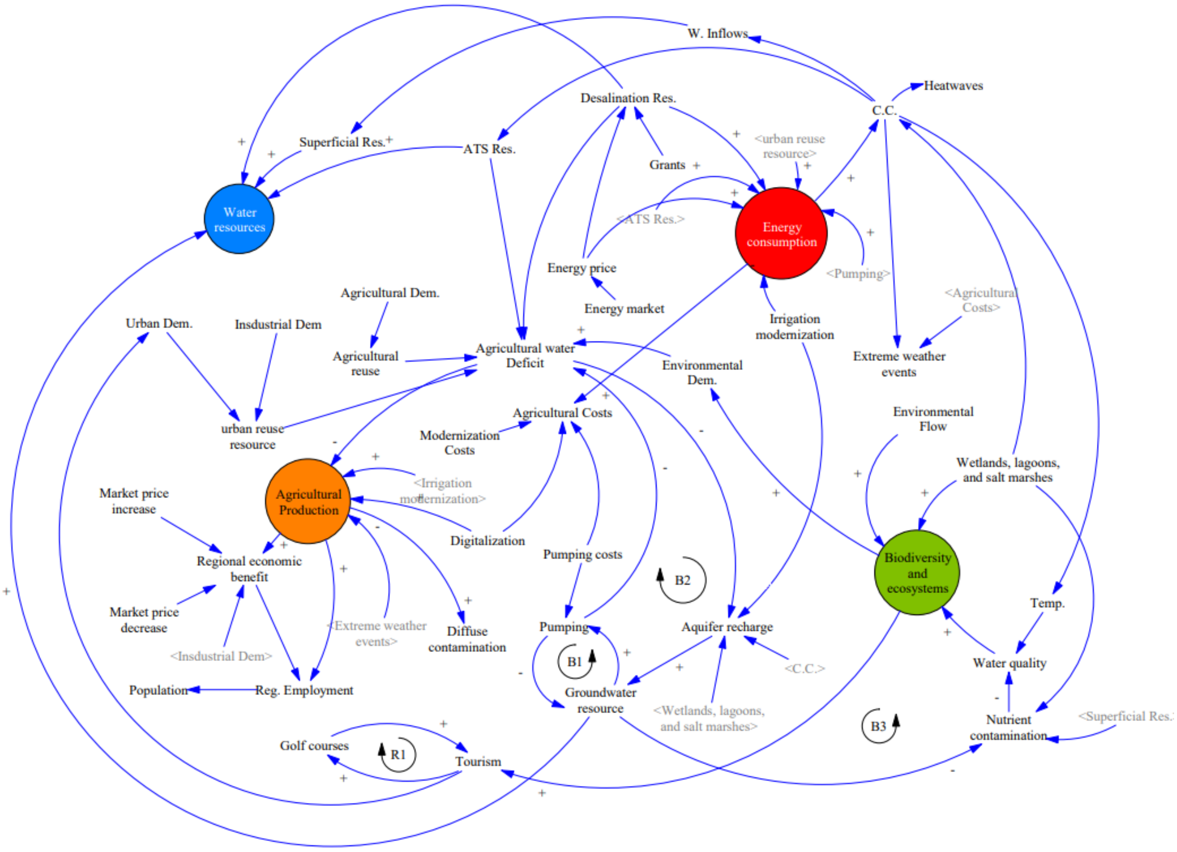

Figure 124. Causal Loop Segura River Basin

Additionally, the water demands considered in the model are collected from public information provided by the CHS (CHS, 2023) and are categorized into environmental demand, urban demand, agricultural demand, industrial demand, and demand for golf courses.

For the TRB two different causal loops were developed due to the differences between the Upper Part (UP) and the Lower Part (LP) for the Spanish part of the basin (Figure 125)

By doing this, spatial differences were captured within the mode and challenges addressed.

As in the SRB, the model interconnects components of the WEFE nexus.

Figure 125. Upper and Lower Part of the TRB

For the UP (Figure 126), the pressure of the city of Madrid on the basin was identified as a primary challenge stressing water quantity and quality. Its urban demand affects directly the Alberche subbasin (its agricultural demand) and the Jarama with the returns.

The LP (Figure 127) is characterized by the energy production within the main channel, being a hyper-controlled river before reaching the border with Portugal.

These two spatial traits were encompassed and represented in the two different Causal Loops and, later, in the Stock and Flow diagrams.

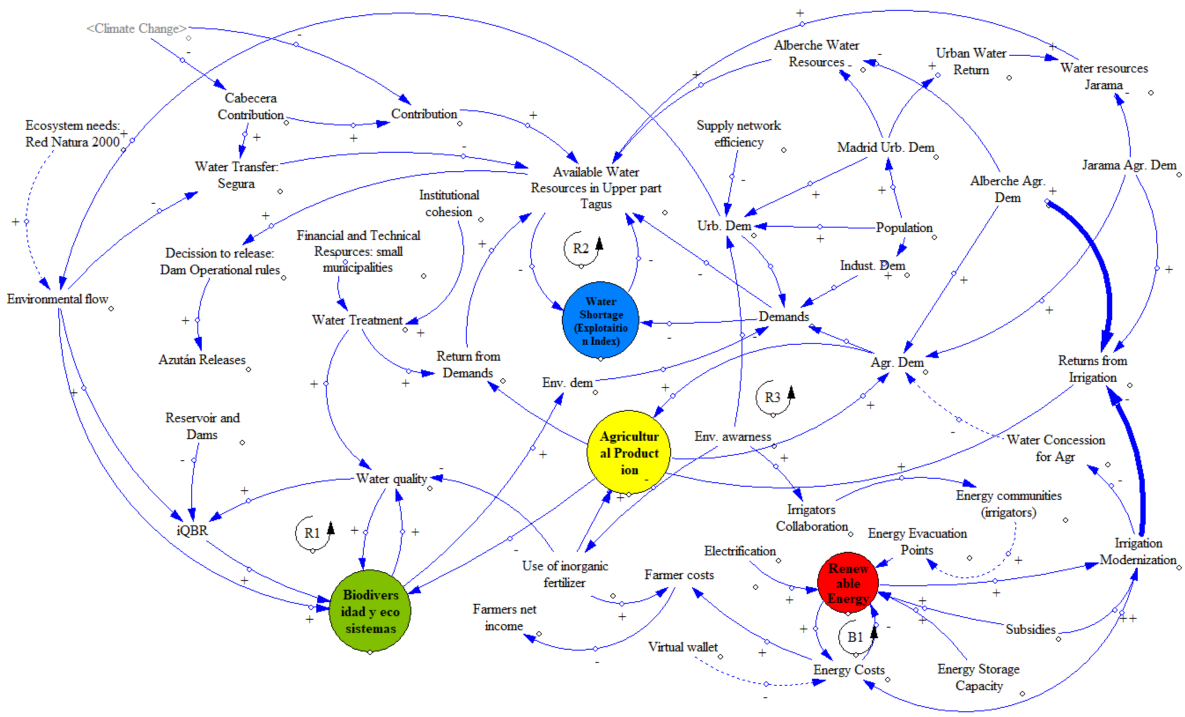

Figure 126. Causal Loop for the UP in the TRB

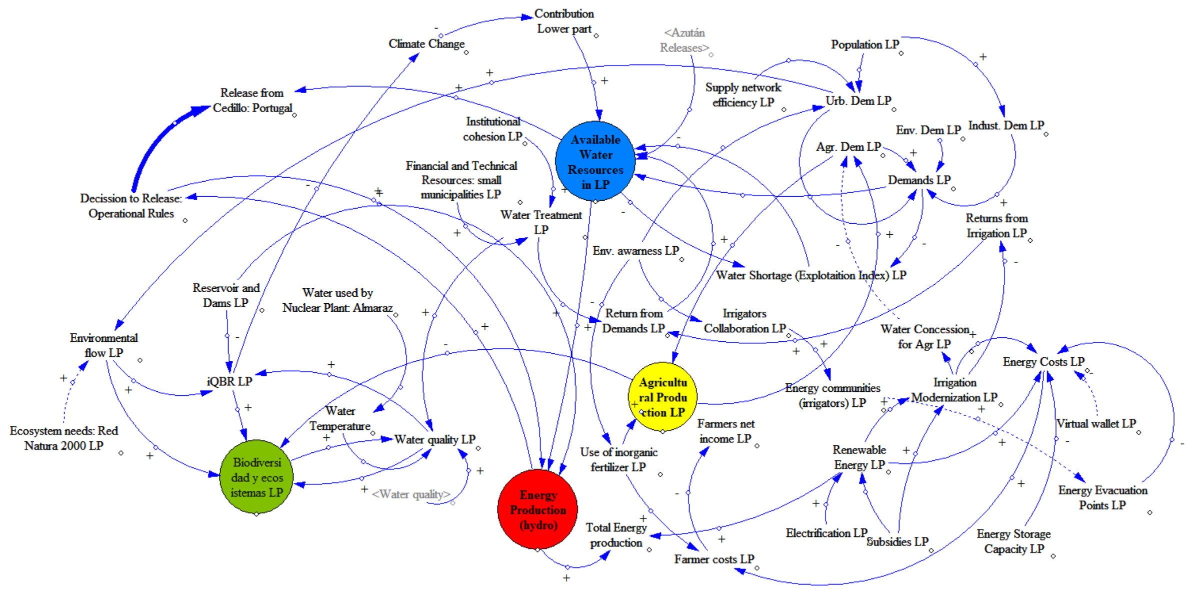

Figure 127. Causal Loop for the LP in the TRB

4.4.2.2 Application Results

The two models SRB (Figure 128) and TRB (Figure 129 and Figure 130) consist of five different sub-modules, each representing one of the components of the Nexus, along with an economic component. These sub-modules are interrelated with each other to capture the complex interactions within the system.

- Water Sub-module: This sub-module focuses on managing available water resources, considering factors such as water availability and water distribution for various purposes like agriculture, industry, and urban consumption. In the case of the TRB, in the LP, for energy production, too.
- Energy Sub-module: In the SRB, the energy sub-module represents the energy consumption within the basin. It considers the energy required for various activities, such as water pumping, agricultural processes, and desalination. In the TRB energy production is calculated.
- Food Sub-module: The food sub-module deals with agricultural production and its interaction with water and energy components. It considers factors like crop types, irrigation methods, and agricultural practices that affect food production. In the case of the TRB, rainfed agriculture plays also a key role within the watershed and it is therefore, represented in the model.
- Ecosystem Sub-module: This sub-module focuses on the ecosystems and their interactions with water availability and usage. It considers ecological factors like aquifers overexploitation for the SRB and fish habitat curves depending on flow in the TRB.
- Economic Sub-module: For the SRB, the economic sub-module represents the economic aspects of the system, including investments and economic impacts of water, energy, and food management decisions.

These sub-modules are designed to interact and influence each other, capturing the feedback loops and interdependencies within the water-energy-food-ecosystems nexus. The overall model helps understand the complexities of the basin functioning and aids in making informed decisions for sustainable resource management.

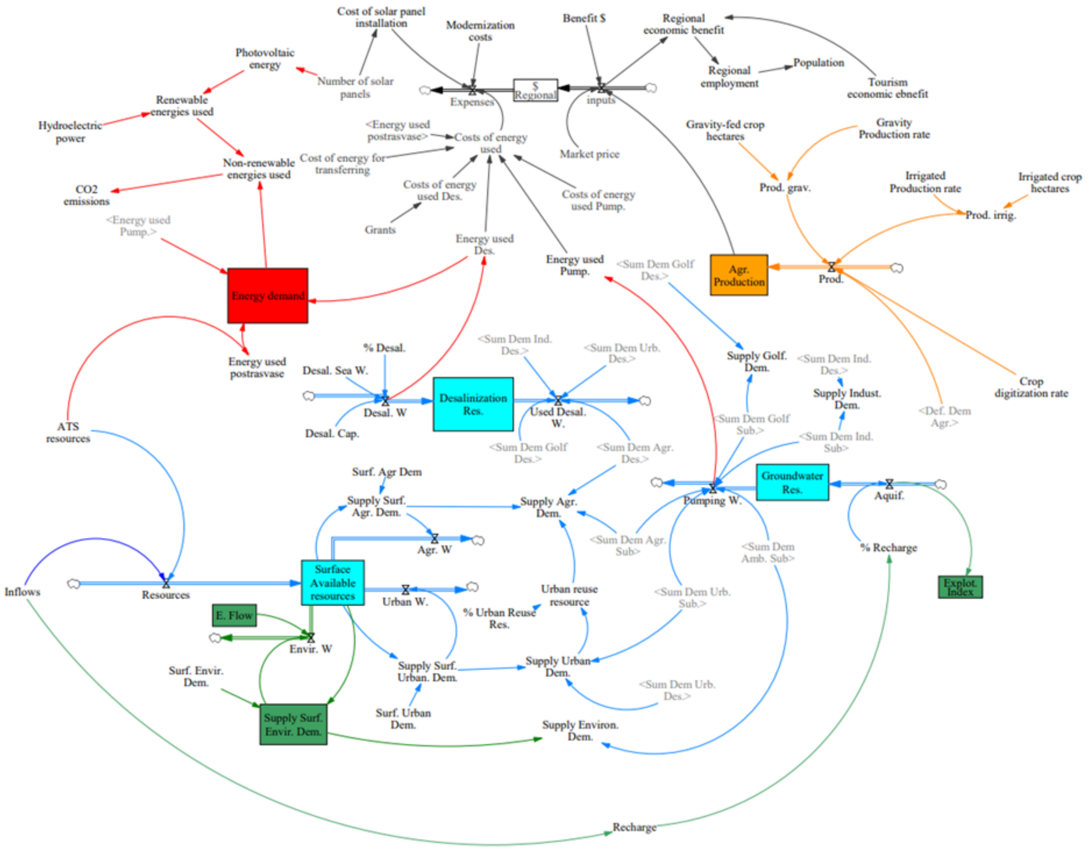

Figure 128. Stock and flow Segura River Basin

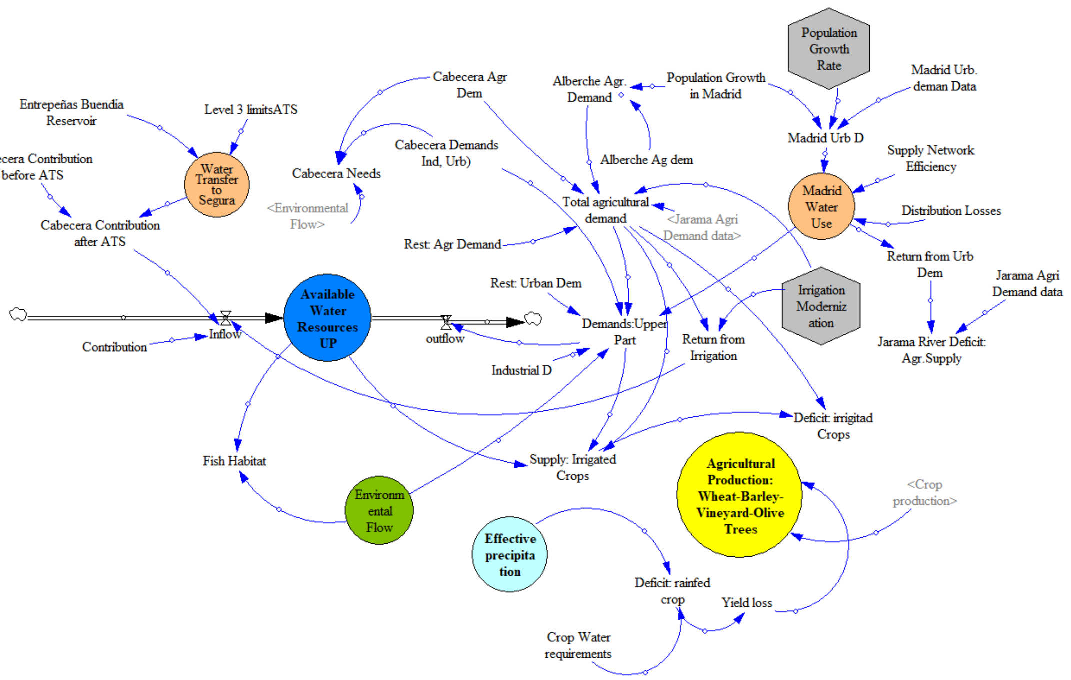

Figure 129. Stock and flow Tagus River Basin (UP)

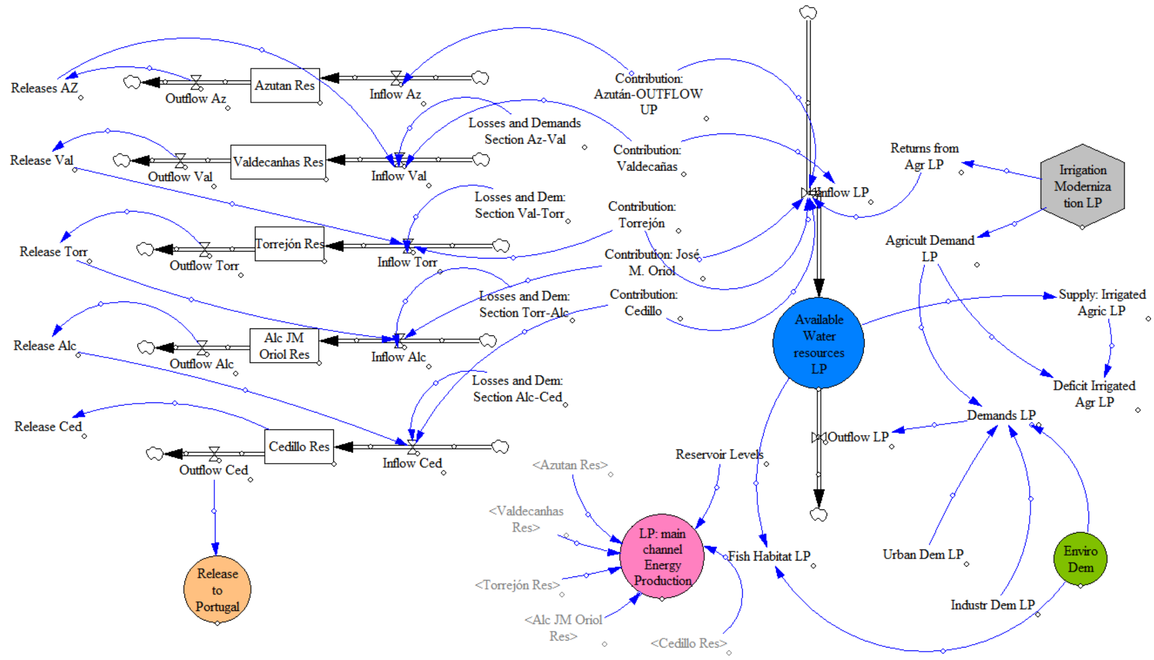

Figure 130. Stock and flow Tagus River Basin (LP)

It is remarkable that the system dynamics model developed for the Segura River basin can effectively replicate the interactions of different systems and follow a very similar trend to a watershed management model. By simulating the historical period considered in the Hydrological Plan of the Segura River Basin, the model resembles the management model for the same period, particularly in variables such as total system storage and monthly evaporation (Figure 131).

This demonstrates the model's capability to capture the complex dynamics and interconnections within the water-energy-food-ecosystems-economic nexus in the basin. The fact that it closely aligns with the management model's results provides confidence in the accuracy and effectiveness of the system dynamics approach for understanding and managing water resources in the Segura River basin.

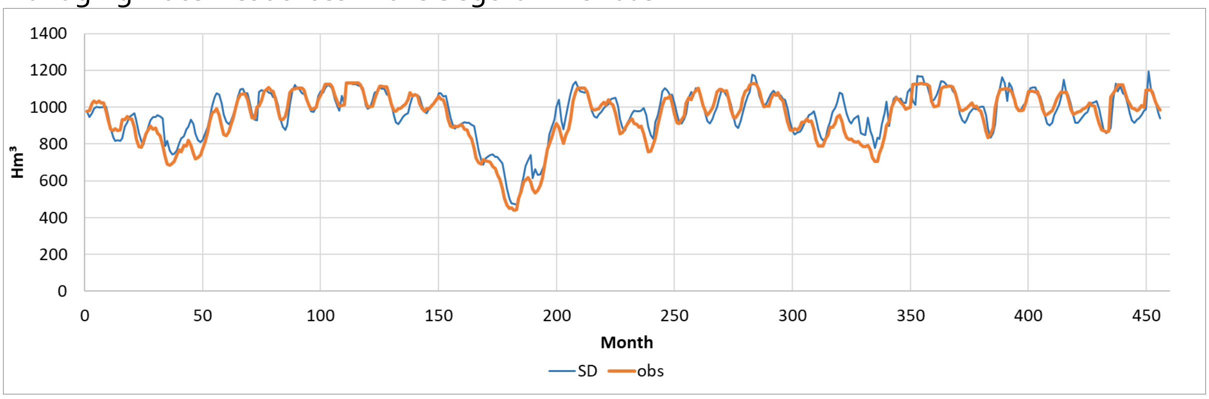

Figure 131. Comparison of the total storage in the SD model and the management model (obs)

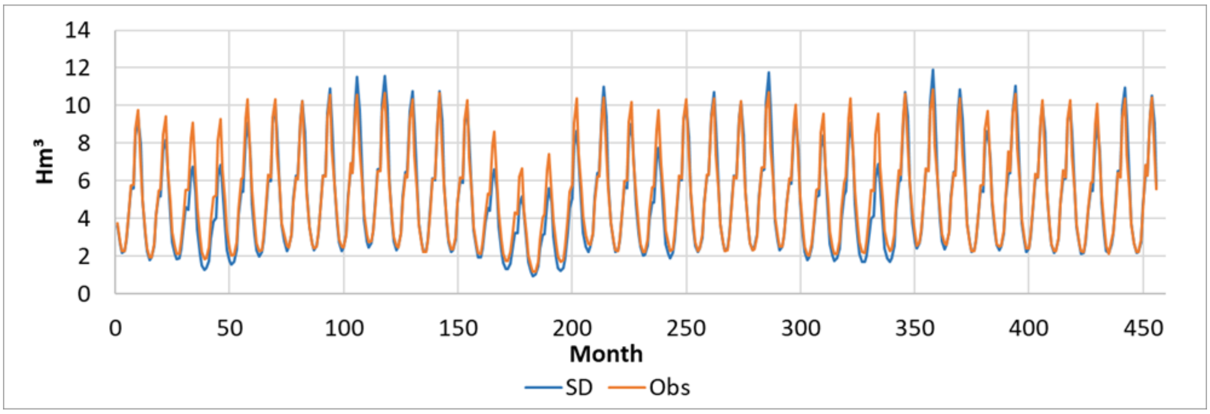

Figure 132. Comparison of the total reservoir evaporation loss in the SD model and the management model (obs)

Undoubtedly, the most significant component of the system is the water resources in the basin. Considering that it is a water-stressed basin with limited resource availability, different sources of water are utilized to compensate for this deficit. Currently, the main sources of water supply include surface water (including resources from the Tagus River basin) and groundwater (Figure 133). However, treated water resulting from urban return flows and desalination plays a fundamental role in meeting the water demands.

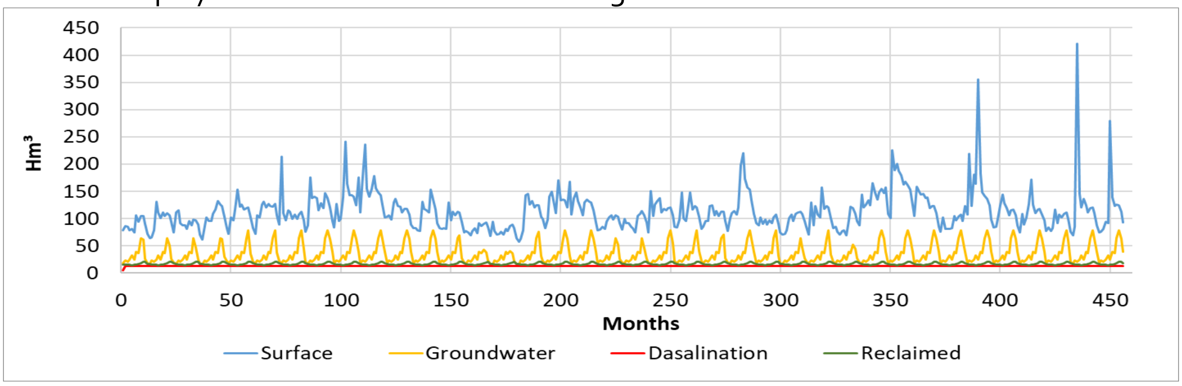

Figure 133. Comparison of the sources of water supply.

Regarding the demands in the system, there are five groups of demands (Figure 134). The agricultural demand represents the largest water needs, followed by the urban demand and the environmental demand. Additionally, the model considers the industrial demand and the demand required for maintaining golf courses.

Figure 134. Average monthly demands [hm³] considered in the modelling.

Agricultural demand is the predominant component within the system, and considering that the basin is water-deficient, it is expected that agricultural demand will experience the highest average monthly deficit (Figure 135). This deficit is defined as the difference between the water demanded by agriculture and the actual water supply available.

The water deficit in agriculture can lead to significant challenges for agricultural productivity. Managing this deficit becomes crucial to ensure the sustainability of agricultural activities in the basin. Strategies such as efficient irrigation practices, water-saving technologies, and crop selection are considered in the model for future scenarios.

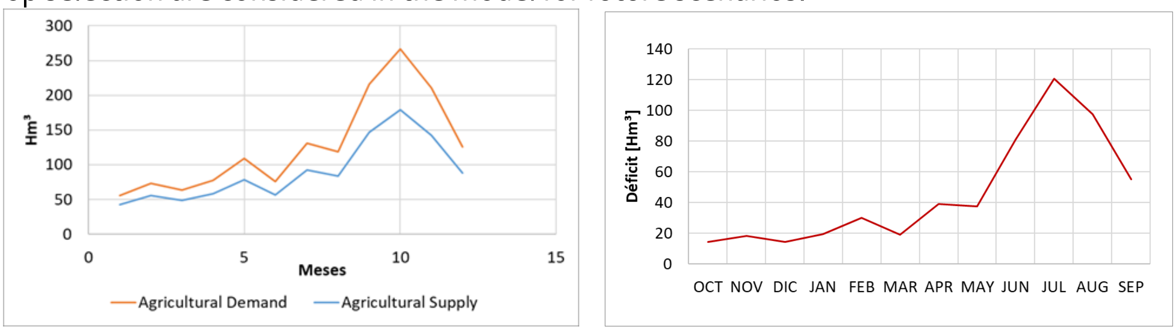

Figure 135. Behaviour of agricultural demand and average monthly supply (left), behaviour of the deficit in agricultural demand (right)

Considering the system's characteristics, the various types of crops present, and the different irrigation methods used, it is possible to estimate the average monthly production of agricultural food and the number of jobs generated by agricultural activities.
The agricultural production can vary depending on factors such as water availability, climate conditions, and the types of crops cultivated. Different irrigation methods, such as drip irrigation, sprinkler irrigation, or flood irrigation, can also impact the productivity of agricultural fields.
Similarly, agricultural activities can be labour-intensive and create employment opportunities for local communities. The number of jobs generated will depend on the scale of agricultural operations and the specific needs of each crop during different stages of the growing season.
Estimating agricultural production and employment is crucial for understanding the socioeconomic impacts of the agricultural sector in the basin (Figure 136). It allows policymakers and stakeholders to make informed decisions regarding water allocation, crop planning, and rural development initiatives, thereby fostering sustainable agricultural practices and supporting livelihoods in the region.

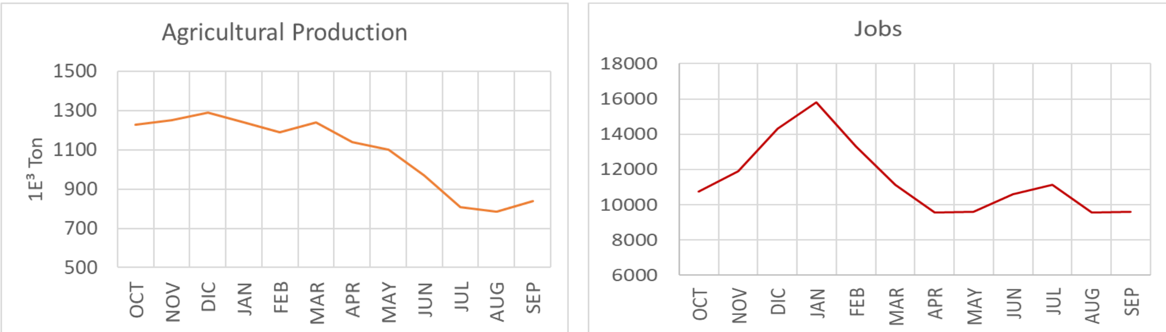

Figure 136.Average monthly agricultural production (left), average monthly employment (right)

The data of monthly work days registered in the agricultural activity per hectare were taken from the Market Report of work 2021 (SEPE, 2022).
The environmental component is of great concern in the Segura River basin, and according to stakeholders and the collected information, one of the most significant impacts on the ecosystems is related to the overexploitation of aquifers (Figure 137). To address this issue, an overexploitation index is established to assess the severity of groundwater overexploitation.

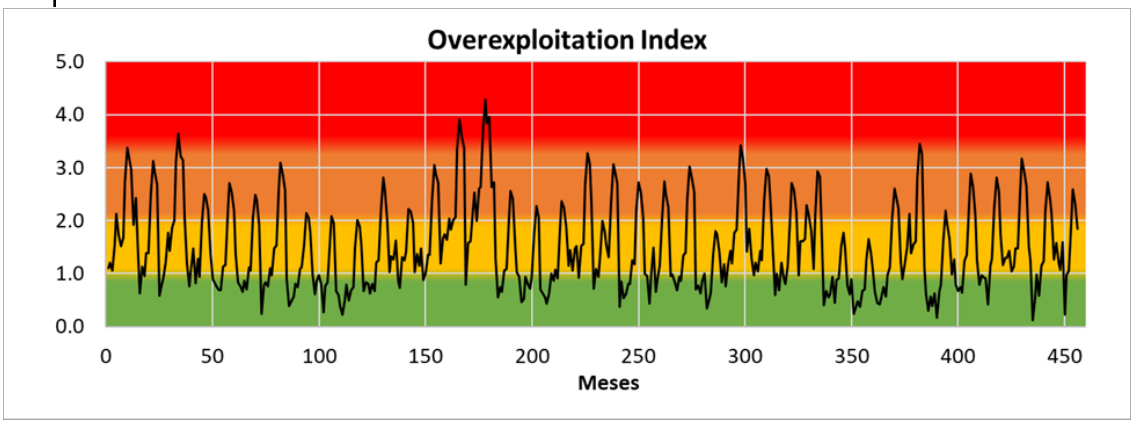

Figure 137. Overexploitation index in the Segura River Basin

For the TRB, inputs for the model (Contribution and Demands) are taken from the River Basin Management Plan (CHT, 23) and for the historical period of 1980-2018. In the graphs, average values are considered at monthly scale.
Main demands in the UP of the watershed are agricultural, with its peak in summer, and the urban demand of Madrid, which remains constant (Figure 138). The rest of demands (industrial and urban) are considered in the model but not show in Figure 138 since, in magnitude, are less significant.

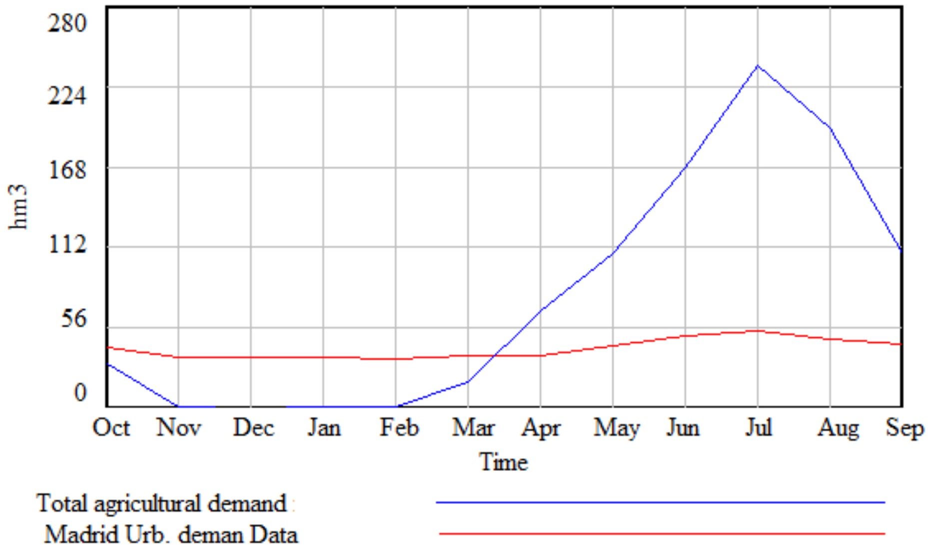

Figure 138. Main demands in the UP of the TRB

The model is also set to simulate a probable population growth in the city of Madrid, which will put more pressure in the system and a future increase in its supply network efficiency. Stakeholders pointed at a strong relationship between the Urban demand of Madrid and its direct influence with the Agricultural demand of Alberche and Jarama rivers. This is also represented and quantified. The model can also explore an increase in the irrigation efficiency as an environmental measurement where the decrease in the water returns will affect the concessions in agricultural demands.
No deficit, defined as the difference between the water demanded by agriculture and the actual water supply available, was found for the period studied. After prioritizing urban and environmental flow, deficit still was not occurring, and all agricultural demands were fully attended.
Rainfed agriculture and its dependency on precipitation patterns will be also considered when implementing climate change scenarios.
The current water transfer rules (Figure 139) are established in the State Official Gazette (Num.179,2021)

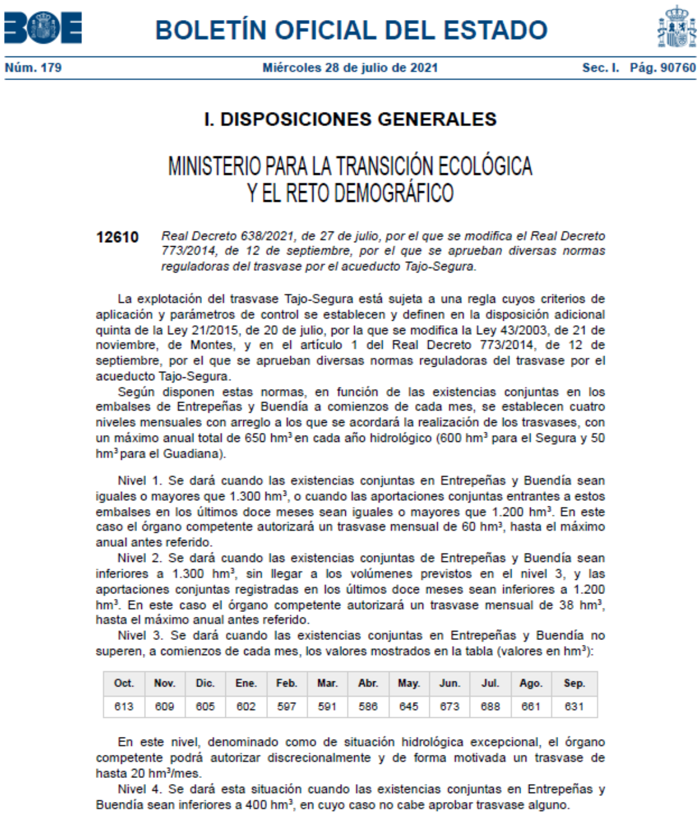

BOLETÍN OFICIAL DEL ESTADO

Núm. 179 Miércoles 28 de julio de 2021 Sec. I. Pág. 90760

I. DISPOSICIONES GENERALES

MINISTERIO PARA LA TRANSICIÓN ECOLÓGICA Y EL RETO DEMOGRÁFICO

12610 *Real Decreto 638/2021, de 27 de julio, por el que se modifica el Real Decreto 773/2014, de 12 de septiembre, por el que se aprueban diversas normas reguladoras del trasvase por el acueducto Tajo-Segura.*

La explotación del trasvase Tajo-Segura está sujeta a una regla cuyos criterios de aplicación y parámetros de control se establecen y definen en la disposición adicional quinta de la Ley 21/2015, de 20 de julio, por la que se modifica la Ley 43/2003, de 21 de noviembre, de Montes, y en el artículo 1 del Real Decreto 773/2014, de 12 de septiembre, por el que se aprueban diversas normas reguladoras del trasvase por el acueducto Tajo-Segura.

Según disponen estas normas, en función de las existencias conjuntas en los embalses de Entrepeñas y Buendía a comienzos de cada mes, se establecen cuatro niveles mensuales con arreglo a los que se acordará la realización de los trasvases, con un máximo anual total de 650 hm³ en cada año hidrológico (600 hm³ para el Segura y 50 hm³ para el Guadiana).

Nivel 1. Se dará cuando las existencias conjuntas en Entrepeñas y Buendía sean iguales o mayores que 1.300 hm³, o cuando las aportaciones conjuntas entrantes a estos embalses en los últimos doce meses sean iguales o mayores que 1.200 hm³. En este caso el órgano competente autorizará un trasvase mensual de 60 hm³, hasta el máximo anual antes referido.

Nivel 2. Se dará cuando las existencias conjuntas de Entrepeñas y Buendía sean inferiores a 1.300 hm³, sin llegar a los volúmenes previstos en el nivel 3, y las aportaciones conjuntas registradas en los últimos doce meses sean inferiores a 1.200 hm³. En este caso el órgano competente autorizará un trasvase mensual de 38 hm³, hasta el máximo anual antes referido.

Nivel 3. Se dará cuando las existencias conjuntas en Entrepeñas y Buendía no superen, a comienzos de cada mes, los valores mostrados en la tabla (valores en hm³):

Oct.	Nov.	Dic.	Ene.	Feb.	Mar.	Abr.	May.	Jun.	Jul.	Ago.	Sep.
613	609	605	602	597	591	586	645	673	688	661	631

En este nivel, denominado como de situación hidrológica excepcional, el órgano competente podrá autorizar discrecionalmente y de forma motivada un trasvase de hasta 20 hm³/mes.

Nivel 4. Se dará esta situación cuando las existencias conjuntas en Entrepeñas y Buendía sean inferiores a 400 hm³, en cuyo caso no cabe aprobar trasvase alguno.

Figure 139. State Official Gazette (Num.179, 2021)

The model encompasses the rules for transferring water to the Segura basin, both models (SRB and TRB) are connected through this variable. The volume of water transferred depends on combined volume storage of the Bolarque and Entrepeñas reservoirs at the beginning of the month.

Four monthly volumes are established with a maximum annual volume of 600 hm3 for the Segura watershed. In Figure 140, an example of water transfer is shown for averages of the historical period.

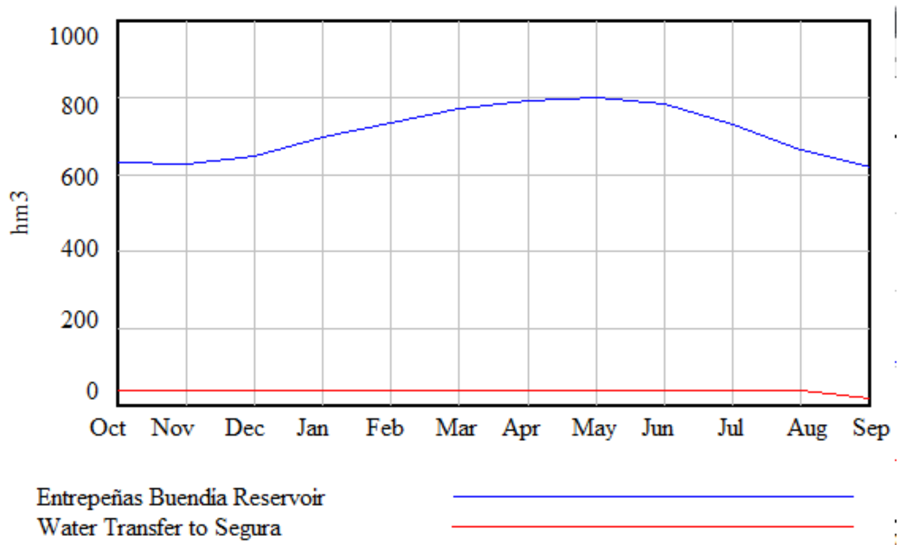

Figure 140. Volume transfer to the Segura basin with average monthly volumes for the historical period.

The model also considers the recent law which establishes a gradual increase of environmental flows which will affect water transfers to the Segura.

This new regime of environmental flows will affect positively ecosystems, where the model will contemplate fish habitat curves.
In the main channel of the LP of the basin, the river is full controlled and fully dedicated to energy production through a cascade of reservoirs until the border with Portugal.
The equation below shows how the Energy production for the main reservoirs (>10MW) is calculated:

$$E\ (Gwh) = H(m) * \mu * V(hm3)$$

Where H, is the height of reservoir level, V is, the turbine flow rate and μ the overall efficiency coefficient, which takes into account the maximum installed power, the maximum turbine flow rate and the maximum height.
In Figure 141, an example of the energy produced in Azután is shown for average values of reservoir releases for the historical period.

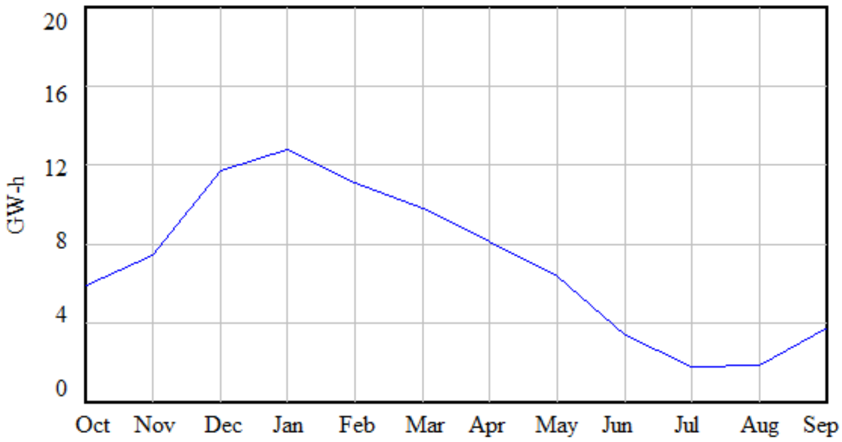

Figure 141. Energy production in Azután reservoir basin with average monthly volumes for the historical period.

4.4.3 Zambezi

4.4.3.1 Application Development

The system dynamics (SD) model developed for the Zambezi Watercourse is intended to represent water management using simple reservoir operating rules. The use of simple operating rules could provide an alternative to the use of more complex functions, given that they could be easier to communicate to the stakeholders and to be implemented by the reservoir managers.
The development of the model was based on a previously developed model by POLIMI for the DAFNE project, which optimizes a set of radial basis functions to calculate the reservoir releases, obtaining Pareto-optimal sets through multi-objective evolutionary optimization, and was intended to translate it into a system dynamics model that could help develop simple operating rules.
The SD model comprises three main components: the stock and flow diagram (Figure 142), where all the mass balances are computed at a monthly time step; the reservoir operation section (Figure 143), where release decisions are determined; and the graphical output, where the main variables, such as water levels and flow rates, are displayed across the simulation.

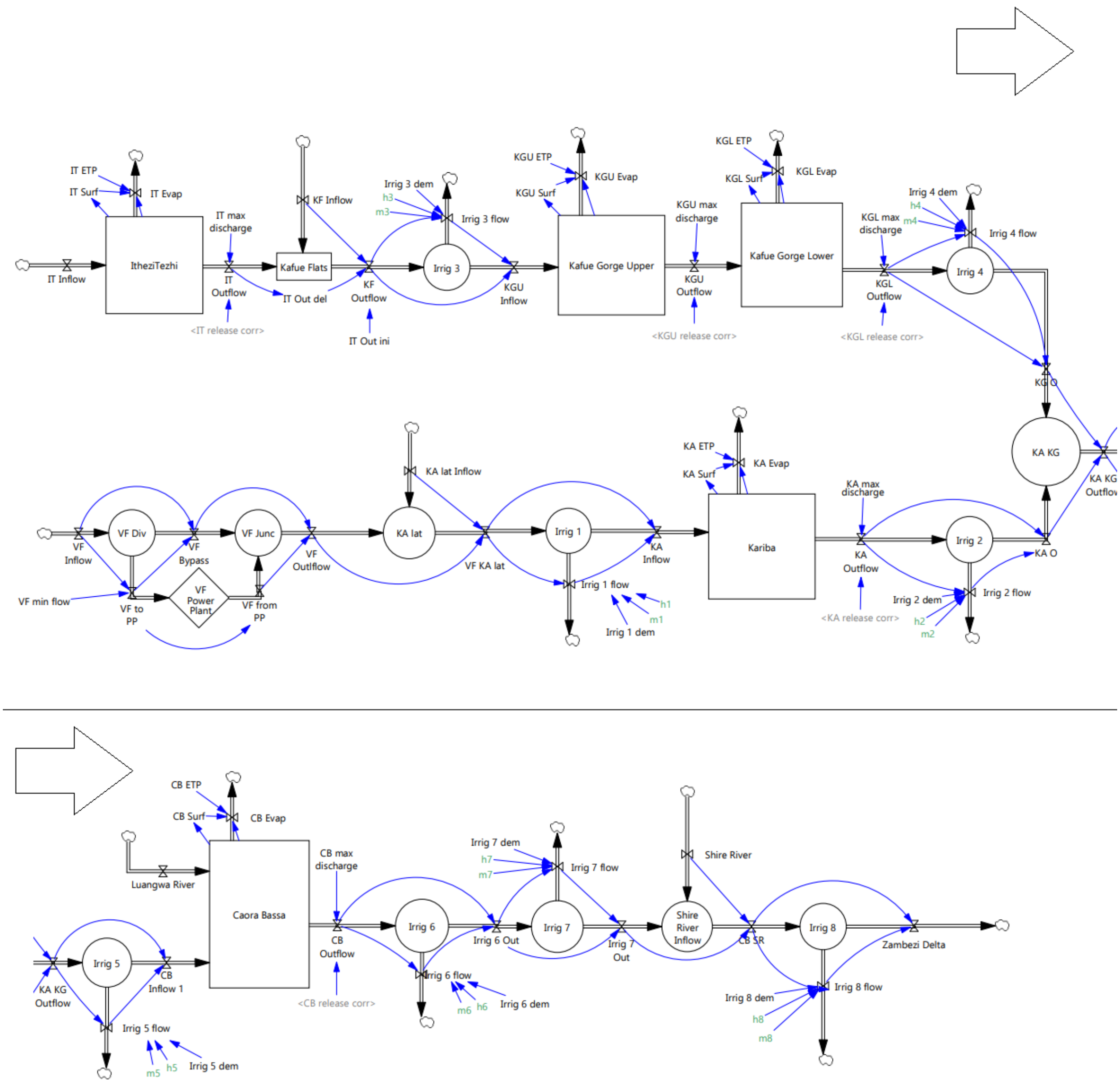

Figure 142. Stock and Flow diagram of the Zambezi system dynamics model

The system schematic is based on the current system state, including the Kafue Gorge Lower reservoir, which was commissioned earlier this year. It includes 6 main inflows, 5 reservoirs with power production capacity, 1 run-of-the-river hydropower plant (Victoria Falls), 8 irrigation abstractions, and 3 environmentally vulnerable areas (Kafue Flats, Victoria Falls, Zambezi Delta). In the first part of the model, all the mass balances are computed through the following equation:

$$S_{t+1} = S_t + I_{t+1} - E_t Sur_t - O_{t+1}$$

where S_t is the storage for that reservoir at the beginning of the month, I_{t+1} are the inflows to that reservoir, O_{t+1} is the outflow dictated by the release decisions of the second part of the model and, if necessary, corrections given physical constraints (lower release or spillage to stay in the reservoir operating range), and $E_t Sur_t$ are the reservoir evaporation losses with E_t the mean monthly evaporation rate and Sur_t the reservoir surface area given by a non-linear relation depending on the storage.

For the irrigation abstractions, water is delivered through diversion channels. The amount of water abstracted depends on the water available in the river and the irrigation demand, and follows a non-linear hedging rule (Celeste and Billib 2009):

$$\omega_{t+1}^{id} = \min\left(q_{t+1}, T_t^{irr,id} * \left[\frac{q_{t+1}}{h^{id}}\right]^{m^{id}}\right) \quad if \quad q_{t+1} \le h^{id} \quad else \ \min\left(q_{t+1}, T_t^{irr,id}\right)$$

Where q_{t+1} is the water flowing through that river segment, $T_t^{irr,id}$ is the demand of that irrigation district, h^{id} and m^{id} are the parameters regulating the diversion channel.
There are two areas protected by Minimum Environmental Flow (MEF) constraints. At Victoria Falls, the minimum flow must be 250 m3/s each month, governing the allocation of water to the run-of-the-river hydropower plant. At Kafue Flats, the releases from the Itezhi-Tezhi reservoir must be at least 40 m3/s every month. However, in March, the minimum release requirement increases to 315 m3/s. For the Zambezi Delta, there is no specific environmental protection in place. However, for the preservation of the river delta's ecosystem, a minimum flow of 7000 m3/s is set as an objective function during the months of February and March.

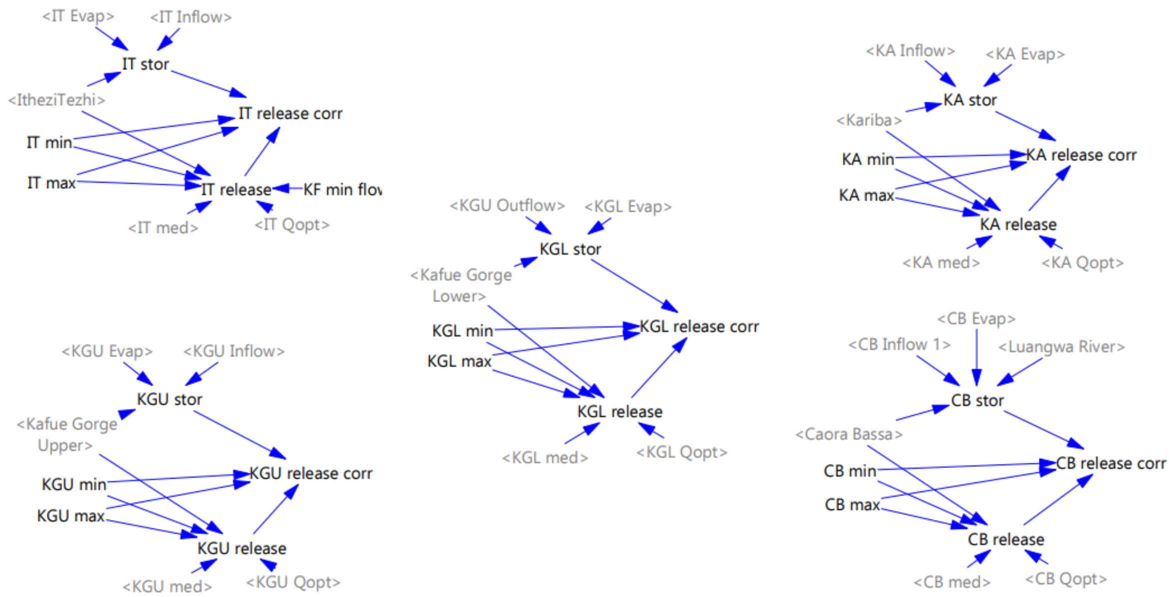

Figure 143. Reservoir operation of the system dynamics model

The reservoir operation is driven by reservoir operating curves that, for each reservoir, associate the storage in the beginning of the month with a release decision. With a similar shape to a Standard Operating Policy, these simple curves (Figure 144) depend on two parameters: the medium level under which the flow is restricted and the optimal release or decision for release when the storage is above the medium level. Also, the rule is a linear hedging rule, in which the release below the medium level (obtained through optimization) is restricted, so that we accept small deficits in current supply in order to reduce the probability of a severe water shortage in the future. The main difference is that Standard Operating Policy rules consider the inflow to the reservoir in that time step, then release water to fulfill the demand according to the available water. In this model, however, the release decision is based on the initial storage in the reservoir, and the parameters are optimized using historical data. Considering this, an additional step is taken to account for physical constraints. If the reservoir level falls below the minimum or rises above the maximum due to inflows and evaporation, the release is modified to stay within that range. The historical data utilized for this model comprises observed streamflow time series for each of the six inflows, spanning the period from 1986 to 2005. This timeframe corresponds to 20 years, or 240 months considering the monthly time step employed.

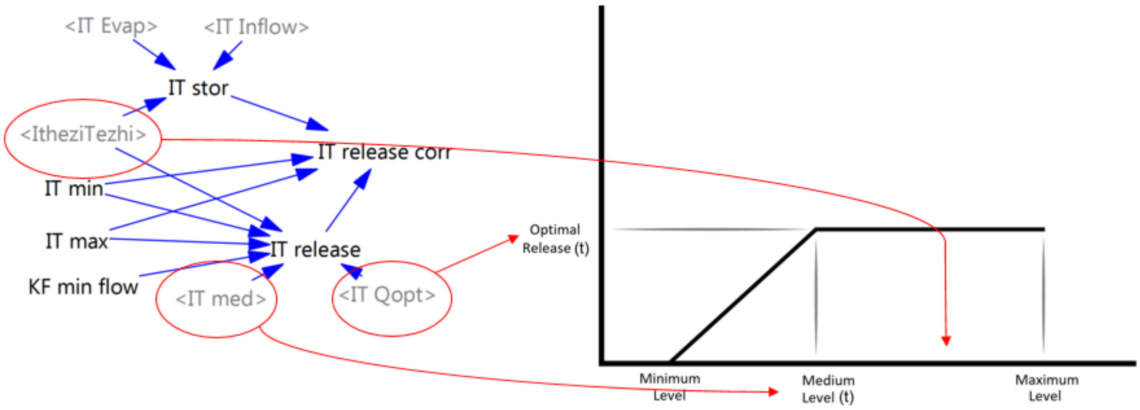

Figure 144. Representation of a release decision curve

The two parameters for each monthly release decision curve, as well as the irrigation abstraction parameters h^{id} and m^{id}, are optimized using the optimization tool included in the selected software (VENSIM), that uses and algorithm based on the Powell's Method (Powell, 1964) that finds the local minimum of a multivariable function without calculating derivatives. The objective functions to minimize where developed in the DAFNE project, aimed to represent the main concerns obtained from the stakeholders, and consist of:

Environmental flow deficit (water):

$$DEF_W = \frac{1}{h}\left[\Sigma_{t=0}^{h-1}\left(\max\left(Qe_t - r_{t+1}, 0\right)\right)^2\right]$$

where Qe_t is the specified monthly minimum flow, which is 7.000 m³/s for the months of February and March only, and r_{t+1} represents the amount of water entering the Zambezi River delta. This deficit is averaged across all the months of the simulation, and its quadratic formulation aims at penalizing severe deficit within a single time step, while allowing more frequent small shortages (Hashimoto, et al., 1982).

Hydropower production deficit (energy):

$$DEF_E = \frac{1}{N_{years}}\left[\Sigma_{t=0}^{h-1}\Sigma_{r=1}^{rmax}\left|Wp_t^r - P_{t+1}^r\right|\right]$$

where Wp_t^r is the target hydropower production, in this case given by the Osemosys energy model used in the DAFNE project, and $P_{t+1}^r = \eta^r g\gamma \bar{h}_t^r q_{t+1}^{turb,r}$ is the actual power production of the r-th power plant, where η^r is the turbines efficiency, $g = 9.81\, m/s^2$ is the gravitational acceleration, $\gamma = 1000\, kg/m^3$ is the water density, $\bar{h}_t^r$ is the net hydraulic head in meters, and $q_{t+1}^{turb,r}$ is the turbinated flow (minimum between the release decision and the turbines flow capacity). The total energy deficit is averaged yearly across the simulation period.

Normalized irrigation deficit (food):

$$DEF_F = \frac{1}{h}\left[\Sigma_{t=0}^{h-1}\Sigma_{id=1}^{idmax}\left(\frac{\max\left(wirr_t^{id} - rirr_{t+1}^{id}, 0\right)}{wirr_t^{id}}\right)^2\right]$$

where $wirr_t^{id}$ and $rirr_{t+1}^{id}$ are the irrigation water demand and abstraction of the id-th irrigation district, respectively. The normalization of the deficit allows to weigh all the irrigation district deficits equally regardless of the magnitude of the demands, and the sum of all the deficits is averaged monthly across the simulation period. As in the environmental flow deficit, the quadratic formulation aims at penalizing severe deficits within a single time step, while allowing more frequent small shortages (Hashimoto, et al., 1982).
To coordinate the dimensions of the objective functions, an equation of the type:

$$F = Minimize(a \cdot DEF_W + b \cdot DEF_E + c \cdot DEF_F)$$

must be solved. This type of equation is entered to the optimization tool, to have in consideration more than one function to optimize. This would correspond with a weighted sum approach to the multi-objective optimization, but in this case, the weight its used to coordinate the dimensions of the deficits (Azari & Tabesh, 2018) as well as to represent the relative weights of each goal. It must be noted that the weights for each deficit were found with a trial an error approach, using as a reference the results of the Pareto-optimal set given by the MORDM of the Zambezi for this configuration to replicate the trend. With this process, we obtain relative weights for three different main objectives: Hydropower Production, Irrigation Supply and Environmental Conservation. With this approach, once the relative weights are set based on the MORDM outputs and stakeholder interaction, this tool can generate simple operating rules for the reservoirs that would approximate that performance.

4.4.3.2 Application Results

4.4.3.2.1 Relative weights

As mentioned before, the relative weights of each deficit were found to approximate the performance and trend of the Pareto-optimal set, the resulting weight of this process are presented in Table 12, where the irrigation supply relative weight was fixed, and the weights of power production and environmental conservation where changed.

Table 12. Relative weights obtained for the optimization of the release decision curves.

Main Goal	Power Production	Irrigation Supply	Environmental Conservation
Power Production	1,5	7	1,0E-06
Irrigation Supply	0,15	7	2,5E-06
Ecological Conservation	0,15	7	5,0E-06

4.4.3.2.2 Model performance

The results in the three indicators for three main goals are presented in Table 13, where we can see the performance that can be reached in this configuration with simple curves like this.

Table 13. Performance in the selected indicators for the obtained release decision curves

Main Goal	Power Production Deficit [TWh/year]	Irrigation Supply Deficit [Normalized Square]	Environmental Deficit $[m^3/s]^2$
Power Production	140.27	1.2345	4.37E+06
Irrigation Supply	186.75	0.0038	8.82E+05
Ecological Conservation	203.58	0.0100	2.52E+05

4.4.3.2.3 Obtained operating rules

While the parameters for the release decision curves obtained in the optimization process are considered too extensive to be shown here, we can illustrate the example of the release decision curves for the Cahora Bassa reservoir in Figure 145, Figure 146, and Figure 147. Here, we can easily observe the differences in the shape and magnitude of these curves.

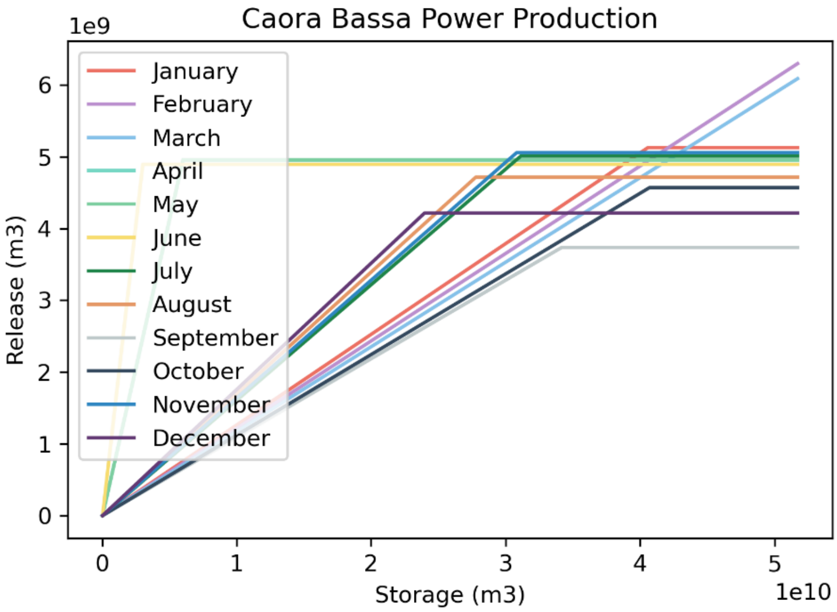

Figure 145. Release decision curves for the Cahora Bassa reservoir. Main goal power production.

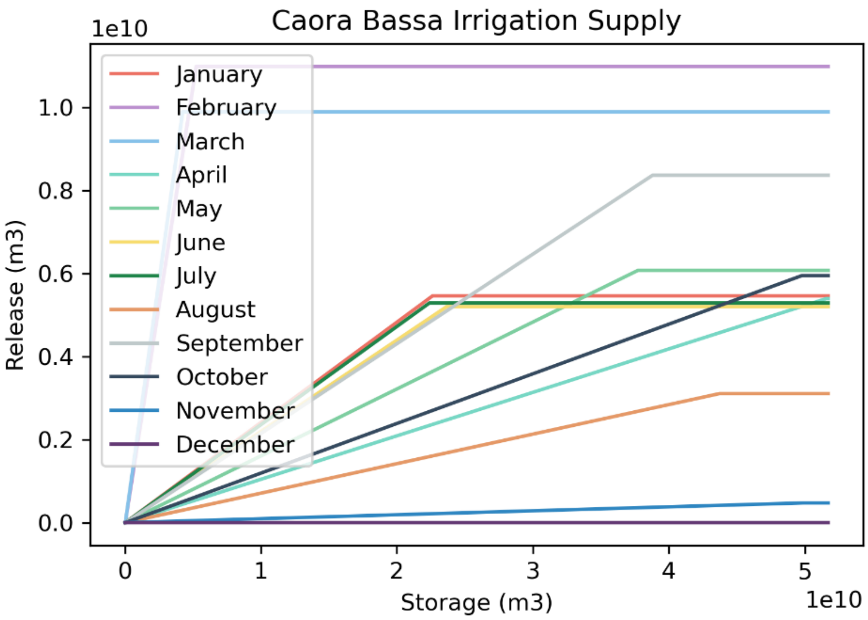

Figure 146. Release decision curves for the Cahora Bassa reservoir. Main goal irrigation supply

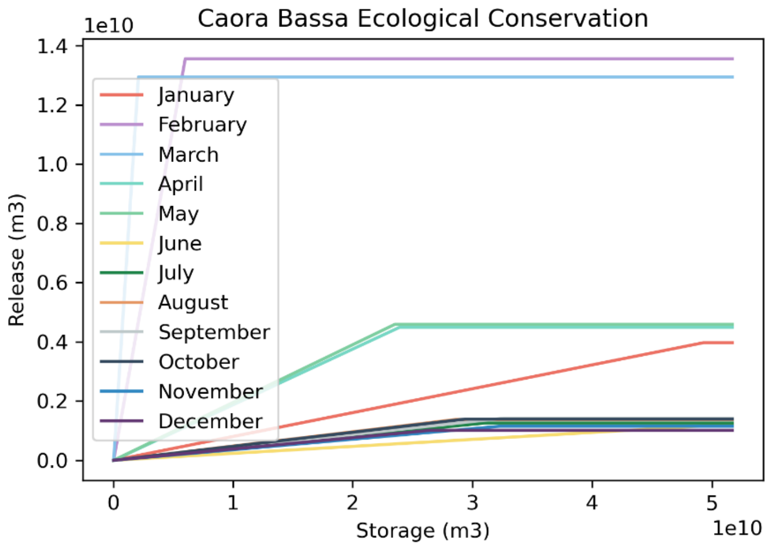

Figure 147. Release decision curves for the Cahora Bassa reservoir. Main goal ecological conservation

Regarding the main goal of power production, the curves mainly fall in the same area of the graph due to the constant target power production throughout the year.

However, for the main goal of irrigation supply, the curves tend to be more scattered and diverse, as the main indicator is linked to the agricultural demand, which fluctuates throughout the year.

In contrast, for the main goal of environmental conservation, the curves for February and March are much higher than in the other months. This is because the performance of the system primarily depends on the flow in the delta during these two months.

It must be noted that this release decision curves are based on a coordinated management of the system, as they have been developed simultaneously. Although these curves are derived based on the storage of each individual reservoir, they were designed with consideration for the operation of the entire system.

Figure 148 illustrates the differences in the alternatives for the flow to the Zambezi delta. It is evident how the primary objectives of environmental conservation and irrigation supply exhibit greater variability in the flows directed to the delta. This variability serves to preserve the natural flood regimes inherent to the ecosystem, which is essential for its ecological balance.

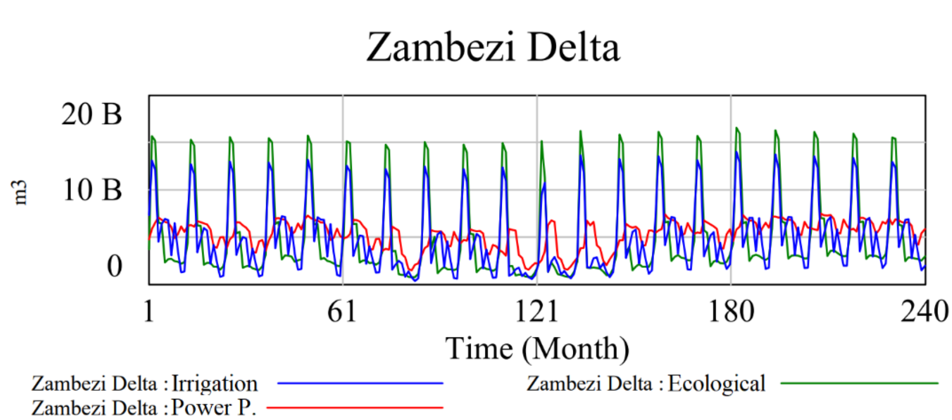

Figure 148. Inflow to the Zambezi Delta in the system dynamics model

5 Synthesis and conclusions

This report has synthesized learnings from the development and application of four complementary WEFE modelling approaches across six diverse river basin case studies in GoNEXUS. The combined application of these quantitative methods provided a more comprehensive understanding of the complex and uncertain nexus dynamics within each unique setting.

The high-resolution modelling generated detailed evaluations of WEFE indicators at local scales, capturing intra-basin variability that is lost in more aggregated models. However, the computational demands limited the extent of uncertainty analysis that could be conducted. Moving forward, opportunities exist to couple key processes for greater model integration and utilize emulators to enable more robustness testing.

The many-objective robust decision making (MORDM) approach effectively explored tradeoffs across conflicting WEFE objectives and assessed the robustness of alternatives across a wide range of plausible futures. A key output was the development of simple operating rules for reservoirs and irrigation diversions co-produced through soft linkage of MORDM and system dynamics models. Testing indicated these rules approximated system behaviour achieved through more complex optimized policies.

Hydroeconomic modelling provided insights into economic tradeoffs and potential synergies from coordinated management of water and interconnected sectors. Limitations in quantitatively representing all nexus components, especially ecosystem services, were partially offset through multi-objective problem formulations. Further method refinement for environmental valuation and integrating climate change uncertainty is an area for future work.

System dynamics modelling enabled the incorporation of qualitative insights from stakeholders into the quantitative modelling, supporting participatory processes. The approach facilitated rapid simulation of scenarios and adaptation pathways. Lack of optimization capability was compensated through soft linkage with the MORDM optimization. Participatory system dynamics helped build trust and transparency with stakeholders.

The relative importance of modelled nexus challenges varied across basins based on their unique socio-environmental contexts. Climate change impacts on water availability were evaluated in all basins, with concerns for increased water scarcity in the Júcar, Tagus-Segura and Senegal. Effects of energy transition and decarbonization policies were analysed in the Júcar case study. Food production sustainability was examined in Lake Como, Júcar, Tagus-Segura and Senegal. Ecosystem preservation and environmental flow considerations were addressed in all basins.

Stakeholder participation in co-developing the case-specific models was critical for ensuring local relevance and adoption. The combined quantitative modelling was able to evidence complex nexus tradeoffs and scenario uncertainties which are difficult to conceptualize qualitatively. This can provide an improved foundation for collaborative and equitable decision-making on sustainable natural resource management.

While the multiple modelling techniques provided complementary insights, limitations remain in representing every nexus aspect quantitatively. Ongoing engagement with diverse stakeholders will be integral to refining the models to address persistent gaps and mismatches with perceived system behaviour. Overall, the case studies demonstrate the value of integrated systems modelling to support management of interconnected WEFE sectors under uncertainty.

6 References

Adams, A. (2000). The River Senegal: flood management and the future of the valley. *The River Senegal: Flood Management and the Future of the Valley.*, *93*. https://www.cabdirect.org/cabdirect/abstract/20001810864

Ahmad, S., & Prashar, D. (2010). Evaluating Municipal Water Conservation Policies Using a Dynamic Simulation Model. *Water Resources Management*, *24*(13), 3371–3395.

Albrecht, T. R., Crootof, A., & Scott, C. A. (2018). The Water-Energy-Food Nexus: A systematic review of methods for nexus assessment. *Environmental Research Letters: ERL [Web Site]*, *13*(4), 043002.

Al-Jawad, J. Y., & Tanyimboh, T. T. (2017). Reservoir operation using a robust evolutionary optimization algorithm. *Journal of Environmental Management*, *197*, 275–286.

Almansa, C., Calatrava, J., & Martínez-Paz, J. M. (2012). Extending the framework of the economic evaluation of erosion control actions in Mediterranean basins. *Land Use Policy*, *29*(2), 294–308.

Amin Zargar, Rehan Sadiq, Bahman Naser, & Faisal I. Khan. (2011). A review of drought indices. *Environmental Reviews*, *19*, 333–349.

Azari, B., & Tabesh, M. (2018). Optimal Design of Stormwater Collection Networks Considering Hydraulic Performance and BMPs. *International Journal of Environmental Research and Public Health*, *12*(5), 585–596.

Bader, J.-C., Lamagat, J.-P., & Guiguen, N. (2003). Management of the Manantali Dam on the Senegal River: quantitative analysis of a conflict of objectives. *Hydrological Sciences Journal*, *48*(4), 525–538.

Bertoni, F., Castelletti, A., Giuliani, M., & Reed, P. M. (2019). Discovering dependencies, trade-offs, and robustness in joint dam design and operation: An ex-post assessment of the kariba dam. *Earth's Future*, *7*(12), 1367–1390.

Bruckmann, L. (2018). Crue et développement rural dans la vallée du Sénégal : entre marginalisation et résilience. *Belgeo*, *2*. https://doi.org/10.4000/belgeo.23158

Burek, P., Greve, P., Wada, Y., Krey, V., Fischer, G., Parkinson, S., Tramberend, S., Byers, E., Satoh, Y., Riahi, K., Veldkamp, T. I. E., Burtscher, R., Djilali, N., Langan, S., & Kahil, T. (2018). A Continental-Scale Hydroeconomic Model for Integrating Water-Energy-Land Nexus Solutions. *Water Resources Research*, *54*(10), 7511–7533.

Calamita, E., Vanzo, D., Wehrli, B., & Schmid, M. (2021). Lake modeling reveals management opportunities for improving water quality downstream of transboundary tropical dams. *Water Resources Research*, *57*(4). https://doi.org/10.1029/2020wr027465

Cañizares, A. O., Cantos, J. O., & Baños Castiñeira, C. J. (2022). The effects of climate change on the Tagus–Segura transfer: Diagnosis of the water balance in the Vega Baja del Segura (Alicante, Spain). *Water*, *14*(13), 2023.

Casadei, S., Peppoloni, F., & Pierleoni, A. (2020). A New Approach to Calculate the Water Exploitation Index (WEI+). *WATER*, *12*(11), 3227.

Celeste, A. B., & Billib, M. (2009). Evaluation of stochastic reservoir operation optimization models. *Advances in Water Resources*, *32*(9), 1429–1443.

Chowdhury, A. F. M. K., Kern, J., Dang, T. D., & Galelli, S. (2020). PowNet: A network-constrained unit commitment/economic dispatch model for large-scale power

systems analysis. *Journal of Open Research Software*, *8*. https://doi.org/10.5334/jors.302
Cohon, J. L., & Marks, D. H. (1975). A review and evaluation of multiobjective programing techniques. In *Water Resources Research* (Vol. 11, Issue 2, pp. 208–220). https://doi.org/10.1029/wr011i002p00208
Conejo, A. J., & Baringo, L. (2018). Unit Commitment and Economic Dispatch. In *Power Electronics and Power Systems* (pp. 197–232). Springer International Publishing.
Conway, D., Dalin, C., Landman, W. A., & Osborn, T. J. (2017). Hydropower plans in eastern and southern Africa increase risk of concurrent climate-related electricity supply disruption. *Nature Energy*, *2*(12), 946–953.
Correia de Araujo, W., Oliveira Esquerre, K. P., & Sahin, O. (2019). Building a System Dynamics Model to Support Water Management: A Case Study of the Semiarid Region in the Brazilian Northeast. *WATER*, *11*(12), 2513.
DAFNE. (2018). *A Decision-Analytic Framework to explore the water-energy-food NExus in complex and transboundary water resources systems of fast growing developing countries*. EU H2020 Project Grant No. 690268.
Degeorges, A., & Reilly, B. K. (2006). Dams and large scale irrigation on the Senegal River: impacts on man and the environment. *The International Journal of Environmental Studies*, *63*(5), 633–644.
Denaro, S., Anghileri, D., Giuliani, M., & Castelletti, A. (2017). Informing the operations of water reservoirs over multiple temporal scales by direct use of hydro-meteorological data. *Advances in Water Resources*, *103*, 51–63.
Denaro, S., Castelletti, A., Giuliani, M., & Characklis, G. (2020). Insurance portfolio diversification through bundling for competing agents exposed to uncorrelated drought and flood risks. *Water Resources Research*, *56*(5). https://doi.org/10.1029/2019wr026443
DiFrancesco, K. N., & Tullos, D. D. (2014). Flexibility in Water Resources Management: Review of Concepts and Development of Assessment Measures for Flood Management Systems. *JAWRA Journal of the American Water Resources Association*, *50*(6), 1527–1539.
Diouf, P., Albaret, J. J., T., B., Diallo, A., Diallo, P., Deme-Gningue, I., Le Reste, L., & Kebe, M. (1993). *Aménagement de la vallée du fleuve Sénégal – Projet d'étude du système Pêche*. Institut Sénégalais des Recherches Agricoles. http://intranet.isra.sn/aurifere/opac_css/docnum/OC0000655.pdf
Do, P., Tian, F., Zhu, T., Zohidov, B., Ni, G., Lu, H., & Liu, H. (2020). Exploring synergies in the water-food-energy nexus by using an integrated hydro-economic optimization model for the Lancang-Mekong River basin. *The Science of the Total Environment*, *728*, 137996.
ERM. (2019). *Proposed Batoka Gorge Hydro-Electric Scheme (Zambia and Zimbabwe) on the Zambezi River: Environmental and Social Impact Assessment (ESIA) for the Project Area of Inundation, Staff Villages and Quarries (V4.0)*. Zambezi River Authority (ZRA). https://www.erm.com/contentassets/6bdbb76b347f4e9fb9b9c14054806210/esia-dam-and-associated-infrastructure.pdf
Escriva-Bou, A., Pulido-Velazquez, M., & Pulido-Velazquez, D. (2017). Economic value of climate change adaptation strategies for water management in Spain's jucar basin. *Journal of Water Resources Planning and Management*, *143*(5), 04017005.

Espanmanesh, V., & Tilmant, A. (2022). Optimizing the management of multireservoir systems under shifting flow regimes. *Water Resources Research*, *58*(6). https://doi.org/10.1029/2021wr030582

Estrela-Segrelles, C., Gómez-Martinez, G., & Pérez-Martín, M. Á. (2021). Risk assessment of climate change impacts on Mediterranean coastal wetlands. Application in Júcar River Basin District (Spain). *The Science of the Total Environment*, *790*(148032), 148032.

European Commission Joint Research Centre. (2022). PVGIS 5.2 [Data set]. In *EU Science Hub*. https://joint-research-centre.ec.europa.eu/pvgis-photovoltaic-geographical-information-system/pvgis-releases/pvgis-52_en

Farinotti, D., Huss, M., Fürst, J. J., Landmann, J., Machguth, H., Maussion, F., & Pandit, A. (2019). A consensus estimate for the ice thickness distribution of all glaciers on Earth. *Nature Geoscience*, *12*(3), 168–173.

Fatichi, S., Rimkus, S., Burlando, P., Bordoy, R., & Molnar, P. (2015). High-resolution distributed analysis of climate and anthropogenic changes on the hydrology of an Alpine catchment. *Journal of Hydrology*, *525*, 362–382.

Friedman, J. H., & Fisher, N. I. (1999). Bump hunting in high-dimensional data. *Statistics and Computing*, *9*(2), 123–143.

Fuso, F., Casale, F., Giudici, F., & Bocchiola, D. (2021). Future Hydrology of the Cryospheric Driven Lake Como Catchment in Italy under Climate Change Scenarios. *Climate*, *9*(1), 8.

Gandolfi, C., Agostani, D., Facchi, A., & Ortuani, B. (2011). *Modello e codice di calcolo IdrAgra*. 93.

Gandolfi, C., Guariso, G., & Togni, D. (1997). Optimal Flow Allocation in the Zambezi River System. *Water Resources Management*, *11*(5), 377–393.

Garcia Galiano, S. G., Olmos Gimenez, P., & Giraldo-Osorio, J. D. (2015). Assessing nonstationary spatial patterns of extreme droughts from long-term high-resolution observational dataset on a semiarid basin (Spain). *Water*, *7*(10), 5458–5473.

Gil, M., Garrido, A., & Gómez-Ramos, A. (2011). Economic analysis of drought risk: An application for irrigated agriculture in Spain. *Agricultural Water Management*, *98*(5), 823–833.

Girard, C., Pulido-Velazquez, M., Rinaudo, J.-D., Pagé, C., & Caballero, Y. (2015). Integrating top–down and bottom–up approaches to design global change adaptation at the river basin scale. In *Global Environmental Change* (Vol. 34, pp. 132–146). https://doi.org/10.1016/j.gloenvcha.2015.07.002

Giudici, F., Anghileri, D., Castelletti, A., & Burlando, P. (2021). Descriptive or normative: How does reservoir operations modeling influence hydrological simulations under climate change? *Journal of Hydrology* , *595*(125996), 125996.

Giuliani, Crochemore, L., Pechlivanidis, I., & Castelletti, A. (2020). From skill to value: isolating the influence of end user behavior on seasonal forecast assessment. *Hydrology and Earth System Sciences*, *24*(12), 5891–5902.

Giuliani, Li, Y., Castelletti, A., & Gandolfi, C. (2016). A coupled human-natural systems analysis of irrigated agriculture under changing climate. *Water Resources Research*, *52*(9), 6928–6947.

Giuliani, M., & Castelletti, A. (2016). Is robustness really robust? How different definitions of robustness impact decision-making under climate change. In *Climatic Change* (Vol. 135, Issues 3–4, pp. 409–424). https://doi.org/10.1007/s10584-015-1586-9

Giuliani, M., Castelletti, A., Pianosi, F., Mason, E., & Reed, P. M. (2016). Curses, tradeoffs, and scalable management: Advancing evolutionary multiobjective direct policy search to improve water reservoir operations. *Journal of Water Resources Planning and Management*, *142*(2), 04015050.

Giuliani, M., Lamontagne, J. R., Hejazi, M. I., Reed, P. M., & Castelletti, A. (2022). Unintended consequences of climate change mitigation for African river basins. *Nature Climate Change*, *12*(2), 187–192.

Giuliani, M., Zaniolo, M., Castelletti, A., Davoli, G., & Block, P. (2019). Detecting the state of the climate system via artificial intelligence to improve seasonal forecasts and inform reservoir operations. *Water Resources Research*, *55*(11), 9133–9147.

Gómez-Martínez, G., Galiano, L., Rubio, T., Prado-López, C., Redolat, D., Paradinas Blázquez, C., Gaitán, E., Pedro-Monzonís, M., Ferriz-Sánchez, S., Añó Soto, M., Monjo, R., Pérez-Martín, M. Á., Almenar Llorens, P., & Macián Cervera, J. (2021). Effects of climate change on water quality in the Jucar River Basin (Spain). *Water*, *13*(17), 2424.

González-Rosell, A., Blanco, M., & Arfa, I. (2020). Integrating Stakeholder Views and System Dynamics to Assess the Water–Energy–Food Nexus in Andalusia. *WATER*, *12*(11), 3172.

Gonzalez-Sanchez, R., Kougias, I., Moner-Girona, M., Fahl, F., & Jäger-Waldau, A. (2021). Assessment of floating solar photovoltaics potential in existing hydropower reservoirs in Africa. *Renewable Energy*, *169*, 687–699.

Goor, Q., Halleux, C., Mohamed, Y., & Tilmant, A. (2010). Optimal operation of a multipurpose multireservoir system in the Eastern Nile River Basin. *Hydrology and Earth System Sciences*, *14*(10), 1895–1908.

Groves, D. G., & Lempert, R. J. (2007). A new analytic method for finding policy-relevant scenarios. *Global Environmental Change: Human and Policy Dimensions*, *17*(1), 73–85.

Guisández, I., Pérez-Díaz, J. I., & Wilhelmi, J. R. (2013). Assessment of the economic impact of environmental constraints on annual hydropower plant operation. *Energy Policy*, *61*, 1332–1343.

Gumindoga, W., Rientjes, T. H. M., Haile, A. T., Makurira, H., & Reggiani, P. (2019). Performance of bias-correction schemes for CMORPH rainfall estimates in the Zambezi River basin. *Hydrology and Earth System Sciences*, *23*(7), 2915–2938.

Gupta, H. V., Kling, H., Yilmaz, K. K., & Martinez, G. F. (2009). Decomposition of the mean squared error and NSE performance criteria: Implications for improving hydrological modelling. *Journal of Hydrology*, *377*(1), 80–91.

Hadka, D., & Reed, P. (2013). Borg: an auto-adaptive many-objective evolutionary computing framework. *Evolutionary Computation*, *21*(2), 231–259.

Harou, J. J., & Lund, J. R. (2008). Ending groundwater overdraft in hydrologic-economic systems. *Hydrogeology Journal*, *16*(6), 1039–1055.

Harou, J. J., Pulido-Velazquez, M., Rosenberg, D. E., Medellín-Azuara, J., Lund, J. R., & Howitt, R. E. (2009). Hydro-economic models: Concepts, design, applications, and future prospects. In *Journal of Hydrology* (Vol. 375, Issues 3–4, pp. 627–643). https://doi.org/10.1016/j.jhydrol.2009.06.037

Herman, J. D., Reed, P. M., Zeff, H. B., & Characklis, G. W. (2015). How Should Robustness Be Defined for Water Systems Planning under Change? *Journal of Water Resources Planning and Management*, *141*(10), 04015012.

Hossen, M. A., Connor, J., & Ahammed, F. (2021). Review of hydro-economic models (HEMs) which focus on transboundary river water sharing disputes. *Water Policy*, *23*(6), 1359–1374.

Huffman, G. J., Bolvin, D. T., Braithwaite, D., Hsu, K.-L., Joyce, R. J., Kidd, C., Nelkin, E. J., Sorooshian, S., Stocker, E. F., Tan, J., Wolff, D. B., & Xie, P. (2020). Integrated Multi-satellite Retrievals for the Global Precipitation Measurement (GPM) Mission (IMERG). In V. Levizzani, C. Kidd, D. B. Kirschbaum, C. D. Kummerow, K. Nakamura, & F. J. Turk (Eds.), *Satellite Precipitation Measurement: Volume 1* (pp. 343–353). Springer International Publishing.

ICPDR. (2004). *The Danube River Basin District*. International Commission for the Protection of the Danube River. https://www.icpdr.org/flowpaper/app/services/view.php?doc=danube_basin_analysis_2004.pdf&format=pdf&page={page}&subfolder=default/files/nodes/documents/

IRD. (1999). *Programme d'optimisation de la gestion des réservoirs. Phase 2 – Analyses et mises à jour des étalonnages*. IRD.

Joyce, R. J., Janowiak, J. E., Arkin, P. A., & Xie, P. (2004). CMORPH: A Method that Produces Global Precipitation Estimates from Passive Microwave and Infrared Data at High Spatial and Temporal Resolution. *Journal of Hydrometeorology*, *5*(3), 487–503.

Kahil, M. T., Dinar, A., & Albiac, J. (2015). Modeling water scarcity and droughts for policy adaptation to climate change in arid and semiarid regions. *Journal of Hydrology*, *522*, 95–109.

Kahil, M. T., Ward, F. A., Albiac, J., Eggleston, J., & Sanz, D. (2016). Hydro-economic modeling with aquifer–river interactions to guide sustainable basin management. *Journal of Hydrology*, *539*, 510–524.

Kantoussan, J., Ecoutin, J. M., Fontenelle, G., Morais, L. T., & Laë, R. (2014). Catch per Unit Effort and yields as indicators of exploited fish communities: application to two West A frican reservoirs. *Lakes and Reservoirs*, *19*(2), 86–97.

Kasprzyk, J. R., Nataraj, S., Reed, P. M., & Lempert, R. J. (2013). Many objective robust decision making for complex environmental systems undergoing change. *Environmental Modelling & Software*, *42*, 55–71.

Kirkpatrick, S., Gelatt, C. D., Jr, & Vecchi, M. P. (1983). Optimization by simulated annealing. *Science*, *220*(4598), 671–680.

Knoben, W. J. M., Freer, J. E., & Woods, R. A. (2019). Technical note: Inherent benchmark or not? Comparing Nash–Sutcliffe and Kling–Gupta efficiency scores. *Hydrology and Earth System Sciences*, *23*(10), 4323–4331.

Kwakkel, J. H., Eker, S., & Pruyt, E. (2016). How robust is a robust policy? Comparing alternative robustness metrics for robust decision-making. In *Robustness Analysis in Decision Aiding, Optimization, and Analytics* (pp. 221–237). Springer International Publishing.

Kwakkel, J. H., & Jaxa-Rozen, M. (2016). Improving scenario discovery for handling heterogeneous uncertainties and multinomial classified outcomes. *Environmental Modelling & Software*, *79*, 311–321.

Lautze, J., Phiri, Z., Smakhtin, V., & Saruchera, D. (Eds.). (2017). *The Zambezi river basin*. Routledge.

Lehner, B., Verdin, K., & Jarvis, A. (2006). Technical documentation version 1.0. *USGS Earth Resources Observation and Science: Sioux Falls, SD, USA*. https://core.ac.uk/download/pdf/5210660.pdf
Lempert, R. J. (2002). A new decision sciences for complex systems. *Proceedings of the National Academy of Sciences of the United States of America*, *99 Suppl 3*, 7309–7313.
Li, L., & Simonovic, S. P. (2002). System dynamics model for predicting floods from snowmelt in North American prairie watersheds. *Hydrological Processes*, *16*(13), 2645–2666.
Li, Y., Giuliani, M., & Castelletti, A. (2017). A coupled human–natural system to assess the operational value of weather and climate services for agriculture. *Hydrology and Earth System Sciences*, *21*(9), 4693–4709.
Liu, Z., & He, X. (2023). Balancing-oriented hydropower operation makes the clean energy transition more affordable and simultaneously boosts water security. *Nature Water*, *1*(9), 778–789.
Lopez-Nicolas, A., Pulido-Velazquez, M., & Macian-Sorribes, H. (2017). Economic risk assessment of drought impacts on irrigated agriculture. *Journal of Hydrology*, *550*, 580–589.
Macian-Sorribes, H., Pulido-Velazquez, M., & Tilmant, A. (2014). *Definition of scarcity-based water pricing policies through hydro-economic stochastic programming*. 814.
Macian-Sorribes, H., Tilmant, A., & Pulido-Velazquez, M. (2017). Improving operating policies of large-scale surface-groundwater systems through stochastic programming. *Water Resources Research*, *53*(2), 1407–1423.
Mahmoud, M., Liu, Y., Hartmann, H., Stewart, S., Wagener, T., Semmens, D., Stewart, R., Gupta, H., Dominguez, D., Dominguez, F., Hulse, D., Letcher, R., Rashleigh, B., Smith, C., Street, R., Ticehurst, J., Twery, M., van Delden, H., Waldick, R., … Winter, L. (2009). A formal framework for scenario development in support of environmental decision-making. *Environmental Modelling & Software*, *24*(7), 798–808.
Maier, H. R., Kapelan, Z., Kasprzyk, J., Kollat, J., Matott, L. S., Cunha, M. C., Dandy, G. C., Gibbs, M. S., Keedwell, E., Marchi, A., Ostfeld, A., Savic, D., Solomatine, D. P., Vrugt, J. A., Zecchin, A. C., Minsker, B. S., Barbour, E. J., Kuczera, G., Pasha, F., … Reed, P. M. (2014). Evolutionary algorithms and other metaheuristics in water resources: Current status, research challenges and future directions. *Environmental Modelling & Software*, *62*, 271–299.
Marques, G. F., & Tilmant, A. (2013). The economic value of coordination in large-scale multireservoir systems: The Parana River case. In *Water Resources Research* (Vol. 49, Issue 11, pp. 7546–7557). https://doi.org/10.1002/2013wr013679
Martinez Santa-Maria, C., Fernández Yuste, J. A., Sanchez, J., Magdaleno Mas, F., & García, E. (2008). Iahris: New Software to Assess Hydrologic Alteration. *Proceedings of 4th ECRR International Conference on River Restoration 2008*, 1057.
Martínez-Paz, J. M., Pellicer-Martínez, F., Fernández, J. R., & Lamonaca, L. (2015). Valoración socioeconómica de la extracción de gas mediante fracturación hidráulica en la Región de Murcia. *Papeles de Geografía*, *61*, 122.
Matalas, N. C., & Fiering, M. B. (1977). *Water-Resource Systems Planning. Chapter 6 in Climate, Climatic Change, and Water Supply*. Washington, DC: National Academy of Sciences.
Matrosov, E. S., Padula, S., & Harou, J. J. (2013). Selecting portfolios of water supply and demand management strategies under uncertainty—contrasting economic

optimisation and 'robust decision making' approaches. *Water Resources Management*, *27*(4), 1123–1148.

McPhail, C., Maier, H. R., Kwakkel, J. H., Giuliani, M., Castelletti, A., & Westra, S. (2018). Robustness Metrics: How Are They Calculated, When Should They Be Used and Why Do They Give Different Results? *Earth's Future*, *6*(2), 169–191.

Mezger, G., De Stefano, L., & González del Tánago, M. (2022). Analysis of the evolution of climatic and hydrological variables in the Tagus River basin, Spain. *Water*, *14*(5), 818.

Mirchi, A., Madani, K., Watkins, D., & Ahmad, S. (2012). Synthesis of System Dynamics Tools for Holistic Conceptualization of Water Resources Problems. In *Water Resources Management* (Vol. 26, Issue 9, pp. 2421–2442). https://doi.org/10.1007/s11269-012-0024-2

Momblanch, A., Connor, J. D., Crossman, N. D., Paredes-Arquiola, J., & Andreu, J. (2016). Using ecosystem services to represent the environment in hydro-economic models. *Journal of Hydrology*, *538*, 293–303.

Muñoz-Sabater, J., Dutra, E., Agustí-Panareda, A., Albergel, C., Arduini, G., Balsamo, G., Boussetta, S., Choulga, M., Harrigan, S., Hersbach, H., Martens, B., Miralles, D. G., Piles, M., Rodríguez-Fernández, N. J., Zsoter, E., Buontempo, C., & Jean-Noël Thépaut. (2021). ERA5-Land: a state-of-the-art global reanalysis dataset for land applications. *Earth System Science Data*, *13*(9), 4349–4383.

Nappo, N., Ferrario, M. F., Livio, F., & Michetti, A. M. (2020). Regression Analysis of Subsidence in the Como Basin (Northern Italy): New Insights on Natural and Anthropic Drivers from InSAR Data. *Remote Sensing*, *12*(18), 2931.

Olesen, J. E., & Bindi, M. (2002). Consequences of climate change for European agricultural productivity, land use and policy. *European Journal of Agronomy: The Journal of the European Society for Agronomy*, *16*(4), 239–262.

Pastor, A. V., Ludwig, F., Biemans, H., Hoff, H., & Kabat, P. (2014). Accounting for environmental flow requirements in global water assessments. *Hydrology and Earth System Sciences*, *18*(12), 5041–5059.

Peleg, N., Fatichi, S., Paschalis, A., Molnar, P., & Burlando, P. (2017). An advanced stochastic weather generator for simulating 2-D high-resolution climate variables. *Journal of Advances in Modeling Earth Systems*, *9*(3), 1595–1627.

Peleg, N., Molnar, P., Burlando, P., & Fatichi, S. (2019). Exploring stochastic climate uncertainty in space and time using a gridded hourly weather generator. *Journal of Hydrology*, *571*, 627–641.

Peleg, N., Sinclair, S., Fatichi, S., & Burlando, P. (2020). Downscaling climate projections over large and data sparse regions: Methodological application in the Zambezi River Basin. *International Journal of Climatology: A Journal of the Royal Meteorological Society*, *40*(15), 6242–6264.

Pereira-Cardenal, S. J., Madsen, H., Arnbjerg-Nielsen, K., Riegels, N., Jensen, R., Mo, B., Wangensteen, I., & Bauer-Gottwein, P. (2014). Assessing climate change impacts on the Iberian power system using a coupled water-power model. *Climatic Change*, *126*(3–4), 351–364.

Perni, Á., & Martínez-Paz, J. M. (2017). Measuring conflicts in the management of anthropized ecosystems: Evidence from a choice experiment in a human-created Mediterranean wetland. *Journal of Environmental Management*, *203*(Pt 1), 40–50.

Piccardi, C., & Soncini-Sessa, R. (1991). Stochastic dynamic programming for reservoir optimal control: Dense discretization and inflow correlation assumption made possible by parallel computing. In *Water Resources Research* (Vol. 27, Issue 5, pp. 729–741). https://doi.org/10.1029/90wr02766
Powell, M. J. D. (1964). An efficient method for finding the minimum of a function of several variables without calculating derivatives. *Computer Journal*, *7*(2), 155–162.
Pulido-Velazquez, M. A., Sahuquillo-Herraiz, A., Camilo Ochoa-Rivera, J., & Pulido-Velazquez, D. (2005). Modeling of stream–aquifer interaction: the embedded multireservoir model. *Journal of Hydrology*, *313*(3–4), 166–181.
Pulido-Velázquez, M., Andreu, J., & Sahuquillo, A. (2006). Economic Optimization of Conjunctive Use of Surface Water and Groundwater at the Basin Scale. *Journal of Water Resources Planning and Management*, *132*(6), 454–467.
Qaiser, K., Ahmad, S., Johnson, W., & Batista, J. (2011). Evaluating the impact of water conservation on fate of outdoor water use: A study in an arid region. In *Journal of Environmental Management* (Vol. 92, Issue 8, pp. 2061–2068). https://doi.org/10.1016/j.jenvman.2011.03.031
Rubio-Martin, A., Pulido-Velazquez, M., Macian-Sorribes, H., & Garcia-Prats, A. (2020). System dynamics modeling for supporting drought-oriented management of the Jucar River system, Spain. *WATER*, *12*(5), 1407.
SAAP. (2017). *SAPP Pool Plan 2017*. Southern African Power Pool. https://www.sapp.co.zw/sites/default/files/SAPP%20Pool%20Plan%202017%20Main%20Volume_0.pdf
Saltelli, A., Ratto, M., Andres, T., Campolongo, F., Cariboni, J., Gatelli, D., Saisana, M., & Tarantola, S. (2008). *Global Sensitivity Analysis: The Primer*. John Wiley & Sons.
Satti, S., Zaitchik, B., & Siddiqui, S. (2015). The question of Sudan: a hydro-economic optimization model for the Sudanese Blue Nile. *Hydrology and Earth System Sciences*, *19*(5), 2275–2293.
Savage, L. J. (1951). The Theory of Statistical Decision. *Journal of the American Statistical Association*, *46*(253), 55–67.
Sehlke, G., & Jacobson, J. (2005). System dynamics modeling of transboundary systems: the bear river basin model. *Ground Water*, *43*(5), 722–730.
Shela, O. N. (2000). Management of shared river basins: the case of the Zambezi River. *Water Policy*, *2*(1), 65–81.
Simon, H. A. (1956). Rational choice and the structure of the environment. *Psychological Review*, *63*(2), 129–138.
Simonovic, S. P. (2020). Application of the Systems Approach to the Management of Complex Water Systems. *WATER*, *12*(10), 2923.
Singh, V. P. (2012). *The Yamuna River Basin*.
Sobol, I. M. (2001). Global sensitivity indices for nonlinear mathematical models and their Monte Carlo estimates. *Mathematics and Computers in Simulation*, *55*(1), 271–280.
Spalding-Fecher, R., Joyce, B., & Winkler, H. (2017). Climate change and hydropower in the Southern African Power Pool and Zambezi River Basin: System-wide impacts and policy implications. *Energy Policy*, *103*, 84–97.
Spalding-Fecher, R., Senatla, M., Yamba, F., Lukwesa, B., Himunzowa, G., Heaps, C., Chapman, A., Mahumane, G., Tembo, B., & Nyambe, I. (2017). Electricity supply and demand scenarios for the Southern African power pool. *Energy Policy*, *101*, 403–414.

Srikrishnan, V., Lafferty, D. C., Wong, T. E., Lamontagne, J. R., Quinn, J. D., Sharma, S., Molla, N. J., Herman, J. D., Sriver, R. L., Morris, J. F., & Lee, B. S. (2022). Uncertainty analysis in multi-sector systems: Considerations for risk analysis, projection, and planning for complex systems. *Earth's Future*. https://doi.org/10.1029/2021ef002644
Sterman, J. D. (2000). *Business Dynamics: Systems Thinking and Modeling for a Complex World*. McGraw-Hill School Education Group.
Suárez-Almiñana, S., Solera, A., Andreu, J., & García-Romero, L. (2020). Análisis de incertidumbre de las proyecciones climáticas en relación a las aportaciones históricas en la Cuenca del Júcar. *Ingeniería Del Agua*, *24*(2), 89.
Susnik, J., Wang, X., & Dong, Z. (2022). System Dynamics Modelling to Simulate Regional Water-Energy-Food Nexus Combined with the Society-Economy-Environment System in Hunan Province, China. In *SSRN Electronic Journal*. https://doi.org/10.2139/ssrn.4209965
Sutanudjaja, E. H., van Beek, R., Wanders, N., Wada, Y., Bosmans, J. H. C., Drost, N., van der Ent, R. J., de Graaf, I. E. M., Hoch, J. M., de Jong, K., Karssenberg, D., López López, P., Peßenteiner, S., Schmitz, O., Straatsma, M. W., Vannametee, E., Wisser, D., & Bierkens, M. F. P. (2018). PCR-GLOBWB 2: a 5 arcmin global hydrological and water resources model. *Geoscientific Model Development*, *11*(6), 2429–2453.
Tesfaye, A., Wolanios, N., & Brouwer, R. (2016). Estimation of the economic value of the ecosystem services provided by the Blue Nile Basin in Ethiopia. *Ecosystem Services*, *17*, 268–277.
Tietenberg, T., & Lewis, L. (2012). *Environmental and Natural Resource Economics*.
Tilmant, A., Kinzelbach, W., Juizo, D., Beevers, L., Senn, D., & Casarotto, C. (2011). Economic valuation of benefits and costs associated with the coordinated development and management of the Zambezi river basin. *Water Policy*, *14*(3), 490–508.
Tilmant, Pina, J., Salman, M., Casarotto, C., Ledbi, F., & Pek, E. (2020). Probabilistic trade-off assessment between competing and vulnerable water users – The case of the Senegal River basin. *Journal of Hydrology*, *587*(124915), 124915.
Trindade, B. C., Reed, P. M., Herman, J. D., Zeff, H. B., & Characklis, G. W. (2017). Reducing regional drought vulnerabilities and multi-city robustness conflicts using many-objective optimization under deep uncertainty. *Advances in Water Resources*, *104*. https://doi.org/10.1016/j.advwatres.2017.03.023
Tweddle, D., Cowx, I. G., Peel, R. A., & Weyl, O. L. F. (2015). Challenges in fisheries management in the Zambezi, one of the great rivers of Africa. *Fisheries Management and Ecology*, *22*(1), 99–111.
Valerio, C., De Stefano, L., Martínez-Muñoz, G., & Garrido, A. (2021). A machine learning model to assess the ecosystem response to water policy measures in the Tagus River Basin (Spain). *The Science of the Total Environment*, *750*(141252), 141252.
Wald, A. (1950). Statistical decision functions. *Biometrika*, *40*(3/4), 475–477.
Walker, W., Haasnoot, M., & Kwakkel, J. (2013). Adapt or perish: A review of planning approaches for adaptation under deep uncertainty. *Sustainability*, *5*(3), 955–979.
Winz, I., & Brierley, G. (2007). *Participatory methods in environmental system dynamics projects*. https://proceedings.systemdynamics.org/2007/proceed/papers/WINZ303.pdf
Winz, I., Brierley, G., & Trowsdale, S. (2009). The Use of System Dynamics Simulation in Water Resources Management. *Water Resources Management*, *23*(7), 1301–1323.

World Bank Group. (2010). *The Zambezi River Basin A Multi-Sector Investment Opportunities Analysis*. World Bank Group. http://documents.worldbank.org/curated/en/724861468009989838/Summary-report

Wu, G. C., Deshmukh, R., Ndhlukula, K., Radojicic, T., Reilly-Moman, J., Phadke, A., Kammen, D. M., & Callaway, D. S. (2017). Strategic siting and regional grid interconnections key to low-carbon futures in African countries. *Proceedings of the National Academy of Sciences of the United States of America*, *114*(15), E3004–E3012.

Yung, L., Louder, E., Gallagher, L. A., Jones, K., & Wyborn, C. (2019). How Methods for Navigating Uncertainty Connect Science and Policy at the Water-Energy-Food Nexus. *Frontiers of Environmental Science & Engineering in China*, *7*. https://doi.org/10.3389/fenvs.2019.00037

Zaniolo, M., Fletcher, S., & Mauter, M. S. (2023). Multi-scale planning model for robust urban drought response. *Environmental Research Letters: ERL [Web Site]*, *18*(5), 054014.

Zhang, Q., Singh, V. P., Li, J., Jiang, F., & Bai, Y. (2012). Spatio-temporal variations of precipitation extremes in Xinjiang, China. *Journal of Hydrology*, *434–435*, 7–18.